OULU 2012
C 434

ACTA

UNIVERSITATIS OULUENSIS

Giuseppe Destino

POSITIONING IN WIRELESS NETWORKS

NON-COOPERATIVE AND COOPERATIVE ALGORITHMS

UNIVERSITY OF OULU GRADUATE SCHOOL;
UNIVERSITY OF OULU,
FACULTY OF TECHNOLOGY,
DEPARTMENT OF COMMUNICATIONS ENGINEERING;
CENTRE FOR WIRELESS COMMUNICATIONS;
INFOTECH OULU

ACTA UNIVERSITATIS OULUENSIS
C Technica 434

GIUSEPPE DESTINO

POSITIONING IN WIRELESS NETWORKS

Non-cooperative and cooperative algorithms

Academic dissertation to be presented with the assent of the Doctoral Training Committee of Technology and Natural Sciences of the University of Oulu for public defence in OP-sali (Auditorium L10), Linnanmaa, on 16 November 2012, at 12 noon

UNIVERSITY OF OULU, OULU 2012

Acta Univ. Oul. C 434, 2012

Supervised by
Professor Giuseppe Thadeus Freitas de Abreu
Professor Jari Iinatti

Reviewed by
Professor José Manuel Fonseca de Moura
Assistant Professor Sinan Gezici

ISBN 978-951-42-9973-5 (Paperback)
ISBN 978-951-42-9974-2 (PDF)

ISSN 0355-3213 (Printed)
ISSN 1796-2226 (Online)

Cover Design
Raimo Ahonen

JUVENES PRINT
TAMPERE 2012

Destino, Giuseppe, Positioning in Wireless Networks. Non-cooperative and cooperative algorithms

University of Oulu Graduate School; University of Oulu, Faculty of Technology, Department of Communications Engineering; Centre for Wireless Communications; Infotech Oulu, P.O. Box 4500, FI-90014 University of Oulu, Finland

Acta Univ. Oul. C 434, 2012
Oulu, Finland

Abstract

In the last few years, location-awareness has emerged as a key technology for the future development of mobile, ad hoc and sensor networks. Thanks to location information, several network optimization strategies as well as services can be developed. However, the problem of determining accurate location, i.e. positioning, is still a challenge and robust algorithms are yet to be developed.

In this thesis, we focus on the development of distance-based non-cooperative and cooperative algorithms, which is derived based on a non-parametric non- Bayesian framework, specifically with a Weighted Least Square (WLS) optimization. From a theoretic perspective, we study the WLS problem and establish the optimality through the relationship with a Maximum Likelihood (ML) estimator. We investigate the fundamental limits and derive the consistency conditions by creating a connection between Euclidean geometry and inference theory. Furthermore, we derive the closed-form expression of a distance-model based Cramér-Rao Lower Bound (CRLB), as well as the formulas, that characterize information coupling in the Fisher information matrix.

Non-cooperative positioning is addressed as follows. We propose a novel framework, namely the Distance Contraction, to develop robust non-cooperative positioning techniques. We prove that distance contraction can mitigate the global minimum problem and structured distance contraction yields nearly optimal performance in severe channel conditions. Based on these results, we show how classic algorithms such as the Weighted Centroid (WC) and the Non-Linear Least Square (NLS) can be modified to cope with biased ranging.

For cooperative positioning, we derive a novel, low complexity and nearly optimal global optimization algorithm, namely the Range-Global Distance Continuation method, to use in centralized and distributed positioning schemes. We propose an effective weighting strategy to cope with biased measurements, which consists of a dispersion weight that captures the effect of noise while maximizing the diversity of the information, and a geometric-based penalty weight, that penalizes the assumption of bias-free measurements. Finally, we show the results of a positioning test where we employ the proposed algorithms and utilize commercial Ultra-Wideband (UWB) devices.

Keywords: estimation error bounds, field trial, mobile positioning, multi-target positioning, optimization, ultra-wideband, weighted least square

Destino, Giuseppe, Paikannus langattomissa verkoissa. Ei-yhteistoiminnalliset ja yhteistoiminnalliset algoritmit
Oulun yliopiston tutkijakoulu; Oulun yliopisto, Teknillinen tiedekunta, Tietoliikennetekniikan osasto; Centre for Wireless Communications; Infotech Oulu, PL 4500, 90014 Oulun yliopisto
Acta Univ. Oul. C 434, 2012
Oulu

Tiivistelmä

Viime vuosina paikkatietoisuudesta on tullut eräs merkittävä avainteknologia mobiili- ja sensoriverkkojen tulevaisuuden kehitykselle. Paikkatieto mahdollistaa useiden verkko-optimointistrategioiden sekä palveluiden kehittämisen. Kuitenkin tarkan paikkatiedon määrittäminen, esimerkiksi kohteen koordinaattien, on edelleen vaativa tehtävä ja robustit algoritmit vaativat kehittämistä.

Tässä väitöskirjassa keskitytään etäisyyspohjaisten, yhteistoiminnallisten sekä ei-yhteistoiminnallisten, algoritmien kehittämiseen. Algoritmit pohjautuvat parametrittömään ei-bayesilaiseen viitekehykseen, erityisesti painotetun pienimmän neliösumman (WLS) optimointimenetelmään. Väitöskirjassa tutkitaan WLS ongelmaa teoreettisesti ja osoitetaan sen optimaalisuus todeksi tarkastelemalla sen suhdetta suurimman todennäköisyyden (ML) estimaattoriin. Lisäksi tässä työssä tutkitaan perustavanlaatuisia raja-arvoja sekä johdetaan yhtäpitävyysehdot luomalla yhteys euklidisen geometrian ja inferenssiteorian välille. Väitöskirjassa myös johdetaan suljettu ilmaisu etäisyyspohjaiselle Cramér-Rao -alarajalle (CRLB) sekä esitetään yhtälöt, jotka karakterisoivat informaation liittämisen Fisherin informaatiomatriisiin.

Väitöskirjassa ehdotetaan uutta viitekehystä, nimeltään etäisyyden supistaminen, robustin ei-yhteistoiminnallisen paikannustekniikan perustaksi. Tässä työssä todistetaan, että etäisyyden supistaminen pienentää globaali minimi -ongelmaa ja jäsennetty etäisyyden supistaminen johtaa lähes optimaaliseen suorituskykyyn vaikeissa radiokanavan olosuhteissa. Näiden tulosten pohjalta väitöskirjassa esitetään, kuinka klassiset algoritmit, kuten painotetun keskipisteen (WC) sekä epälineaarinen pienimmän neliösumman (NLS) menetelmät, voidaan muokata ottamaan huomioon etäisyysmittauksen harha.

Yhteistoiminnalliseksi paikannusmenetelmäksi johdetaan uusi, lähes optimaalinen algoritmi, joka on kompleksisuudeltaan matala. Algoritmi on etäisyyspohjainen globaalin optimoinnin menetelmä ja sitä käytetään keskitetyissä ja hajautetuissa paikannusjärjestelmissä. Lisäksi tässä työssä ehdotetaan tehokasta painotusstrategiaa ottamaan huomioon mittausharha. Strategia pitää sisällään dispersiopainon, joka tallentaa häiriön aiheuttaman vaikutuksen maksimoiden samalla informaation hajonnan, sekä geometrisen sakkokertoimen, joka rankaisee harhattomuuden ennakko-oletuksesta. Lopuksi väitöskirjassa esitetään tulokset kokeellisista mittauksista, joissa ehdotettuja algoritmeja käytettiin kaupallisissa erittäin laajakaistaisissa (UWB) laitteissa.

Asiasanat: estimoinnin raja-arvot, mobiilipaikannus, monikohdepaikannus, optimointi, painotettu pienin neliösumma, ultra-laajakaista ja kenttäkoe

A mio padre

- To my father -

Preface

The research work presented in this doctoral thesis has been carried out at the Centre for Wireless Communications (CWC), Department of Communications Engineering (DCE), University of Oulu, Oulu, Finland. This work has been financially supported by the European projects PULSERS Phase II, EUWB and BUTLER as well as by the Infotech Oulu Graduate School. I also acknowledge the foundations Nokia Oyj:n säätiö, Oulun Yliopiston tukisäätiö, Riitta ja Jorma J. takasen säätiö, Tekniikan edistämissäätiö and Walter Ehström-säätiö, from which I received personal research grants.

This research started back in September 2005 when, at my first working day as a Ph.D. student, my advisor Prof. Giuseppe Abreu gave me the article "Improved MDS-based Localization" and asked me to understand what the problem of "Positioning in Wireless Networks" is about. It turned out that such a problem was a fascinating, curious and challenging combination of Euclidean geometry and estimation theories applied to wireless networks.

Throughout the years of my Ph.D. study, nice and difficult moments occurred. There have been situations in which the stress was high and the work did not progress. However, the encouragement from my colleagues as well as from my family helped me to continue. I am very thankful to those persons and hereby I would like to express my sincere gratitude.

I thank my advisor and friend Prof. Giuseppe Abreu. I met him during my first visit in CWC, in 2004, when I was working for my Master thesis. Our relationship started as a friendship and over time it became also professional. In 2005 he asked me to be his first Ph.D student. The amount of hours spent on the whiteboard to discuss ideas, formalize problems and derive equations are countless. His constructive criticism, preciseness and high standard helped me to produce novel and significant research results. His availability to sit with me and teach me the technical writing will never be forgotten. If today, I am an independent, self-critical and creative scientist it is on great part thanks to him.

I thank my supervisor Prof. Jari Iinatti. I have had the opportunity to work with him only in the last few years, but his contributions have been important to the accomplishment of this thesis. I would like to thank him for his reinsuring

words, efficient work planning, availability to supervise my research and all valuable comments that he gave me to improve the quality of the manuscript.

I also thank my group leader Prof. Markku Juntti for his useful advice during the years as well as for his guidance in my current research.

A special gratitude goes to my reviewers Prof. José Manuel Fonseca de Moura and Prof. Sinan Gezici that provided a professional and careful inspection of the thesis as well as accurate corrections to enhance the level of the content. An acknowledgement is also directed to Aleksandrs Malinovskis for the proofreading.

I would like to thank also the Head of the DCE, Prof. Matti Latva-aho, as well as the former and current CWC director, Lisc. Tech. Ari Pouttu and Dr. Harri Posti respectively, for providing a great working environment. My gratitude also goes to the administration group, Hanna Saarela, Kirsi Ojutkangas, Eija Pajunen, Elina Komminaho, Timo Äikäs and Jari Sillanpää for their efficient and always prompt cooperation in the work-related issues.

Sincere thanks are inexorable to my Friend and office-mate Davide Macagnano, with whom I did spend a lot of time! More than any other colleague, I shared with Davide a lot of nice and difficult time at work. If with my advisor I had countless hours spent on technical problems, then that number must be exponentially increased when referring to the technical (and loud) discussions that I had with Davide. His criticism has always been constructive and, his advice have helped to steer the work into the right direction.

I would like to express my gratitude also to other colleagues for the free-time spent together: (the brasilian churrascu team) Pedro Nardelli, Carlos Lima and Hirley Alves; (the lunch-break team) Jani Saloranta, Jari Ylionas, Esa Kunnari and Markus Myllyla; (the occasianlly party team) Jussi Haapola, Leonardo Goratti, Marko Härkönen, Brett Kaufman, Stefano Severi and Antti Tölli. Additional thanks go to Jani Saloranta who helped me with a pre-screen of the thesis as well as Finnish translations. I also thank Prof. Behnaam Aazhang for both his professional advice and the nice time spent together outside the office.

My warmest gratitude goes to my dearly loved wife, Miia. This chapter of my life is also due to her. She was the person that, better than any others, knew my feelings without me expressing any word. I thank her for all the advice, her objective considerations, her understanding of my work and her joyfulness for my successes. I also thank her very much for the precious help to read the text of this thesis and to provide useful corrections.

I would like to thank my little step-son Joona who cheered up my personal life with his young energy and let me forget the problems at work while watching his exciting football games. Another special thank goes to my little son Alessio, now, a nine months old baby. During the editing of the thesis, he made sure that I would wake up at five o'clock in the morning to write a few paragraphs before going to work.

Finally, I thank my parent-in-law Pentti and Sirpa as well as my brother-in-law Marko and his fiancé Kati for their kind and always reliable help.

In conclusione, un ringraziamento molto speciale a mio padre Angelo, mia madre Maria Antonietta, i miei fratelli Luigi e Gianni e le rispettive moglie e fiancé Antonella e Angela. Loro mi son stati accanto in ogni momento e, anche se da lontano, hanno sempre saputo consigliarmi per il meglio. A mio padre, che purtroppo oggi non é più con noi, voglio dedicare questa tesi. Le sue parole e i suoi consigli mi son serviti per crescere e i suoi sacrifici mi han consentito di arrivare a questo punto. Grazie.

Oulu, October 24, 2012 Giuseppe Destino

Symbols and abbreviations

AoA	Angle-of-Arrival
AHB	Abel Hybrid Bound
BB	Battacharyya Bound
BFGS	Broyden-Fletcher-Goldfarb-Shanno
CRLB	Cramér-Rao Lower Bound
C-WLS	Constraint Weighted Least Square
DoA	Direction-of-Arrival
DC	Distance Contraction
DE	Distance Error
EDF	Euclidean Distance Function
EDM	Euclidean Distance Matrix
FCC	Federal Communications Commission
FIM	Fisher Information Matrix
GDC	Global Distance Continuation
GDOP	Geometric Dilution of Precision
GPS	Global Positioning System
HCRB	Hammersley-Chapmann-Robbins Bound
i.i.d.	independent identically distributed
LQ	Link-Quality
LBS	Location Based Service
LOS	Line-of-Sight
LLS	Linearised Least Square
LS	Least Square
LT	Location-Tracking
MDS	Multi-Dimensional Scaling
ML	Maximum Likelihood
MSE	Mean Square Error
MSPE	Mean-Squared-Position-Error
MUSIC	MUltiple SIgnal Classification
NLOS	Non-Line-of-Sight
NLS	Non-Linear Least Square

PE	Position Error
PEB	Position Error Bound
PSM	Positive Semi-definite Matrix
R-GDC	Range-Global Distance Continuation
RMSE	Root-Mean-Squared-Error
RSS	Received Signal Strength
SB	Stochastic Bound
SDP	Semi Definite Programming
SMACOF	Stress-of-a-MAjorizing-Complex-Objective-Function
SNR	Signal-to-Noise-Ratio
SQP	Sequential Quadratic Programming
SR-GDC	Square Range-Global Distance Continuation
SR-LS	Squared-Range Least Square
ToA	Time-of-Arrival
UWB	Ultra-WideBand
WC	Weighted Centroid
WLS	Weighted Least Square
$\mathbf{0}_{\eta}$	Vector of zeros with η columns
$\mathbf{0}_{\eta\eta}$	Matrix of all zeros and size $\eta \times \eta$
$\mathbf{1}_N$	Vector of ones with N rows
$\|\cdot\|_{\mathrm{F}}$	Frobenius norm
$\circ$	Hadamard product
$\otimes$	Kronecker product
$\nabla_{\mathbf{x}}(\cdot)$	Gradient vector of the function given as the argument derived with respect to the variable vector $\mathbf{x}$
$\nabla^2_{\mathbf{x}}(\cdot)$	Hessian matrix of the function given as the argument derived with respect to the variable vector $\mathbf{x}$
$\frac{\mathrm{d}}{\mathrm{d}x}$	First derivative with respect to the variable x
$\frac{\partial}{\partial x}$	Partial derivative with respect to the variable x
$\frac{\partial^2}{\partial x \partial y}$	Second Partial derivative with respect to the variables x and y
$\frac{\partial^n}{\partial \mathbf{x}^{\otimes n}}$	Vector of all partial derivatives with respect to the vector $\mathbf{x}$ up to the n-th order
$\mathrm{abs}(\cdot)$	Absolute value function
${}_1F_1(a;b;\cdot)$	Confluent hypergeometric function of parameters a and b
$\mathrm{AHB}_{\mathrm{LOS}}(\cdot)$	AHB function derived from the LOS assumptions

$\mathcal{C}(\cdot)$	Convex-hull of the coordinate matrix given as argument
$\mathrm{CRLB}_{\mathrm{LOS}}(\cdot)$	CRLB function derived from the LOS assumptions
$\mathrm{CRLB}_{\mathrm{NLOS}}(\cdot)$	CRLB function derived from the NLOS assumptions
$\mathcal{D}(\cdot)$	Euclidean distance function
$\mathrm{diag}(\cdot)$	Diagonal function
$\mathrm{dom}(\cdot)$	Domain of the function given as argument
$\mathrm{E}_x\{\cdot\}$	Expectation with respect to the random variable x
$\mathscr{E}_i(\cdot)$	i-th eigenvalue of the matrix given as argument
$f_e(\cdot)$	General estimator function
$f_{\mathrm{T}}(\cdot; a)$	T-distribution of a degree of freedom
$f_{\mathrm{R}}(\cdot)$	Weighted least square function
$f_{ij}^{\mathrm{R}}(\cdot;\lambda)$	ij-th term of the Gaussian transform of f_{R}
$f_{\text{A-R}}(\cdot)$	Location ambiguity function
$f_{ij}(\tilde{d}_{ij}\|d_{ij})$	Probability density function of $\tilde{d}_{ij}$ parametrised by d_{ij}
$f_{\mathrm{Fp}}(\tilde{\mathbf{y}}\|\mathbf{X}_{m_p})$	Conditioned probability density function of the fingerprint $\tilde{\mathbf{y}}$
$g(\cdot;\lambda)$	Gaussian kernel with parameter λ
$g_m(\cdot)$	Gaussian mixture function
$g_{mi}(\cdot)$	i-th term of the Gaussian mixture
$\mathcal{G}(\cdot,\cdot,\cdot)$	Graph function
$\mathcal{H}(\cdot)$	Entropy function
$\mathrm{HCRB}_{\mathrm{LOS}}(\cdot)$	HCRB function derived from the LOS assumptions
$\mathcal{J}_{\mathbf{x}}(\cdot)$	Jacobian function of the vector function given as the argument with respect to the variable vector $\mathbf{x}$
$\mathcal{K}(\cdot)$	Double centering Euclidean kernel transformation
$\mathcal{K}^{-1}(\cdot)$	Inverse of the double centering Euclidean kernel transformation
$\mathcal{L}(\vec{\mathbf{p}}\|\tilde{\mathbf{d}})$	Generalised Likelihood function of $\vec{\mathbf{p}}$ given $\vec{\tilde{\mathbf{d}}}$
$\mathcal{L}_{\mathrm{LOS}}(\vec{\mathbf{p}}\|\vec{\tilde{\mathbf{d}}})$	Likelihood function of $\vec{\mathbf{p}}$ given $\vec{\tilde{\mathbf{d}}}$ in LOS
$\mathcal{L}_{\mathrm{NLOS}}(\vec{\tilde{\mathbf{p}}}\|\vec{\tilde{\mathbf{d}}})$	Likelihood function of $\vec{\tilde{\mathbf{p}}}$ given $\vec{\tilde{\mathbf{d}}}$ in NLOS
$\mathrm{MSE}(\cdot)$	Mean square error function
$\mathcal{N}(\cdot)$	Null-space function
$\mathcal{O}(\cdot)$	Asymptotic upper bound notation
$p_y(\tilde{\mathbf{y}})$	Distribution of the observation vector $\tilde{\mathbf{y}}$ (general)
$\Pr\{\cdot\}$	Probability of the event described in the argument
$Q(\cdot)$	Tail probability of the standard normal distribution

$\mathrm{rank}(\cdot)$	Rank function
$\mathscr{S}(\cdot)$	Minimiser deviation
$S_1(\cdot;\lambda)$	Auxiliary function used in the derivation of the gradient and Hessian of $\langle f_{\mathrm{R}} \rangle_\lambda$
$S_2(\cdot;\lambda)$	Auxiliary function used in the derivation of the Hessian of $\langle f_{\mathrm{R}} \rangle_\lambda$
$\mathrm{tr}(\cdot)$	Trace function
$\mathcal{T}(\cdot)$	Majorising and integrable function
$\mathcal{U}(a,b)$	Uniform distribution defined in the interval (a,b)
$W_d(\cdot,\cdot;\gamma)$	Dispersion weighing function parametrized by γ
$\Gamma(\cdot)$	Gamma function
$\Delta(\mathbf{x}_1,\mathbf{x}_2;\mathbf{y})$	Difference of the likelihood function at $\mathbf{a}$ and $\mathbf{b}$, and parametrized by $\mathbf{y}$
$\Pi(\cdot)$	Minimisation effectiveness function
$\phi(\cdot)$	Generic unbiased ranging distribution
$(\cdot)^{\mathrm{T}}$	Transpose operation
$(\cdot) \preceq 0$	Negative semi-definite
$(\cdot) \succeq 0$	Positive semi-definite
$\{\cdots\}$	Finite set
$\langle\cdot\rangle_\lambda$	Gaussian transform with the smoothing parameter λ
$(\cdot,\cdot)$	Pair of elements
$[\cdot]_{ij}$	ij-th element of a matrix
$[\cdot]_{ij}^{\eta}$	ij-th block-matrix of $\eta \times \eta$ elements
$[\cdot]_{:i}$	i-th column of a matrix
$[\cdot]_{i:}$	i-th row of a matrix
$[\cdot,\cdot]$	column-wise concatenation
$[\cdot;\cdot]$	row-wise concatenation
i,j,k,t,q,s,n	Index counter
A_i	Label of the i-th anchor node
A_{gi}	Multiplicative coefficient of the Gaussian function g_{mi}
$\mathbf{a}_i$	Coordinate vector of the i-th anchor node
$\mathbf{A}_{\mathrm{dc}}$	Auxiliary matrix in the distance-contraction algorithm
$\mathbf{A}_{\mathrm{SR}}$	Auxiliary matrix in the SR-LS algorithm
b_i	Ranging bias associated to the distance d_i
$\hat{b}_i$	Estimate of the ranging bias b_i
b_i^u	Upper bound of the ranging bias b_i

b_{ij}	Ranging bias associated to the distance d_{ij}
b_{MAX}	Maximum ranging bias
B	Hypersphere set
B'	Extended hypersphere set of B
B_i	Hypersphere set associated to the i-th anchor
B_P	Compact set
B_D	Target feasibility region
$\mathbf{b}_{\mathrm{dc}}$	Auxiliary vector in the distance-contraction algorithm
$\mathbf{b}_{\mathrm{SR}}$	Auxiliary vector in the SR-LS algorithm
$\mathbf{b}_{\mathbf{x}}$	Bias vector on the estimate of a general parameter $\mathbf{x}$
c	Speed of light in the vacuum
c_{ij}	ij-th element of $\mathbf{C}$
C_{ijq}	Number of triplets with the elements of the i, j and q sets
$\vec{\mathbf{c}}$	Vectorised form of $\mathbf{C}$
$\mathbf{C}$	Connectivity matrix
d_i	Euclidean distance between the i-th anchor and the target
d_i^{R}	Euclidean distance between the i-th anchor and the point $\mathbf{p}_{\mathrm{R}}$
d_{ik}^{r}	Euclidean distance between the i-th anchor and the test point $\mathbf{r}_k$
d_{ij}	Euclidean distance between the i-th and the j-th nodes
$\tilde{d}_{ij}$	Measurement of the distance d_{ij}
$\tilde{d}_{ij}^{(k)}$	k-th element of a measurement set of the distance d_{ij}
$\hat{d}_i$	Estimate of d_i
$\hat{d}_i^B$	Distance between the i-th anchor node and the point $\hat{\mathbf{z}}_B$
$\hat{d}_{ij}$	Estimate of d_{ij}
$\bar{d}_{ij}$	Sample-mean of the set $\{\tilde{d}_{ij}^{(k)}\}$
$\vec{\mathbf{d}}$	Vectorised form of $\mathbf{D}$
$\vec{\tilde{\mathbf{d}}}$	Vectorised form of $\tilde{\mathbf{D}}$
$\vec{\hat{\mathbf{d}}}$	Vectorised form of $\hat{\mathbf{D}}$
$\mathbf{D}$	Euclidean distance matrix in the natural coordinates of $\mathbf{P}$
$\mathbf{D}^{(i)}$	Euclidean distance matrix in the natural coordinates of $\mathbf{P}^{(i)}$
$\mathbf{D}'$	Euclidean distance matrix in the natural coordinates of $\mathbf{P}'$
$\mathbf{D}^{\circ 2}$	Euclidean distance matrix in the squared coordinates of of $\mathbf{P}$
$\tilde{\mathbf{D}}$	Sample of the Euclidean distance matrix $\mathbf{D}$
$\hat{\mathbf{D}}$	Estimate of the Euclidean distance matrix $\mathbf{D}$

$\mathbf{D}_{\mathrm{SR}}$	Auxiliary matrix in the SR-LS algorithm
e_{ij}^{G}	ij-th edge in the network graph G
$\mathbf{e}_{ij}$	Row-vector with $[\mathbf{e}_{ij}]_i = 1$, $[\mathbf{e}_{ij}]_j = -1$ and all other elements equal to 0
E	Set of edges of the network graph G
$E^{(i)}$	Set of edges of the network graph $G^{(i)}$
E_F	Set all possible edges of the network G
$\mathbb{EDM}^N$	Cone of the $N \times N$ Euclidean distance matrices in the natural coordinates
$\mathbb{EDM}_2^N$	Cone of the $N \times N$ Euclidean distance matrices in the squared coordinates
$\mathbf{E}_k$	Equivocation matrix associated with the k-th node
$\mathbf{E}_k^{(i)}$	Equivocation matrix associated with the k-th node in the i-th network
$\bar{\mathbf{E}}_k$	Block-off diagonal part of the Equivocation matrix
$\breve{\mathbf{E}}_d$	Block-diagonal part of the Equivocation matrix
$\hat{\boldsymbol{\mathcal{F}}}$	Matrix form of the weighted distance squared errors
$\hat{\boldsymbol{\mathcal{F}}}$	Matrix form of the weighted distance squared errors
$\dot{\hat{\boldsymbol{\mathcal{F}}}}_i^n$	Partial derivative of $\hat{\boldsymbol{\mathcal{F}}}$ with respect to $\hat{p}_i^n$
$\ddot{\hat{\boldsymbol{\mathcal{F}}}}_{ij}^{mn}$	Second partial derivative of $\hat{\boldsymbol{\mathcal{F}}}$ with respect to $\hat{p}_i^n$ and $\hat{p}_j^m$
$\mathbf{f}_{\mathrm{SR}}$	Auxiliary vector in the SR-LS algorithm
$\mathbf{F}^{\nu}$	Information matrix relative to the information vector ν
$\mathbf{F}_{\mathrm{LOS}}^{hcr}$	Hammersley-Chapmann-Robbins Information matrix with the LOS assumptions
$\mathbf{F}_{\mathrm{LOS}}^{a}$	Hybrid Abel Information matrix with the LOS assumptions
$\mathbf{F}_d$	Fisher Information matrix (general ranging model)
$\bar{\mathbf{F}}_d$	Block-off-diagonal matrix of $\mathbf{F}_d$
$\breve{\mathbf{F}}_d$	Block-diagonal matrix of $\mathbf{F}_d$
$\breve{\mathbf{F}}_d^k$	k-th diagonal block of $\breve{\mathbf{F}}_d$
$\mathbf{F}_d^{(i)}$	Fisher Information matrix associated to $\mathbf{P}^{(i)}$
$\breve{\mathbf{F}}_d^{k,A}$	Part of $\breve{\mathbf{F}}_d^k$ associated to the anchor-to-target links
$\breve{\mathbf{F}}_d^{k,T}$	Part of $\breve{\mathbf{F}}_d^k$ associated to the target-to-target links
$\bar{\mathbf{F}}_d^{ij}$	ij-th off-diagonal block of $\bar{\mathbf{F}}_d$
$\mathbf{F}_{\mathrm{LOS}}$	Fisher Information matrix with the LOS assumptions

$\bar{\mathbf{F}}_{\mathrm{LOS}}$	Block-off-diagonal matrix of $\mathbf{F}_{\mathrm{LOS}}$
$\breve{\mathbf{F}}_{\mathrm{LOS}}$	Block-diagonal matrix of $\mathbf{F}_{\mathrm{LOS}}$
$\breve{\mathbf{F}}^{k}_{\mathrm{LOS}}$	k-th block-diagonal part of $\mathbf{F}_{\mathrm{LOS}}$
$\bar{\mathbf{F}}^{ij}_{\mathrm{LOS}}$	ij-th off-diagonal block of $\mathbf{F}_{\mathrm{LOS}}$
$\mathbf{F}_{\mathrm{NLOS}}$	Fisher Information matrix with the NLOS assumptions
$\bar{\mathbf{F}}_{\mathrm{NLOS}}$	Block-off diagonal part of $\mathbf{F}_{\mathrm{NLOS}}$
$\breve{\mathbf{F}}_{\mathrm{NLOS}}$	Block-diagonal part of $\mathbf{F}_{\mathrm{NLOS}}$
$\breve{\mathbf{F}}^{k}_{\mathrm{NLOS}}$	k-th block-diagonal part of $\mathbf{F}_{\mathrm{NLOS}}$
$\bar{\mathbf{F}}^{ij}_{\mathrm{NLOS}}$	ij-th off-diagonal block of $\mathbf{F}_{\mathrm{NLOS}}$
G	Network graph
$\hat{\mathbf{g}}^{\mathrm{R}}_{k}$	k-th row-vector of the matrix $\mathbf{G}_{\mathrm{R}}$
$\mathbf{G}_{P}$	Gram-kernel
$\mathbf{G}_{\theta}$	Auxiliary matrix in the angle-based Maximum-likelihood estimator
$\mathbf{G}_{k}$	Upper-left partition of $\mathbf{F}_{d}$ with $k\eta \times k\eta$ elements
$\mathbf{G}^{(i)}_{k}$	Upper-left partition of of $\mathbf{F}^{(i)}_{d}$ with $k\eta \times k\eta$
$\mathbf{G}^{a}_{N_R}$	Upper-left partition of $\mathbf{F}^{a}_{\mathrm{LOS}}$ with $\eta \times N_R\eta$ elements
h_l	Location hypothesis
H_0	Null hypothesis
H_1	Alternative hypothesis
$\hat{\boldsymbol{H}}$	Hessian matrix evaluated at the point $\hat{\vec{\mathbf{p}}}$
$\bar{\boldsymbol{H}}$	Block-off diagonal part of the Hessian matrix
$\breve{\boldsymbol{H}}$	Block-diagonal part of the Hessian matrix
$\breve{\boldsymbol{H}}^{k}$	k-th block-diagonal part of the Hessian matrix
$\breve{\boldsymbol{H}}^{ij}$	ij-th off-diagonal block of the Hessian matrix
ij	ij-th link
I_g	Number of components in the Gaussian mixture g_m
$\mathcal{I}_i$	i-th integral used in the derivation of $\langle f_{\mathrm{R}} \rangle_{\lambda}$
$\mathbf{I}_a$	Identity matrix of a dimensions
$\mathbf{J}$	Double centering projection matrix
$\mathbf{J}_d$	Inverse of $\mathbf{F}_d$
$\mathbf{J}^{c}_{\mathrm{LOS}}$	Inverse of $\mathbf{F}_{\mathrm{LOS}}$
$\mathbf{J}^{hcr}_{\mathrm{LOS}}$	Inverse of $\mathbf{F}^{hcr}_{\mathrm{LOS}}$
$\mathbf{J}^{c}_{\mathrm{NLOS}}$	Inverse of $\mathbf{F}_{\mathrm{NLOS}}$
$\mathbf{J}^{\mathrm{R}}_{di}$	Jacobian of the function $\|\mathbf{p}_{\mathrm{R}} - \mathbf{a}_i\|_{\mathrm{F}}$ with respect to $\mathbf{p}_{\mathrm{R}}$

$\mathbf{K}$	Double centering Euclidean kernel
$\tilde{\mathbf{K}}$	Sample of the double centering Euclidean kernel
$\hat{\mathbf{K}}$	Estimate of the double centering Euclidean kernel
$\mathbf{K}_{\mathrm{P}}$	Equivalent double centering Euclidean kernel
K_{ij}	Number of measurements of the distance d_{ij}
K_{MAX}	Maximum number of distance measurements
K_{MIN}	Minimum number of distance measurements
$\mathcal{L}_{\lambda}^{K}$	Set of K smoothing parameters λ
m	Meshness ratio
M_H	Total number of location hypothesis
M_T	Total number of tests
M_A	Total number of algorithms
n_{ij}	Ranging noise
N	Total number of nodes
N_{A}	Total number of anchor nodes
N_R	Total number of test points
N_{T}	Total number of target nodes
N_v	Number of the vertices of B_D
N_V	Total number of the optimisation variables
$\vec{\mathbf{o}}$	Centre of the hypersphere
$\vec{\mathbf{o}}^{B_D}$	Centre of B_D
$\hat{\vec{\mathbf{o}}}^{B_D}$	Estimate of $\vec{\mathbf{o}}^{B_D}$
$\mathbf{o}_i$	i-th block matrix of $\vec{\mathbf{o}}$
$\hat{p}_i^n$	n-th component of the vector $\hat{\mathbf{p}}_i$
p_{NLOS}	Probability of NLOS
P_i	Label of the i-th node
P^G	Realisation of the network graph G
$\mathcal{P}_{ij}$	Penalty weight
P_{FA}	Probability of NLOS false-alarm
P_{MD}	Probability of LOS miss-detection
$\overline{\mathrm{PEB}}_{\mathrm{LOS}}$	Position error bound derived from the LOS assumptions
$\overline{\mathrm{PEB}}_{\mathrm{NLOS}}$	Position error bound derived from the NLOS assumptions
$\mathbf{p}_i$	Coordinate vector of the i-th node (i-th row-vector of $\mathbf{P}$)
$\mathbf{p}_i^{B_D}$	Coordinate vector of the i-th intersection point forming B_D
$\hat{\mathbf{p}}_i$	Estimate of the i-th node location

$\vec{\mathbf{p}}$	Vectorised form of $\mathbf{P}$
$\vec{\mathbf{p}}^{(i)}$	Vectorised form of $\mathbf{P}_i$
$\hat{\vec{\mathbf{p}}}$	Vectorised form of $\hat{\mathbf{P}}$
$\mathbf{P}$	Coordinate matrix
$\mathbf{P}_i$	Coordinate matrix of the i-th network realisation
$\mathbf{P}'$	Perturbed coordinate matrix
$\hat{\mathbf{P}}$	Estimate of the coordinate matrix $\mathbf{P}$
$\hat{\mathbf{P}}_{\mathrm{ML}}$	Maximum-likelihood estimate of $\mathbf{P}$
$\hat{\mathbf{p}}_{\mathrm{ML}}(\tilde{\boldsymbol{\theta}})$	Angle-based maximum-likelihood estimate of a node location
$\mathbf{p}_{\mathrm{R}}$	Reference point
$\hat{\vec{\mathbf{p}}}_{\mathrm{ML}}$	Vectorised form of $\hat{\mathbf{P}}_{\mathrm{ML}}$
$\vec{\mathbf{p}}_s$	Supporting point used in the SMACOF algorithm
$\mathbf{Q}_k$	Right-upper partition of $\mathbf{F}_d$ with $k\eta \times \eta$ elements
$\mathbf{Q}_{k,n}$	Upper partition of $\mathbf{Q}_k$ with $n\eta \times \eta$ elements
R_{MAX}	Maximum connectivity range
$\mathbf{r}_i$	i-th test point for the derivation of the hybrid-bound
$\mathbb{R}^a$	Real space of a dimensions
$\hat{\mathbf{R}}_{ik}^h$	Auxiliary matrix in the expression of $\breve{\mathbf{H}}_k$
$\mathbb{S}^N$	Space of the $N \times$ N symmetric matrices
$\mathbb{S}_+^N$	Space of the $N \times$ N positive semi-definite symmetric matrices
$\mathbb{S}_h^N$	Space of the $N \times$ N hollow symmetric matrices
$\mathbf{S}_k$	Equivalent FIM associated with the k-th node
$\mathbf{S}_k^{(i)}$	Equivalent FIM associated with the k-th node in the i-th network
$\bar{\mathbf{S}}_n$	Shur-complement of the matrix $\mathbf{G}_n$
t_{ij}	t-score associated to the statistics $\bar{d}_{ij}$
T_{MAX}	Maximum number of iterations of an iterative optimisation algorithm
$\mathbf{T}$	Matrix of the differences between the test points $\mathbf{r}_i$ and $\hat{\mathbf{x}}$
u^x	First component of the variable $\mathbf{u}$
u^y	Second component of the variable $\mathbf{u}$
u^2	Squared norm of $\mathbf{u}$
$\mathbf{u}$	Integration variable
$\mathbf{U}_{\mathrm{R}}$	Auxiliary matrix in the derivation of the Abel hybrid bound
$\mathbf{U}_\eta$	Matrix with the η-th highest left singular-vectors of $\hat{\mathbf{K}}$
v_i^G	i-th vertex of the network graph G

V	Set of vertexes of the network graph G
$\hat{\mathbf{v}}_{kj}$	Normalised direction vector
$\mathbf{V}_\eta$	Matrix with the η-th highest right singular-vectors of $\hat{\mathbf{K}}$
w_i	Weight to the distance d_i
w_{ij}	Weight to the distance d_{ij}
w_{ij}^D	Dispersion weight to the distance d_{ij}
w_{ij}^G	Edge-weight of the ij-th edge in the network graph G
W	Set of edge-weights of the network graph G
$\mathscr{W}$	Field of the dispersion weighing function
$\mathbf{W}$	Weight matrix
$\varkappa_{ijq}$	Critical value of the geometric test
$\mathbf{x}$	Parameter to be estimated (general)
$\hat{\mathbf{x}}$	Estimate of $\mathbf{x}$
$\mathbf{X}_{h_l}$	fingerprint parameters
y_{ij}	ij-th element of the matrix $\mathbf{Y}$
$\tilde{\mathbf{y}}$	observation vector (general)
$\mathbf{y}_f$	fingerprint observation
$\mathbf{y}_{\mathrm{SR}}$	Variable of the SR-LS algorithm
$\mathbf{Y}$	Hollow symmetric matrix
Z_i	Label of i-th target node
$\vec{\boldsymbol{z}}$	Integration variable
$\vec{\mathbf{z}}$	Vectorised form of $\mathbf{Z}$
$\bar{\mathbf{z}}$	Local minimum of the function $f_{\mathrm{R}}(\hat{\mathbf{z}})$
$\vec{\hat{\mathbf{z}}}$	Vectorised form of $\hat{\mathbf{Z}}$
$\hat{\mathbf{z}}^*$	Global minimum of the function $f_{\mathrm{R}}(\hat{\mathbf{z}})$
$\mathbf{z}_{\text{A-R}}$	Minimum of the location ambiguity function
$\hat{\mathbf{z}}_B$	Coordinate vector of a node at the boundary of the set B
$\hat{\mathbf{z}}_\ell$	Solution of the ℓ-th algorithm
$\mathbf{z}_i$	Coordinate vector of the i-th target node
$\hat{\mathbf{z}}_i$	Estimate of vector of $\mathbf{z}_i$
$\hat{\mathbf{Z}}$	Estimate of the target coordinate matrix
$\mathbf{Z}$	Target coordinate matrix
$\aleph$	Auxiliary matrix used for the derivation of $\lambda^{(1)}$
α_{nk}	Coefficient of $\boldsymbol{\Upsilon}_{nk}$
α_{ink}	Coefficient of $\boldsymbol{\Upsilon}_{ik}$

$\hat{\alpha}_z$	Component of $\hat{\boldsymbol{\omega}}_z$
β_{nk}	Coefficient of the sum $(\boldsymbol{\Upsilon}_{nk}^{ki} + \boldsymbol{\Upsilon}_{ik}^{kn})$
β_{ijnk}	Coefficient of $\boldsymbol{\Upsilon}_{ik}^{kj}$
γ	Confidence bound
γ_{opt}	Optimum confidence bound
$\hat{\gamma}_{\text{opt}}$	Estimate of the optimum confidence bound
$\boldsymbol{\gamma}_\nu$	Translation matrix
δ_{ij}	Distance error between $\bar{d}_{ij}$ and d_{ij}
δ_{TX-RX}	Measurement of the round-trip time of packet transmission
$\hat{\Delta}_{ij}^x$	Difference of the coordinates $\hat{p}_i^x$ and $\hat{p}_j^x$
$\hat{\Delta}_{ij}^y$	Difference of the coordinates $\hat{p}_i^y$ and $\hat{p}_j^y$
Δ_B	Increase of the hypersphere radius ϱ_B
Δd_{ij}	Range-difference
Δt_{ij}	Time-difference-of-arrival
$\boldsymbol{\Delta}_{\text{P}}$	Perturbation of the coordinate matrix $\mathbf{P}$
ϵ	Tolerance on the sample mean $\bar{d}_{ij}$
ϵ_{te}	Delay of the radio-frequency circuits
ϵ_{ts}	Delay of synchronisation algorithm
ϵ_{tl}	Delay of the leading edge algorithm
ϵ_L	Threshold on the generalised likelihood function
$\varepsilon_{q,\ell}$	Location error of the ℓ-th algorithm for the q-th network
$\bar{\varepsilon}_\ell$	Location accuracy of the ℓ-th algorithm
ζ_{ij}	Ranging information intensity
ζ_{ij}^{e}	Equivalent ranging information intensity
η	Euclidean dimension
θ_{ij}^*	Characteristic angle
$\tilde{\boldsymbol{\theta}}$	Bearing measurement vector
$\boldsymbol{\theta}_{\text{R}}$	Bearing vector of the reference point
$\hat{\theta}_{kj}$	Angle between the vectors centred at $\hat{\mathbf{p}}_k$ pointing towards $\hat{\mathbf{p}}_j$ and $\hat{\mathbf{p}}_k + [1, \mathbf{0}]$
$\hat{\theta}_{iZ\hat{z}_B}$	Differential angle between the vectors $\mathbf{a}_i$ and $\hat{\mathbf{z}}_B$ centred at the target Z
κ_{ik}^{kj}	Information coupling coefficient
λ	Smoothing parameter
λ^*	Infimum of the set $\mathscr{L}$

λ_{S}^{*}	Initial smoothing parameter for source-localisation
λ_{N}^{*}	Initial smoothing parameter for network-localisation
$\lambda^{(i)}$	i-th smoothing parameter of the set $\mathcal{L}_{\lambda}^{K}$
$\boldsymbol{\Lambda}_{\mathrm{SR}}$	Diagonal matrix with all anchor-to-target weights
μ_{ij}	Bias of the ranging distribution
μ_{gi}	Mean of the Gaussian function g_{mi}
$\tilde{mu}_{ijq}$	Random variable obtained as $(\tilde{d}_{ij} - \tilde{d}_{iq} - \tilde{d}_{jq})$
$\bar{\mu}_{ijq}$	Sample mean of the random variable $\tilde{mu}_{ijq}$
ν_{ij}	Random variable obtained from the generic unbiased ranging distribution
$\boldsymbol{\nu}$	Information vector
$\boldsymbol{\nu}_{c}$	Information vector associate to the CRLB
$\boldsymbol{\nu}_{b}^{(q)}$	Information vector associate to the BB of the q-th order
$\boldsymbol{\nu}_{hcr}$	Information vector associate to HCRB
$\boldsymbol{\nu}_{a}^{(q)}$	Information vector associate to tha AHB of the q-th order
ξ_{ij}	Cross-scaling of the ranging information intensity
ξ_{H}	LOS/NLOS decision threshold
$\boldsymbol{\Xi}$	Matrix with the i-th row-vector equals to $[\cos\theta_{iN}, \sin\theta_{iN}]$
ξ_{p}	Quality-of-Location
π_{h_l}	Probability density function of the location hypothesis
π_{o}	Outage of the location accuracy
π_{s}	Strong localisability test
ϖ_{ik}	Asymptotic eigenvalue of the Hessian matrix
ρ_{i}	i-th element of the vector $\boldsymbol{\rho}$
ϱ	Module of a vector in the polar coordinates
ϱ_{b}	Radius of an hypersphere
$\boldsymbol{\rho}$	Perturbation vector
$\hat{\boldsymbol{\rho}}$	Estimate of the perturbation vector
σ	Standard deviation of a Gaussian distribution
σ_{gi}	Standard deviation of the Gaussian function g_{mi}
σ_{ij}	Standard deviation of the ranging noise
$\hat{\sigma}_{ij}$	Estimate of standard deviation of the ranging noise
$\hat{\sigma}_{\mu_{ijq}}$	Estimate of standard deviation of the random variable $\tilde{\mu}_{ijq}$
σ_{MAX}	Maximum standard deviation of the ranging noise
σ_{MIN}	Minimum standard deviation the ranging noise

$\boldsymbol{\Sigma}_\theta$	Covariance matrix of the bearing measurements
$\boldsymbol{\Sigma}_\eta$	Diagonal matrix with the η-th highest singular values of $\hat{\mathbf{K}}$
τ_{ik}	Scaling of the ranging information intensity
$\boldsymbol{\tau}_i$	Difference between the i-th test point and the vector $\hat{\mathbf{x}}$
$\boldsymbol{\Upsilon}_{kj}$	Ranging direction matrix
$\boldsymbol{\Upsilon}_{ik}^{kj}$	Cross-ranging direction matrix
$\hat{\boldsymbol{\Upsilon}}_{kj}$	Ranging direction matrix derived from $\hat{\mathbf{p}}_k$ and $\hat{\mathbf{p}}_j$
$\bar{\boldsymbol{\Upsilon}}$	Weighted sum of $\hat{\boldsymbol{\Upsilon}}_{kj}$
ϕ	Angle a vector in the polar coordinates
φ_i^ρ	Perturbed-to-estimate distance ratio
φ_i	Sample-to-estimate distance ratio
$\boldsymbol{\Phi}_\mathrm{R}$	Auxiliary matrix in the derivation of the AHB
χ_Z	Tolerance on the relative changes of the optimization variable
χ_F	Tolerance on the relative changes of the function value
ω_i^ρ	Weighing coefficient for the definition of a minimum of $f_\mathrm{R}(\hat{\mathbf{z}})$ with perturbed distances
ω_i	Weighing coefficient for the definition of the convex-hull
$\boldsymbol{\omega}_\mathrm{WC}$	Weighing vector in the WC algorithm
$\boldsymbol{\omega}_\mathrm{WC\text{-}DC}$	Weighing vector in the WC-DC algorithm
$\hat{\boldsymbol{\omega}}$	Component of $\hat{\boldsymbol{\omega}}_z$
$\hat{\boldsymbol{\omega}}_z$	Initialisation variable of the distance-contraction algorithm
$\boldsymbol{\Omega}$	Relative angle kernel
$\hat{\boldsymbol{\Omega}}$	Estimate of the relative angle kernel

Contents

1 Introduction

1.1 Positioning in wireless networks: a key technology

The history of wireless positioning dates back to 1994, when the Federal Communications Commission (FCC) issued a Notice of Proposed Rule-making (NPRM) for the development of the first location-based emergency service, the E-911 [1]. Since then, in North America many location platforms were developed for emergency services, whereas in Europe, Japan and South-Korea, the early deployment of location platforms focused on commercial services.

Wireless positioning was initially conceived for cellular networks, and mobile operators were the key partners and the main distribution channels for location-based applications and services. Nowadays, their central role is being challenged by the rising of heterogeneous smart-device (mobile phones, computers, tablets, etc.) ecosystems that in many cases offer self-sustained applications and seemless interfaces to various wireless networks. Location information has become a crucial component for a number of mobile context-aware applications, and companies such as Facebook, Twitter and Google have successfully exploited it for the implementation of effective market penetration strategies.

In 2011, statistics published by the International Telecommunication Union (ITU) [2] showed that there are 6 billion mobile phone subscribers worldwide. The number of mobile-broadband subscriptions have grown 45% annually over the last four years, and today there are twice as many mobile-broadband as fixed-broadband subscriptions. Only in Europe, the penetration of mobile-broadband technology has reached 54%.

Today, the number of mobile applications is countless and covering a vast variety of services. In particular, market analysts forecast that the revenue from the Location Based Services (LBS) market in Europe will grow from 205 million Euro in 2010 to about 435 million Euro in 2016 [3]. In addition to this, we also foresee that the profit from positioning applications will sky rocket with the coming internet-of-things, machine-to-machine and sensor networks technologies. The integration of these new ecosystems, commonly referred to near-field communications, in the world of mobile communications is foreseen within

the year 2020. By then, over 2.1 billion devices will be interconnected forming the largest wireless network worldwide [4]. It is considered that positioning will be one of the fundamental features of this network so as to optimize the networking and enable smart, personalized and pervasive services.

From all of the above, it is no wonder that wireless positioning has become a key technology surging the interest of both industry and academia.

1.2 Open challenges

The central problem of positioning is the estimation of physical location. This information can be provided as geographical coordinates or a semantic position such as "I am in the room", "I am at home", etc. To obtain this information from a wireless network, it is necessary that devices can communicate, that position-related information such as distances or angles can be extracted from a receiving waveform, and that an algorithm (the positioning engine) processes the measurements to get the sought information. Considering that the network operates on a wireless channel with multi-paths and fading, several challenges are met in the design of a positioning system.

Firstly, at the radio-hardware, low power-consumption and robust radios are necessary to enable communications in harsh environments and over a sufficiently large coverage area. Secondly, at the physical layer, low-complexity and fast signal processing is required to extract the position-related information from the waveform, *e.g.* ranging [5] or angle-estimation [6] algorithms. Thirdly, at the link-layer, new positioning-enabling primitives as well as scheduling protocols are needed to perform contention-free measurements, *e.g.* ranging functionality in the IEEE.802.15.4a [5]. Finally, at the middle-ware, a lightweight and robust localisation algorithm is necessary to estimate node locations.

The research presented in this thesis focuses on the development of low-complexity and robust positioning techniques. We address the problem from both theoretical and algorithmic perspectives, and deal with non-cooperative and cooperative scenarios. We restrict the assumptions to the case where no *a priori* information is available about the measurement statistics. The positioning problem is therefore formulated with a non-Bayesian non-parametric framework, namely a Weighted Least Square (WLS) optimization problem.

This approach has been widely considered by many researchers in industry and academia, and in the pursuit of an optimal and computational efficient minimization algorithm, several techniques have been proposed in the literature. The main problem is the non-convexity of the objective function, which becomes more and more irregular with the increase of measurement errors. To exemplify, in Figure 1 we illustrate the WLS objective function when distances are free of – Figure 1(a) – and affected by – Figure 1(b) – errors. It can be noticed that with imperfect measurements, the global minimum is placed away from the sought location (indicated with the marker "$\circ$"), and a local minimum appears. The design of mitigation techniques that circumvent the local minima problem and minimize the localization error is still an open challenge. The same problem extended to multi-target positioning becomes even more difficult since a large number of variables are involved, many more minima can occur and the complexity of the algorithm can rapidly increase.

From a theoretical perspective, a deep understanding of the fundamental limits of this type of estimation problem is crucial. Considering the positioning problem as a mere estimation problem is restrictive. Localization is also an Euclidean embedding problem, which is governed by other fundamental limits. How to bundle these two aspects is yet a subject of investigation.

1.3 Outline and author's contributions

In this thesis we tackle the problem of positioning in a wireless network. We consider a distance-based approach and, specifically, a multilateration scheme. Restricting the assumptions to unknown measurement statistics, a non-Bayesian non-parametric framework is employed, namely a WLS optimisation. The reminder of the thesis is organised as follows.

In Chapter 2 we provide a comprehensive overview of the state-of-the-art algorithms for non-cooperative and cooperative positioning. Specifically, we survey the most common and effective optimisation techniques as well as mitigation methods to bias errors. Based on simulations, a comparison of the performance of a selected set of techniques is also provided.

In Chapter 3, we describe the WLS formulation of a distance-based localisation problem. In addition, we also summarize the alternative matrix-proximity approach and discuss three different variations.

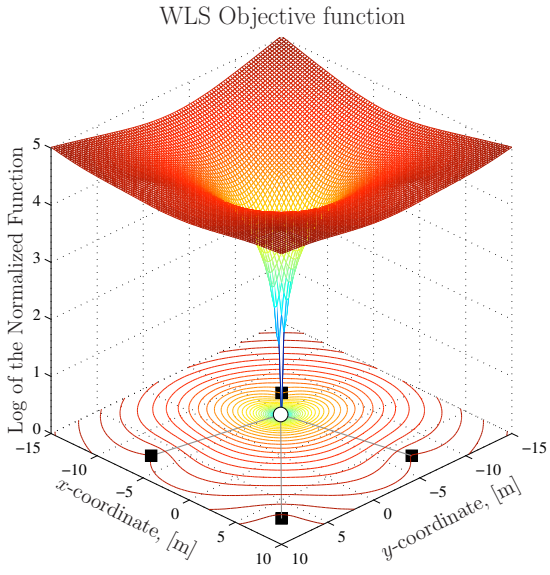

(a) Exact distances

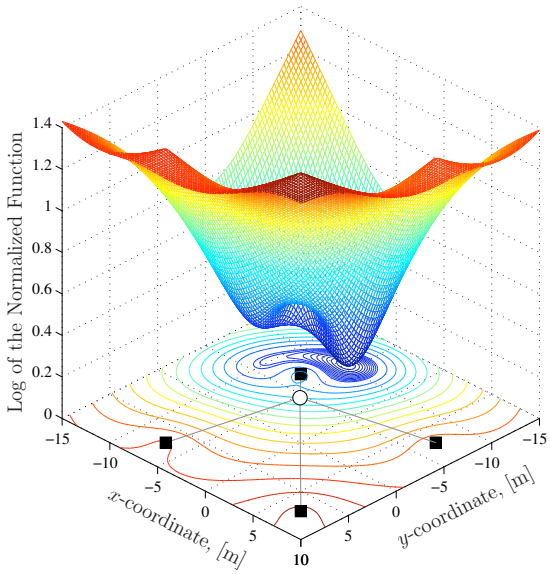

(b) Imperfect distances

Fig 1. Contour plots and surface of the normalised (shifted down by the minimum value) WLS objective function. The black squares and the white circle indicate the locations of the anchors and target, respectively.

In Chapter 4, we derive the fundamental limits of distance-based positioning, and create a bundle between the positioning estimation problem and the Euclidean embedding problem. Specifically, we prove that a distance-based positioning problem is fundamentally solvable if the network is strongly localisable in a pre-defined Euclidean embedding space. We derive the closed-form expressions for a distance-model based Cramér-Rao Lower Bound (CRLB) and provide the formulas for the evaluation of the information-couplings established with inter-node cooperation. Additionally, we discuss the limitations of the CRLB in the low-Signal-to-Noise Ratio (SNR) régime and, based on the Abel's framework [7], propose a hybrid bound that accounts for large estimation errors.

The remaining part of the thesis is devoted to algorithms and their test. Specifically, in Chapter 5 we propose two robust non-cooperative positioning algorithms, both based on the principle of Distance Contraction (DC), which is one of our contributions whose main idea is explained in Section 5.1. Essentially, we prove that if the target node lies within the convex-hull formed by the anchors, the target-to-anchor distances are subject to a negative errors and such errors lie in the null subspace of the relative angle matrix $\mathbf{\Omega}$, then: 1) the associated WLS objective is a convex function, and 2) its global minimum coincides with the true target location. The proposed DC-based techniques, namely the WC-DC and the NLS-DC algorithms, will exploit this principle to improve the location accuracy in Non-Line-of-Sight (NLOS) scenarios.

In Chapter 6, we address the problem of cooperative positioning. In this regard, we propose a robust global optimisation algorithm to minimize the WLS objective function and a weighing strategy to mitigate the effects of ranging errors. The proposed optimisation method, hereafter referred to as the *Range-Global Distance Continuation* (R-GDC) algorithm, solves the WLS problem via iterative minimisations of smoothed variations of the objective, each obtained by convolution with a Gaussian kernel of progressively smaller variances. Regarding the weighing strategy, we propose a non-parametric mechanism to compute a weight formed by a *dispersion* and a *penalty* term. The dispersion component captures the effect of noise under the assumption of bias-free samples, whereas the penalty term quantifies the risk of the latter assumption and penalises it proportionally.

In Chapter 7 we show the results of an experiment where the aforementioned algorithms locate the nodes of a real wireless network. The experiment was performed at the Centre for Wireless Communications of the University of Oulu using commercial Ultra-WideBand (UWB) devices (Time Domain PulseON 210). Finally, in Chapter 8 we provide final conclusions and discuss future works.

1.4 Author's contributions to the publications

The thesis is based on research that has been published in two IEEE journals [8, 9] and six IEEE international conference papers [10–15] In addition, the thesis includes novel results that will be submitted to IEEE journals.

In [10], we addressed for the first time the localisation problem as a WLS optimisation problem. We derived the gradient and the Hessian for the WLS function with squared ranges and compare the results to a Semi Definite Programming (SDP)-based optimisation. The analytical tools employed in [10] are reused in Chapter 3 to derive the closed form expressions of the gradient and the Hessian for the WLS function without squaring.

In [9, 13], the Range-Global Distance Continuation (R-GDC) optimisation algorithm was proposed as a nearly optimal solution to a WLS-based positioning. The derivation of this minimisation algorithm as well as the comparison to the state-of-the-art optimisation methods, namely the Stress-of-a-MAjorizing-Complex-Objective-Function (SMACOF), the NLS-Levenberg-Marquardt (LM) and SDP, are offered in Section 6.1.

In [8, 11] we dealt with the problem of a non-parametric weighing strategy design for WLS-based positioning. Specifically, in [11] we derived the dispersion weight and the entropy-based confidence-bound optimisation, whereas in [8] we proposed the penalty weight as a correction to the dispersion weight in the case of biased measurements. In Section 6.2, the derivation of such dispersion-penalty weighing strategy is provided and, the effectiveness of this technique, jointly with the aforementioned R-GDC algorithm, is shown via simulations.

In [14] we originally proposed the DC principle presented in Chapter 5. This paper was appointed to the Finalists for the Best Student Paper Contest in the IEEE 43th Asilomar Conference on Signals, Systems and Computers. In [15], the DC principle was used to derive an initial version of a DC-based

algorithm which has been replaced by the WC-DC and the NLS-DC algorithms proposed in Section 5.2. The performance of these new non-cooperative schemes are compared to the state-of-the-art and, their advantages are shown in both Line-of-Sight (LOS) and mixed LOS/NLOS scenarios. Chapter 5 contains novel results to use in a new IEEE journal publication.

In [12], we utilized state-of-the-art optimisation methods and the dispersion-penalty weighing strategy to evaluate the performance of cooperative positioning with UWB devices. In Chapter 7, the measurements are reused to evaluate the performance of the R-GDC cooperative localisation technique as well as the DC-based non-cooperative methods.

Finally, Chapter 4 includes novel contributions on the analysis of the Fisher Information Matrix (FIM) for distance-based positioning. These results will be used for a new IEEE journal publication.

2 Literature review

In this chapter, a review on the literature related to the scope of the thesis is provided. We categorise positioning systems based on the objective (source and network localisation), the application (self and network-centric positioning) and algorithm strategy (cooperative and non-cooperative). We survey on the types of information used for positioning, and classify the localisation techniques into fingerprinting or profile-based, angle-based and distance-based methods. Amongst these, we focus on the latter due to the inherent accuracy as well as theoretical and algorithmic challenges. In this regard, we devote our attention to WLS based algorithms because of the ease of implementation, minimum requirements and flexibility to different technologies. We survey on the most fundamental WLS-based localisation algorithms, and discuss their performance and limitations via numerical results.

2.1 Overview of positioning technologies

In its most comprehensive form, location information is intended as the knowledge on the position of all nodes in the network (*i.e. network localisation*); and in its simpler form, as the knowledge on the position of a specific node (*i.e. source localisation*). This information can be obtained by means of an estimation technique, commonly referred to as *positioning*.

In a localisation system, we distinguish two types of devices, namely, *anchors* and *targets*. The former refers to nodes with a fixed known location, while the latter to nodes whose position is yet to be determined. In practice, an anchor can be a base station in a cellular network or an access point in a local area network, or in some application scenarios, a node located via Global Positioning System (GPS). A target, instead, can be any other device such as laptops, tablets, mobile phones, tags, etc.

The objective of a positioning algorithm is to estimate the unknown target locations. In this regard, if a target node can communicate and acquire information only from the anchors, then the positioning method is considered *non-cooperative*. In turn, if all nodes can communicate and exchange information with each other, then such a system is referred to as *cooperative*.

Algorithmically, non-cooperative and cooperative positioning can be performed in a distributed (*self-positioning*) or centralised (*network-centric positioning*) manner. The advantages of distributed methods are essentially the scalability and low-complexity. Nevertheless, they may not reach optimality in a global sense [16], they are sensitive to the error propagation due to the exchange of imperfect information, and they may require a long convergence time [17]. In contrast, centralised methods are fundamentally optimum, stable, but the computational complexity can grow with the number of nodes. Therefore, the choice between centralised or distributed is often a matter of the application scenario and a trade-off between complexity and performance.

One of the key challenges, that has motivated the research of novel positioning systems, is the accuracy. The inherent uncertainty in localisation arises from the small number of nodes with known locations (anchors), the large number of nodes with unknown locations (targets), their limited connectivity and the harshness of the radio propagation channel where the network is deployed. Positioning is indeed performed on the basis of wireless measurements of distance, angle or power-profile. For instance, the angle between a transmitter and a receiver can be estimated from the Angle-of-Arrival (AoA) of a signal, the distance between two nodes can be obtained from the receiving power (Received Signal Strength (RSS), link-quality) or the time-of-flight estimates, and the power-profile from measurements of Channel Impulse Response (CIR). In severe radio propagation channel conditions [18–20], distance, angle and power-profile measurements are typically affected by errors, that in the case of distance and angle are manifested in the form of noise and bias of unknown statistics, whereas in the case of power-profile as amplitude fluctuations and jitter [21].

To overcome these short-comings, several technological and algorithmic solutions can be considered. For instance, accurate CIR can be obtained through wideband channel sounder, or more pragmatically from the Inverse Fourier Transform (IFT) of a wideband Orthogonal Frequency-Division Multiplexing (OFDM) signal spread over a large number of sub-carriers [22]. Angle estimation can be improved by employing robust estimation algorithms such as MUltiple SIgnal Classification (MUSIC) [6] and multiple antennas with a large number of elements. Accurate distance measurements can be achieved with wideband technologies, *e.g.* UWB [5] and Direct Sequence Spread Spectrum (DSSS) [23].

Based on the type of information, different positioning techniques can be designed upon. To the best of our knowledge, three main categories can be identified: fingerprinting (based on CIR), angle-based (based on AoA) and distance-based methods (based on Received Signal Strength Index (RSSI), Time-of-Arrival (ToA) and Time-Difference-of-Arrival (TDoA)) [21, 24].

In Figure 2 a matrix based chart depicts a technology-wise taxonomy of wireless positioning systems, where different types of methods are cross-correlated with the radio technologies and application scenarios [22, 25–32]. For instance, consider a distance-based wireless positioning system. This solution can be designed with UWB devices and by employing either a cooperative or a non-cooperative trilateration technique. Environmental monitoring, for example, is a typical application scenarios for cooperative positioning since sensors are connected in a mesh network and are capable to communicate data and perform ranging. On the other hand, indoor navigation is classic example of a non-cooperative positioning system since each device is typically connected to fixed base stations, *e.g.* cellular base stations, to which can perform ranging.

2.1.1 Fingerprinting positioning

Fingerprinting can be generally described as a multiple hypothesis testing decision problem, where the objective is to infer the best hypothesis (location of the node) based on an observation of the fingerprint $\mathbf{y}_f$ (CIR). The method relies also on a set of a priori information represented by the hypothesis h_l's, the associated a priori probability density function (pdf) π_{h_l} and the conditioned pdf $f_{\mathrm{Fp}}(\mathbf{y}|\mathbf{X}_{h_l})$ that models an observation of the fingerprint $\mathbf{y}$ and the fingerprint parameters $\mathbf{X}_{h_l}$ associated to the hypothesis h_l. Mathematically, the fingerprinting positioning problem can be formulated as [33]

$$\hat{h}_l = \arg \max_{h_l=1,\cdots,M_H} \pi_{h_l} f_{\mathrm{Fp}}(\mathbf{y}_f|\mathbf{X}_{h_l}), \tag{1}$$

where $\hat{m}_p$ is the estimated hypothesis and M_H the number of hypothesis.

In practice, a fingerprinting positioning method requires two phases: the training and the localization phases. During the training, fingerprints are collected in sample locations and, for each location, the parameter $\mathbf{X}_{h_l}$ is estimated [33].

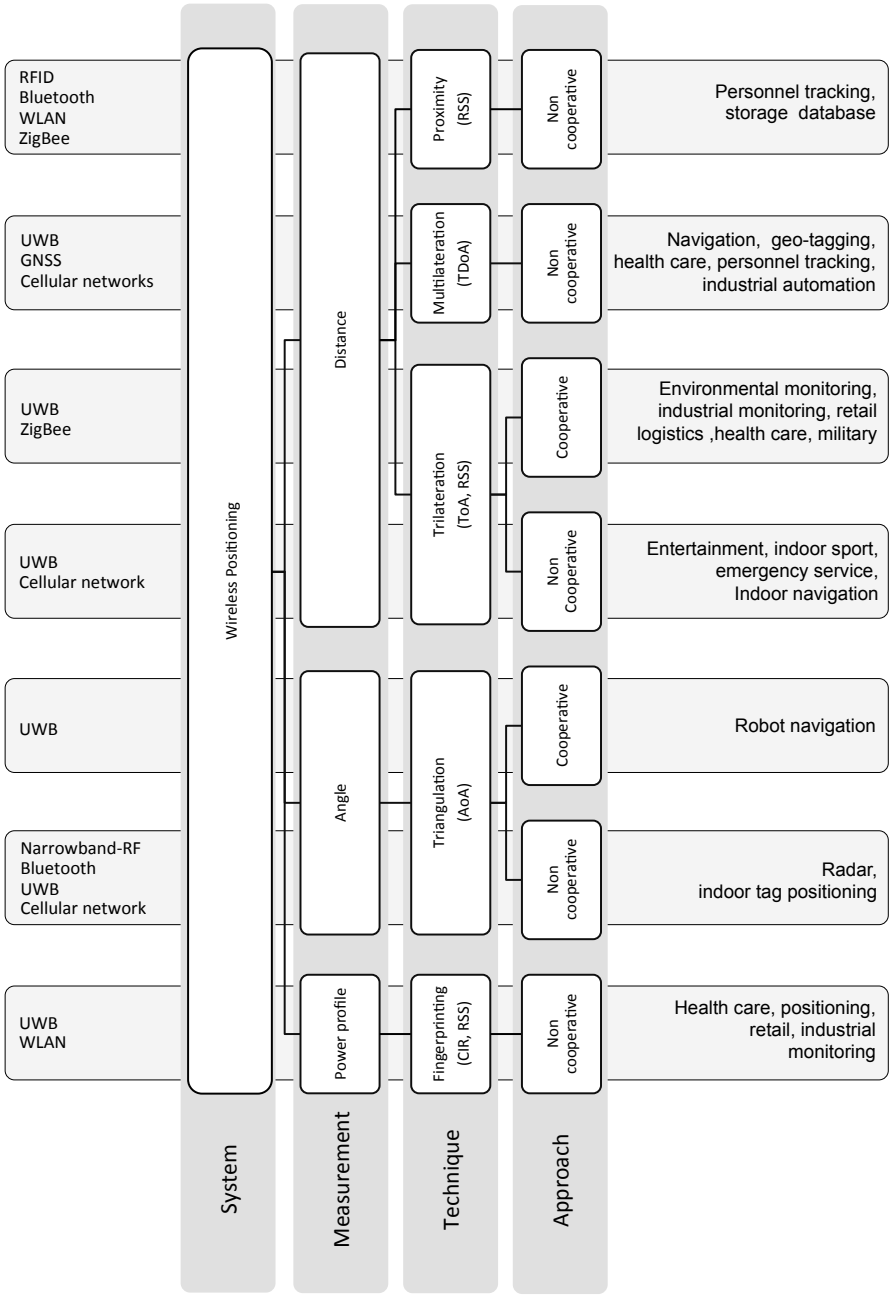

Fig 2. Taxonomy of current wireless positioning systems.

During the second phase, positioning is performed in real-time by searching for the best hypothesis that maximizes the problem defined above.

The main advantage of this technique is the flexibility to any radio interface, indeed, solutions for narrowband and wideband technologies exist [28, 33–37]. The position accuracy, however, depends on the reliability (quantity and up-to-date) of the training data, the error in the synthesis of the fingerprint parameters, and the sensitivity of the algorithm to changes of the environment.

To improve the robustness of the location estimation with respect to the inaccuracy of training data, several techniques are proposed in the literature. For instance, in [28] statistical learning is used to design an algorithm based on support vector machine. In [22] a non-parametric kernel regression method is adopted to estimate the location from an approximation of the CIR. Other methods can be found in [34–37].

2.1.2 Angle-based positioning

Angle-based positioning is another class of localisation methods based on the well-known triangulation principle [38], *i.e.* intersections of bearing lines from two or more receivers. In the literature, this type of positioning technique has been widely investigated and, different formulations have been proposed, such as a Maximum Likelihood (ML) [39, 40], a Least Square (LS) [41] and a probabilistic [42, 43]. For instance, the ML solution to the angle-based positioning of a single target is given by

$$\hat{\mathbf{p}}_{\mathrm{ML}}(\tilde{\boldsymbol{\theta}}) = \mathbf{p}_{\mathrm{R}} + \left(\mathbf{G}_{\theta}^{\mathrm{T}}\boldsymbol{\Sigma}_{\theta}^{-1}\mathbf{G}_{\theta}\right)^{-1}\mathbf{G}_{\theta}\boldsymbol{\Sigma}_{\theta}^{-1}\left(\tilde{\boldsymbol{\theta}} - \boldsymbol{\theta}_{\mathrm{R}})\right), \tag{2}$$

with

$$\mathbf{G}_{\theta} \triangleq \begin{bmatrix} -\sin(\theta_{R1})/d_{R1} & \cos(\theta_{R1})/d_{R1} \\ \vdots & \vdots \\ -\sin(\theta_{RN_{\mathrm{A}}})/d_{RN_{\mathrm{A}}} & \cos(\theta_{RN_{\mathrm{A}}})/d_{RN_{\mathrm{A}}} \end{bmatrix}, \tag{3}$$

and where $\tilde{\boldsymbol{\theta}} \in \mathbb{R}^{N_{\mathrm{A}}}$ is the bearing measurement vector, $^{\mathrm{T}}$ denotes transpose, $\boldsymbol{\Sigma}_{\theta}$ is the covariance matrix of the bearing measurements, $\mathbf{p}_{\mathrm{R}}$ are the coordinates of a reference point (*e.g.* a point in the middle of the polygon bounded by the measured bearing lines), N_{A} is the number of anchor nodes, d_{Ri} is the distance between the i-th anchor and the reference point, $\boldsymbol{\theta}_{\mathrm{R}}$ is the vector of the angles θ_{Ri} given by

$$\theta_{Ri} \triangleq \tan^{-1}\left(\frac{p^1_{\mathrm{R}} - p^1_{\mathrm{A}_i}}{p^2_{\mathrm{R}} - p^2_{\mathrm{A}_i}}\right), \tag{4}$$

and $p^j_{\mathrm{A}_i}$ and p^j_{R} corresponds to the j-th coordinate of the i-th anchor and the reference point, respectively.

The aforementioned techniques, however, refer to a source localisation problem. The generalization to network positioning (multi-triangulation) is indeed more difficult, and as shown in [27, 44], it requires more sophisticated optimisation with a large number of variables. The key idea is to cast the angle-based positioning problem into a distance-based localisation by exploiting the angle properties of a triangle circumscribed by a circle of radius r_o. For instance, from the example illustrated in Figure 3, the distance between the points A_1 and X, denoted by d_{XA_1} can be computed as

$$d_{XA_1} = \sqrt{2r_o^2 - (1 - \cos(2\beta))}, \tag{5}$$

where β is a measurable angle.

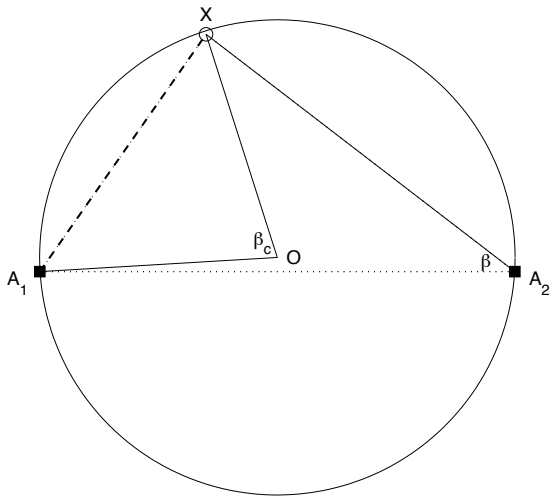

Fig 3. Illustration of the geometric property for the transformation of angle information to distance information.

2.1.3 Distance-based positioning

Distance-based positioning is perhaps the approach that has attracted the most interest because of the potential high accuracy, the applicability to different radio technologies and the ease of implementation. Within this category, we can distinguish between range and range-difference based methods. Specifically, the former refers to distance-based positioning systems where the information is a direct measure of the distance (ranging) between two nodes. The latter, instead, corresponds to systems where the information (range-difference) is a differential measure of the distances d_{ij} and d_{ik} that separates the pair of nodes (i,j) and (i,k), respectively. In practice, range-based positioning can be designed with the requirement that either ToA or RSS can be measured, while a range-difference-based localisation needs TDoA estimates [5]. Consequently, the former method is applicable to both asynchronous and synchronous systems, while the latter requires a precise synchronisation between any pair of receivers during the TDoA estimation procedure. Due to this issue, range-difference-based positioning is rarely used for cooperative schemes since a global network synchronisation is difficult to achieve. On the other hand, range-difference-based positioning is often used for non-cooperative localisation schemes, where anchors are synchronised while the target can also not be.

Given the different type of information (range and range-difference), localisation algorithms also differ conceptually. In fact, the former and the latter rely on the trilateration and multilateration principle, respectively.

In a trilateration method, the ranging d_{ij} defines a circle for the position of the j-th node with respect to i-th node. Thus, from a set of ranging $\{d_{ij}, \cdots, d_{iN}\}$, multiple circles can be drawn and their intersection coincides with the sought location. For instance, in Figure 4(a) we show a trilateration scenario where four ranging (one per anchor) are used to locate the position of the unknown target. In the multilateration technique, instead, each range-difference defines a hyperbola where the focal points (foci) are represented by the location of the receivers, and the curve gives the possible location of the target. The point of intersection of multiple hyperbolas coincides with the target location. In Figure 4(b), for example, we illustrate a scenario where three range-differences (one per each pair of anchors $(\mathrm{A}_1, \mathrm{A}_j)$) are used for positioning.

Mathematically, the trilateration and the multilateration approaches can be

formulated as follows. Let $\mathbf{z}$ and $\mathbf{a}_i$ denote the coordinate vector of the target and the i-th anchor locations, respectively. The trilateration can be synthesised with the non-linear system

$$\begin{cases} \|\mathbf{z}-\mathbf{a}_1\|_{\mathrm{F}} = d_{za_1}, \\ \vdots \\ \|\mathbf{z}-\mathbf{a}_{N_{\mathrm{A}}}\|_{\mathrm{F}} = d_{za_{N_{\mathrm{A}}}}, \end{cases} \tag{6}$$

where N_{A} is the number of anchors, $\|\cdot\|_{\mathrm{F}}$ denotes the Frobenius norm and d_{za_i} is the distance between the target and the i-th anchor.

The multilateration, instead, can be described as

$$\begin{cases} \|\mathbf{z}-\mathbf{a}_1\|_{\mathrm{F}} - \|\mathbf{z}-\mathbf{a}_R\|_{\mathrm{F}} = \Delta d_{za_1}, \\ \vdots \\ \|\mathbf{z}-\mathbf{a}_{N_{\mathrm{A}}-1}\|_{\mathrm{F}} - \|\mathbf{z}-\mathbf{a}_R\|_{\mathrm{F}} = \Delta d_{za_{N_{\mathrm{A}}-1}}, \end{cases} \tag{7}$$

where $\Delta d_{za_i} \triangleq c\Delta t_{za_i}$ is the i-th range-difference, c equals to the speed-of-light and Δt_{za_i} denotes the TDoA measured with respect to a reference anchor A_R and an anchor A_i.

Because of the non-linearity of the norm function, a closed-form solution to either equation (6) or (7) is difficult to derive. Furthermore, in a real application scenarios, range and range-difference measurements are affected by errors thus, only an estimate of the coordinate vector $\mathbf{z}$ can be inferred.

In this regard, the estimation problem can be formulated with non-Bayesian (*e.g.* ML, LS, etc.) and Bayesian, (*e.g.* Maximum A Posteriori (MAP), Minimum Mean Squared Error (MMSE), etc.), frameworks, whether the unknown node location is considered as a parameter of the system or as a realisation of a random variable [45], respectively. To the best of our knowledge, none of the algorithms proposed in the literature can solve optimally the estimation problem in closed-form. Most of the techniques are either iterative or approximate solutions.

For instance, in [46] a factor-graph based algorithm is proposed to solve a Bayesian formulation of a cooperative range-based positioning. In [47], approximate ML (non-Bayesian parametric) solutions are proposed for the cases of source range and range-difference positioning.

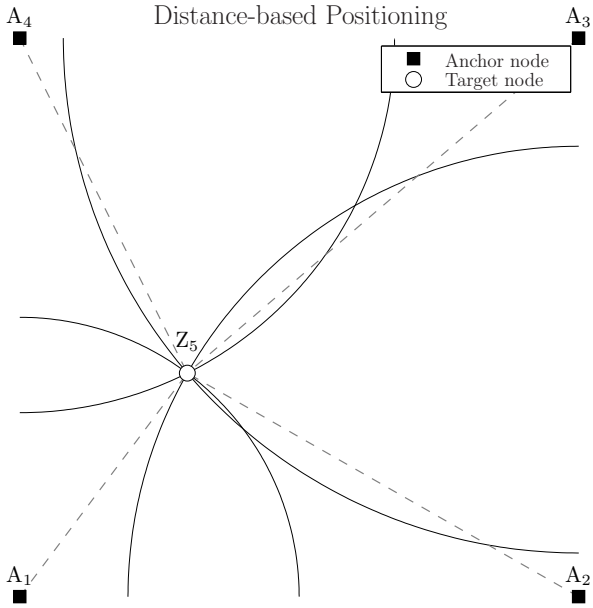

(a) Trilateration

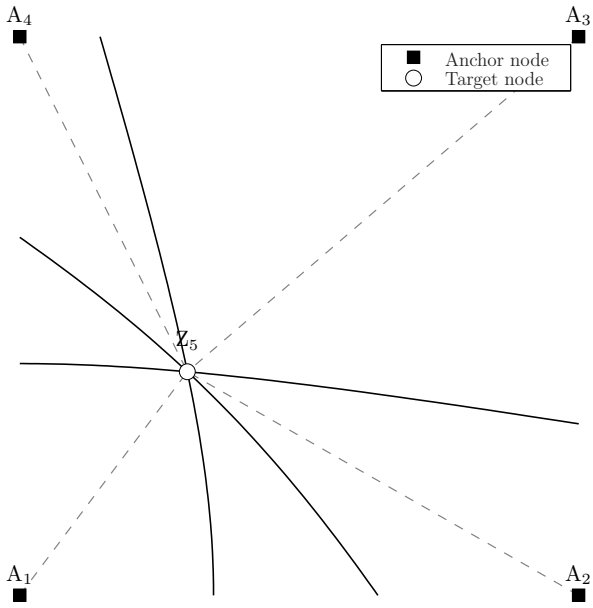

(b) Multilateration

Fig 4. Illustration of the trilateration and multilateration principles.

For the specific case of three co-linear anchors, the exact solutions to ML range and range-difference localisation problems can be found in [47] and [48], respectively. In [49], the authors derived a closed-form solution to a LS (non-Bayesian non-parametric) formulation of a single target positioning problem with squared range and squared range-difference information. In addition to the above, many other techniques can be found in [50–58] and reference thereby.

In this thesis, we aim at the development of non-cooperative and cooperative positioning algorithms with the assumptions that no information on the ranging statistics and the distribution of the node locations are available. To this end, we adopt a non-Bayesian non-parametric approach and we formulate the problem with a non-linear non-convex WLS optimisation [59–61]

$$\min_{\vec{\hat{\mathbf{p}}}\in\mathbb{R}^{\eta N}} \sum_{i=1}^{N}\sum_{j>i}^{N} w_{ij}^2 \left(\tilde{d}_{ij} - \hat{d}_{ij}\right)^2, \tag{8}$$

where $\vec{\hat{\mathbf{p}}} \triangleq [\hat{\mathbf{p}}_1, \cdots, \hat{\mathbf{p}}_N]$ is a row-vector with all the unknown variables $\hat{\mathbf{p}}_i \in \mathbb{R}^\eta$, $\mathbb{R}$ is the real space, N is the number of the nodes in the network, η is the Euclidean dimension of the embedding space, w_{ij}^2 is a weighing factor that is proportional to the reliability of the measurement [62], $\tilde{d}_{ij}$ and $\hat{d}_{ij} \triangleq \|\hat{\mathbf{p}}_i - \hat{\mathbf{p}}_j\|_{\mathrm{F}}$ denote a measurement and an estimate of the distance d_{ij}, respectively.

It is well known that this optimisation problem is difficult and with several pitfalls. Firstly, in spite of the exactness of the ranging, the uniqueness of the solution may not be guaranteed. In fact, in [54, 63] it is shown that the connectivity as well as the node locations determine the unique localisability of the network, *i.e.* the resolvability and uniqueness of the solution to the positioning problem. Secondly, there is the local minima problem due to the non-convexity of the objective function. In [61, 64], it is indeed shown that the number of minima grows with the increase of the measurement errors, the number of nodes and the dimensionality of the problem. Finally, there is the issue of the error on the location estimates due to imperfect measurements.

In light of all the above, the design of an accurate WLS-based positioning algorithm is a two-fold research problem. First, there is the issue of seeking the global minimum of the objective function. Second, the challenge of developing robust error mitigation techniques. In what follows, a survey of the state-of-the-art optimisation and error mitigation methods is provided.

2.2 Optimization techniques for WLS-based positioning

In the literature, several techniques are proposed for the minimisation of the WLS objective function. Generally, an algorithm used for cooperative positioning can be adopted for non-cooperative methods too. The contrary, instead, is not typically possible since, the WLS formulation of non-cooperative positioning posses properties that can not be generalised. For this reason, the following optimisation techniques will be classified as general methods and approximate methods for non-cooperative schemes.

2.2.1 General methods

Gradient-based techniques

As any other cost function, the WLS objective function can be minimised with standard gradient-based algorithms [65]. Amongst all, the least complex technique is the Broyden-Fletcher-Goldfarb-Shanno (BFGS) method, where no matrix inversion is required. In this algorithm, a line-search method is typically employed for the calculation of the descending step. This technique is slow-convergent and sensitive to the local minima problem.

Another algorithm, especially designed for NLS problems is the LM method. This algorithm is typically implemented with a trust region optimization sub-problem that calculates an appropriate descending step-size. Based on our experience, this technique offers a good convergence rate and a reliable performance. However, the computational complexity is higher than that of the BFGS technique since the inversion of a large matrix (a positive semi-definite approximation of the Hessian matrix) is required. The utilization of the LM algorithm for positioning is, for example, proposed in [66].

Majorisation techniques

A low-complexity alternative to the gradient-based methods is the SMACOF algorithm. This technique is well-known in the Multidimensional Scaling (MDS) analysis, where the WLS function is referred to as the *stress* function. The fundamental idea is to minimize the WLS objective with an iterative procedure, where at each step a simple convex function (a quadratic function), which

both bounds the WLS objective from above and touches its surface at a point $\hat{\vec{\mathbf{p}}}_s \in \mathbb{R}^{N\eta}$ (supporting point), is minimised. Based on our experience, the algorithm converges to a solution, a minimum (maybe global) of the WLS objective, after a few iterations, *e.g.* 40.

Likewise the aforementioned gradient-based methods, the effectiveness of the SMACOF technique depends on the reliability of the initialisation point and the number of local minima. The advantage, however, is the low-complexity since the minimisation of the quadratic function can be solved in closed-form through a Guttman transform. The detail of this algorithms can be found in [59].

Semi-definite programming techniques

Considering global optimisation methods, the most powerful, yet more complex algorithms are based on SDP. The basic idea of an SDP approach is to consider the WLS minimisation problem as a matrix proximity optimisation problem, where the properties of Euclidean embedding space can be exploited [67].

Given the relevance of SDP methods, more details on the general technique as well as formulations will be provided in Section 3.3. At this point, we can simply remark that in general, SDP algorithms do not find the minimum of the WLS objective, but they provide a central (average) solution that yields the best compromise with respect to the constraints. To achieve a minimum of the WLS function, a refinement of this solution is necessary and, to this end, any gradient-based technique can be applied after the SDP optimisation [68].

As mentioned above, the complexity of an SDP-based optimisation for positioning is high. It depends on the number of constraints used in the formulation, the noise and the number of unmeasured links. It can be shown that the computational complexity of this method can reach the order $\mathcal{O}(N_{\mathrm{T}}^6)$ [69], (N_{T} is the number of targets) which makes it prohibitive in large-scale centralised network localisation problems.

Smoothing-continuation methods

Another type of global optimisation algorithm can be obtained with the combination of global smoothing and numeric continuation techniques [70]. The basic idea is to use a smoothed variation of the original objective to reduce the

number of minima, and to apply a continuation method to track a candidate minimum. The smoothing method can be designed either as local or global technique. The former is typically adopted to remove local cusps of the objective function, which come from the utilisation of square-root, absolute value, or, generally, non-differentiable functions [64]. The latter, instead, can be applied to minimise the fluctuations of the objective in the whole domain. In this case, smoothing is performed via a convolution of the original objective with regular functions, such as the Gaussian kernel [71]. One of the main advantage of global smoothing with respect to local smoothing is that the former can be designed to obtain a convex function, which eliminates any sensitivity to initial estimates. However, a typical problem is to determine the "right" amount of smoothing. In other words, too much smoothing will yield a convex function that has little correlation with the original one, and consequently, it will increase the number of unnecessary iterations. On the other hand, too little smoothing will not be sufficient to convex the original objective. Thus, a trade-off is necessary.

An example of global smoothing technique for a localisation problem was proposed in [71]. However, the optimisation algorithm described in [71] – hereafter referred to as Square Range-Global Distance Continuation (SR-GDC) – relies on a WLS formulation with squared distances, which is not optimal [72] .

Stochastic techniques

Finally, we discuss global optimisation algorithms based on stochastic search techniques. A typical example is the Simulated-Annealing (SA) [73].

Briefly, in SA the search of the minimum is performed in a pseudo-random manner. In other words, the algorithm can move "uphill" or "downhill" with a certain probability that depends both on the difference between the current and the new function values and on a global parameter, called the temperature, that from a high value (hot state) goes to 0 (frozen state) while the randomness of the search decreases. In [73], SA was applied to the minimisation of the WLS objective function in a network localisation problem. The authors remarked that the optimum performance out of the SA technique can be obtained if the temperature slowly decreases while the minimisation proceeds. Clearly, this implies that the SA converges after many iterations and this may increase prohibitively the complexity of the algorithm.

2.2.2 Approximate solutions for single-target positioning

In the specific case of non-cooperative positioning, *i.e.* where a target node exchange information only with the anchors, the WLS optimisation problem given in equation (8) reduces to

$$\min_{\hat{\mathbf{z}}\in\mathbb{R}^{\eta}} \sum_{i=1}^{N_{\mathrm{A}}} w_i^2 \left(\tilde{d}_i - \hat{d}_i\right)^2, \tag{9}$$

where $\hat{\mathbf{z}}$ denotes the estimate of the target location, $w_i^2, \tilde{d}_i$ and $\hat{d}_i$ refer to the weight, the ranging and the distance estimate associated with the link between the i-th anchor and the target.

Typically, this optimisation problem is solved with an iterative algorithm that, at each iteration, computes the minimum of the linear approximation of WLS objective given by [39]

$$\sum_{i=1}^{N_{\mathrm{A}}} w_i^2 \left(\tilde{d}_i - \hat{d}_i\right)^2 \approx \sum_{i=1}^{N_{\mathrm{A}}} w_i^2 \left(\tilde{d}_i - (d_i^{\mathrm{R}} + \mathbf{J}_{di}^{\mathrm{R}}(\hat{\mathbf{z}} - \mathbf{p}_{\mathrm{R}})^{\mathrm{T}})\right)^2, \tag{10}$$

where $d_i^{\mathrm{R}} \triangleq \|\mathbf{a}_i - \mathbf{p}_{\mathrm{R}}\|_{\mathrm{F}}$, $\mathbf{p}_{\mathrm{R}}$ is the approximation point and $\mathbf{J}_{di}^{\mathrm{R}} \triangleq (\mathbf{p}_{\mathrm{R}} - \mathbf{a}_i)/d_i^{\mathrm{R}}$.

The success of this iterative technique depends on the choice of the initial approximation point $\mathbf{p}_{\mathrm{R}}$ as well as the number of minima of the objective. A reliable point, for instance, can be obtained from the solution of the Squared Range (SR)-LS minimisation problem

$$\begin{aligned} \min_{\hat{\mathbf{z}}\in\mathbb{R}^{\eta}} \quad & \sum_{i=1}^{N_{\mathrm{A}}} w_i^2 \left(\tilde{d}_i^2 - (\alpha_{\mathrm{SR}} - 2\mathbf{a}_i^{\mathrm{T}}\hat{\mathbf{z}} + \|\mathbf{a}_i\|_F^2)\right)^2, \\ \text{s.t.} \quad & \|\hat{\mathbf{z}}\|_F^2 = \alpha_{\mathrm{SR}}, \end{aligned} \tag{11}$$

which can be written in a matrix form as

$$\begin{aligned} \min_{\hat{\mathbf{z}}\in\mathbb{R}^{\eta}} \quad & (\mathbf{A}_{\mathrm{SR}}\mathbf{y}_{\mathrm{SR}} - \mathbf{b}_{\mathrm{SR}})^{\mathrm{T}} \, \mathbf{\Lambda}_w \, (\mathbf{A}_{\mathrm{SR}}\mathbf{y}_{\mathrm{SR}} - \mathbf{b}_{\mathrm{SR}}), \\ \text{s.t.} \quad & \mathbf{y}_{\mathrm{SR}}^{\mathrm{T}}\mathbf{D}_{\mathrm{SR}}\mathbf{y}_{\mathrm{SR}} + 2\,\mathbf{f}_{\mathrm{SR}}^{\mathrm{T}}\mathbf{y}_{\mathrm{SR}} = 0, \end{aligned} \tag{12}$$

where $\mathbf{\Lambda}_w \in \mathbb{R}^{N_{\mathrm{A}}\times N_{\mathrm{A}}}$ is a diagonal matrix with the i-th diagonal element equals

to w_i^2, $\mathbf{y}_{\mathrm{SR}} \triangleq [\hat{\mathbf{z}}, \alpha_{\mathrm{SR}}]^{\mathrm{T}}$ and

$$\mathbf{A}_{\mathrm{SR}} \triangleq \begin{bmatrix} -2\mathbf{a}_1^{\mathrm{T}} & 1 \\ \vdots & \vdots \\ -2\mathbf{a}_{N_{\mathrm{A}}}^{\mathrm{T}} & 1 \end{bmatrix}, \ \mathbf{b}_{\mathrm{SR}} \triangleq \begin{bmatrix} \tilde{d}_1^2 - \|\mathbf{a}_1\|_{\mathrm{F}}^2 \\ \vdots \\ \tilde{d}_{N_{\mathrm{A}}}^2 - \|\mathbf{a}_{N_{\mathrm{A}}}\|_{\mathrm{F}}^2 \end{bmatrix}, \tag{13}$$

$$\mathbf{D}_{\mathrm{SR}} \triangleq \begin{bmatrix} \mathbf{I}_\eta & \mathbf{0}_\eta \\ \mathbf{0}_1 & 0 \end{bmatrix}, \ \mathbf{f}_{\mathrm{SR}} \triangleq \begin{bmatrix} \mathbf{0}_\eta \\ -0.5 \end{bmatrix}. \tag{14}$$

In the literature, exact [49, 74] and approximate [75–77] solutions to the above optimisation problem exist. The exact solutions are derived from the Lagrangian function [49, 74], while the approximation, known as the Linearised Least Square (LLS) solution, are obtained by considering the quadratic constraint as a part of the objective function [75–77].

2.3 Error mitigation techniques

Notwithstanding that a robust minimisation is necessary for accurate positioning, the performance of a localisation algorithm, especially in NLOS scenarios, can be improved with error mitigation techniques. In this regard, WLS based methods offer two possibilities: a soft-mitigation scheme by means of weights and hard mitigation scheme by means of constraints.

The calculation of weights is typically costless with respect to the overall computational complexity of the minimisation algorithm. Indeed, the utilisation of weights does not modify any part of the optimisation technique, except for the objective. Obviously, different weighing strategies yield different results, and the challenge is to derive the best method under scarce information.

On the other hand, constrained minimisations can be more effective than weight-based methods, but they come with an increase of computational complexity. For this reason, in network (cooperative) localisation, where the number of variables is large and the complexity is a concern, error mitigation schemes typically rely on weighing strategies. In contrast, in source (non-cooperative) positioning, constrained optimisation can be used with no restrictions.

2.3.1 Weighing strategies

In the words of Stephen Boyd [62, pp. 5] when speaking of least square problems, "*weights are chosen to reflect differing levels of concern about the sizes of the terms*" in the sum of the objective function. This means that the solution of a WLS optimisation problem can be influenced by emphasizing some terms of the cost-function over others, so that the higher the weight, the tighter is the requirement over the corresponding least square error. With this perspective, the general rule-of-thumb is to give higher weight to accurate measurements, less to the others and zero to the unmeasured links [78].

In spite of the known benefits of weighing, a few strategies have so far been proposed for positioning which are applicable to cooperative approaches, can cope with scarce ranging information, and require no a priori information on either the ranging error model nor the channel conditions. To the best of our knowledge, the only weighing strategies proposed in the literature are the following.

In [79, 80] w_{ij}^2 is computed as the inverse of the ranging noise variance σ_{ij}^2, *i.e.*

$$w_{ij}^2 = 1/\sigma_{ij}^2, \tag{15}$$

This strategy is directly derived from the ML formulation of a distance-based localisation problem with the assumption that the noise is a random variable with a zero-mean Gaussian distribution and variance σ_{ij}^2. However, if the real ranging statistics do not match this assumption, *e.g.* in the case of NLOS channel conditions, or if the variance is not known a priori, or if the measurements are scarce and the variance can not be estimated, than such a strategy may degrade the localisation accuracy.

An alternative solution was proposed in [81], and in this case, the weights were derived from the kurtosis, mean excess delay and root-mean-square delay spread of the received signal. The assumption, which may not be realistic in unknown environments, is the a priori knowledge of a statistical model of the multipath propagation.

In [69], the weight was proposed as the inverse of the square of the distance measurement, *i.e.*

$$w_{ij}^2 = 1/\tilde{d}_{ij}^2. \tag{16}$$

This strategy was derived from the assumption that the variance of the ranging error increases proportionally with the distance between the transmitter

and the receiver. In many application scenarios, *e.g.* outdoor navigation and environmental monitoring in large space environments, this assumption is realistic and this strategy is sufficient to mitigate the errors.

A similar idea, this time based on a non-parametric Locally weighted Scatter plot Smoothing (LOESS) filtering mechanism, was proposed in [82]. In this case, there is no assumptions on the measurement model, and the weights are computed simply to emphasize shorter connections rather than longer ones. The LOESS-based weight w_{ij}^2 is given by

$$w_{ij}^2 = \exp\left(-\frac{\tilde{d}_{ij}^2}{(\max_j\{\tilde{d}_{ij}\})^2}\right). \tag{17}$$

In [8], we proposed another alternative, yet over performing, weighing strategy. In contrast to all of the above, the weight w_{ij}^2 is computed without any assumptions on the ranging statistics, and is derived based on the maximisation criterion of the measurement diversity as well as geometrical properties. More details are provided in Section 6.2.

2.3.2 Constrained optimisations

As mentioned in the introduction of Section 2.3.1, constrained optimisations are typically designed for source localisation where the computational complexity of the algorithm is not a crucial restriction. Typically, the constraints are derived from geometric considerations and/or statistical information of the ranging. The basic idea is to determine a *feasibility region* of the target location, and force the optimisation to search in such a region.

For instance, based on the assumption that a range estimate is typically larger than the true distance, the feasibility region of the target location can be determined by the intersection of the convex sets $B_D^i \triangleq \{\hat{\mathbf{z}}|0 \leq \hat{d}_i \leq \tilde{d}_i\}$. Convex optimisation based on Projection On Convex Sets (POCS) techniques can be utilised to compute an estimate of $\mathbf{z}$ from the intersection of all B_D^is [83, 84]. However, a more accurate solution can be obtained via a constrained WLS minimisation problem such as

$$\begin{aligned} \min_{\hat{\mathbf{z}}\in\mathbb{R}^\eta} \quad & \sum_{i=1}^{N_\mathrm{A}} w_i^2(\tilde{d}_i - \hat{d}_i)^2, \\ \text{s.t.} \quad & \hat{d}_i \leq \tilde{d}_i \ \forall i, \end{aligned} \tag{18}$$

which can be solved either with Sequential Quadratic Programming (SQP), or via barrier methods as described in [85], or approximated with a Linear Programming (LP) formulation as proposed in [86].

Based on the same considerations, in [87] a two-step LLS-based algorithm, hereafter referred to as Geometric-constrained Location Estimation (GLE), was proposed. In this technique, the first step consists of estimating the target location through a modified LLS method where, the geometric constraints are incorporated in the LLS formulation by means of a virtual distance, *i.e.* the average distance between a reference point and the intersection points of the circles derived from the ranges. In the second step, the algorithm attempts to correct the bias by using the solution obtained at the first step.

In [88], another two-step algorithm was proposed. In this case, the first step is to estimate the target location via a LLS technique, and the second step is to estimate the bias with an interior-point optimisation. To use this algorithm, the a priori information on the bias statistics is needed to set the lower and the upper bounds to the bias estimates. Finally, in [57], a constrained WLS optimisation, that can be solved with a standard SQP technique, was proposed to perform a joint estimation of the target location and bias errors. Specifically, this technique is based on the minimisation problem

$$\begin{aligned} \min_{\hat{\mathbf{z}}\in\mathbb{R}^{\eta},\{\hat{b}_i\}} \quad & \sum_{i=1}^{N_{\mathrm{A}}} w_i^2(\tilde{d}_i - \hat{d}_i - \hat{b}_i)^2, \\ \text{s.t.} \quad & \hat{d}_i \leq \tilde{d}_i \ \forall i, \\ & 0 \leq \hat{b}_i \leq b_i^u \ \forall i, \end{aligned} \tag{19}$$

where $\hat{b}_i$ is an estimate of the bias b_i and b_i^u denotes an upper bound to $\hat{b}_i$.

2.4 Comparison of the state-of-the-art methods

The objective of this section is to discuss the advantages and disadvantages of the aforementioned algorithms and mitigation techniques with numerical results. To this end, we consider non-cooperative and cooperative algorithms separately, and evaluate their performance in LOS and NLOS scenarios.

For each algorithm we calculate the average location accuracy, which is defined as the Root-Mean-Squared-Error (RMSE) of the position estimate, *i.e.*

$$\bar{\varepsilon}_\ell \triangleq \frac{1}{M_T N_{\mathrm{T}}} \sqrt{\sum_{q=1}^{M_T} \varepsilon_{q,\ell}^2}, \tag{20}$$

where $\varepsilon_{q,\ell}^2 \triangleq \|(\vec{\mathbf{z}}_\ell^{(q)} - \vec{\mathbf{z}}^{(q)}\|_{\mathrm{F}}^2$, $\vec{\mathbf{z}}^{(q)} \in \mathbb{R}^{\eta N_{\mathrm{T}}}$ is a row-vector with all target coordinates and $\vec{\hat{\mathbf{z}}}_\ell^{(q)}$ the corresponding estimate obtained the ℓ-th out of M_A algorithms and the q-th network out of M_T realisations.

For non-cooperative positioning, the RMSE will be studied as a function of the noise variance in LOS and the maximum bias in NLOS channel conditions. Whereas, in the case of cooperative positioning we also consider the meshness-ratio[1] given by

$$m \triangleq \frac{(|E| - N + 1)}{(|E_F| - N + 1)}, \tag{21}$$

where $|\cdot|$ indicates the cardinal number of a set, E and E_F are the set of measured distances and the set of all pairwise distances in the network, respectively.

2.4.1 Non-cooperative positioning

Consider a network with $N_{\mathrm{A}} = 4$ anchors equispaced around a circle of radius 10 meters and, $N_{\mathrm{T}} = 10$ targets uniformly distributed within the convex-hull of the anchors[2]. All anchors are connected to the target ($m = 1$), and all anchor-to-target distances are measured once. Assume LOS scenarios, *i.e.* ranging errors as random variables with a zero mean Gaussian distribution and variance σ^2.

We evaluate the RMSE obtained with the Squared-Range Least-Square (SR-LS) method described in [49], the closed-form solutions LLS-1 [75] LLS-2 [76], LLS-3 [77], the Taylor's Series (TS)-WLS approximation [39] and the iterative LM-WLS algorithm [65]. Both the TS-WLS and LM-WLS methods are initialised with the solution obtained from the LLS-1 algorithm. For the sake of optimality, we also evaluate the RMSE obtained with a global optimisation performed via exhaustive search and, this performance is indicated as Optimum-WLS.

[1]The meshness-ratio is a metric commonly used in algebraic topology and graph-theory [89] that captures in one number information on the planarity of a graph. In practice, $m \to 1$ indicates that the network is fully connected and, $m \to 0$ vice versa.

[2]This scenario typically models a localisation system for indoors as well as cellular networks, where base-stations surround the target.

The comparison, shown in Figure 5(a), reveals that all techniques have similar performance, thus any of them can be utilized for positioning. Nevertheless, we notice that amongst the LLS methods, the LLS-3 provides the closest result to the optimum SR-LS. However, due to the squared ranging, the latter cannot achieve the performance of the Optimum-WLS, which in turn are reached by both the TS-WLS and the LM-WLS techniques. In light of this test, the TS-WLS and the LM-WLS can be considered equivalent state-of-the-art solutions for source-positioning in LOS channel conditions.

Next, we assume NLOS scenarios. In this regard, the ranging error is modelled as the sum of two random variables, one that models the noise (zero-mean Gaussian random variable with variance σ^2) and the other the bias (positive value with uniform distribution within 0 and b_{MAX}). The algorithms compared in this simulation are: the TS-WLS, the Constraint Non-linear Least Square (C-NLS) [85], the GLE [87] and the C-NLS modified [57]. We assume full connectivity, one ranging per distance and unknown ranging statistics.

The result illustrated in Figure 5(b) shows that all constrained methods offer an advantage with respect to the TS-WLS. However, the C-NLS modified provides the lowest location accuracy since it performs a joint estimation of the node locations and bias errors.

First we consider LOS scenarios (see description in the previous section), one ranging per distance and optimal weighing strategy[3]. We test the gradient-based method LM-WLS [66], the majorizing technique SMACOF [60], the smoothing-continuation algorithm SR-GDC [71] and the SDP-based minimisation with projection on the Euclidean Distance Matrix (EDM) space [69].

2.4.2 Cooperative positioning

Next, we consider cooperative positioning and we evaluate both the difference amongst optimisation methods and weighing strategies. The typical network consists of $N_{\mathrm{A}} = 4$ anchors equispaced around a circle of radius 10 meters and, $N_{\mathrm{T}} = 10$ targets uniformly distributed in the convex-hull formed by the anchors[4].

[3]The optimal weighing strategy with unbiased Gaussian error is given by equation (15) [79–81].
[4]This scenario typically models a localisation system for indoor positioning, where anchors can be placed at the outer border of a building.

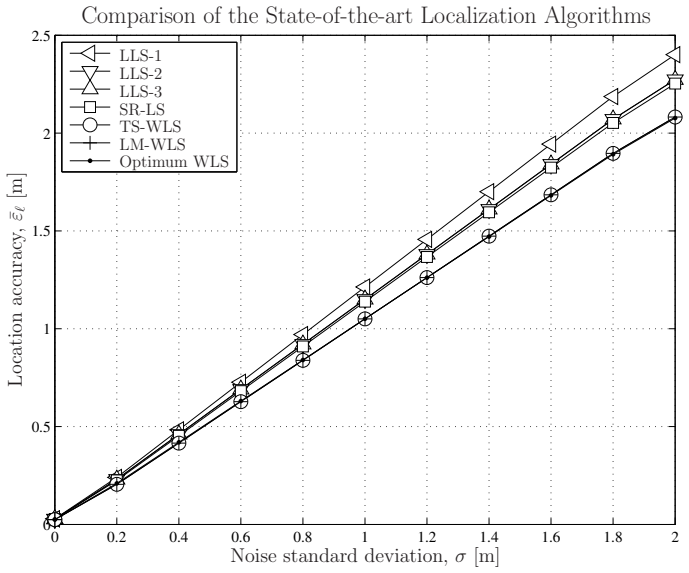

(a) LOS scenario

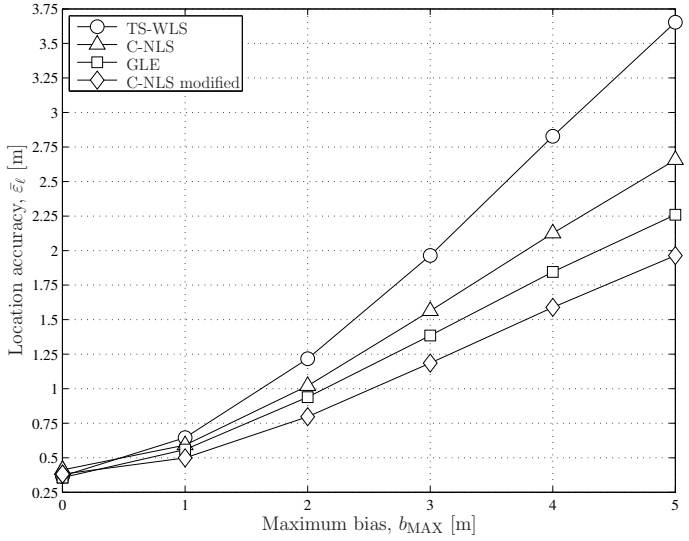

(b) NLOS scenario

Fig 5. Comparison of the state-of-the-art algorithms for source localisation. The network is deployed in a square of 14.14×14.14 meters. In a) and b) the results refer to LOS (unbiased measurements) and NLOS (biased measurements) scenarios, respectively.

In Figures 6(a) and 6(b) we show the RMSE as a function of the noise standard deviation σ while $m = 1$ and, the RMSE as a function the meshness-ratio[5] m while $\sigma = 0.3$ meter. From both tests, it can be noticed that the SDP-based optimisation (which is followed by a refinement) achieves the lowest RMSE. The SR-GDC algorithm provides a similar result. The difference however is due to the sub-optimality of the formulation that relies on squared ranges. Indeed, from Figure 6(a), it can be observed that the gap between the RMSE achieved with SR-GDC and that obtained with the SDP grows with the increase of the noise.

On the other hand, the performance of the SMACOF and LM-WLS methods are in general comparable to those obtained with the SDP. The difference between the SMACOF, LM-WLS and SDP can be noticed only for $m \to 0$. This indicates that the MDS-based technique proposed in [90] is a reliable initial estimate only for high connectivity. Indeed, at $m = 1$ the MDS solution is equivalent to the solution obtained with a SDP formulation based on the projection on the Positive Semi-definite Matrix (PSM) cone (see Section 3.3). However, we remark that the initialisation method proposed in [90] relies on a centralised algorithm. For distributed positioning it can be expected that the performance of the SMACOF and the LM-WLS degrade since an MDS-based algorithm – which is based on eigendecomposition – is difficult to implement.

From these results, we conclude that the SDP-based solution proposed in [69] is the best performing optimisation method, but it is also the most complex. On the other hand, the SMACOF and LM-WLS are less complex than the SDP, but inaccurate at low meshness. Furthermore, they need a reliable initial point. The best compromise amongst accuracy, robustness to initial estimate and complexity, instead, is obtained with the SR-GDC algorithm.

The second set of simulations is devoted to the comparison of different weighing strategies in NLOS scenarios. Specifically, we compare a connectivity based ($w_{ij}^2 = 1$ if two nodes are connected and 0 otherwise), the variance-based (equation (15)), the inverse-distance based (equation (16)) and the LOESS based (equation (17)) methods. The minimisation is performed with the SDP algorithm proposed in [69].

[5]The meshness ratio is varied by assuming that two nodes are connected if $d_{ij} \leq R_{\mathrm{MAX}}$ and by changing R_{MAX} within 8 and 20 meters.

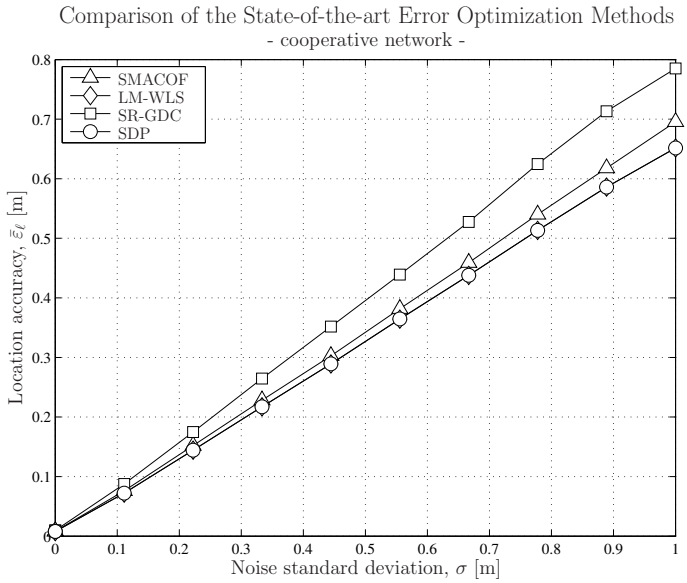

(a) RMSE as a function of the noise

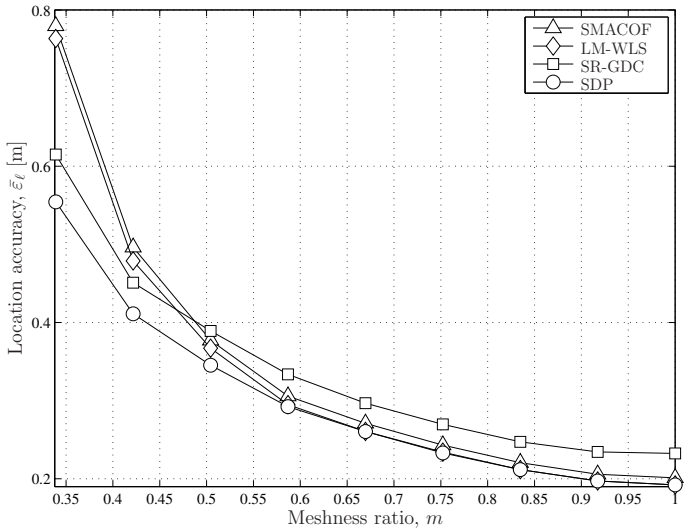

(b) RMSE as a function of the meshness

Fig 6. Comparison of the state-of-the-art optimizations for cooperative positioning in LOS scenarios. The network consists of $N_{\mathbf{A}} = 4$ anchors, $N_{\mathbf{T}} = 10$ targets and it is deployed in a square of 14.14×14.14 square meters. In a) and b) the results are plotted as a function of the noise standard deviation $\sigma_{ij} = \sigma \; \forall ij$ with $m = 1$, and the mesheness ratio m with $\sigma_{ij} = 0.3$ meters $\forall ij$, respectively.

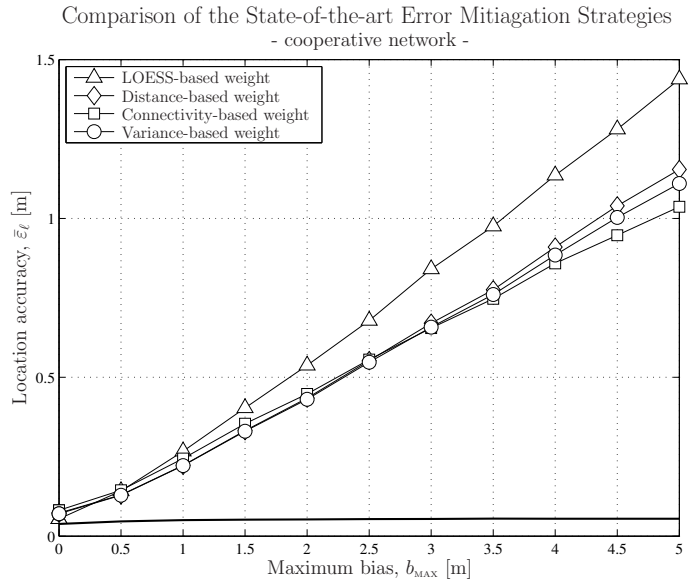

(a) RMSE as a function of the bias

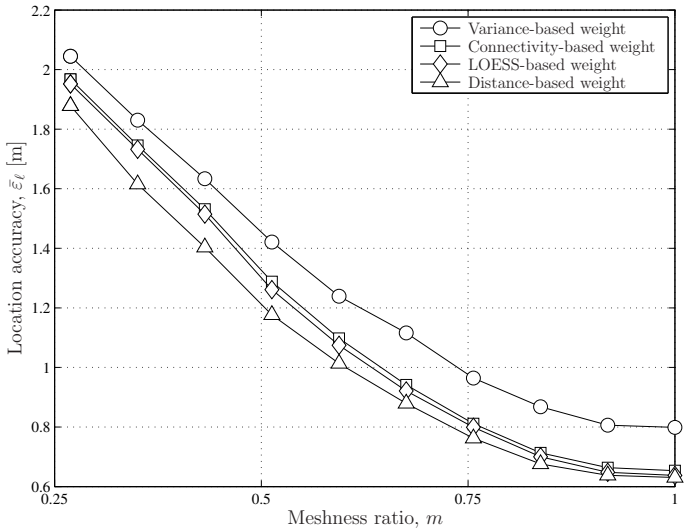

(b) RMSE as a function of the meshness

Fig 7. Comparison of the weighing strategies for cooperative positioning in NLOS scenarios. The network consists of $N_{\mathbf{A}} = 4$ anchors, $N_{\mathbf{T}} = 10$ targets and it is deployed in a square of 14.14×14.14 square meters. In a) and b) the results are plotted as a function of $b_{\mathbf{MAX}}$ with $m = 1$, and m with $b_{\mathbf{MAX}} = 5$ meters, respectively.

We assume that a link is in NLOS channel conditions with a probability $p_{\text{NLOS}} = 0.3$. The noise is modelled with a random variable with a zero-mean Gaussian distribution and a random standard deviation of σ_{ij} selected in the interval $(0.01, 0.3)$ meters, and the bias b_{ij} as a random variable with uniform distribution between 0 and b_{MAX}. A distance can be measured K_{ij} times, where K_{ij} is also a random variable governed by a uniform distribution defined in the interval $(K_{\text{MIN}}, K_{\text{MAX}})$[6]. The average distance $\bar{d}_{ij}$ computed out of the K_{ij} samples is used in the WLS objective function instead of $\tilde{d}_{ij}$.

In Figures 7(a) and 7(b) we show the RMSE as a function of the maximum bias b_{MAX} while $m = 1$ and, the RMSE as a function the meshness-ratio m while $b_{\text{MAX}} = 3$ meter. From these results, it can be noticed that the variance-based method, which was optimal in LOS scenario, is the worse strategy in NLOS. The connectivity based strategy is a good trade-off if all errors follow the same distribution. The inverse-distance and the LOESS based strategies are instead the best performing methods. In fact, both strategies penalised longer distances than short ones.

2.5 Summary and discussions

In this chapter we offered an overview as well as a comparison of existing positioning algorithms and show that robust non-cooperative techniques can rely on constrained optimisation problems, whereas efficient cooperative methods can be developed with global optimisation methods such as the SDP and weighing strategies. In this thesis, we propose novel solutions to both problems by developing in Chapter 5 and Chapter 6, robust non-cooperative and cooperative localisation methods, respectively.

[6]To minimise the traffic overhead as well as the energy consumption due to ranging, we assume that $(K_{\min}, K_{\text{MAX}})$ are small numbers, *e.g.* $K_{\min} = 2$ and $K_{\text{MAX}} = 5$.

3 Fundamentals of ranging-based positioning

In this Chapter, the distance-based positioning problem is formulated as a WLS optimisation problem. We derive the gradient and the Hessian of the WLS objective function in closed form so as to provide the fundamental tools for the theoretical and algorithmic results shown in the following chapters. In addition, we also revise the matrix-proximity formulation of the WLS optimization problem and describe the principles of three SDP formulations. In particular, the technique referred to as SDP-method 1 will be considered the state-of-the-art optimisation algorithm.

3.1 Ranging-based positioning system model

Consider a wireless network composed of N_{A} anchor, and N_{T} target nodes distributed in the Euclidean space of η dimensions. An *anchor* is a node with a known fixed location, and a *target* is a node whose location is yet to be determined. Let $\mathbf{a}_i \in \mathbb{R}^\eta$ and $\mathbf{z}_j \in \mathbb{R}^\eta$ denote the coordinate vectors of the i-th anchor and j-th target, respectively. Let $\mathbf{P} \in \mathbb{R}^{N\times\eta}$ with $N = N_{\mathrm{A}} + N_{\mathrm{T}}$, be the matrix with all coordinate vectors of the nodes in the network. Assume that the first N_{A} rows of $\mathbf{P}$ refer to the anchors' coordinates and the remaining to coordinates of the targets, *i.e.*

$$\mathbf{p}_j \triangleq \begin{cases} \mathbf{a}_i, & 1 \leq i \leq N_{\mathrm{A}}, \quad \text{and } 1 \leq j \leq N_{\mathrm{A}}, \\ \mathbf{p}_i, & 1 \leq i \leq N_{\mathrm{T}}, \quad \text{and } N_{\mathrm{A}}+1 \leq j \leq N, \end{cases} \tag{22}$$

where $\mathbf{p}_j$ denotes the j-th row-vector of $\mathbf{P}$. The matrix $\mathbf{P}$ will be hereafter referred to as the *coordinate-matrix* of the network.

The *Euclidean distance*, or *exact* ranging, between the i-th and the j-th nodes is denoted by d_{ij} and is computed as

$$d_{ij} \triangleq \|\mathbf{p}_i - \mathbf{p}_j\|_{\mathrm{F}}, \tag{23}$$

where $\|\|_{\mathrm{F}}$ is the Frobenius norm[7].

[7]The Frobenius norm of vectors is equivalent to the Euclidean norm (2-norm). Indeed, both norms can be referred to as the Euclidean norms [91].

The distance d_{ij} is also the ij-th element of a matrix $\mathbf{D} \in \mathbb{R}^{N\times N}$, hereafter, referred to as the EDM associated with $\mathbf{P}$. Such a matrix can be directly computed from $\mathbf{P}$ as

$$\mathbf{D} = \mathcal{D}(\mathbf{P}) \triangleq \sqrt{\mathbf{1}_{\mathrm{N}}\mathrm{diag}\left(\mathbf{P}\mathbf{P}^{\mathrm{T}}\right)^{\mathrm{T}} + \mathrm{diag}\left(\mathbf{P}\mathbf{P}^{\mathrm{T}}\right)\mathbf{1}_{\mathrm{N}}^{\mathrm{T}} - 2\mathbf{P}\mathbf{P}^{\mathrm{T}}}, \tag{24}$$

where $\mathcal{D} : \mathbb{R}^{N\times\eta} \to \mathbb{R}^{N\times N}$ is the Euclidean Distance Function (EDF) [67], $^{\mathrm{T}}$ indicates transpose, $\mathbf{1}_{\mathrm{N}} \in \mathbb{R}^{N}$ is a column vector with all elements equal to one, and diag() is the diagonal function that returns a column vector containing the diagonal elements of the matrix given as argument.

The connectivity of the network is described by the connectivity matrix $\mathbf{C} \in \mathbb{R}^{N\times N}$ and the ij-th element of $\mathbf{C}$, denoted by c_{ij}, is equal to 1 if and only if the i-th and the j-th nodes are connected, and 0 otherwise. If $c_{ij} = 1$, it is assumed that the distance d_{ij} can be measured.

Let $\tilde{\mathbf{D}}$ denote the EDM-sample, or observation, of the true EDM $\mathbf{D}$. The ij-th element of $\tilde{\mathbf{D}}$, denoted by $\tilde{d}_{ij}$, is referred to as a measurement (ranging) of d_{ij} and it is assumed that $\tilde{d}_{ij} = \tilde{d}_{ji}$. For analytical purpose, each ranging is considered as an independent identically distributed (iid) random variable and modelled as

$$\tilde{d}_{ij} = d_{ij} + n_{ij} + b_{ij}, \tag{25}$$

where n_{ij} and b_{ij} refer to small-scale (noise) and large-scale (bias) ranging errors, respectively.

The noise n_{ij} is governed by a zero-mean Gaussian distribution of variance σ_{ij}^2. The distribution of the bias b_{ij}, instead, is given by a uniform distribution $\mathcal{U}(0, b_{\mathrm{MAX}})$ where $b_{\mathrm{MAX}} = 0$ in LOS and $b_{\mathrm{MAX}} > 0$ in NLOS channel conditions [86, 92]. In [93, 94], it was shown that such a model is a valid approximation of the ranging statistics obtained with UWB devices in indoor environments. However, alternative ranging models that best apply to other application scenarios can be found in the literature. For instance, in [80, 95] the bias is modelled as a random variable with exponential distribution, in [56] as an unknown constant value and, in [96] as a Gaussian mixture whose parameters are derived from measurements.

3.2 Weighted least square problem formulation

The distance-based positioning problem can be defined as an estimation problem in which, given an EDM-sample $\tilde{\mathbf{D}}$, the variables $\mathbf{p}_i$'s are computed to minimise the distance-based squared error criteria given by

$$f_{\mathrm{R}}(\vec{\hat{\mathbf{p}}}) \triangleq \left\| \mathbf{C} \circ \left(\tilde{\mathbf{D}} - \hat{\mathbf{D}} \right) \right\|_{\mathrm{F}} = \left\| \vec{\mathbf{c}} \circ (\vec{\tilde{\mathbf{d}}} - \vec{\hat{\mathbf{d}}}) \right\|_{\mathrm{F}} = \sum_{i=1}^{N} \sum_{\substack{j=1 \\ j \neq i}}^{N} c_{ij} \left(\tilde{d}_{ij} - \hat{d}_{ij} \right)^2, \quad (26)$$

where $\circ$ is the Hadamard product, $\hat{d}_{ij} \triangleq \|\hat{\mathbf{p}}_i - \hat{\mathbf{p}}_j\|_{\mathrm{F}}$, $\hat{\mathbf{p}}_i$ is the estimate of the i-th node location and corresponds to the i-th row-vector of $\hat{\mathbf{P}}$, $\hat{\mathbf{D}} \triangleq \mathcal{D}(\hat{\mathbf{P}})$ and $\vec{\hat{\mathbf{p}}}$, $\vec{\mathbf{c}}$, $\vec{\hat{\mathbf{d}}}$, $\vec{\tilde{\mathbf{d}}}$ are the vectorised forms of the matrices $\hat{\mathbf{P}}$, $\mathbf{C}$, $\hat{\mathbf{D}}$ and $\tilde{\mathbf{D}}$, respectively.

In the literature, this problem is known as a LS formulation of the distance-based positioning problem [51, 58, 69, 97]. The following Theorem provides the optimality conditions from which the WLS optimisation problem can be considered a ML estimation problem.

Theorem T1 (Equivalence of WLS-based and LOS ML-based Positioning [69])**.** *Let $\tilde{d}_{ij}$ be an iid random variable with Gaussian distribution of mean d_{ij} and variance σ_{ij}^2. Then the ML formulation of the localisation problem is equivalent to a distance-based WLS minimisation problem where $w_{ij}^2 = c_{ij}/\sigma_{ij}^2$.*

Proof. Given $\tilde{d}_{ij}$ as an iid Gaussian random variable of mean d_{ij} and variance σ_{ij}^2, the likelihood function of the parameters $\vec{\hat{\mathbf{p}}}$ is given by

$$L(\vec{\hat{\mathbf{p}}}|\vec{\tilde{\mathbf{d}}}) \triangleq \prod_{i=1}^{N} \prod_{\substack{j=1 \\ j \neq i}}^{N} \frac{1}{\sqrt{2\pi}\sigma_{ij}} \exp\left(-\frac{c_{ij}\left(\tilde{d}_{ij} - \hat{d}_{ij}\right)^2}{2\sigma_{ij}^2} \right). \quad (27)$$

Taking the logarithm of $L(\vec{\hat{\mathbf{p}}}|\vec{\tilde{\mathbf{d}}})$ and computing the maximum, it yields

$$\begin{aligned} \max_{\vec{\hat{\mathbf{p}}} \in \mathbb{R}^{\eta N}} \log L(\vec{\hat{\mathbf{p}}}|\vec{\tilde{\mathbf{d}}}) &= \sum_{i=1}^{N} \sum_{\substack{j=1 \\ j \neq i}}^{N} \frac{1}{\sqrt{2\pi}\sigma_{ij}} - \max_{\vec{\hat{\mathbf{p}}} \in \mathbb{R}^{\eta N}} \sum_{i=1}^{N} \sum_{\substack{j=1 \\ j \neq i}}^{N} \frac{c_{ij}}{2\sigma_{ij}^2} \left(\tilde{d}_{ij} - \hat{d}_{ij} \right)^2 \quad (28) \\ &= \min_{\vec{\hat{\mathbf{p}}} \in \mathbb{R}^{\eta N}} \sum_{i=1}^{N} \sum_{j>i}^{N} \frac{c_{ij}}{\sigma_{ij}^2} \left(\tilde{d}_{ij} - \hat{d}_{ij} \right)^2, \end{aligned}$$

where the last equality holds because of the symmetric properties of $\tilde{\mathbf{D}}$. □

3.2.1 Analysis of the WLS objective

In this subsection, we carry on an analytical study of the WLS objective function given in equation (26). We derive closed-form expressions of its gradient and Hessian, and investigate the convexity of $f_{\mathrm{R}}(\vec{\hat{\mathbf{p}}})$.

To begin with, rewrite equation (26) in a matrix form as

$$f_{\mathrm{R}}(\vec{\hat{\mathbf{p}}}) = \|\hat{\boldsymbol{\mathcal{F}}}\|_{\mathrm{F}}^2, \tag{29}$$

where

$$\hat{\boldsymbol{\mathcal{F}}} \triangleq \mathbf{W} \circ \left(\tilde{\mathbf{D}} - \mathcal{D}(\hat{\mathbf{P}})\right), \tag{30}$$

in which $\mathbf{W} \in \mathbb{R}^{N\times N}$ is a general weighing matrix ($\mathbf{W} = \mathbf{C}$ gives the function in equation (26)) with $w_{ij} > 0$ if $c_{ij} = 1$ and $w_{ij} = 0$ otherwise.

From the above, the gradient and the Hessian of $f_{\mathrm{R}}(\vec{\hat{\mathbf{p}}})$, respectively denoted as $\nabla_{\vec{\hat{\mathbf{p}}}} f_{\mathrm{R}}(\vec{\hat{\mathbf{p}}}) \in \mathbb{R}^{N\eta}$ and $\nabla^2_{\vec{\hat{\mathbf{p}}}} f_{\mathrm{R}}(\vec{\hat{\mathbf{p}}}) \in \mathbb{R}^{N\eta\times N\eta}$, can be derived as follows.

Derivation of the gradient

By definition, the gradient of $f_{\mathrm{R}}(\vec{\hat{\mathbf{p}}})$ is given by the vector of all first partial derivatives $\frac{\partial}{\partial \hat{p}_i^n}$, where $\hat{p}_i^n$ denotes the variable in $\vec{\hat{\mathbf{p}}}$ corresponding to the n-th coordinate of the i-th node. Hence, from equation (29) we obtain

$$\begin{aligned}\nabla_{\vec{\hat{\mathbf{p}}}} f_{\mathrm{R}}(\vec{\hat{\mathbf{p}}}) &\triangleq \frac{\partial}{\partial \vec{\hat{\mathbf{p}}}} f_{\mathrm{R}}(\vec{\hat{\mathbf{p}}}) = \frac{\partial \mathrm{tr}(\hat{\boldsymbol{\mathcal{F}}}\hat{\boldsymbol{\mathcal{F}}}^T)}{\partial \vec{\hat{\mathbf{p}}}} \\ &= \left[\mathrm{tr}\left(\frac{\partial \hat{\boldsymbol{\mathcal{F}}}\hat{\boldsymbol{\mathcal{F}}}^{\mathrm{T}}}{\partial \hat{\boldsymbol{\mathcal{F}}}}\frac{\partial \hat{\boldsymbol{\mathcal{F}}}}{\partial \hat{p}_1^1}\right), \cdots, \mathrm{tr}\left(\frac{\partial \hat{\boldsymbol{\mathcal{F}}}\hat{\boldsymbol{\mathcal{F}}}^{\mathrm{T}}}{\partial \hat{\boldsymbol{\mathcal{F}}}}\frac{\partial \hat{\boldsymbol{\mathcal{F}}}}{\partial \hat{p}_i^n}\right) \cdots, \mathrm{tr}\left(\frac{\partial \hat{\boldsymbol{\mathcal{F}}}\hat{\boldsymbol{\mathcal{F}}}^{\mathrm{T}}}{\partial \hat{\boldsymbol{\mathcal{F}}}}\frac{\partial \hat{\boldsymbol{\mathcal{F}}}}{\partial \hat{p}_N^\eta}\right)\right],\end{aligned} \tag{31}$$

where $\mathrm{tr}()$ denotes the trace and $\frac{\partial}{\partial \hat{\boldsymbol{\mathcal{F}}}}$ is the partial derivative with respect to $\hat{\boldsymbol{\mathcal{F}}}$ and $\frac{\partial}{\partial \vec{\hat{\mathbf{p}}}}$ is the vector of all partial derivatives $\frac{\partial}{\partial \hat{p}_i^n}$.

From the above, the (n,i)-th element of the gradient, *i.e.* the derivative with respect to $\hat{p}_i^n$, is given by

$$\frac{\partial f_{\mathrm{R}}(\vec{\hat{\mathbf{p}}})}{\partial \hat{p}_i^n} = \mathrm{tr}\left(\frac{\partial \hat{\boldsymbol{\mathcal{F}}}\hat{\boldsymbol{\mathcal{F}}}^{\mathrm{T}}}{\partial \hat{\boldsymbol{\mathcal{F}}}}\frac{\partial \hat{\boldsymbol{\mathcal{F}}}}{\partial \hat{p}_i^n}\right), \tag{32}$$

where

$$\frac{\partial \hat{\boldsymbol{\mathcal{F}}}\hat{\boldsymbol{\mathcal{F}}}^{\mathrm{T}}}{\partial \hat{\boldsymbol{\mathcal{F}}}} = 2\hat{\boldsymbol{\mathcal{F}}}, \tag{33}$$

and

$$\frac{\partial \hat{\boldsymbol{\mathcal{F}}}}{\partial \hat{p}_i^n} \triangleq \dot{\hat{\boldsymbol{\mathcal{F}}}}_i^n = \begin{bmatrix} 0 & \cdots & -w_{1i}\dfrac{\hat{p}_1^n - \hat{p}_i^n}{\hat{d}_{1i}} & \cdots & 0 \\ \vdots & & \vdots & & \vdots \\ w_{i1}\dfrac{\hat{p}_i^n - \hat{p}_1^n}{\hat{d}_{i1}} & \cdots & 0 & \cdots & w_{iN}\dfrac{\hat{p}_i^n - \hat{p}_N^n}{\hat{d}_{iN}} \\ \vdots & & \vdots & & \vdots \\ 0 & \cdots & -w_{Ni}\dfrac{\hat{p}_N^n - \hat{p}_i^n}{\hat{d}_{Ni}} & s & 0 \end{bmatrix}. \quad (34)$$

Combining equations (33) and (34) in equation (32), the gradient vector $\nabla_{\vec{\mathbf{p}}} f_{\mathrm{R}}(\vec{\hat{\mathbf{p}}})$ can be written in a compact form as

$$\nabla_{\vec{\mathbf{p}}} f_{\mathrm{R}}(\vec{\hat{\mathbf{p}}}) = 2\left[\sum_{j=1}^{N} w_{1j}^2 \frac{\tilde{d}_{1j} - \hat{d}_{1j}}{\hat{d}_{1j}}(\hat{\mathbf{p}}_1 - \hat{\mathbf{p}}_j), \cdots, \sum_{j=1}^{N} w_{Nj}^2 \frac{\tilde{d}_{Nj} - \hat{d}_{Nj}}{\hat{d}_{Nj}}(\hat{\mathbf{p}}_N - \hat{\mathbf{p}}_j)\right]. \quad (35)$$

Considering that an anchor node has a known location, *i.e.*$\hat{\mathbf{p}}_i = \mathbf{a}_i$, then all partial derivatives $\frac{\partial f_{\mathrm{R}}(\vec{\hat{\mathbf{p}}})}{\partial \hat{p}_i^n}$ with $i \leq N_{\mathrm{A}}$ are equal to 0. Consequently, $\nabla_{\vec{\mathbf{p}}} f_{\mathrm{R}}(\vec{\hat{\mathbf{p}}})$ can be reduced to $\nabla_{\vec{\mathbf{p}}} f_{\mathrm{R}}(\vec{\hat{\mathbf{z}}}) \in \mathbb{R}^{\eta N_{\mathrm{T}}}$, where $\vec{\hat{\mathbf{z}}}$ is the vectorised form of the target coordinate-matrix estimate $\hat{\mathbf{Z}} \in \mathbb{R}^{N_{\mathrm{T}} \times \eta}$, $\hat{\mathbf{Z}} \triangleq [\hat{\mathbf{p}}_{N_{\mathrm{A}}+1}; \cdots; \hat{\mathbf{p}}_N]$, where $[;]$ indicates a row-wise concatenation of vectors. Furthermore, due to the symmetric assumption over $\tilde{\mathbf{D}}$, equation (35) can be simplified by a factor of 2.

Derivation of the Hessian

The Hessian of $f_{\mathrm{R}}(\vec{\hat{\mathbf{p}}})$, denoted by $\nabla^2_{\vec{\mathbf{p}}} f_{\mathrm{R}}(\vec{\hat{\mathbf{p}}})$, is derived as

$$\nabla^2_{\vec{\mathbf{p}}} f_{\mathrm{R}}(\vec{\hat{\mathbf{p}}}) \triangleq \frac{\partial^2}{\partial \vec{\hat{\mathbf{p}}}^{\mathrm{T}} \vec{\hat{\mathbf{p}}}} f_{\mathrm{R}}(\vec{\hat{\mathbf{p}}}) = \mathcal{J}_{\vec{\mathbf{p}}}(\nabla_{\vec{\mathbf{p}}} f_{\mathrm{R}}(\vec{\hat{\mathbf{p}}})), \quad (36)$$

where $\mathcal{J}_{\vec{\mathbf{p}}}(\cdot)$ denotes the Jacobian of the vector functions given in the argument.

In the equation above, the second partial derivative $\dfrac{\partial^2 f_{\mathrm{R}}(\vec{\hat{\mathbf{p}}})}{\partial \hat{p}_j^s \hat{p}_i^n}$ is given by

$$\frac{\partial^2 f_{\mathrm{R}}(\vec{\hat{\mathbf{p}}})}{\partial \hat{p}_j^s \hat{p}_i^n} = \frac{\partial}{\partial \hat{p}_j^s} \mathrm{tr}\left(2\hat{\boldsymbol{\mathcal{F}}} \frac{\partial \hat{\boldsymbol{\mathcal{F}}}}{\partial \hat{p}_i^n}\right) = \mathrm{tr}\left(2\frac{\partial \hat{\boldsymbol{\mathcal{F}}}}{\partial \hat{p}_j^s}\frac{\partial \hat{\boldsymbol{\mathcal{F}}}}{\partial \hat{p}_i^n} + 2\hat{\boldsymbol{\mathcal{F}}}\frac{\partial^2 \hat{\boldsymbol{\mathcal{F}}}}{\partial \hat{p}_j^s \hat{p}_i^n}\right), \quad (37)$$

where $\dfrac{\partial \hat{\boldsymbol{\mathcal{F}}}}{\partial \hat{p}_i^n}$ is given in equation (34) and $\dfrac{\partial^2 \hat{\boldsymbol{\mathcal{F}}}}{\partial \hat{p}_j^s \hat{p}_i^n} \triangleq \ddot{\hat{\boldsymbol{\mathcal{F}}}}_{ji}^{mn} = \ddot{\hat{\boldsymbol{\mathcal{F}}}}_{ij}^{mn} \in \mathbb{R}^{N \times N}$ is

– for $i \neq j$,

$$\left[\ddot{\hat{\boldsymbol{\mathcal{F}}}}_{ji}^{sn}\right]_{tq} = \begin{cases} -\dfrac{w_{tq}}{\hat{d}_{tq}}\left(\dfrac{(\hat{p}_t^n - \hat{p}_q^n)(\hat{p}_t^s - \hat{p}_q^s)}{\hat{d}_{tq}^2} - 1\right), & n = s, t = i, \\ -\dfrac{w_{tq}}{\hat{d}_{tq}}\dfrac{(\hat{p}_t^n - \hat{p}_q^n)(\hat{p}_t^s - \hat{p}_q^s)}{\hat{d}_{tq}^2}, & n \neq s, t = i, \\ 0, & \text{otherwise}, \end{cases} \tag{38}$$

– for $i = j$,

$$\left[\ddot{\hat{\boldsymbol{\mathcal{F}}}}_{ii}^{sn}\right]_{tq} = \begin{cases} \dfrac{w_{tq}}{\hat{d}_{tq}}\left(\dfrac{(\hat{p}_t^n - \hat{p}_q^n)(\hat{p}_t^s - \hat{p}_q^s)}{\hat{d}_{tq}^2} - 1\right), & n = s, t = i, q \neq i, \\ \dfrac{w_{tq}}{\hat{d}_{tq}}\dfrac{(\hat{p}_t^n - \hat{p}_q^n)(\hat{p}_t^s - \hat{p}_q^s)}{\hat{d}_{tq}^2}, & n \neq s, t = i, q \neq i, \\ 0, & \text{otherwise}, \end{cases} \tag{39}$$

where $[\cdot]_{tq}$ indicates the tq-th element of a matrix.

Replacing equations (34), (38) and (39) in (37), the ij-the element of the Hessian reduces to

– for $i \neq j$,

$$\begin{aligned} \frac{\partial^2 f_{\mathrm{R}}(\vec{\hat{\mathbf{p}}})}{\partial \hat{p}_j^s \hat{p}_i^n} &= 2\mathrm{tr}\left(\frac{\partial \hat{\boldsymbol{\mathcal{F}}}}{\partial \hat{p}_j^s}\frac{\partial \hat{\boldsymbol{\mathcal{F}}}}{\partial \hat{p}_i^n}\right) + 2\mathrm{tr}\left(\hat{\boldsymbol{\mathcal{F}}}\frac{\partial^2 \hat{\boldsymbol{\mathcal{F}}}}{\partial \hat{p}_j^s \hat{p}_i^n}\right) \\ &= 4\left[\dot{\hat{\boldsymbol{\mathcal{F}}}}_j^s\right]_{ij}\left[\dot{\hat{\boldsymbol{\mathcal{F}}}}_i^n\right]_{ij} + 4\left[\hat{\boldsymbol{\mathcal{F}}}\right]_{ij}\left[\ddot{\hat{\boldsymbol{\mathcal{F}}}}_{ij}^{ns}\right]_{ij} \\ &= 4w_{ij}^2\left(\frac{(\hat{p}_j^s - \hat{p}_i^s)(\hat{p}_i^n - \hat{p}_j^n)}{\hat{d}_{ij}^2} - \frac{(\tilde{d}_{ij} - \hat{d}_{ij})}{\hat{d}_{ij}}\left(1 + \frac{(\hat{p}_i^n - \hat{p}_j^n)(\hat{p}_i^s - \hat{p}_j^s)}{\hat{d}_{ij}^2}\right)\right) \\ &= -4w_{ij}^2\left(\frac{(\tilde{d}_{ij} - \hat{d}_{ij})}{\hat{d}_{ij}} + \frac{\tilde{d}_{ij}}{\hat{d}_{ij}}\frac{(\hat{p}_i^s - \hat{p}_j^s)(\hat{p}_i^n - \hat{p}_j^n)}{\hat{d}_{ij}^2}\right), \end{aligned} \tag{40}$$

– for $i = j$,

$$\begin{aligned}\frac{\partial^2 f_{\mathrm{R}}(\vec{\hat{\mathbf{p}}})}{\partial \hat{p}_i^s \hat{p}_i^n} &= 2\mathrm{tr}\left(\frac{\partial \hat{\boldsymbol{\mathcal{F}}}}{\partial \hat{p}_i^s}\frac{\partial \hat{\boldsymbol{\mathcal{F}}}}{\partial \hat{p}_i^n}\right) + 2\mathrm{tr}\left(\hat{\boldsymbol{\mathcal{F}}}\frac{\partial^2 \hat{\boldsymbol{\mathcal{F}}}}{\partial \hat{p}_i^s \hat{p}_i^n}\right) \\ &= 4\left[\dot{\hat{\boldsymbol{\mathcal{F}}}}_i^s\right]_{i:}\left[\dot{\hat{\boldsymbol{\mathcal{F}}}}_i^n\right]_{:i} + 4\left[\hat{\boldsymbol{\mathcal{F}}}\right]_{i:}\left[\ddot{\hat{\boldsymbol{\mathcal{F}}}}_{ii}^{ns}\right]_{:i} \\ &= 4\sum_{j=1}^{N} w_{ij}^2\left(\frac{(\hat{p}_i^s - \hat{p}_j^s)(\hat{p}_i^n - \hat{p}_j^n)}{\hat{d}_{ij}^2} + \frac{(\tilde{d}_{ij} - \hat{d}_{ij})}{\hat{d}_{ij}}\left(1 + \frac{(\hat{p}_j^n - \hat{p}_i^n)(\hat{p}_j^s - \hat{p}_i^s)}{\hat{d}_{ij}^2}\right)\right) \\ &= 4\sum_{j=1}^{N} w_{ij}^2\frac{(\tilde{d}_{ij} - \hat{d}_{ij})}{\hat{d}_{ij}} + 4\sum_{j=1}^{N} w_{ij}^2\frac{\tilde{d}_{ij}}{\hat{d}_{ij}}\frac{(\hat{p}_i^s - \hat{p}_j^s)(\hat{p}_i^n - \hat{p}_j^n)}{\hat{d}_{ij}^2},\end{aligned} \tag{41}$$

where $[\cdot]_{i:}$ and $[\cdot]_{:i}$ indicate the i-th row and the i-th column of a matrix.

As for the gradient, if $\hat{p}_i^n$ refers to an anchor then all mixed derivative with $\frac{\partial}{\partial \hat{p}_i^n}$ are 0. Consequently, also the Hessian $\nabla^2_{\vec{\hat{\mathbf{p}}}} f_{\mathrm{R}}(\vec{\hat{\mathbf{p}}})$ can be reduced to $\nabla^2_{\vec{\hat{\mathbf{z}}}} f_{\mathrm{R}}(\vec{\hat{\mathbf{z}}}) \in \mathbb{R}^{N_{\mathrm{T}}\eta \times N_{\mathrm{T}}\eta}$. Furthermore, due to the symmetric assumption over $\tilde{\mathbf{D}}$, equations (40) and (41) can be simplified by a factor of 4.

Non-convexity property

It is well-known that the function $f_{\mathrm{R}}(\vec{\hat{\mathbf{p}}})$ is not convex in its domain $\mathrm{dom}(f_{\mathrm{R}}) \triangleq \mathbb{R}^{\eta N}$. In particular, $f_{\mathrm{R}}(\vec{\hat{\mathbf{p}}})$ is characterised by a concave surface with support defined in an hypersphere with centre $\vec{\mathbf{o}} \in \mathbb{R}^{N_{\mathrm{T}}\eta}$ given by $\vec{\mathbf{o}} \triangleq [\mathbf{o}_1, \cdots, \mathbf{o}_i, \cdots, \mathbf{o}_{N_{\mathrm{T}}}]$ with $\mathbf{o}_k \in \mathbb{R}^{\eta}$, $\mathbf{o}_k = \mathbf{a}_i$ and $\mathbf{o}_j = \mathbf{0}_\eta \ \forall j \neq k$. This property can be put as the following Lemma.

Lemma L1 (Multiple Targets: concavity of $f_{\mathrm{R}}(\vec{\hat{\mathbf{p}}})$ around anchors)**.**

Let B_i denote the hypersphere $\{\vec{\hat{\mathbf{z}}} \mid \|\vec{\mathbf{o}} - \vec{\hat{\mathbf{z}}}\| \leq \varrho_b$ and $\vec{\hat{\mathbf{z}}} \in \mathrm{dom}(f_{\mathrm{R}})\}$. Then

$$\exists\ \varrho_b \mid \nabla^2_{\vec{\hat{\mathbf{z}}}} f_{\mathrm{R}}(\vec{\hat{\mathbf{z}}}) \preceq 0, \ \ \forall\ \vec{\hat{\mathbf{z}}} \in B_i. \tag{42}$$

Proof. Using equations (40) and (41) the Hessian matrix, hereafter also denoted by $\hat{\boldsymbol{H}}$, can be decomposed as

$$\hat{\boldsymbol{H}} = \breve{\boldsymbol{H}} + \bar{\boldsymbol{H}}, \tag{43}$$

where $\breve{\boldsymbol{H}} \in \mathbb{R}^{\eta N \times \eta N}$ and $\bar{\boldsymbol{H}} \in \mathbb{R}^{\eta N \times \eta N}$ are a block-diagonal and a block-off-diagonal matrices, respectively, defined as

$$[\breve{\boldsymbol{H}}]_{kj}^{\eta} \ \triangleq\ \begin{cases} [\hat{\boldsymbol{H}}]_{kk}^{\eta} & k = j, \\ \mathbf{0}_{\eta\eta} & k \neq j, \end{cases} \tag{44}$$

$$[\bar{\boldsymbol{H}}]_{kj}^{\eta} \triangleq \begin{cases} \mathbf{0}_{\eta\eta} & k=j, \\ [\hat{\boldsymbol{H}}]_{kj}^{\eta} & k\neq j, \end{cases} \tag{45}$$

where $\mathbf{0}_{\eta\eta} \in \mathbb{R}^{\eta\times\eta}$ is a matrix of all zeros, $[\hat{\boldsymbol{H}}]_{kj}^{\eta} \in \mathbb{R}^{\eta\times\eta}$ denotes the kj-th block-matrix of $\hat{\boldsymbol{H}}$ with size $\eta\times\eta$.

The k-th block of $\breve{\boldsymbol{H}}$, denoted by $\breve{\boldsymbol{H}}_k \in \mathbb{R}^{\eta\times\eta}$, is given by

$$\breve{\boldsymbol{H}}^k \triangleq [\hat{\boldsymbol{H}}]_{kk}^{\eta} = \left(\sum_{j=1}^{N} w_{kj}^2 \tfrac{\hat{d}_{kj}-\tilde{d}_{kj}}{\hat{d}_{kj}}\right)\mathbf{I}_\eta + \sum_{j=1}^{N} w_{kj}^2 \tfrac{\tilde{d}_{kj}}{\hat{d}_{kj}}\hat{\boldsymbol{\Upsilon}}_{kj}, \tag{46}$$

where

$$\hat{\boldsymbol{\Upsilon}}_{kj} \triangleq \hat{\mathbf{v}}_{kj}^{\mathrm{T}}\hat{\mathbf{v}}_{kj} = \begin{bmatrix} \cos^2\hat{\theta}_{kj} & \sin\hat{\theta}_{kj}\cos\hat{\theta}_{kj} \\ \sin\hat{\theta}_{kj}\cos\hat{\theta}_{kj} & \sin^2\hat{\theta}_{kj} \end{bmatrix}, \tag{47}$$

$\hat{\mathbf{v}}_{kj} \triangleq (\hat{\mathbf{p}}_k - \hat{\mathbf{p}}_j)/\hat{d}_{kj}$, and $\hat{\theta}_{kj}$ is the angle between the vectors centred at $\hat{\mathbf{p}}_k$ pointing towards $\hat{\mathbf{p}}_j$ and $\hat{\mathbf{p}}_k + [1, 0]$, respectively.

The kj-th off diagonal block of $\bar{\boldsymbol{H}}$, denoted by $\bar{\boldsymbol{H}}^{kj}$ is

$$\bar{\boldsymbol{H}}^{kj} \triangleq [\hat{\boldsymbol{H}}]_{kj}^{\eta} = -\left(w_{kj}^2 \tfrac{\hat{d}_{kj}-\tilde{d}_{kj}}{\hat{d}_{kj}}\right)\mathbf{I}_\eta - w_{kj}^2 \tfrac{\tilde{d}_{kj}}{\hat{d}_{kj}}\hat{\boldsymbol{\Upsilon}}_{kj}. \tag{48}$$

Without lost of generality, assume that the k-th target is connected to the i-th anchor. Then, in equation (46) we isolate the term $j=i$, which corresponds to the link between the k-th target and the i-th anchor, in order to obtain

$$\breve{\boldsymbol{H}}^k = \hat{\varpi}_{ik}(\hat{\boldsymbol{\Upsilon}}_{ik} - \mathbf{I}_\eta) + \underbrace{\left(w_{ik}^2 + \sum_{j\neq i}^{N} w_{jk}^2\left(1 - \tfrac{\tilde{d}_{jk}}{\hat{d}_{jk}}\right)\right)\mathbf{I}_\eta + \sum_{j\neq i}^{N} w_{jk}^2 \tfrac{\tilde{d}_{jk}}{\hat{d}_{jk}}\hat{\boldsymbol{\Upsilon}}_{kj}}_{\hat{\mathbf{R}}_{ik}^h}, \tag{49}$$

where $\hat{\varpi}_{ik} \triangleq w_{ik}^2\tilde{d}_{ik}/\|\mathbf{a}_i - \hat{\mathbf{p}}_k\|_{\mathrm{F}}$.

Notice that $\vec{\tilde{\mathbf{z}}} \in B_i$ implies that the distance $\|\mathbf{a}_i - \hat{\mathbf{p}}_k\|_{\mathrm{F}}$ is upper bounded by ϱ_b. Thus, the smaller ϱ_b, the smaller $\|\mathbf{a}_i - \hat{\mathbf{p}}_k\|_{\mathrm{F}}$ is. Furthermore, we remark that the eigenvalues of the matrix difference $(\hat{\boldsymbol{\Upsilon}}_{ik} - \mathbf{I}_\eta)$ are -1 and 0, and that the coefficient $\hat{\varpi}_{ik}$ is positive and grows proportionally with decreasing ϱ_b, therefore $\hat{\varpi}_{ik}(\hat{\boldsymbol{\Upsilon}}_{ik} - \mathbf{I}_\eta) \preceq 0$, where the notation $(\cdot) \preceq 0$ indicates that the matrix on the left-side is negative semi-definite. In contrast, the matrix $\hat{\mathbf{R}}_{ik}^h$ is finite for all $\vec{\tilde{\mathbf{z}}} \in B_i$ as long as there is no $\mathbf{a}_j$ such that $\|\mathbf{a}_i - \mathbf{a}_j\| \leq \varrho_b$, which can be ensured by a sufficiently small ϱ_b. In conclusion, the eigenspectrum of each $\breve{\boldsymbol{H}}^k$ can be controlled by ϱ_b in such a way that, for a sufficiently small ϱ_b, $\breve{\boldsymbol{H}}^k$ is

a negative semi-definite matrix with an eigenvalue that decreases boundlessly. Invoking the generalised Geshgorian theorem to block-diagonal matrices [98], the eigenspectrum of $\nabla^2_{\hat{\mathbf{p}}} f_{\mathrm{R}}(\hat{\mathbf{p}})$ can be modified by ϱ_b such that it includes an eigenvalue that asymptotically approaches $-\hat{\varpi}_{ik}$. Specifically, ϱ_b can be selected such that $\|(\breve{\boldsymbol{H}}^k + \hat{\varpi}_{ik}\mathbf{I}_\eta)^{-1}\|_{\mathrm{F}}^{-1} \leq \sum_{j=1}^{N} |\bar{\boldsymbol{H}}^{kj}\|_{\mathrm{F}}$. □

In light of the above result, it is proven that regardless of the node locations, a concave region of the WLS objective function is always located around each anchor $\mathbf{a}_i$. Thus, the objective function $f_{\mathrm{R}}(\vec{\hat{\mathbf{p}}})$ is not convex.

3.3 Matrix proximity problem formulation

Consider the optimisation problem given in equation (26) and assume $\hat{\mathbf{D}}$ is the unknown variable to be estimated. In this perspective, a LS-based positioning problem can be reformulated as a matrix-proximity problem, in which $\hat{\mathbf{P}}$ is computed from the *closest* EDM $\hat{\mathbf{D}}$ to the EDM-sample $\tilde{\mathbf{D}}$.

Due to unique properties of the EDMs, the matrix $\hat{\mathbf{D}}$ can be obtained as the solution of a convex optimisation problem based on the SDP formulation described in [54, 67].

3.3.1 Properties of the Euclidean distance matrices

In equation (24), we generally refer to $\mathbf{D}$ as an EDM. However, an EDM is mathematically defined as a distance matrix where the ij-th element is given by the squared-distance d_{ij}^2 [67, Chapter 6, pp. 493]. For the sake of clarity, hereafter, the EDM with absolute distances d_{ij}, will be denoted by $\mathbf{D}$ and referred to as an EDM in the *natural coordinates*. An EDM with squared distances d_{ij}^2, instead, will be denoted by $\mathbf{D}^{\circ 2}$ and referred to as an EDM in the *squared coordinates*.

Respectively, the subspaces of $\mathbf{D}$ and $\mathbf{D}^{\circ 2}$ are named as the EDM-subspace in the *natural* and *squared* coordinates and are defined as

$$\mathbb{EDM}^N \triangleq \{\mathbf{D} \,|\, \mathbf{D} = \mathcal{D}(\mathbf{P})\}, \tag{50}$$

$$\mathbb{EDM}_2^N \triangleq \{\mathbf{D}^{\circ 2} \,|\, \mathbf{D}^{\circ 2} = \mathcal{D}^{\circ 2}(\mathbf{P})\}, \tag{51}$$

where $^{\circ 2}$ indicates the point-wise squaring and N is the subspace dimensions.

In [67, Section 6.3, pp 498], it is shown that these subspaces are characterised by the following properties

i) $\mathbb{EDM}_2^N$ is a convex cone
ii) $\mathbb{EDM}^N$ is a non-convex cone
iii) $\mathbb{EDM}^N \subseteq \mathbb{EDM}_2^N$.

Furthermore, the subspace $\mathbb{EDM}_2^N$ benefits from an injective correspondence to the cone of the PSM described below.

Lemma L2 (Characterisation of an EDM in square coordinates via a PSM [67])**.**

Let $\mathcal{K}$ denote the double-centring Euclidean Kernel Transformation (EKT) given by

$$\mathbf{K} = \mathcal{K}(\mathbf{D}^{\circ 2}) \triangleq -\frac{1}{2}\,\mathbf{J}\cdot(\mathbf{D})^{\circ 2}\cdot\mathbf{J}^{\mathrm{T}}, \tag{52}$$

where $\mathbf{J}$ is the double-centring projection matrix defined as

$$\mathbf{J} \triangleq \mathbf{I}_{\mathrm{N}} - (\mathbf{1}_{\mathrm{N}}\cdot\mathbf{1}_{\mathrm{N}}^{\mathrm{T}})/N, \tag{53}$$

and $\mathbf{I}_{\mathrm{N}}$ is the identity matrix of N dimensions.

A matrix $\mathbf{D}^{\circ 2}$ is an EDM in squared-coordinates if and only if

$$\mathbf{D}^{\circ 2} \in \mathbb{EDM}_2^N \Leftrightarrow \begin{cases} \mathbf{K} \in \mathbb{S}_+^N, \\ \mathbf{D}^{\circ 2} \in \mathbb{S}_h^N, \end{cases} \tag{54}$$

where $\mathbb{S}_+^N$ and $\mathbb{S}_h^N$ denote the space of positive semi-definite and symmetric-hollow matrices of N dimensions.

Proof. See [67, Sec. 6.3, pp 498]. □

The matrix $\mathbf{K}$ obtained from equation (52) is referred to as the *double-centring Euclidean kernel*. Such a kernel is also associated to an endomorphism on the space of the *Gram-kernel* $\mathbf{G}_P \triangleq \mathbf{P}\cdot\mathbf{P}^{\mathrm{T}}$, *i.e.*

$$\mathbf{K}\cdot\mathbf{1}_{\mathrm{N}} = \mathbf{0}_{\mathrm{N}} \Leftrightarrow \mathbf{G}_P\cdot\mathbf{1}_{\mathrm{N}} = \mathbf{0}_{\mathrm{N}}. \tag{55}$$

Therefore, the matrix $\mathbf{K}$ preserves the same rank-deficiency property of $\mathbf{G}_P$ as, indeed, stated in the following corollary.

Corollary C1 (Rank-deficiency of the Euclidean Kernel [67])**.**
Let $\mathbf{D} = \mathcal{D}(\mathbf{P})$ *with* $\mathbf{P} \in \mathbb{R}^{N\times\eta}$*. Then*

$$\operatorname{rank}(\mathcal{K}(\mathbf{D}^{\circ 2})) = \eta. \tag{56}$$

Proof. See [67, Sec. 6.3, pp 498]. □

3.3.2 Projection techniques

As mentioned above, a LS-based positioning problem can be cast onto a matrix proximity problem, and specifically to an EDM proximity problem. In [67], four different approaches are proposed. In this subsection, however, we focus only on the three main principles on which a large variety of SDP-based positioning techniques have been developed [54, 68, 69, 78, 99–101].

Method 1: Projection on the $\mathbb{EDM}^N$ cone

The first approach is to find the closest EDM in $\mathbb{EDM}^N$. Specifically, the proximity problem is formulated as an optimisation constrained to the non-convex cone $\mathbb{EDM}^N$.

Problem PR1 (Projection on the $\mathbb{EDM}^N$ cone)**.**
Given an EDM-sample $\tilde{\mathbf{D}}$*, the closest* $\hat{\mathbf{D}} \in \mathbb{EDM}^N$ *is the minimizer of*

$$\begin{aligned} \min_{\hat{\mathbf{D}}} \quad & \left\| \mathbf{W} \circ \left(\tilde{\mathbf{D}} - \hat{\mathbf{D}} \right) \right\|_F^2, \\ \text{s.t.} \quad & \hat{\mathbf{D}} \in \mathbb{EDM}^N, \\ & \operatorname{rank}(\mathcal{K}(\hat{\mathbf{D}}^{\circ 2})) = \eta. \end{aligned} \tag{57}$$

Due to the non-convexity of both the domain and the rank-constraint, which is used to further refine the search-space of $\hat{\mathbf{D}}$, the above optimization problem is not convex. To circumvent this issue, the following changes were proposed [69].

Rewrite the ij-th term $(\tilde{d}_{ij} - \hat{d}_{ij})^2$ as a function of $\hat{d}_{ij}^2$

$$(\tilde{d}_{ij} - \hat{d}_{ij})^2 = \tilde{d}_{ij}^2 - 2\tilde{d}_{ij}\sqrt{\hat{d}_{ij}^2} + \hat{d}_{ij}^2, \tag{58}$$

and replace $\tilde{d}_{ij}\sqrt{\hat{d}_{ij}^2}$ by a new variable y_{ij}.

Impose the constraint $\tilde{d}_{ij}^2 - 2y_{ij} + \hat{d}_{ij}^2 \geq 0$, derived from the fact that the difference $(\tilde{d}_{ij} - \hat{d}_{ij})$ is squared, yields

$$\begin{bmatrix} \hat{d}_{ij}^2 & y_{ij} \\ y_{ij} & \tilde{d}_{ij}^2 \end{bmatrix} \succeq 0. \tag{59}$$

Finally, relax the rank-constraint $\text{rank}(\mathcal{K}(\hat{\mathbf{D}}^{\circ 2})) = \eta$ by the semi-definite property of the kernel, *i.e.* $\mathcal{K}(\hat{\mathbf{D}}^{\circ 2}) \succeq 0$, $(\cdot) \succeq 0$ indicates that the matrix on the left-side is positive semi-definite.

With all the above, the "convexised" formulation of equation (57) is given by

$$\begin{aligned} \min_{\hat{\mathbf{D}}^{\circ 2}, \mathbf{Y}} \quad & \sum_{i=1}^{N} \sum_{\substack{j=1 \\ j \neq i}}^{N} w_{ij}^2 (\hat{d}_{ij}^2 - 2y_{ij}), \\ \text{s.t.} \quad & \begin{bmatrix} \hat{d}_{ij}^2 & y_{ij} \\ y_{ij} & \tilde{d}_{ij}^2 \end{bmatrix} \succeq 0 \, \forall i, j, \\ & \mathbf{Y} \in \mathbb{S}_h^N, \\ & \hat{\mathbf{D}}^{\circ 2} \in \mathbb{EDM}_2^N, \\ & \mathcal{K}(\hat{\mathbf{D}}^{\circ 2}) \succeq 0, \end{aligned} \tag{60}$$

Method 2: Projection on the $\mathbb{EDM}_2^N$ cone

The second approach is to find the closest $\hat{\mathbf{D}}^{\circ 2}$ in $\mathbb{EDM}_2^N$. This time, the proximity problem is formulated as an optimisation constrained to the convex cone of EDM in squared coordinates.

Problem PR2 (Projection on the $\mathbb{EDM}_2^N$ cone)**.**

Given a EDM-sample $\tilde{\mathbf{D}}$*, the closest* $\hat{\mathbf{D}}^{\circ 2} \in \mathbb{EDM}_2^N$ *is the minimiser of*

$$\begin{aligned} \min_{\hat{\mathbf{D}}^{\circ 2}} \quad & \sum_{i=1}^{N} \sum_{\substack{j=1 \\ j \neq i}}^{N} w_{ij}^2 (\tilde{d}_{ij}^2 - \hat{d}_{ij}^2)^2, \\ \text{s.t.} \quad & \hat{\mathbf{D}}^{\circ 2} \in \mathbb{EDM}_2^N, \\ & \text{rank}(\mathcal{K}(\hat{\mathbf{D}}^{\circ 2})) = \eta. \end{aligned} \tag{61}$$

In contrast to the optimisation problem given in equation (57), this formulation benefits from a strictly convex quadratic objective function in the variable $\hat{\mathbf{D}}^{\circ 2}$

and a convex domain given by the EDM cone $\mathbb{EDM}_2^N$. However, the non-convex rank constraint shown in equation (61) makes the minimisation problem difficult to solve. In [68], it is proposed to relax such constraint with $\mathcal{K}(\hat{\mathbf{D}}^{\circ 2}) \succeq 0$. This relaxation changes the non-convex optimisation problem into a convex one, which can be solved with SDP-based minimisation techniques.

Method 3: Projection on the $\mathbb{S}_+^N$ cone

The third method is based on the injective correspondence between the subspaces of EDM and PSM. Specifically, the new objective is to estimate the closest Euclidean Kernel (EK) $\hat{\mathbf{K}} \in \mathbb{S}_+^N$ to the EK-sample $\tilde{\mathbf{K}} \triangleq \mathcal{K}(\tilde{\mathbf{D}}^{\circ 2})$ [55, 78].

Problem PR3 (Projection on the $\mathbb{S}_+^N$ cone)**.**

Given an EDM-sample $\tilde{\mathbf{D}}$ *and the associated EK-sample* $\tilde{\mathbf{K}}$*, the closest kernel* $\hat{\mathbf{K}} \in \mathbb{S}_+^N$ *is the minimiser of*

$$\begin{aligned} \min_{\hat{\mathbf{K}}} \quad & \left\| \mathbf{W} \circ \left(\mathcal{K}^{-1}(\tilde{\mathbf{K}}) - \mathcal{K}^{-1}(\hat{\mathbf{K}}) \right) \right\|_F^2, \\ \text{s.t.} \quad & \hat{\mathbf{K}} \in \mathbb{S}_+^N, \\ & \operatorname{rank}(\hat{\mathbf{K}}) = \eta, \end{aligned} \tag{62}$$

where $\mathcal{K}^{-1}$ *is the Inverse Euclidean Kernel Transformation (I-EKT) given by*

$$\mathcal{K}^{-1}(\mathbf{K}) = \mathbf{1}_{\mathrm{N}} \cdot \operatorname{diag}(\mathbf{K})^{\mathrm{T}} + \operatorname{diag}(\mathbf{K}) \cdot \mathbf{1}_{\mathrm{N}}^{\mathrm{T}} - 2\mathbf{K}. \tag{63}$$

As in methods 1 and 2, the rank-constraint implies non-convexity. Therefore, the relaxation $\hat{\mathbf{K}} \succeq 0$ is necessary to convex the problem. To this end, relax the equality $\hat{\mathbf{K}} = \hat{\mathbf{P}}^{\mathrm{T}}\hat{\mathbf{P}}$ to the matrix inequality $\hat{\mathbf{K}} - \hat{\mathbf{P}}^{\mathrm{T}}\hat{\mathbf{P}} \succeq 0$. It is well known that by the Schur's complement [102], the aforementioned matrix inequality is equivalent to

$$\hat{\mathbf{K}}_{\mathrm{P}} \triangleq \begin{bmatrix} \mathbf{I}_\eta & \hat{\mathbf{P}}^{\mathrm{T}} \\ \hat{\mathbf{P}} & \hat{\mathbf{K}} \end{bmatrix} \succeq 0. \tag{64}$$

Based on the above, both constraints in equation (62) can be replaced with the above convex relaxation to obtain the following convexised formulation of problem PR3

$$\begin{aligned}
\min_{\hat{\mathbf{K}}_{\mathrm{P}}} \quad & \sum_{i=1}^{N}\sum_{\substack{j=1\\ i\neq j}}^{N} w_{ij}^2(\tilde{d}_{ij}^2 - \hat{d}_{ij}^2)^2, \\
\text{s.t.} \quad & \left[\hat{\mathbf{K}}_{\mathrm{P}}\right]_{1:\eta,1:\eta} = \mathbf{I}_\eta, \\
& \hat{d}_{ij}^2 = [\mathbf{0}, \mathbf{e}_{ij}]\hat{\mathbf{K}}_{\mathrm{P}}[\mathbf{0}, \mathbf{e}_{ij}]^{\mathrm{T}} \ \ \forall i,j, \\
& \hat{\mathbf{K}}_{\mathrm{P}} \succeq 0,
\end{aligned} \tag{65}$$

where $\mathbf{e}_{ij} \in \mathbb{R}^N$ is a row-vector with $[\mathbf{e}_{ij}]_i = 1$, $[\mathbf{e}_{ij}]_j = -1$ and 0 elsewhere.

A special case of the minimization shown in equation (62) is obtained when all distances are measured and $\tilde{d}_{ij} \geq 0$, $\forall ij$. The closest kernel, indeed, can be computed via a spectrum-truncation in which only the η-highest eigenvectors and eigenvalues are kept, *i.e.*

$$\hat{\mathbf{K}} = \mathbf{U}_\eta \cdot \mathbf{\Sigma}_\eta \cdot \mathbf{V}_\eta^{\mathrm{T}}, \tag{66}$$

where the matrix $\mathbf{\Sigma}_\eta \in \mathbb{R}^{\eta\times\eta}$ is a diagonal matrix with $\left[\mathbf{\Sigma}_\eta\right]_{ii}$ corresponding to the i-th highest singular values of $\hat{\mathbf{K}}$, and $\mathbf{U}_\eta \in \mathbb{R}^{N\times\eta}$ and $\mathbf{V}_\eta \in \mathbb{R}^{N\times\eta}$ are the corresponding left and right singular-vector matrices, respectively.

This algebraic solution is the basis for the class of MDS-based positioning algorithms proposed in the literature [66, 103, 104].

Graphical interpretation of the SDP-methods

To conclude this subsection, in Figure 8 we offer an illustration of the aforementioned projection methods.

To begin with, consider all subspaces of interest, namely the $\mathbb{EDM}^N$, the $\mathbb{EDM}_2^N$ and the $\mathbb{S}_+^N$. The EDM cones (in natural and squared coordinates) are defined in the intersection $\mathbb{S}^N \cap \mathbb{R}_+^{N\times N}$, where $\mathbb{S}^N$ and $\mathbb{R}_+^{N\times N}$ denote the subspace of symmetric and real-positive matrices of N dimensions, respectively. Following the EDM properties described in Section 3.3.1, the subspace $\mathbb{EDM}^N$ is drawn as a non-convex cone included in the convex cone $\mathbb{EDM}_2^N$. The subspace of the PSMs, which is defined as a convex subset of $\mathbb{S}^N$, is represented by a cone that intersects $\mathbb{EDM}_2^N$ and $\mathbb{EDM}^N$ only at the origin, *i.e.* $\mathbb{EDM}_2^N \cap \mathbb{S}_+^N = \mathbf{0}_N$ [67]. The EKT given in equation (52) is represented as a mapping from $\mathbb{EDM}_2^N$ to

$\mathbb{S}_+^N$, while the I-EKT goes from $\mathbb{S}_+^N$ to $\mathbb{EDM}_2^N$. These two functions form a cycle that is indicated by the black arrows.

The projection of $\tilde{\mathbf{D}}$ onto the non-convex $\mathbb{EDM}^N$ cone (Method 1) is represented by the blue-arrow, Method 2 by the green arrow and finally, Method 3 is represented by the red arrows. In the latter, we have specifically illustrated that the EK-sample $\tilde{\mathbf{K}}$ is computed from $\tilde{\mathbf{D}}$, that $\tilde{\mathbf{K}}$ is approximated with the closest EK $\hat{\mathbf{K}}$, and that $\hat{\mathbf{D}}^{\circ 2}$ is obtained from $\hat{\mathbf{K}}$ via the I-EKT projection. Notice that in Figure 8, we have also indicated that each method finds a solution on the boundary of the corresponding cone of projection.

The reason is that in most of the cases, $\tilde{\mathbf{D}} \notin \mathbb{EDM}^N$, $\tilde{\mathbf{D}}^{\circ 2} \notin \mathbb{EDM}_2^N$ and $\tilde{\mathbf{K}} \notin \mathbb{S}_+^N$, therefore the closest matrices are at the boundary of the cones. Furthermore, we have also illustrated that $\hat{\mathbf{D}} \neq \hat{\mathbf{D}}^{\circ 2} \neq \mathcal{K}^{-1}(\hat{\mathbf{K}})$ since each projection strategy operates on different subspaces where errors are propagated differently. For this reason, it is difficult to decide a priori which method can be superior to all the others since the accuracy of the estimation method depends on the particular scenario and on the perturbation.

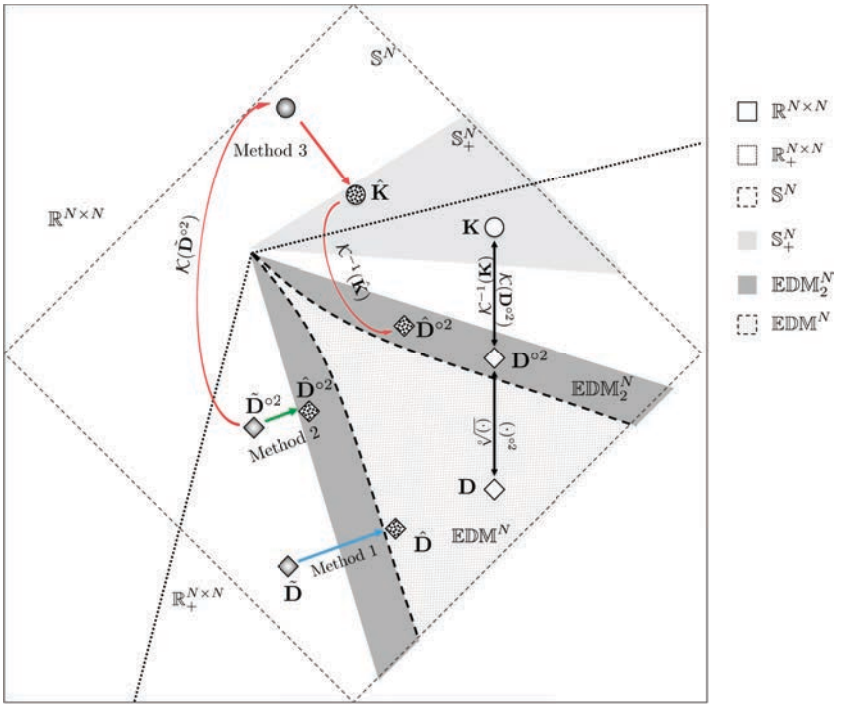

Fig 8. Intuitive representation of the SDP Methods 1, 2 and 3.

3.4 Summary and discussions

In this chapter, we formulated the distance-based positioning problem as a WLS optimisation. By Theorem T1, we have shown that under the assumptions of ranging error with zero-mean Gaussian distribution (LOS), such a formulation is equivalent to a ML estimation problem. We have provided a comprehensive analysis of the WLS-objective, derived the Gradient and the Hessian in closed-form and shown that the considered objective function is not convex. Finally, we have discussed the equivalent matrix-proximity problem formulation of the problem, which is the basis of the SDP-based algorithms, used as a comparison to the algorithms proposed in this thesis.

4 Error analysis of distance-based positioning

In this chapter, we continue the analysis of the positioning problem with the derivation of its fundamental limits. We investigate the conditions for which the ML-estimator, or equivalently a WLS-estimator, is asymptotically convergent to the true parameters, *i.e.* it is *consistent*. Specifically, we show that the consistency of ML estimator can be determined by the condition of strong-localisability of a network (Theorem T6). In addition to the above, we offer a generalised study on the fundamental limits to the achievable Mean Square Error (MSE)

$$\mathrm{MSE}(\mathbf{P}) \triangleq \mathrm{E}_{\tilde{\mathbf{d}}}\left\{(\hat{\mathbf{P}}-\mathbf{P})(\hat{\mathbf{P}}-\mathbf{P})^{\mathrm{T}}\right\}, \tag{67}$$

where $\mathrm{E}\{\cdot\}_{\tilde{\mathbf{d}}}$ denotes the expectation with respect to the variables $\vec{\tilde{\mathbf{d}}}$.

In contrast to previous works [51, 92, 105–108], we propose a distance-model dependent CRLB for cooperative positioning (Theorem T7) and derive a recursive decomposition of the Equivalent Fisher Information Matrix (EFIM) – information matrix associated to k-th target location – (Theorem T8) that permits the quantification of the information-couplings established with inter-node cooperation (Corollary C2) in an arbitrary large network.

We apply these findings to gain useful insights about the coupling/decoupling effects in a network, to prove that the addition of a cooperative link can not degrade the location accuracy of any other node in the network (Corollary C3), and to compute the closed-form expressions of the CRLB of a cooperative network in LOS (Lemma L3) and NLOS (Lemma L3) scenarios.

In addition to all of the above, we also consider the case of low SNR regimé (large noise) and study the difference between the CRLB and the performance of a ML estimator in a simple non-cooperative scenario. We demonstrate that location ambiguities often occur when the target is outside the convex-hull formed by the anchors, and that such a problem can be predicted by the Hammersley-Chapmann-Robbins Bound (HCRB) and the Abel Hybrid Bound (AHB) derived in the thesis (Section 4.5 as well as by the minimum entropy bound proposed in [109].

4.1 Fundamentals of the network localisability theory

We start with a brief review of the fundamentals of the theory of network localisability [54, 63, 78, 110–122].

Let $G = (V, E, W)$ be a weighted graph representing the network of coordinate matrix $\mathbf{P}$, EDM $\mathbf{D}$ and connectivity $\mathbf{C}$, where $V \triangleq \{v_i^G\}$, $E \triangleq \{e_{ij}^G\}$ and $W \triangleq \{w_{ij}^G\}$ denote the set of nodes, connected links and edge-weights with $w_{ij}^G = d_{ij}$, respectively. Let P^G denote a realisation of the graph G in the Euclidean space of η dimensions, such that the distance between a pair of vertexes v_i^G and v_j^G connected by the edge e_{ij}^G is equal to w_{ij}^G.

Definition D1 (Localisable Network [63, 115])**.**

The network of coordinate matrix $\mathbf{P}$*, EDM* $\mathbf{D}$ *and connectivity* $\mathbf{C}$ *is localisable if the corresponding graph realization* P^G *embedded in the Euclidean space of* η *dimensions, is uniquely determined up to rotations, translations and reflections.*

The problem of recognising the uniqueness of a graph realisation, *i.e.* to assert that exists only one P^G such that the length of the edge e_{ij}^G is equal to the edge-weight w_{ij}^G, is known in the literature as the graph realisation problem and in [123], it was proved to be an Non-deterministic Polynomial-time hard (NP-hard) problem. In [63] and later also in [110, 111], the authors demonstrated that with the aid of rigidity theory [120] this problem can be solved in polynomial time if $\eta = 2$ and the following theorem holds.

Theorem T2 (Uniqueness of a Graph Realisation [63, 115])**.**

The realisation of a graph G *is unique in the Euclidean space of two dimensions if and only if* P^G *is tri-connected and redundantly rigid.*

Proof. See [63]. □

Recently, on the basis of the theory of SDP, it was shown that with the assumptions of a graph (network) with $N_\mathrm{A} \geq \eta + 1$ known vertices (anchors), Theorem T2 can be generalised to any η Euclidean dimensions.

Theorem T3 (Network Localisability [54])**.**

Suppose that a network P^G *with* $N_\mathrm{A} = \eta + 1$ *fixed locations is connected. Then, the following statements are equivalent*

1) The network is uniquely localisable

2) The max rank solution of the SDP problem given in equation (65) *with* $\tilde{\mathbf{D}} = \mathbf{D}$ *and modified with the constraints* $\hat{\mathbf{p}}_i = \mathbf{a}_i$*, has rank* η

3) The solution matrix of the problem (65) *with* $\tilde{\mathbf{D}} = \mathbf{D}$ *and modified with the constraints* $\hat{\mathbf{p}}_i = \mathbf{a}_i$*, represented by* $\hat{\mathbf{K}}_{\mathrm{P}}$*, satisfies* $\hat{\mathbf{K}} = \mathbf{P}^{\mathrm{T}}\mathbf{P}$*.*

Proof. See [54]. □

Based on the above, the fact that a network is localisable implies that for a given coordinate matrix $\mathbf{P}$, $N_{\mathrm{A}} = \eta + 1$ anchors, EDM $\mathbf{D}$ and connectivity $\mathbf{C}$, the positioning problem defined as in equation (65) admits only the exact solution $\hat{\mathbf{P}} = \mathbf{P}$.

Finally, we introduce the definition of strongly-localisable network and, the SDP-based theorem used for its characterisation.

Definition D2 (Strongly-localisable network [54])**.**

We say that a network with coordinate matrix $\mathbf{P}$*,* $N_{\mathrm{A}} = \eta + 1$ *anchors, EDM* $\mathbf{D}$ *and connectivity* $\mathbf{C}$ *is strongly-localisable, if the dual of the SDP-based optimisation problem given in equation* (65) *with* $\tilde{\mathbf{D}} = \mathbf{D}$ *and modified with the constraints* $\hat{\mathbf{p}}_i = \mathbf{a}_i$*, has an optimal dual slack matrix with rank* N_{T}*.*

In plain words, a strongly-localisable network is a network that is uniquely localisable and remains so if the location of the nodes is slightly modified, *i.e.* the network with coordinate matrix $\mathbf{P'} = \mathbf{P'} + \mathbf{\Delta}_{\mathrm{P}}$, where $\mathbf{\Delta}_{\mathrm{P}} \in \mathbb{R}^{N \times \eta}$ is a small perturbation, $\mathbf{D'} = \mathcal{D}(\mathbf{P'})$ and connectivity $\mathbf{C}$ is uniquely localisable.

Theorem T4 (Strong-Localisability [54])**.**

If a localisation problem contains a sub-problem (sub-graph) that is strongly localisable, then the sub-matrix solution corresponding to the sub-problem in the SDP formulation of equation (65) *with* $\tilde{\mathbf{D}} = \mathbf{D}$ *and modified with the constraints* $\hat{\mathbf{p}}_i = \mathbf{a}_i$ *has rank* η*. That is, the SDP relaxation of a positioning problem with exact distances computes a solution that localises all possibly localisable targets.*

Proof. See Theorem 4 of [54]. □

4.2 Consistency of a ML location estimator

Consider a general formulation of a distance based estimation problem and let $\vec{\hat{\mathbf{p}}}$ be an estimate of $\vec{\mathbf{p}}$. The consistency of $\vec{\hat{\mathbf{p}}}$ can be defined as follows.

Definition D3 (Consistent estimator)**.**

Let $\vec{\hat{\mathbf{p}}}$ be an estimate of $\vec{\mathbf{p}}$. We say that $\vec{\hat{\mathbf{p}}}$ is consistent if [45]

$$\lim_{K_{ij}\to\infty} \Pr\{\vec{\hat{\mathbf{p}}} - \vec{\mathbf{p}}\} = 0, \tag{68}$$

where K_{ij} is the number of samples of each ranging d_{ij}.

Next, focus on the case of a ML estimator which can be designed over the following generalised likelihood function.

Definition D4 (Generalised likelihood function of $\vec{\hat{\mathbf{p}}}$)**.**

Consider iid distance measurements $\{\tilde{d}_{ij}\}$ and let $f_{ij}(\tilde{d}_{ij}|d_{ij})$ denote the pdf of $\tilde{d}_{ij}$ parametrised by d_{ij}. The generalised likelihood function of the estimate $\vec{\hat{\mathbf{p}}}$ of $\vec{\mathbf{p}}$, denoted by $\mathcal{L}(\vec{\hat{\mathbf{p}}}|\tilde{\mathbf{d}})$, is defined as

$$\mathcal{L}(\vec{\hat{\mathbf{p}}}|\tilde{\mathbf{d}}) \triangleq \prod_{ij\in E} f_{ij}(\tilde{d}_{ij}|\hat{d}_{ij}). \tag{69}$$

Theorem T5 (Properties of a consistent ML estimator [124])**.**

Let $\hat{\mathbf{P}}_{\mathrm{ML}}$ (the matrix form of $\vec{\hat{\mathbf{p}}}_{\mathrm{ML}}$) be the ML estimate of $\mathbf{P}$. Then, $\hat{\mathbf{P}}_{\mathrm{ML}}$ is consistent if all the following properties hold

a) Identification, *i.e. $\nexists \mathbf{P}^{(1)} \in \mathbb{R}^{N\times\eta}$ with $\mathbf{P}^{(1)} \neq \mathbf{P}$ such that $\mathcal{L}\big(\vec{\hat{\mathbf{p}}}|\vec{\mathbf{d}}\big) = \mathcal{L}\big(\vec{\hat{\mathbf{p}}}|\vec{\mathbf{d}}^{(1)}\big)$, where $\mathcal{L}\big(\vec{\hat{\mathbf{p}}}|\vec{\mathbf{d}}\big)$ is the limiting likelihood function parametrized by $\vec{\mathbf{d}}$ and $\vec{\mathbf{d}}^{(1)}$ is the vectorised form of $\mathbf{D}_1 \triangleq \mathcal{D}(\mathbf{P}^{(1)})$*

b) Compactness, *i.e. the limiting likelihood function $\mathcal{L}\big(\vec{\hat{\mathbf{p}}}|\vec{\mathbf{d}}\big)$ cannot approach the maximum value arbitrarily close to some other point than $\vec{\mathbf{p}}^{(1)} \neq \vec{\mathbf{p}}$, $\vec{\mathbf{p}}^{(1)} \in B_P$, where B_P is a compact set with $\vec{\mathbf{p}} \in B_P$*

c) Continuity, *i.e. $\ln \mathcal{L}\big(\vec{\hat{\mathbf{p}}}|\vec{\tilde{\mathbf{d}}}\big)$ is continuous with probability one*

d) Dominance, *i.e. $|\ln \mathcal{L}\big(\vec{\hat{\mathbf{p}}}|\vec{\tilde{\mathbf{d}}}\big)| < \mathcal{T}(\vec{\hat{\mathbf{p}}})$, where $\mathcal{T}(\vec{\hat{\mathbf{p}}})$ is an integrable function.*

Proof. See Theorem 2.5 of [124]. □

Theorem T6 (Consistency of a ML-based Position Estimator)**.**

Consider a positioning problem in a network with coordinate matrix $\mathbf{P}$, $N_{\mathrm{A}} = \eta + 1$ anchors, EDM $\mathbf{D}$ and connectivity $\mathbf{C}$. If the network is strongly-localisable and the likelihood function $\mathcal{L}(\vec{\hat{\mathbf{p}}}|\tilde{\mathbf{d}})$ is obtained as the product of unbiased pdf of $\tilde{d}_{ij}$ with maximum in d_{ij}, then $\hat{\mathbf{P}}$ is consistent.

Proof. The continuity and dominance properties of a ML-estimator can be readily shown by the facts that the $\ln \mathcal{L}\big(\vec{\tilde{\mathbf{p}}}|\vec{\tilde{\mathbf{d}}}\big)$ is a regular function [45, 124].

To prove the identification and the compactness properties, on the other hand, we exploit the facts that the distributions $f_{ij}(\tilde{d}_{ij}|d_{ij})$, $\forall\, i,j$ are unbiased and the network is strongly-localisable. The former implies that $\forall\, i,j$, then for $K_{ij} \to \infty$ the likelihood function $\mathcal{L}\big(\vec{\tilde{\mathbf{p}}}|\vec{\tilde{\mathbf{d}}}\big)$ converges to the limiting likelihood function $\mathcal{L}\big(\vec{\tilde{\mathbf{p}}}|\vec{\mathbf{d}}\big)$. The latter implies that the network is uniquely localisable [54]. Therefore, by Theorem T3, $\nexists \mathbf{P}^{(1)} \in \mathbb{R}^{N\times\eta}$ with $\mathbf{P}^{(1)} \neq \mathbf{P}$ such that $\mathbf{D}^{(1)} = \mathbf{D}$. In other words the distances $\vec{\mathbf{d}}$, and consequently, $\mathcal{L}\big(\vec{\tilde{\mathbf{p}}}|\vec{\mathbf{d}}\big)$ are uniquely determined by $\mathbf{P}$. Hence, the identification property holds.

Finally, we consider the compactness condition. By definition, if a network with coordinate matrix $\mathbf{P}$ is strongly-localisable, then a network with $\mathbf{P}^{(1)}$ obtained from a small perturbation of $\mathbf{P}$, *i.e.* $\mathbf{P}^{(1)} = \mathbf{P} + \mathbf{\Delta}_{\mathrm{P}}$ is still uniquely localisable. This implies that if $\mathbf{P}$ is strongly-localisable, $\mathbf{P}$ and $\mathbf{P}^{(1)} \in B_P$, and given that $\mathcal{L}$ is a regular function, we can derive $\mathbf{P}^{(1)}$ such that $\mathcal{L}\big(\vec{\tilde{\mathbf{p}}}|\vec{\mathbf{d}}\big) - \mathcal{L}\big(\vec{\tilde{\mathbf{p}}}|\vec{\mathbf{d}}^{(1)}\big) < \epsilon_L$, with ϵ_L arbitrarily small. Finally, since $\mathbf{P}^{(1)}$ is uniquely localisable, $\nexists \mathbf{P}^{(2)} \in \mathbb{R}^{N\times\eta}$ such that $\vec{\mathbf{d}}^{(1)} = \vec{\mathbf{d}}^{(2)}$, and consequently, $\mathcal{L}\big(\vec{\tilde{\mathbf{p}}}|\vec{\mathbf{d}}^{(1)}\big) = \mathcal{L}\big(\vec{\tilde{\mathbf{p}}}|\vec{\mathbf{d}}^{(2)}\big) > \mathcal{L}\big(\vec{\tilde{\mathbf{p}}}|\vec{\mathbf{d}}\big) - \epsilon_L$. Thus the assumption that the network of coordinate $\mathbf{P}$ is strongly-localisable implies that the compactness property holds. □

Notice that in order to verify the aforementioned properties it is required that the locations of all nodes in the network are known *a priori*. Clearly, this is not the case when the objective is to estimate the node locations of a network. Therefore, the consistency of a ML-based positioning algorithm can not be guaranteed in real scenarios. However, it is possible to infer about consistency from measurable metrics, such as the meshness-ratio given by equation (21). To investigate the relationship between the meshness-ratio and the strong localisability of a network, we use the definition provided in [54, pp. 11] and derive the empirical cumulative distribution function (cdf) of the strong localisability test defined as

$$\pi_s \triangleq \begin{cases} 1 & \text{if the network is strong localisable,} \\ 0 & \text{if the network is not strong localisable.} \end{cases} \tag{70}$$

The result shown in Figure 9 illustrates that the cdf of π_s increases with m and that it grows earlier when the number of targets is larger.

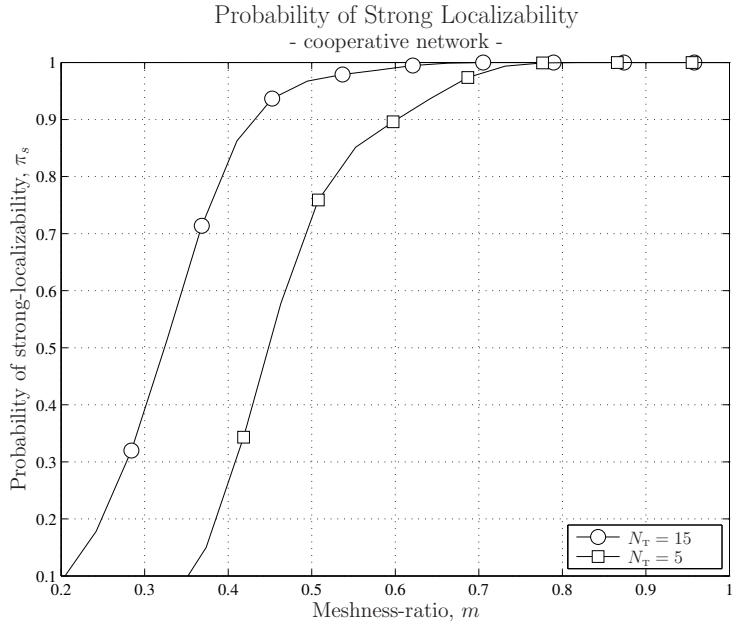

Fig 9. Probability of strong-localizability as a function of the meshness-ratio. Networks are randomly generated within a square of 14.14×14.14 squared meters, with anchors at the corner of the square. Meshness is varied by changing the connectivity range $R_{\mathbf{MAX}}$ within $[8, 20]$ meters.

The reason is obviously related to the number of connections in the network, *i.e.* the larger the number of connections, the higher the rigidity of the network [63, 117]. Indeed, comparing a network of $N_T = 15$ targets with a network of $N_T = 5$ targets, it is noticed that in the former the probability of strong-localisabile network is equal to 0.95 when $m = 0.45$, while in the latter the same probability is achieved with $m = 0.65$.

4.3 The Cramér-Rao lower bound for range-positioning

The derivation of the CRLB for cooperative and non-cooperative positioning has been widely addressed in the literature tackling specific scenarios and/or assumptions. For instance, in [51] the CRLB was derived under the assumptions that ranging errors are random variables with zero-mean Gaussian distribution. In [92], the bound was derived from a more generic ranging model, but addressing

a non-cooperative positioning scenario. In [106, 107], the authors focused on wideband technologies and derived a generic CRLB based on the information inherent in the receiving waveform.

In contrast to the aforementioned solutions, the proposed CRLB derivation relies only on the knowledge of the ranging error pdf (biased or unbiased). Therefore it can be considered an alternative to [106, 107] as well as a generalisation of [92].

Theorem T7 (Generalised CRLB for Range-Positioning)**.**

Given a network with coordinate matrix $\mathbf{P}$*,* $N_{\mathrm{A}} = \eta + 1$ *anchors, EDM* $\mathbf{D}$*, connectivity* $\mathbf{C}$ *and likelihood function* $\mathcal{L}(\vec{\tilde{\mathbf{p}}}|\tilde{\mathbf{d}})$*, the* CRLB *on the covariance matrix of* $\vec{\hat{\mathbf{p}}}$ *is given by*

$$\mathrm{CRLB}(\mathbf{P}) \triangleq \mathbf{J}_d, \tag{71}$$

where $\mathbf{J}_d$ *is the inverse of FIM* $\mathbf{F}_d$ *given by*

$$\mathbf{F}_d \triangleq \breve{\mathbf{F}}_d + \bar{\mathbf{F}}_d, \tag{72}$$

with $\breve{\mathbf{F}}_d$ *and* $\bar{\mathbf{F}}_d$ *denoting a block-diagonal and a block-off-diagonal matrices, respectively obtained as*

$$[\breve{\mathbf{F}}_d]_{ii}^{\eta} = \breve{\mathbf{F}}_d^k \triangleq \sum_{j=1}^{N} \zeta_{ij} \boldsymbol{\Upsilon}_{ij}, \tag{73}$$

$$[\bar{\mathbf{F}}_d]_{ij}^{\eta} = \bar{\mathbf{F}}_d^{ij} \triangleq -\zeta_{ij} \boldsymbol{\Upsilon}_{ij}, \tag{74}$$

where

$$\zeta_{ij} \triangleq c_{ij} \int_{-\infty}^{\infty} \frac{\phi^2(\nu_{ij})}{\mathcal{L}_{ij}(\hat{\mathbf{p}}_i \hat{\mathbf{p}}_j | \tilde{d}_{ij})} \, \mathrm{d}\nu_{ij}, \tag{75}$$

$\mathcal{L}_{ij}(\hat{\mathbf{p}}_i \hat{\mathbf{p}}_j | \tilde{d}_{ij}) = f_{ij}(\tilde{d}_{ij} | \hat{d}_{ij})$ *is the likelihood of* $(\hat{\mathbf{p}}_i, \hat{\mathbf{p}}_j)$ *given* $\tilde{d}_{ij}$ *and* $\phi(\nu_{ij})$ *is the unbiased distribution of* $\tilde{d}_{ij}$*, i.e.* $\mathrm{E}_{\nu_{ij}}\{\nu_{ij} - d_{ij}\} = 0$*.*

Proof. Consider the log-likelihood function of $\vec{\hat{\mathbf{p}}}$ given by

$$\ln(\mathcal{L}(\vec{\hat{\mathbf{p}}}|\tilde{\mathbf{d}})) \triangleq \sum_{i=1}^{N} \sum_{\substack{j=1 \\ j \neq i}}^{N} c_{ij} \ln\left(\mathcal{L}_{ij}(\mathbf{p}_i, \mathbf{p}_j | \tilde{d}_{ij})\right). \tag{76}$$

The FIM, denoted by $\mathbf{F}_d$, is by definition equal to

$$\mathbf{F}_d \triangleq \mathrm{E}_{\tilde{\mathbf{d}}} \left\{ \nabla_{\vec{\hat{\mathbf{p}}}}^{\mathrm{T}} \ln\left(\mathcal{L}(\vec{\hat{\mathbf{p}}}|\vec{\tilde{\mathbf{d}}})\right) \nabla_{\vec{\hat{\mathbf{p}}}} \ln\left(\mathcal{L}(\vec{\hat{\mathbf{p}}}|\vec{\tilde{\mathbf{d}}})\right) \right\} \Big|_{\vec{\hat{\mathbf{p}}} = \vec{\mathbf{p}}}, \tag{77}$$

where the partial derivative $\frac{\partial}{\partial \hat{p}_i^n} \ln\left(\mathcal{L}(\vec{\hat{\mathbf{p}}}|\vec{\tilde{\mathbf{d}}})\right)$ is given by

$$\frac{\partial}{\partial \hat{p}_i^n} \ln\left(\mathcal{L}(\vec{\hat{\mathbf{p}}}|\vec{\tilde{\mathbf{d}}})\right) = -\sum_{j=1}^{N} \frac{(\hat{p}_i^n - \hat{p}_j^n)}{\hat{d}_{ij}} \frac{c_{ij}}{\mathcal{L}_{ij}(\hat{\mathbf{p}}_i\hat{\mathbf{p}}_j|\tilde{d}_{ij})} \frac{\mathrm{d}}{\mathrm{d}\hat{d}_{ij}} f_{ij}(\tilde{d}_{ij}|\hat{d}_{ij}), \quad (78)$$

where we intentionally used $f_{ij}(\tilde{d}_{ij}|\hat{d}_{ij})$ instead of $\mathcal{L}_{ij}(\hat{\mathbf{p}}_i\hat{\mathbf{p}}_j|\tilde{d}_{ij})$ to explicate the dependence to $\hat{d}_{ij}$.

From equation (77), we decompose $\mathbf{F}_d$ in a block-diagonal and a block-off-diagonal matrices, as

$$\mathbf{F}_d = \breve{\mathbf{F}}_d + \bar{\mathbf{F}}_d, \quad (79)$$

where $\breve{\mathbf{F}}_d$ and $\bar{\mathbf{F}}_d$.

In order to compute the CRLB, that is the bound to the covariance matrix of an unbiased estimator of $\vec{\mathbf{p}}$, we replace $\tilde{d}_{ij}$ by the unbiased random variable $\nu_{ij} \triangleq \tilde{d}_{ij} - \mu_{ij}$, where $\mu_{ij} \triangleq \mathrm{E}_{\tilde{d}_{ij}}\{\tilde{d}_{ij} - d_{ij}\}$. Consequently, the pdf $f_{ij}(\tilde{d}_{ij}|\hat{d}_{ij})$ is also replaced by the unbiased distribution $\phi_{ij}(\nu_{ij})$.

With these changes, the block-matrices of $\breve{\mathbf{F}}_d$ and $\bar{\mathbf{F}}_d$ can be computed as

$$\begin{aligned}[\breve{\mathbf{F}}_d]_{ii}^{\eta} = \breve{\mathbf{F}}_d^i &\triangleq \mathrm{E}_{\boldsymbol{\nu}}\left\{\sum_{j=1}^{N}\sum_{q=1}^{N} \frac{c_{ij}c_{iq}\phi(\nu_{iq})\phi(\nu_{kj})(\hat{\mathbf{p}}_i - \hat{\mathbf{p}}_j)^{\mathrm{T}}(\hat{\mathbf{p}}_i - \hat{\mathbf{p}}_q)}{\mathcal{L}_{ij}(\hat{\mathbf{p}}_i\hat{\mathbf{p}}_j|\tilde{d}_{ij})\mathcal{L}_{iq}(\hat{\mathbf{p}}_i\hat{\mathbf{p}}_q|\tilde{d}_{iq})\hat{d}_{ij}\hat{d}_{iq}}\right\}\Bigg|_{\vec{\hat{\mathbf{p}}}=\vec{\mathbf{p}}} \quad (80)\\ &= \sum_{j=1}^{N} \mathrm{E}_{\boldsymbol{\nu}}\left\{\frac{c_{ij}c_{iq}\phi^2(\nu_{ij})}{\mathcal{L}_{ij}^2(\hat{\mathbf{p}}_i\hat{\mathbf{p}}_j|\tilde{d}_{ij})}\right\}\Bigg|_{\vec{\hat{\mathbf{p}}}=\vec{\mathbf{p}}} \boldsymbol{\Upsilon}_{ij} = \sum_{j=1}^{N} \zeta_{ij}\boldsymbol{\Upsilon}_{ij},\end{aligned}$$

$$\begin{aligned}[\bar{\mathbf{F}}_d]_{ij}^{\eta} = \bar{\mathbf{F}}_d^{ij} &\triangleq \mathrm{E}_{\boldsymbol{\nu}}\left\{\sum_{t=1}^{N}\sum_{q=1}^{N} \frac{c_{it}c_{jq}\phi(\nu_{it})\phi(\nu_{jq})(\hat{\mathbf{p}}_i - \hat{\mathbf{p}}_t)^{\mathrm{T}}(\hat{\mathbf{p}}_j - \hat{\mathbf{p}}_q)}{\mathcal{L}_{it}(\hat{\mathbf{p}}_i\hat{\mathbf{p}}_t|\tilde{d}_{it})\mathcal{L}_{jq}(\hat{\mathbf{p}}_j\hat{\mathbf{p}}_q|\tilde{d}_{jq})\hat{d}_{it}\hat{d}_{jq}}\right\}\Bigg|_{\vec{\hat{\mathbf{p}}}=\vec{\mathbf{p}}} \quad (81)\\ &= -\mathrm{E}_{\boldsymbol{\nu}}\left\{\frac{c_{ij}c_{ji}\phi^2(\nu_{ij})}{\mathcal{L}_{ij}^2(\hat{\mathbf{p}}_i\hat{\mathbf{p}}_j|\tilde{d}_{ij})}\right\}\Bigg|_{\vec{\hat{\mathbf{p}}}=\vec{\mathbf{p}}} \boldsymbol{\Upsilon}_{ij} = -\zeta_{ij}\boldsymbol{\Upsilon}_{ij}.\end{aligned}$$

□

Formulating the CRLB as a function of the ranging error distributions offers several advantages. First, this approach eases the simultaneous integration of different ranging models obtained from measurements or practical considerations. Second, it permits the integration of simultaneously mixed LOS/NLOS scenarios.

Finally, it offers the possibilities to evaluate the performance of a localisation system with heterogeneous devices that have different ranging performance.

In fact, for a given network positioning problem, it will be sufficient to define the pdfs $\phi_{ij}(\nu_{ij})$, compute ζ_{ij} and $\mathbf{\Upsilon}_{ij}$ as in equations (75) and (47), respectively. The parameter ζ_{ij}, hereafter referred to as Ranging Information Intensity (RII), will vary upon the pdf $\phi_{ij}(\nu_{ij})$, while the matrix $\mathbf{\Upsilon}_{ij}$, referred to as Ranging Direction Matrix (RDM), will depend on the locations of the i-th and j-th nodes.

In [106, 107], it was also shown that the CRLB of a specific target's location estimate, *e.g.* $\hat{\mathbf{p}}_k$ with $k = N$, can be determined as the inverse of the EFIM of $\mathbf{p}_k$, defined as the Schur-complement of $\mathbf{F}_d$ with respect to the minor $\mathbf{G}_{k-1}$, *i.e.*

$$\mathbf{S}_k \triangleq \breve{\mathbf{F}}_d^{k,A} + \breve{\mathbf{F}}_d^{k,T} - \mathbf{E}_k, \tag{82}$$

where

$$\breve{\mathbf{F}}_d^{k,A} \triangleq \sum_{n=1}^{N_\mathrm{A}} \zeta_{nk} \mathbf{\Upsilon}_{nk}, \tag{83}$$

$$\breve{\mathbf{F}}_d^{k,T} \triangleq \sum_{n=N_\mathrm{A}+1}^{k-1} \zeta_{nk} \mathbf{\Upsilon}_{nk}, \tag{84}$$

$$\mathbf{E}_k \triangleq \mathbf{Q}_k^\mathrm{T} \mathbf{G}_{k-1}^{-1} \mathbf{Q}_k, \tag{85}$$

and $\mathbf{G}_{k-1}$ and $\mathbf{Q}_k$ are obtained by partitioning $\mathbf{F}_d$ as

$$\mathbf{F}_d = \begin{bmatrix} \mathbf{G}_{k-1} & \mathbf{Q}_k \\ \mathbf{Q}_k^\mathrm{T} & \breve{\mathbf{F}}_d^k, \end{bmatrix}. \tag{86}$$

The term *equivalent* indicates that $\mathbf{S}_k$ is not a "true" FIM as the one defined in equation (71), however, its inverse can be used to determine the CRLB of $\hat{\mathbf{p}}_k$.

Respectively, the three terms shown in equation (82), namely $\breve{\mathbf{F}}_d^{k,A}$, $\breve{\mathbf{F}}_d^{k,T}$ and $\mathbf{E}_k$ correspond to the information obtained from the cooperation with the anchors, the cooperation with the neighbouring[8] targets and, in the presence of a negative sign, the *equivocation*[9] on the information of $\mathbf{p}_k$ due to the uncertainties of other target nodes.

[8]The j-th target is a neighbour of the k-th node if $c_{jk} = 1$.

[9]The term equivocation is typically adopted in information theory to refer to the remaining entropy (i.e. uncertainty) of a random variable.

Notice that $\mathbf{S}_k$ is a positive semi-definite (psd) matrix, *i.e.* $\mathbf{S}_k \succeq 0$, therefore $\breve{\mathbf{F}}_d^{k,A} + \breve{\mathbf{F}}_d^{k,T} \succeq \mathbf{E}_k$. This inequality implies that $\breve{\mathbf{F}}_d^{k} \triangleq \breve{\mathbf{F}}_d^{k,A} + \breve{\mathbf{F}}_d^{k,T}$ is the upper bound to EFIM of the $\mathbf{p}_k$. In fact, this Information will be achieved when all the nodes connected to the k-th target are anchors.

Our objective is to study the equivocation term $\mathbf{E}_k$ and the dependency to all RIIs and RDMs of other nodes in the network. To this end, we first decompose the EFIM as follows.

Theorem T8 (Decomposition of the EFIM)**.**

Consider a connected network with N_{A} anchors and N_{T} targets, the EFIM of corresponding to the estimation error of the k-th target node location, with $k = N$, can be decomposed as

$$\begin{aligned}\mathbf{S}_k \;=\; & \breve{\mathbf{F}}_d^{k,A} + \left(\zeta_{1k}\boldsymbol{\Upsilon}_{1k}^{\mathrm{T}} - \boldsymbol{\Upsilon}_{1k}^{\mathrm{T}}\bar{\mathbf{S}}_1^{-1}\boldsymbol{\Upsilon}_{k1}\right) + \\ & + \sum_{n=2}^{k-1}\left(\zeta_{nk}\boldsymbol{\Upsilon}_{nk} - \mathbf{Q}_{k,n}^{\mathrm{T}}\begin{bmatrix} -\mathbf{G}_{n-1}^{-1}\mathbf{Q}_n \\ \mathbf{I}\end{bmatrix}\bar{\mathbf{S}}_n^{-1}\begin{bmatrix} -\mathbf{G}_{n-1}^{-1}\mathbf{Q}_n \\ \mathbf{I}\end{bmatrix}^{\mathrm{T}}\mathbf{Q}_{k,n}\right),\end{aligned} \tag{87}$$

where

$$\mathbf{Q}_k \triangleq [\boldsymbol{\Upsilon}_{1k};\cdots;\boldsymbol{\Upsilon}_{(k-1)k}], \tag{88}$$

$$\mathbf{Q}_{k,n} \triangleq [\boldsymbol{\Upsilon}_{1k};\cdots;\boldsymbol{\Upsilon}_{nk}], \tag{89}$$

$$\mathbf{G}_n \triangleq [\mathbf{F}_d]_{1:(N-n)\eta,1:(N-n)\eta} = \begin{bmatrix}\mathbf{G}_{n-1} & \mathbf{Q}_n \\ \mathbf{Q}_n^{\mathrm{T}} & \breve{\mathbf{F}}_d^{n}\end{bmatrix}, \tag{90}$$

$$\bar{\mathbf{S}}_n \triangleq \breve{\mathbf{F}}_d^{n} - \mathbf{Q}_n^{\mathrm{T}}\mathbf{G}_{n-1}^{-1}\mathbf{Q}_n. \tag{91}$$

and $\bar{\mathbf{S}}_1^{-1} = \mathbf{G}_1^{-1} \triangleq (\breve{\mathbf{F}}_d^{1})^{-1}$.

Proof. Compute $\mathbf{G}_{k-1}^{-1}$ with a classic block matrix inversion algorithm [91] as

$$\mathbf{G}_{k-1}^{-1} = \begin{bmatrix}\mathbf{G}_{k-2}^{-1} & \mathbf{0} \\ \mathbf{0} & \mathbf{0}\end{bmatrix} + \begin{bmatrix} -\mathbf{G}_{k-2}^{-1}\mathbf{Q}_{k-1} \\ \mathbf{I}\end{bmatrix}\bar{\mathbf{S}}_{k-1}^{-1}\begin{bmatrix} -\mathbf{G}_{k-2}^{-1}\mathbf{Q}_{k-1} \\ \mathbf{I}\end{bmatrix}^{\mathrm{T}}, \tag{92}$$

where $\bar{\mathbf{S}}_{k-1}$ is the Schur-complement of $\mathbf{G}_{k-1}$ with respect to the minor $\mathbf{G}_{k-2}$.

Replace (92) in equation (85) and rewrite $\mathbf{E}_k$ as

$$\mathbf{E}_k = \mathbf{Q}_{k,k-2}^{\mathrm{T}}\mathbf{G}_{k-2}^{-1}\mathbf{Q}_{k,k-2} + \mathbf{Q}_k^{\mathrm{T}}\begin{bmatrix} -\mathbf{G}_{k-2}^{-1}\mathbf{Q}_{k-1} \\ \mathbf{I}\end{bmatrix}\bar{\mathbf{S}}_{k-1}^{-1}\begin{bmatrix} -\mathbf{G}_{k-2}^{-1}\mathbf{Q}_{k-1} \\ \mathbf{I}\end{bmatrix}^{\mathrm{T}}\mathbf{Q}_k. \tag{93}$$

Next, apply the inversion algorithm to decompose $\mathbf{G}_{k-2}^{-1}$ in the sum above and iterate the decomposition until the matrix $\mathbf{G}_{k-n} = \breve{\mathbf{F}}_d^1$.

After $N-2$ iterations, the equivocation matrix $\mathbf{E}_k$ can be expressed as

$$\mathbf{E}_k = \boldsymbol{\Upsilon}_{1k}^{\mathrm{T}} \bar{\mathbf{S}}_1^{-1} \boldsymbol{\Upsilon}_{k1} + \sum_{n=2}^{k-1} \mathbf{Q}_{k,n}^{\mathrm{T}} \begin{bmatrix} -\mathbf{G}_{n-1}^{-1}\mathbf{Q}_n \\ \mathbf{I} \end{bmatrix} \bar{\mathbf{S}}_n^{-1} \begin{bmatrix} -\mathbf{G}_{n-1}^{-1}\mathbf{Q}_n \\ \mathbf{I} \end{bmatrix}^{\mathrm{T}} \mathbf{Q}_{k,n}. \quad (94)$$

Finally, replace equation (94) in equation (82) and reorder the term of the sums to obtain equation (87). □

Based on this result, we can further decompose the equivocation matrix $\mathbf{E}_k$ in order to identify the information-dependency amongst nodes in the network.

Corollary C2 (Decomposition of the Equivocation Matrix)**.**

Consider a connected network with N_{A} anchors and N_{T} targets, the equivocation matrix of the k-th target node with $k = N$ can be decomposed as

$$\mathbf{E}_k = \breve{\mathbf{E}}_k + \bar{\mathbf{E}}_k, \quad (95)$$

where

$$\breve{\mathbf{E}}_k \triangleq \sum_{i=m_a}^{k-1} \zeta_{ik}^{\mathrm{e}} \boldsymbol{\Upsilon}_{ik}, \quad (96)$$

$$\bar{\mathbf{E}}_k \triangleq \sum_{i=m_a}^{k-1} \sum_{\substack{j=m_a \\ j\neq i}}^{k-1} \kappa_{ik}^{kj} \boldsymbol{\Upsilon}_{ik}^{kj}, \quad (97)$$

with

$$\zeta_{ik}^{\mathrm{e}} \triangleq \zeta_{ik}^2 \tau_{ik}, \quad (98)$$

$$\kappa_{ik}^{kj} \triangleq \zeta_{ik}\zeta_{kj}\chi_{ij}, \quad (99)$$

$$\tau_{ik} \triangleq \sum_{n=i+1}^{k-1} \sum_{t=m_a}^{n-1} \sum_{q=1}^{n-1} \zeta_{nt}\zeta_{nq} (\mathbf{v}_{ik}[\mathbf{G}_n^{-1}]_{iq}^{\eta} \mathbf{v}_{nq}^{\mathrm{T}})(\mathbf{v}_{nq}\bar{\mathbf{S}}_n^{-1}\mathbf{v}_{nt}^{\mathrm{T}})(\mathbf{v}_{nt}[\mathbf{G}_n^{-1}]_{ti}^{\eta}\mathbf{v}_{ik}^{\mathrm{T}}) + \left(\mathbf{v}_{ik}\bar{\mathbf{S}}_i^{-1}\mathbf{v}_{ik}^{\mathrm{T}}\right), \quad (100)$$

$$\chi_{ij} \triangleq \sum_{t=m_a}^{j-1} \zeta_{tj} \left(\mathbf{v}_{ik}[\mathbf{G}_j^{-1}]_{it}^{\eta}\mathbf{v}_{tj}^{\mathrm{T}}\right)\left(\mathbf{v}_{tj}\bar{\mathbf{S}}_j^{-1}\mathbf{v}_{kj}^{\mathrm{T}}\right) + \sum_{n=s_a}^{k-1} \sum_{t=m_a}^{n-1} \sum_{q=m_a}^{n-1} \zeta_{nt}\zeta_{nq} (\mathbf{v}_{ik}[\mathbf{G}_n^{-1}]_{iq}^{\eta}\mathbf{v}_{nq}^{\mathrm{T}})(\mathbf{v}_{nq}\bar{\mathbf{S}}_n^{-1}\mathbf{v}_{nt}^{\mathrm{T}})(\mathbf{v}_{nt}^{\mathrm{T}}[\mathbf{G}_n^{-1}]_{tj}^{\eta}\mathbf{v}_{kj}^{\mathrm{T}}), \quad (101)$$

$$\boldsymbol{\Upsilon}_{ik}^{kj} \triangleq \mathbf{v}_{ik}^{\mathrm{T}}\mathbf{v}_{kj}, \quad (102)$$

and $m_a = N_{\mathrm{A}} + 1$ and $s_a = \max(i,j) + 1$.

Proof. Consider a matrix product $\mathbf{AB}$, with $\mathbf{A} \in \mathbb{R}^{nq \times mq}$ and $\mathbf{B} \in \mathbb{R}^{mq \times tq}$. The ij-th block-matrix of $q \times q$ elements of $\mathbf{AB}$ is equal to

$$[\mathbf{AB}]_{ij}^{q} = \sum_{k=1}^{n} [\mathbf{A}]_{ik}^{q} [\mathbf{B}]_{kj}^{q}, \tag{103}$$

where $[\mathbf{A}]_{ik}^{q} \in \mathbb{R}^{q \times q}$ and $[\mathbf{B}]_{kj}^{q} \in \mathbb{R}^{q \times q}$ denote the ik-th and the kj-th blocks of $\mathbf{A}$ and $\mathbf{B}$, respectively.

From the above, the n-th term of equation (94)

$$\mathbf{Q}_{k,n}^{\mathrm{T}} \begin{bmatrix} -\mathbf{G}_{n-1}^{-1}\mathbf{Q}_n \\ \mathbf{I} \end{bmatrix} \bar{\mathbf{S}}_n^{-1} \begin{bmatrix} -\mathbf{G}_{n-1}^{-1}\mathbf{Q}_n \\ \mathbf{I} \end{bmatrix}^{\mathrm{T}} \mathbf{Q}_{k,n}, \tag{104}$$

can be resolved as

$$\begin{aligned} &\boldsymbol{\Upsilon}_{nk}\bar{\mathbf{S}}_n^{-1}\boldsymbol{\Upsilon}_{nk} + \mathbf{Q}_{k,n-1}^{\mathrm{T}}\mathbf{G}_{n-1}^{-1}\mathbf{Q}_n\bar{\mathbf{S}}_n^{-1}\mathbf{Q}_n^{\mathrm{T}}\mathbf{G}_{n-1}^{-1}\mathbf{Q}_{k,n-1} + \\ &-\mathbf{Q}_{k,n-1}^{\mathrm{T}}\mathbf{G}_{n-1}^{-1}\mathbf{Q}_{n-1}\bar{\mathbf{S}}_n^{-1}\boldsymbol{\Upsilon}_{kn} - \boldsymbol{\Upsilon}_{kn}\bar{\mathbf{S}}_n^{-1}\mathbf{Q}_{n-1}^{\mathrm{T}}\mathbf{G}_{n-1}^{-1}\mathbf{Q}_{k,n-1}^{\mathrm{T}}. \end{aligned} \tag{105}$$

Now, notice that all matrix products similar to $\boldsymbol{\Upsilon}_{ik}[\mathbf{A}]_{iq}^{\eta}\boldsymbol{\Upsilon}_{qk}$ can be simplified as

$$\boldsymbol{\Upsilon}_{ik}[\mathbf{A}]_{iq}^{\eta}\boldsymbol{\Upsilon}_{qk} = \zeta_{ik}\zeta_{qk}\mathbf{v}_{ik}^{\mathrm{T}}(\mathbf{v}_{ik}[\mathbf{A}]_{iq}^{\eta}\mathbf{v}_{qk}^{\mathrm{T}})\mathbf{v}_{qk} = \zeta_{ik}\zeta_{qk}(\mathbf{v}_{ik}[\mathbf{A}]_{iq}^{\eta}\mathbf{v}_{qk}^{\mathrm{T}})\mathbf{v}_{ik}^{\mathrm{T}}\mathbf{v}_{qk},$$

where the last equality holds because the term in the brackets is a scalar.

By resolving equation (105) with the rule (73) and applying the above simplification to each term in the form of $\boldsymbol{\Upsilon}_{ik}[\mathbf{A}]_{iq}^{\eta}\boldsymbol{\Upsilon}_{qk}$, it follows that equation (105) can be reduced to

$$\alpha_{nk}\boldsymbol{\Upsilon}_{nk} + \sum_{i=m}^{n-1} \alpha_{ink}\boldsymbol{\Upsilon}_{ik} + \sum_{i=m_a}^{n-1} \sum_{\substack{j=m_a \\ j\neq i}}^{n-1} \beta_{ink}(\boldsymbol{\Upsilon}_{nk}^{ki} + \boldsymbol{\Upsilon}_{ik}^{kn}) + \beta_{ijnk}\boldsymbol{\Upsilon}_{ik}^{kj}, \tag{106}$$

and the equivocation matrix $\mathbf{E}_k$ can be written as

$$\mathbf{E}_k = \sum_{n=m_a}^{k-1} \sum_{i=m_a}^{n-1} \sum_{\substack{j=m_a \\ j\neq i}}^{n-1} \alpha_{nk}\boldsymbol{\Upsilon}_{nk} + \alpha_{ink}\boldsymbol{\Upsilon}_{ik} + \beta_{ink}(\boldsymbol{\Upsilon}_{nk}^{ki} + \boldsymbol{\Upsilon}_{ik}^{kn}) + \beta_{ijnk}\boldsymbol{\Upsilon}_{ik}^{kj}, \tag{107}$$

where the coefficients $\alpha_{nk}, \alpha_{ink}, \beta_{ink}$ and β_{ijnk} are given by

$$\alpha_{nk} \triangleq \zeta_{nk}^2 \left(\mathbf{v}_{nk} \bar{\mathbf{S}}_n^{-1} \mathbf{v}_{nk}^{\mathrm{T}}\right), \tag{108}$$

$$\alpha_{ink} \triangleq \zeta_{ik}^2 \sum_{t=m_a}^{n-1} \sum_{q=1}^{n-1} \zeta_{nt}\zeta_{nq} (\mathbf{v}_{ik} [\mathbf{G}_n^{-1}]_{iq}^{\eta} \mathbf{v}_{nq}^{\mathrm{T}})(\mathbf{v}_{nq} \bar{\mathbf{S}}_n^{-1} \mathbf{v}_{nt}^{\mathrm{T}})(\mathbf{v}_{nt} [\mathbf{G}_n^{-1}]_{ti}^{\eta} \mathbf{v}_{ik}^{\mathrm{T}}), \tag{109}$$

$$\beta_{ink} \triangleq \zeta_{ik}\zeta_{kn} \sum_{t=m_a}^{n-1} \zeta_{tn} \left(\mathbf{v}_{nk} [\mathbf{G}_j^{-1}]_{it}^{\eta} \mathbf{v}_{tn}^{\mathrm{T}}\right) \left(\mathbf{v}_{tn} \bar{\mathbf{S}}_n^{-1} \mathbf{v}_{kn}^{\mathrm{T}}\right), \tag{110}$$

$$\beta_{ijnk} \triangleq \zeta_{ik}\zeta_{kj} \sum_{t=m_a}^{n-1} \sum_{q=m_a}^{n-1} \zeta_{nt}\zeta_{nq} (\mathbf{v}_{ik} [\mathbf{G}_n^{-1}]_{iq}^{\eta} \mathbf{v}_{nq}^{\mathrm{T}})(\mathbf{v}_{nq} \bar{\mathbf{S}}_n^{-1} \mathbf{v}_{nt}^{\mathrm{T}})(\mathbf{v}_{nt}^{\mathrm{T}} [\mathbf{G}_n^{-1}]_{tj}^{\eta} \mathbf{v}_{kj}^{\mathrm{T}}). \tag{111}$$

Finally, equations (96) and (97) can be obtained by resolving the sums in equation (107) and grouping all terms with the same RDM $\boldsymbol{\Upsilon}_{ik}$ and Cross-Ranging Direction Matrix (C-RDM) $\boldsymbol{\Upsilon}_{ik}^{kj}$. □

Corollary C2 shows that the equivocation matrix can be decomposed as a sum of ζ_{ik}^{e}'s and a sum of κ_{ik}^{kj}'s, which respectively denote the *equivalent ranging error* due to the uncertainty of the i-th node location and the *information coupling* between the i-th and j-th node established by fact that also such nodes cooperate with each other.

This result generalises Theorem 1 of [108], in which the decomposition was derived for $N_{\mathrm{T}} = 3$. From equation (99), in particular, it is found that the information coupling between two nodes i and j, namely κ_{ik}^{kj} is proportional to the product of the RIIs corresponding to the links ζ_{ik} and ζ_{kj}. The coefficient of proportionality, namely χ_{ij}, is given by equation (101), and it is equal to a weighted sum of the RIIs ζ_{tj} with $N_{\mathrm{A}} + 1 \leq t < j$ as well as the products ζ_{ni}^2, ζ_{nj}^2, $\zeta_{ni}\zeta_{nj}$ and $\zeta_{nq}\zeta_{nt}$ with $n > \max(i, j)$, $q \neq \{i, j\}$ and $t \neq \{i, j\}$.

Based on this result, it is trivial to show that $\kappa_{ik}^{kj} = 0$ can be obtained if either $c_{ik} = 0$, $c_{jk} = 0$, or $\chi_{ij} = 0$. The more interesting case, however, is when $\chi_{ij} = 0$, which results either if the j-th node becomes an anchor since $\bar{\mathbf{S}}_j \to \infty$ and $[\mathbf{G}_n]_{tj} \to \infty$ or, if the location of the nodes are such that in each term of the sums, at least one of the matrix products written in the form of $(\mathbf{v}_{ik} [\mathbf{A}]_{iq}^{\eta} \mathbf{v}_{qk}^{\mathrm{T}})$ is 0. Without loss of generality, assume $j = k - 1$ for instance that then the latter condition implies that

$$\sum_{t=N_{\mathrm{A}}+1}^{j-1} \zeta_{tj} \left(\mathbf{v}_{ik} [\mathbf{G}_j^{-1}]_{it}^{\eta} \mathbf{v}_{tj}^{\mathrm{T}}\right) \left(\mathbf{v}_{tj} \bar{\mathbf{S}}_j^{-1} \mathbf{v}_{kj}^{\mathrm{T}}\right) = 0. \tag{112}$$

Obviously, this is typically a rare fact and, especially can not be controlled *a priori* since the locations of the target nodes are not known. More useful insights, however, can be gained from the example with $N_{\mathrm{T}} = 3$ targets proposed in [108].

In this Thesis, we propose two different examples to learn about the effects of information coupling/decoupling in more general networks. For instance, in Figure 10 we consider a small network with $N_{\mathrm{A}} = 3$ anchors and $N_{\mathrm{T}} = 4$ targets indicated with the labels Z_i with $4 \leq i \leq 7$. We assume $\sigma_{ij} = \sigma = 1$ meter $\forall ij \in E$ and compare the location accuracy, represented by the corresponding error-ellipse [40], of the node obtained Z_7 with and without the information coupling κ_{67}^{75}. The scenario corresponding to $\kappa_{67}^{75} \neq 0$ is obtained with a network fully connected. Based on equation (112), $\kappa_{67}^{75} = 0$ is achieved, for instance, if $\zeta_{46} = 0$ and $\zeta_{56} = 0$, *i.e.* the links $Z_4 - Z_6$ and $Z_5 - Z_6$ are disconnected. In this case, the lack of information coupling increases the uncertainty represented by the equivocation matrix (topic addressed in Corollary 3), and therefore decreases the Position Error Bound (PEB) of the node Z_7.

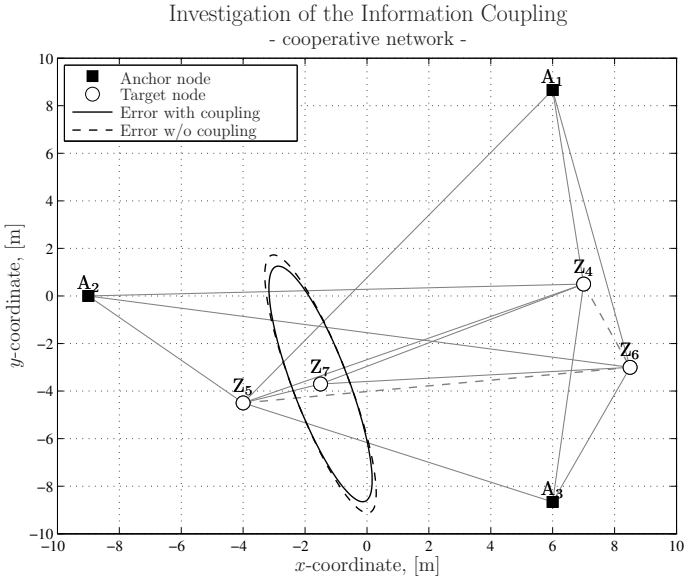

Fig 10. Study of the information coupling effects on a small network with $N_{\mathbf{A}} = 4$ anchors and $N_{\mathbf{T}} = 4$ targets. The ellipses with solid and dashed lines refer to the PEB obtained with and without coupling, respectively.

In Figure 11, we consider a larger network with $N_{\mathrm{T}} = 17$ targets separated in two sub-networks identified with negative and positive x-coordinates and referred to the SN_1 and SN_2, respectively. In contrast to the previous study, we show that information decoupling (this time caused by the replacement of a node with an anchor) can improve the average location accuracy of the nodes. Notice however that this result can not be obtained from the work in [108] since, their result was developed for a small network of $N_{\mathrm{T}} = 3$ nodes.

For instance, consider the PEB of the node Z_{22}, which can be computed as the inverse of the EFIM $\mathbf{S}_{22}$ given by equation (82). The equivocation matrix $\mathbf{E}_{22}$ is obtained from (85), in which we focus on the coupling coefficient κ_{ik}^{kj} where the indexes i, j and k refer to the number $20, 21$ and 22, respectively.

From equation (99), $\kappa_{ik}^{kj} = \zeta_{ik}\zeta_{jk}\chi_{ij}$, and in particular χ_{ij} is given by

$$\chi_{ij} = \sum_{t=N_{\mathrm{A}}+1}^{j-1} \zeta_{tj} \left(\mathbf{v}_{ik}[\mathbf{G}_j^{-1}]_{it}^{\eta}\mathbf{v}_{tj}^{\mathrm{T}}\right)\left(\mathbf{v}_{tj}\bar{\mathbf{S}}_j^{-1}\mathbf{v}_{kj}^{\mathrm{T}}\right). \tag{113}$$

From all of the above, it is shown that κ_{ik}^{kj} is a function of all the RIIs corresponding to the nodes connected to Z_{21} as well as on their uncertainties. As illustrated in Figure 11(a), this dependence generates a correlation between the location error of the nodes in SN_2 to those in SN_1, and vice versa. In fact, in the example we show that the PEB of all nodes in the network are affected by a larger uncertainty due to the cancellation of some edges in SN_2. Clearly, this correlation is undesired, especially if the two networks refer to different application scenarios with different location error requirements.

To decouple SN_1 from SN_2, while preserving the connectivity, we replace Z_{21} with the anchor A_6. This replacement implies $\chi_{ij} = 0$, and therefore the decoupling of the two networks. The benefits can be appreciated in Figure 11(b), from which it can be noticed that not only all PEBs are slightly smaller but, especially that the location errors of the nodes in SN_1 are unchanged regardless of the removal of the links in SN_2.

The study of the information coupling and the understanding of its impacts on the fundamental limits of range based positioning are still subject of investigations. Indeed, as mentioned in [108], useful insights can be gained from these studies in order to improve localization techniques as well as to the design of optimal anchor deployment criteria.

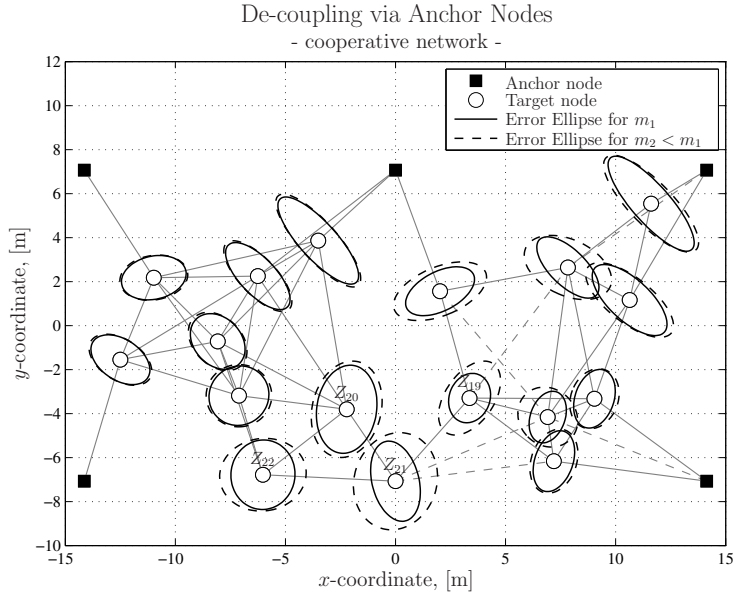

(a) Coupled network

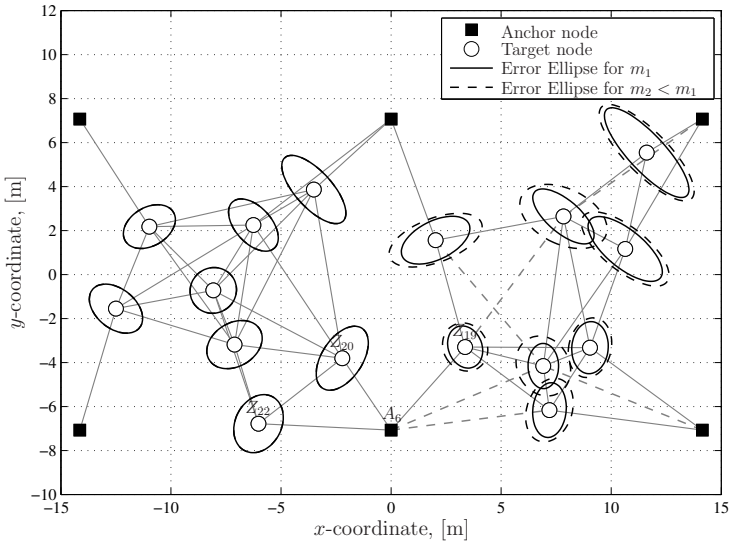

(b) Decoupled network

Fig 11. Study of the error propagation due to information coupling. Sub-figures (a) and (b) show a coupled and decoupled network, respectively. The PEBs of each node obtained before and after the removal of the links are represented by the error ellipses in solid and dashed lines, respectively.

Finally, we investigate the relationship between the meshness ratio and the EFIM in order to establish the advantages of network cooperation onto the location accuracy. To this end, consider the following result.

Corollary C3 (EFIM and Meshness-Ratio)**.**

Consider a network with $N_{\rm A}$ anchors, $N_{\rm T}$ targets and let E_1 and E_2 be two sets of connected edges of the same network with $E_1 \subset E_2$. Let $\mathbf{S}_k^{(1)}$, $\mathbf{S}_k^{(2)}$ be the EFIMs of k-th node obtained with the set of edges E_1 and E_2, respectively. Then,

$$\mathbf{S}_k^{(2)} \succeq \mathbf{S}_k^{(1)}. \tag{114}$$

Proof. Consider a network with connectivity matrix $\mathbf{C}$ and a set of edges E_1, and assume that the pair of nodes (q, j) are not connected, *i.e.* $c_{jq} = 0$. Next, consider a new set of edges $E_2 \triangleq E_1 \cup jq$. The objective of the proof is to verify that the matrix inequality (114) holds for all following scenarios:

a) $j = k$ and $q \leq N_{\rm A}$, *i.e.* the q-th node is an anchor connected to the k-th node,
b) $j = k$ and $q > N_{\rm A}$, *i.e.* the q-th node is a target connected to the k-th node,
c) $j \neq q \neq k$, *i.e.* the j-th and q-th nodes are disconnected from the k-th target.

Scenario a) From equation (82), we compute $\mathbf{S}_k^{(2)}$ and $\mathbf{S}_k^{(1)}$ as

$$\mathbf{S}_k^{(1)} = \sum_{n=1}^{q-1} \zeta_{nk} \boldsymbol{\Upsilon}_{nk} + \sum_{n=m_a}^{k-1} \zeta_{nk} \boldsymbol{\Upsilon}_{nk} - \mathbf{Q}_k^{\rm T} \mathbf{G}_k^{-1} \mathbf{Q}_k, \tag{115}$$

$$\mathbf{S}_k^{(2)} = \mathbf{S}_k^{(1)} + \zeta_{qk} \boldsymbol{\Upsilon}_{qk}, \tag{116}$$

from which it follows that

$$\mathbf{S}_k^{(2)} - \mathbf{S}_k^{(1)} = \zeta_{qk} \boldsymbol{\Upsilon}_{qk} \succeq 0. \tag{117}$$

Scenario b) Compute $\mathbf{S}_k^{(2)}$ and $\mathbf{S}_k^{(1)}$ as in equation (82), and evaluate the difference

$$\mathbf{S}_k^{(2)} - \mathbf{S}_k^{(1)} = \zeta_{qk} \boldsymbol{\Upsilon}_{qk} - (\mathbf{E}_k^{(2)} - \mathbf{E}_k^{(1)}), \tag{118}$$

where $\mathbf{E}_k^{(2)}$ and $\mathbf{E}_k^{(1)}$ are calculated as in equation (95).

Without loss of generality, assume that $q = (k-1)$, thus

$$\mathbf{S}_k^{(2)} - \mathbf{S}_k^{(1)} = \underbrace{\zeta_{qk}\boldsymbol{\Upsilon}_{qk} - \left(\mathbf{Q}_k^{\mathrm{T}}\begin{bmatrix} -\mathbf{G}_{q-1}^{-1}\mathbf{Q}_q \\ \mathbf{I} \end{bmatrix}(\bar{\mathbf{S}}_q^{(2)})^{-1}\begin{bmatrix} -\mathbf{G}_{q-1}^{-1}\mathbf{Q}_q \\ \mathbf{I} \end{bmatrix}^{\mathrm{T}}\mathbf{Q}_k\right)}_{\text{Part 1}}$$
$$+ \underbrace{\mathbf{Q}_{k,q-1}^{\mathrm{T}}\mathbf{G}_{q-1}^{-1}\mathbf{Q}_q(\bar{\mathbf{S}}_q^{(1)})^{-1}\mathbf{Q}_q^{\mathrm{T}}\mathbf{G}_{q-1}^{-1}\mathbf{Q}_{k,q-1}}_{\text{Part 2}}, \tag{119}$$

where both parts are psd. Thus, the inequality shown in equation (114) holds.

Scenario c) In this scenario, the difference of EFIMs is given by

$$\mathbf{S}_k^{(2)} - \mathbf{S}_k^{(1)} = \mathbf{E}_k^{(1)} - \mathbf{E}_k^{(2)} = \mathbf{Q}_k^{\mathrm{T}}\big((\mathbf{G}_k^{(1)})^{-1} - (\mathbf{G}_k^{(2)})^{-1}\big)\mathbf{Q}_k. \tag{120}$$

The fact that $\mathbf{G}_k^{(2)} \succeq \mathbf{G}_k^{(1)} \succeq 0$ implies

$$(\mathbf{G}_k^{(1)})^{-1} \succeq (\mathbf{G}_k^{(2)})^{-1} \succeq 0, \tag{121}$$

and, therefore, $\big((\mathbf{G}_k^{(1)})^{-1} - (\mathbf{G}_k^{(2)})^{-1}\big) \succeq 0$ and $\mathbf{S}_k^{(2)} \succeq \mathbf{S}_k^{(1)}$. □

The above Corollary proves that despite the location of a new cooperation, the location accuracy of a generic k-th node improves. However, the impact onto the PEB of the k-th node can be more or less significant if such a cooperation is established between the k-th target and an neighbour anchor, or a neighbour target, or if it is a consequence of a new cooperation between two other nodes. If the RII are the same for all links, the strongest impact is due to a cooperation with an anchor since no further uncertainty is introduced in the equivocation matrix. On the other hand, if the cooperation is established with a neighbouring node the impact can still be significant if the number of the previous connections is small. If the cooperation is established between another pair of nodes, the impact can also be null if the local portion of the network of the k-th node is decoupled from the rest.

4.4 CRLB in LOS and NLOS channel conditions

Consider the ranging model proposed in Section 3.1, in which the noise and the bias errors are modelled with the random variables n_{ij} and b_{ij} that are governed by a Gaussian and an uniform distribution, respectively.

With the assumption that all links are in LOS channel conditions, *i.e.* $b_{ij} = 0$ (no bias), then the likelihood function of $\vec{\mathbf{p}}$ can be computed as in equation (27) and, the CRLB can be derived as follows.

Lemma L3 (Cramér-Rao Lower Bound in LOS [51])**.**

Assume LOS channel conditions, i.e. $b_{ij} = 0 \ \forall i, j$*. Let* $\vec{\hat{\mathbf{p}}} \in \mathbb{R}^{\eta N}$ *be an estimator of* $\vec{\mathbf{p}}$ *governed by the likelihood function* $\mathcal{L}(\vec{\hat{\mathbf{p}}}|\vec{\tilde{\mathbf{d}}}) = L(\vec{\hat{\mathbf{p}}}|\vec{\tilde{\mathbf{d}}})$*. Then the CRLB on the covariance matrix of* $\vec{\hat{\mathbf{p}}}$ *is given by*

$$\mathrm{CRLB}_{\mathrm{LOS}}(\mathbf{P}) \triangleq \mathbf{J}^{c}_{\mathrm{LOS}}, \tag{122}$$

where $\mathbf{J}^{c}_{\mathrm{LOS}}$ *is the inverse of the information matrix* $\mathbf{F}_{\mathrm{LOS}}$ *given by*

$$\mathbf{F}_{\mathrm{LOS}} \triangleq \breve{\mathbf{F}}_{\mathrm{LOS}} + \bar{\mathbf{F}}_{\mathrm{LOS}}, \tag{123}$$

with $\breve{\mathbf{F}}_{\mathrm{LOS}}$ *and* $\bar{\mathbf{F}}_{\mathrm{LOS}}$ *denoting a block-diagonal and a block-off-diagonal matrices, respectively obtained as*

$$[\breve{\mathbf{F}}_{\mathrm{LOS}}]^{\eta}_{kk} = \breve{\mathbf{F}}^{k}_{\mathrm{LOS}} \triangleq \sum_{j=1}^{N} \frac{c_{kj}}{\sigma^2_{kj}} \boldsymbol{\Upsilon}_{kj}, \tag{124}$$

$$[\bar{\mathbf{F}}_{\mathrm{LOS}}]^{\eta}_{kj} = \bar{\mathbf{F}}^{kj}_{\mathrm{LOS}} \triangleq -\frac{c_{kj}}{\sigma^2_{kj}} \boldsymbol{\Upsilon}_{kj}. \tag{125}$$

Proof. From Theorem T1, the log-likelihood function $\ln L(\vec{\hat{\mathbf{p}}}|\tilde{\mathbf{d}})$ is given by equation (27) with $w^2_{ij} = c_{ij}/\sigma^2_{ij}$.

Invoking Theorem T7, $\hat{\mathbf{F}}$ can be decomposed as in equation (123) with

$$\begin{aligned} \breve{\mathbf{F}}^{k}_{\mathrm{LOS}} &\triangleq \mathrm{E}_{\tilde{\mathbf{d}}} \left\{ \left(\sum_{j=1}^{N} \frac{c_{kj}}{\sigma^2_{kj}} \frac{\hat{d}_{kj} - \tilde{d}_{kj}}{\hat{d}_{kj}} \right) \mathbf{I}_{\eta} + \sum_{j=1}^{N} \frac{c_{kj}}{\sigma^2_{kj}} \frac{\tilde{d}_{kj}}{\hat{d}_{kj}} \boldsymbol{\Upsilon}_{kj} \right\} \Bigg|_{\vec{\hat{\mathbf{p}}} = \vec{\mathbf{p}}} \\ &= \sum_{j=1}^{N} \frac{c_{kj}}{\sigma^2_{kj}} \boldsymbol{\Upsilon}_{kj} = \sum_{j=1}^{N_{\mathrm{A}}} \frac{c_{kj}}{\sigma^2_{kj}} \boldsymbol{\Upsilon}_{kj} + \sum_{jm}^{N} \frac{c_{kj}}{\sigma^2_{kj}} \boldsymbol{\Upsilon}_{kj}, \end{aligned} \tag{126}$$

and,

$$\bar{\mathbf{F}}^{kj}_{\mathrm{LOS}} \triangleq -\mathrm{E}_{\tilde{\mathbf{d}}} \left\{ \left(\frac{c_{kj}}{\sigma^2_{kj}} \frac{\hat{d}_{kj} + \tilde{d}_{kj}}{\hat{d}_{kj}} \right) \mathbf{I}_{\eta} - \frac{c_{kj}}{\sigma^2_{kj}} \frac{\tilde{d}_{kj}}{\hat{d}_{kj}} \boldsymbol{\Upsilon}_{kj} \right\} \Bigg|_{\vec{\hat{\mathbf{p}}} = \vec{\mathbf{p}}} = -\frac{c_{kj}}{\sigma^2_{kj}} \boldsymbol{\Upsilon}_{kj}. \tag{127}$$

Notice that under the assumption of ranging errors with a zero-mean Gaussian distribution $\zeta_{kj} = c_{kj}/\sigma^2_{kj}$.

Finally, the CRLB is given by

$$\mathrm{CRLB}_{\mathrm{LOS}}(\mathbf{P}) \triangleq \mathbf{J}^{c}_{\mathrm{LOS}} = \mathbf{F}^{-1}_{\mathrm{LOS}}. \tag{128}$$

□

Next, we focus on the derivation of the CRLB with the assumptions of NLOS channel conditions. Specifically, we consider the ranging model described in Section 3.1 where the noise and the bias are modelled with random variables governed by a Gaussian and uniform distribution, respectively. Under these assumptions, the likelihood function of $\vec{\mathbf{p}}$ can be computed as in [92] and the CRLB can be derived as follows.

Lemma L4 (Cramér-Rao Lower Bound in NLOS)**.**

Assume NLOS channel conditions, i.e. $b_{ij} = \mathcal{U}(0, b_{\mathrm{MAX}})\ \forall\, i, j$. *Let* $\vec{\hat{\mathbf{p}}} \in \mathbb{R}^{\eta N_{\mathrm{T}}}$ *be an estimator of* $\vec{\mathbf{z}}$ *governed by the likelihood function* $\mathcal{L}(\vec{\hat{\mathbf{p}}}|\vec{\tilde{\mathbf{d}}}) = \bar{L}(\vec{\hat{\mathbf{p}}}|\vec{\tilde{\mathbf{d}}})$ *given by*

$$\bar{L}(\vec{\hat{\mathbf{p}}}|\vec{\tilde{\mathbf{d}}}) \triangleq \prod_{ij \in E} \bar{L}_{ij}(\vec{\hat{\mathbf{p}}}_i \vec{\hat{\mathbf{p}}}_j | \tilde{d}_{ij}), \tag{129}$$

where

$$\bar{L}_{ij}(\vec{\hat{\mathbf{p}}}_i \vec{\hat{\mathbf{p}}}_j | d_{ij}) \triangleq Q\left(\frac{\tilde{d}_{ij} - \hat{d}_{ij} - b_{\mathrm{MAX}}}{\sigma_{ij}}\right) - Q\left(\frac{\tilde{d}_{ij} - \hat{d}_{ij}}{\sigma_{ij}}\right), \tag{130}$$

and $Q(x) \triangleq \frac{1}{\sqrt{2\pi}} \int_{x}^{\infty} \exp\left(-\frac{t^2}{2}\right) \mathrm{d}t$.

Then the CRLB on the covariance matrix of $\vec{\hat{\mathbf{z}}}$ *is given by*

$$\mathrm{CRLB}_{\mathrm{NLOS}}(\mathbf{P}) \triangleq \mathbf{J}^{c}_{\mathrm{NLOS}}, \tag{131}$$

where $\mathbf{J}^{c}_{\mathrm{NLOS}}$ *is the inverse of the information matrix* $\mathbf{F}_{\mathrm{NLOS}}$ *given by*

$$\mathbf{F}_{\mathrm{NLOS}} \triangleq \breve{\mathbf{F}}_{\mathrm{NLOS}} + \bar{\mathbf{F}}_{\mathrm{NLOS}}, \tag{132}$$

with $\breve{\mathbf{F}}_{\mathrm{NLOS}}$ *and* $\bar{\mathbf{F}}_{\mathrm{NLOS}}$ *denoting a block-diagonal and a block-off-diagonal matrices, respectively obtained as*

$$\breve{\mathbf{F}}^{i}_{\mathrm{NLOS}} \triangleq \sum_{j=1}^{N} \zeta_{ij} \boldsymbol{\Upsilon}_{ij}, \tag{133}$$

$$\bar{\mathbf{F}}^{ij}_{\mathrm{NLOS}} \triangleq -\zeta_{ij} \boldsymbol{\Upsilon}_{ii}, \tag{134}$$

where

$$\zeta_{ij} \triangleq c_{ij} \int_{-\infty}^{\infty} \frac{\phi^2(\nu_{ij})}{\bar{L}_{ij}(\vec{\hat{\mathbf{p}}}_i \vec{\hat{\mathbf{p}}}_j | \tilde{d}_{ij})} \, \mathrm{d}\nu_{ij}, \tag{135}$$

$$\phi(\nu_{ij}) \triangleq \frac{1}{\sqrt{2\pi\sigma_{ij}^2}} \left(\exp\!\left(\tfrac{-(\nu_{ij} - 0.5\, b_{\mathrm{MAX}})^2}{2\sigma_{ij}^2} \right) - \exp\!\left(\tfrac{-(\nu_{ij} + 0.5\, b_{\mathrm{MAX}})^2}{2\sigma_{ij}^2} \right) \right). \tag{136}$$

Proof. From [92], we obtain that the likelihood function of $\vec{\hat{\mathbf{p}}}$ is given by equation (129). From the definition of the Q-function, it follows that

$$\frac{\mathrm{d}}{\mathrm{d}x} Q(x) = -\frac{1}{\sqrt{2\pi}} \exp\left(-\frac{x^2}{2} \right), \tag{137}$$

thus

$$\frac{\partial}{\partial \hat{p}_i^n} \ln\left(\bar{L}(\vec{\hat{\mathbf{z}}} | \vec{\tilde{\mathbf{d}}}) \right) = \sum_{j=1}^{N} \frac{c_{ij}}{\bar{L}_{ij}(\vec{\hat{\mathbf{z}}}_i \vec{\hat{\mathbf{z}}}_j | \tilde{d}_{ij})} \left(\frac{1}{\sqrt{2\pi\sigma_{ij}^2}} \exp\!\left(\tfrac{-(\tilde{d}_{ij} - \hat{d}_{ij} - b_{\mathrm{MAX}})^2}{2\sigma_{ij}^2} \right) + \right.$$
$$\left. - \frac{1}{\sqrt{2\pi\sigma_{ij}^2}} \exp\!\left(\tfrac{-(\tilde{d}_{ij} - \hat{d}_{ij})^2}{2\sigma_{ij}^2} \right) \right) \frac{(\hat{p}_i^n - \hat{p}_j^n)}{\hat{d}_{ij}}. \tag{138}$$

The FIM is therefore given by

$$\mathbf{F}_{\mathrm{NLOS}} \triangleq \mathrm{E}_{\tilde{\mathbf{d}}} \left\{ \nabla_{\vec{\hat{\mathbf{p}}}}^{\mathrm{T}} \ln\left(\bar{L}(\vec{\hat{\mathbf{p}}} | \vec{\tilde{\mathbf{d}}}) \right) \nabla_{\vec{\hat{\mathbf{p}}}} \ln\left(\bar{L}(\vec{\hat{\mathbf{p}}} | \vec{\tilde{\mathbf{d}}}) \right) \right\} \Big|_{\vec{\hat{\mathbf{p}}} = \vec{\mathbf{p}}} = \breve{\mathbf{F}}_{\mathrm{NLOS}} + \bar{\mathbf{F}}_{\mathrm{NLOS}}, \tag{139}$$

where $\breve{\mathbf{F}}_{\mathrm{NLOS}}$ and $\bar{\mathbf{F}}_{\mathrm{NLOS}}$ are obtained as

$$\breve{\mathbf{F}}_{\mathrm{NLOS}}^{k} \triangleq \mathrm{E}_{\boldsymbol{\nu}} \left\{ \sum_{j=1}^{N} \sum_{q=1}^{N} \frac{c_{kj} c_{kq} \phi(\nu_{kq}) \phi(\nu_{kj}) (\hat{\mathbf{p}}_k - \hat{\mathbf{p}}_j)^{\mathrm{T}} (\hat{\mathbf{p}}_k - \hat{\mathbf{p}}_q)}{\bar{L}_{kj}(\vec{\hat{\mathbf{p}}}_k \vec{\hat{\mathbf{p}}}_j | \tilde{d}_{kj}) \bar{L}_{kq}(\vec{\hat{\mathbf{p}}}_k \vec{\hat{\mathbf{p}}}_q | \tilde{d}_{kq}) \hat{d}_{kj} \hat{d}_{kq}} \right\} \Bigg|_{\vec{\hat{\mathbf{p}}} = \vec{\mathbf{p}}}, \tag{140}$$
$$= \sum_{j=1}^{N} \mathrm{E}_{\boldsymbol{\nu}} \left\{ \frac{c_{kj} c_{kq} \phi^2(\nu_{kj})}{\bar{L}_{kj}^2(\vec{\hat{\mathbf{p}}}_k \vec{\hat{\mathbf{p}}}_j | \tilde{d}_{kj})} \right\} \Bigg|_{\vec{\hat{\mathbf{p}}} = \vec{\mathbf{p}}} \boldsymbol{\Upsilon}_{kj} = \sum_{j=1}^{N} \zeta_{kj} \boldsymbol{\Upsilon}_{kj},$$

$$\breve{\mathbf{F}}_{\mathrm{NLOS}}^{kj} \triangleq \mathrm{E}_{\boldsymbol{\nu}} \left\{ \sum_{t=1}^{N} \sum_{q=1}^{N} \frac{c_{kt} c_{jq} \phi(\nu_{kt}) \phi(\nu_{jq}) (\hat{\mathbf{p}}_k - \hat{\mathbf{p}}_t)^{\mathrm{T}} (\hat{\mathbf{p}}_j - \hat{\mathbf{p}}_q)}{\bar{L}_{kt}(\vec{\hat{\mathbf{p}}}_k \vec{\hat{\mathbf{p}}}_t | \tilde{d}_{kt}) \bar{L}_{jq}(\vec{\hat{\mathbf{p}}}_j \vec{\hat{\mathbf{p}}}_q | \tilde{d}_{jq}) \hat{d}_{kt} \hat{d}_{jq}} \right\} \Bigg|_{\vec{\hat{\mathbf{p}}} = \vec{\mathbf{p}}}, \tag{141}$$
$$= -\mathrm{E}_{\boldsymbol{\nu}} \left\{ \frac{c_{kj} c_{jk} \phi^2(\nu_{kj})}{\bar{L}_{kj}^2(\vec{\hat{\mathbf{p}}}_k \vec{\hat{\mathbf{p}}}_j | \tilde{d}_{kj})} \right\} \Bigg|_{\vec{\hat{\mathbf{p}}} = \vec{\mathbf{p}}} \boldsymbol{\Upsilon}_{kj} = -\zeta_{kj} \boldsymbol{\Upsilon}_{kj},$$

where $\nu_{kj} = b_{ij} + n_{ij} - 0.5\, b_{\mathrm{MAX}}$.

Finally, the CRLB is given by

$$\mathrm{CRLB}_{\mathrm{NLOS}}(\mathbf{P}) \triangleq \mathbf{J}^{c}_{\mathrm{NLOS}} = \mathbf{F}^{-1}_{\mathrm{NLOS}}. \tag{142}$$

□

Lemma L4 is the generalisation of the CRLB derived in [92] and the alternative to the signal-model based bound proposed in [106, 107]. The new formulas, in fact, can be used to compute the error bounds for large-scale network in closed-forms relying only on the statistics of the ranging measurements. In this way, the proposed error analysis framework is flexible and suitable for heterogeneous scenarios, where ranging errors can have different distributions due to either diverse channel conditions or dissimilar ranging technologies.

4.5 Alternative bounds to MSE in single-target positioning

The CRLB is perhaps the most known and utilised tool to benchmark the results of an estimation algorithm. However, it is also known that in low SNR regimé (large noise) the CRLB is devalued because it cannot predict the large estimation errors due to estimation ambiguities. To overcome this issue, alternative bounds can be derived either based on a deterministic or a Bayesian approach.

For instance, in [109] a Bayesian bound (also referred to as Stochastic Bound (SB)) was derived from the matrix inequality

$$\mathrm{E}_{\tilde{\mathbf{y}}}\{(\hat{\mathbf{z}}-\mathbf{z})^{\mathrm{T}}(\hat{\mathbf{z}}-\mathbf{z})\} \succeq \mathrm{SB}(\mathbf{z}) \triangleq \int_{\mathbb{R}^{\eta}} (\boldsymbol{z}-\bar{\boldsymbol{z}})^{\mathrm{T}}(\boldsymbol{z}-\bar{\boldsymbol{z}})\, p_L\big(\boldsymbol{z}|\vec{\mathbf{d}}\big)\, \mathrm{d}\boldsymbol{z}, \tag{143}$$

in which $\boldsymbol{z}$ is the integration variable, $\bar{\boldsymbol{z}}$ is given by

$$\bar{\boldsymbol{z}} \triangleq \int_{\mathbb{R}^{\eta}} \boldsymbol{z}\, p_L\big(\boldsymbol{z}|\vec{\mathbf{d}}\big)\, \mathrm{d}\boldsymbol{z}. \tag{144}$$

and $p_L(\boldsymbol{z}|\vec{\mathbf{d}})$ is the a posteriori distribution of the estimate $\hat{\mathbf{z}}$ with the minimum entropy, and it is equal to

$$p_L\big(\boldsymbol{z}|\vec{\mathbf{d}}\big) \triangleq \frac{L\big(\boldsymbol{z}|\vec{\mathbf{d}}\big)}{\int\limits_{\mathbb{R}^{\eta}} L\big(\boldsymbol{z}|\vec{\mathbf{d}}\big)\, \mathrm{d}\boldsymbol{z}}. \tag{145}$$

This bound, hereafter referred to as $\mathrm{SB}_{\mathrm{LOS}}$, can provide an accurate estimate to the MSE of a ML estimator, however, a closed-form solution of the integral is difficult to obtain and numeric techniques are needed. On the other hand, deterministic bounds such as the Bhattacharyya Bound (BB) [125], the HCRB [126] and the AHB [7] are less precise, but can be derived in closed form. A neat derivation method, for instance, was proposed by in [7].

Unifying framework for the derivation of deterministic MSE bounds

Let $p_y(\tilde{\mathbf{y}})$ be the distribution of the observation vector $\tilde{\mathbf{y}}$ and $\hat{\mathbf{x}} \triangleq f_e(\tilde{\mathbf{y}})$ be an estimate of $\mathbf{x} \in \mathbb{R}^n$, and f_e is the estimation function. Based on the covariance inequality [127, p. 123], it can be shown that

$$\mathrm{E}_{\tilde{\mathbf{y}}}\{(\hat{\mathbf{x}}-\mathbf{x})^{\mathrm{T}}(\hat{\mathbf{x}}-\mathbf{x})\} \succeq \mathbf{b}_{\mathrm{x}}^{\mathrm{T}}\mathbf{b}_{\mathrm{x}} + \left(\mathrm{E}_{\tilde{\mathbf{y}}}\{\hat{\boldsymbol{\xi}}^{\mathrm{T}}\hat{\boldsymbol{\nu}}\}\mathrm{E}_{\tilde{\mathbf{y}}}\{\hat{\boldsymbol{\nu}}^{\mathrm{T}}\hat{\boldsymbol{\nu}}\}^{-1}\mathrm{E}_{\tilde{\mathbf{y}}}\{\hat{\boldsymbol{\nu}}^{\mathrm{T}}\hat{\boldsymbol{\xi}}\}\right)\Big|_{\hat{\mathbf{x}}=\mathbf{x}}, \quad (146)$$

where $\mathrm{E}_{\tilde{\mathbf{y}}}$ denotes the expectation with respect to the distribution $p_y(\tilde{\mathbf{y}})$, $\mathbf{b}_{\mathrm{x}} \triangleq \mathrm{E}_{\tilde{\mathbf{y}}}\{\hat{\mathbf{x}}-\mathbf{x}\}$, $\hat{\boldsymbol{\xi}} \triangleq \hat{\mathbf{x}} - \mathrm{E}_{\tilde{\mathbf{y}}}\{\hat{\mathbf{x}}\}$ and $\hat{\boldsymbol{\nu}}$ is a free-choice vector that depends on $\hat{\mathbf{x}}$. Let $\hat{\boldsymbol{\nu}}$ be referred to as the *information vector* and let

$$\hat{\boldsymbol{\gamma}}_{\hat{\nu}} \triangleq \mathrm{E}_{\tilde{\mathbf{y}}}\{\hat{\boldsymbol{\xi}}^{\mathrm{T}}\hat{\boldsymbol{\nu}}\}, \quad (147)$$

$$\hat{\mathbf{F}}^{\hat{\nu}} \triangleq \mathrm{E}_{\tilde{\mathbf{y}}}\{\hat{\boldsymbol{\nu}}^{\mathrm{T}}\hat{\boldsymbol{\nu}}\}, \quad (148)$$

be the *information matrix* and the *translation matrix* relative to $\hat{\boldsymbol{\nu}}$, respectively.

Abel proved that the CRLB, the BB, the HCRB and the AHB can be derived from equation (146) by considering different expressions of the information vector. Specifically,

i) The CRLB is obtained with

$$\hat{\boldsymbol{\nu}} = \hat{\boldsymbol{\nu}}_c \triangleq \frac{1}{l(\hat{\mathbf{x}}|\tilde{\mathbf{y}})}\left[\frac{\partial l(\hat{\mathbf{x}}|\tilde{\mathbf{y}})}{\partial \hat{\mathbf{x}}}\right] = \nabla_{\hat{\mathbf{x}}} \ln l(\hat{\mathbf{x}}|\tilde{\mathbf{y}}) \in \mathbb{R}^n, \quad (149)$$

ii) The m-th order BB is obtained with

$$\hat{\boldsymbol{\nu}} = \hat{\boldsymbol{\nu}}_b^{(q)} \triangleq \frac{1}{l(\hat{\mathbf{x}}|\tilde{\mathbf{y}})}\left[\frac{\partial l(\hat{\mathbf{x}}|\tilde{\mathbf{y}})}{\partial \hat{\mathbf{x}}}, \cdots, \frac{\partial^m l(\hat{\mathbf{x}}|\tilde{\mathbf{y}})}{\partial \hat{\mathbf{x}}^{\otimes m}}\right] \in \mathbb{R}^{n^m}, \quad (150)$$

iii) The HCRB is obtained with

$$\hat{\boldsymbol{\nu}} = \hat{\boldsymbol{\nu}}_{hcr} \triangleq \frac{1}{l(\hat{\mathbf{x}}|\tilde{\mathbf{y}})}\left[\Delta(\mathbf{r}_1, \hat{\mathbf{x}}; \tilde{\mathbf{y}}), \cdots, \Delta(\mathbf{r}_n, \hat{\mathbf{x}}; \tilde{\mathbf{y}})\right] \in \mathbb{R}^n, \quad (151)$$

iv) The AHB is obtained with

$$\hat{\boldsymbol{\nu}} = \hat{\boldsymbol{\nu}}_a^{(q)} \triangleq \left[\hat{\boldsymbol{\nu}}_b^{(q)}, \hat{\boldsymbol{\nu}}_{hcr}\right] \in \mathbb{R}^{n+n^m}, \tag{152}$$

where $l(\hat{\mathbf{x}}|\tilde{\mathbf{y}})$ is the likelihood function of $\hat{\mathbf{x}}$ given the observations $\tilde{\mathbf{y}}$, $(\cdot)^{(q)}$ indicates the order of partial derivatives used in the information vector, $\frac{\partial^m}{\partial \hat{\mathbf{x}}^{\otimes m}}$ is the vector of all derivatives with respect to the vector $\hat{\mathbf{x}}$ up to the m-th order, the function

$$\Delta(\mathbf{r}_i, \hat{\mathbf{x}}; \tilde{\mathbf{y}}) \triangleq l(\mathbf{r}_i|\tilde{\mathbf{y}}) - l(\hat{\mathbf{x}}|\tilde{\mathbf{y}}), \tag{153}$$

and the vector $\mathbf{r}_i \in \mathbb{R}^\eta$, referred to as the i-th test point, is given by $\mathbf{r}_i \triangleq \mathrm{E}_{\tilde{\mathbf{y}}}\{\hat{\mathbf{x}}\} + \boldsymbol{\tau}_i$ where $\boldsymbol{\tau}_i \in \mathbb{R}^n$ is an arbitrary vector.

Assuming that the estimator $\hat{\mathbf{x}}$ is unbiased, *i.e.* $\mathrm{E}_{\tilde{\mathbf{y}}}\{\hat{\mathbf{x}}\} = \mathbf{x}$, we obtain

$$\mathrm{E}_{\tilde{\mathbf{y}}}\{(\hat{\mathbf{x}} - \mathbf{x})^{\mathrm{T}} \cdot (\hat{\mathbf{x}} - \mathbf{x})\} \succeq \left(\mathrm{E}_{\tilde{\mathbf{y}}}\{\hat{\boldsymbol{\xi}}^{\mathrm{T}}\hat{\boldsymbol{\nu}}\}\mathrm{E}_{\tilde{\mathbf{y}}}\{\hat{\boldsymbol{\nu}}^{\mathrm{T}}\hat{\boldsymbol{\nu}}\}^{-1}\mathrm{E}_{\tilde{\mathbf{y}}}\{\hat{\boldsymbol{\nu}}^{\mathrm{T}}\hat{\boldsymbol{\xi}}\}\right)\Big|_{\hat{\mathbf{x}}=\mathbf{x}}, \tag{154}$$

and $\mathbf{r}_i = \mathbf{x} + \boldsymbol{\tau}_i$.

In possession of this framework, the HCRB and the AHB, which are conceived for large-scale estimation errors, can be derived as follows.

Derivation of the HCRB and AHB

Replace $\hat{\mathbf{x}}$ by $\hat{\mathbf{z}}$ and $\tilde{\mathbf{y}} = \tilde{\mathbf{d}}$, and for the sake of mathematical convenience, consider $l(\hat{\mathbf{x}}|\tilde{\mathbf{y}}) = L(\hat{\mathbf{z}}|\tilde{\mathbf{d}})$ (LOS likelihood function).

To derive the HCRB, we compute the information vector $\hat{\boldsymbol{\nu}}_{hcr}$ as

$$\hat{\boldsymbol{\nu}}_{hcr} \triangleq \frac{1}{L(\hat{\mathbf{z}}|\tilde{\mathbf{d}})}\left[\Delta(\mathbf{r}_1, \hat{\mathbf{z}}; \tilde{\mathbf{d}}), \cdots, \Delta(\mathbf{r}_{N_R}, \hat{\mathbf{z}}; \tilde{\mathbf{d}})\right], \tag{155}$$

where the i-th test point is given by $\mathbf{r}_i = \mathbf{z} + \tau_i$.

Next we compute the translation vector $\hat{\boldsymbol{\gamma}}_{hcr}$ as

$$\begin{aligned} \hat{\boldsymbol{\gamma}}_{hcr} &\triangleq \mathbb{E}_{\vec{\mathbf{d}}}\{\left(\hat{\mathbf{z}} - \mathbb{E}_{\vec{\mathbf{d}}}\{\hat{\mathbf{z}}\}\right)^{\mathrm{T}}\hat{\boldsymbol{\nu}}_{hcr}\} \\ &= \mathbb{E}_{\vec{\mathbf{d}}}\{\hat{\mathbf{z}}^{\mathrm{T}}\hat{\boldsymbol{\nu}}_{hcr}\} - \mathbb{E}_{\vec{\mathbf{d}}}\{\mathbb{E}_{\vec{\mathbf{d}}}\{\hat{\mathbf{z}}^{\mathrm{T}}\}\hat{\boldsymbol{\nu}}_{hcr}\} \\ &= \left[\tau_1^{\mathrm{T}}, \cdots, \tau_{N_R}^{\mathrm{T}}\right], \end{aligned} \tag{156}$$

where we used the fact that $\mathbb{E}_{\vec{\mathbf{d}}}\{\hat{\mathbf{z}}^{\mathrm{T}}\hat{\boldsymbol{\nu}}_{hcr}\} = 0$.

Replacing equation (155) in (148), we obtain that the ij-th element of HCRB information matrix is equal to

$$
\begin{aligned}
[\hat{\mathbf{F}}^{hcr}_{\mathrm{LOS}}]_{ij} \triangleq & \mathrm{E}_{\tilde{\mathbf{d}}}\left\{ \frac{L(\mathbf{r}_i|\tilde{\mathbf{d}})L(\mathbf{r}_j|\tilde{\mathbf{d}})}{L^2(\hat{\mathbf{z}}|\tilde{\mathbf{d}})} \right\} - 1 \qquad (157)\\
= & \int_{-\infty}^{\infty}\cdots\int_{-\infty}^{\infty}\prod_{q=1}^{N_{\mathrm{A}}} \frac{\exp\left(\frac{(\tilde{d}_q-\hat{d}_q)^2-(\tilde{d}_q-d^{\mathrm{r}}_{qi})^2-(\tilde{d}_q-d^{\mathrm{r}}_{qj})^2}{2\sigma_q^2} \right)}{\sqrt{2\pi}\sigma_q} \mathrm{d}\tilde{d}_1\cdots\mathrm{d}\tilde{d}_{N_{\mathrm{A}}} - 1\\
= & \prod_{q=1}^{N_{\mathrm{A}}} \exp\left(\frac{\hat{d}_q^2-d^{\mathrm{r}}_{qi}-d^{\mathrm{r}}_{qj}}{2\sigma^2} \right) \int_{-\infty}^{\infty}\cdots\int_{-\infty}^{\infty}\prod_{q=1}^{N_A} \exp\left(\frac{-\tilde{d}_q(\tilde{d}_q+2\hat{d}_q-2d^{\mathrm{r}}_{qi}-2d^{\mathrm{r}}_{qj})}{2\sigma_q^2} \right) \mathrm{d}\tilde{d}_1\cdots\mathrm{d}\tilde{d}_{N_{\mathrm{A}}} - 1\\
= & \prod_{q=1}^{N_{\mathrm{A}}} \exp\left(\frac{\hat{d}_q^2+d^{\mathrm{r}}_{qi}d^{\mathrm{r}}_{qj}-\hat{d}_q(d^{\mathrm{r}}_{qi}+d^{\mathrm{r}}_{qj})}{\sigma_q^2} \right) - 1.
\end{aligned}
$$

Finally, replacing the HCRB information $\hat{\mathbf{F}}^{hcr}_{\mathrm{LOS}}$ and the translation matrix (156) in equation (154) yields

$$
\mathrm{HCRB}_{\mathrm{LOS}}(\mathbf{z}) \triangleq \hat{\boldsymbol{\gamma}}_{hcr}\, \hat{\mathbf{J}}^{hcr}_{\mathrm{LOS}}\, \hat{\boldsymbol{\gamma}}^{\mathrm{T}}_{hcr}\Big|_{\hat{\mathbf{z}}=\mathbf{z}}, \qquad (158)
$$

where $\hat{\mathbf{J}}^{hcr}_{\mathrm{LOS}} = \left(\hat{\mathbf{F}}^{hcr}_{\mathrm{LOS}}\right)^{-1}$.

To derive the AHB, first we combine the CRLB and the HCRB information vector to obtain

$$
\hat{\boldsymbol{\nu}}_a \triangleq [\hat{\boldsymbol{\nu}}_c, \hat{\boldsymbol{\nu}}_{hcr}], \qquad (159)
$$

where

$$
\hat{\boldsymbol{\nu}}_c = \nabla_{\hat{\mathbf{z}}} \ln L(\hat{\mathbf{z}}|\tilde{\mathbf{d}}) = -2\sum_{i=1}^{N_{\mathrm{A}}} \left(\frac{\left(\tilde{d}_i - \hat{d}_i\right)}{\sigma_i^2} \left[\cos(\hat{\theta}_i), \sin(\hat{\theta}_i)\right] \right). \qquad (160)
$$

Replacing equation (159) in (148), the AHB information matrix is equal to

$$
\hat{\mathbf{F}}^{a}_{\mathrm{LOS}} \triangleq \mathrm{E}_{\tilde{\mathbf{d}}}\{\hat{\boldsymbol{\nu}}_a^{\mathrm{T}}\hat{\boldsymbol{\nu}}_a\} = \begin{bmatrix} \hat{\mathbf{F}}_{\mathrm{LOS}} & \hat{\mathbf{G}}_{\mathrm{R}}^{\mathrm{T}} \\ \hat{\mathbf{G}}_{\mathrm{R}} & \hat{\mathbf{F}}^{hcr}_{\mathrm{LOS}} \end{bmatrix}. \qquad (161)
$$

where the matrix $\hat{\mathbf{G}}_{\mathrm{R}}$ is formed as the stack of the row vectors $\hat{\mathbf{g}}^{\mathrm{R}}_k$

$$
\hat{\mathbf{g}}^{\mathrm{R}}_k \triangleq \mathrm{E}_{\tilde{\mathbf{d}}}\left\{ \frac{\Delta(\mathbf{r}_k)}{L(\hat{\mathbf{z}}|\tilde{\mathbf{d}})} \frac{\partial L(\hat{\mathbf{z}}|\tilde{\mathbf{d}})}{\hat{\mathbf{z}}} \right\} = \sum_{i=1}^{N_{\mathrm{A}}} \frac{[\cos\hat{\theta}_i, \sin\hat{\theta}_i]}{\sigma_i^2}(d^{\mathrm{r}}_{ik} - \hat{d}_i), \qquad (162)
$$

with $d^{\mathrm{r}}_{ik} \triangleq \|\mathbf{a}_i - \mathbf{r}_k\|_{\mathrm{F}}$.

Next, replacing equation (152) in (147), we obtain

$$\hat{\boldsymbol{\gamma}}_a = [\hat{\boldsymbol{\gamma}}_c, \hat{\boldsymbol{\gamma}}_{hcr}]\,, \tag{163}$$

where $\hat{\boldsymbol{\gamma}}_c = \mathbf{I}_\eta$.

Finally, replacing equations (163) and (161) in equation (146) we obtain that the AHB is given by

$$\mathrm{AHB}_{\mathrm{LOS}}(\mathbf{z}) \triangleq \left([\mathbf{I}_\eta, \hat{\boldsymbol{\gamma}}_{hcr}] \cdot \begin{bmatrix} \hat{\mathbf{F}}_{\mathrm{LOS}} & \hat{\mathbf{G}}_{\mathrm{R}}^{\mathrm{T}} \\ \hat{\mathbf{G}}_{\mathrm{R}} & \hat{\mathbf{F}}_{\mathrm{LOS}}^{hcr} \end{bmatrix}^{-1} \cdot [\mathbf{I}_\eta, \hat{\boldsymbol{\gamma}}_{hcr}]^{\mathrm{T}} \right) \Bigg|_{\hat{\mathbf{z}}=\mathbf{z}}, \tag{164}$$

which can be rewritten as

$$\mathrm{AHB}_{\mathrm{LOS}}(\mathbf{z}) = \left(\mathbf{F}_{\mathrm{LOS}}^{-1} + \mathbf{U}_{\mathrm{R}} \cdot \boldsymbol{\Phi}_{\mathrm{R}}^{-1} \cdot \mathbf{U}_{\mathrm{R}}^{\mathrm{T}} \right), \tag{165}$$

where

$$\mathbf{U}_{\mathrm{R}} \triangleq \mathbf{F}_{\mathrm{LOS}}^{-1} \cdot \mathbf{G}_{\mathrm{R}}^{\mathrm{T}} - \hat{\boldsymbol{\gamma}}_{hcr}, \tag{166}$$

and

$$\boldsymbol{\Phi}_{\mathrm{R}} \triangleq \mathbf{F}_{\mathrm{LOS}}^{hcr} - \mathbf{G}_{N_R}^{a} \cdot \mathbf{F}_{\mathrm{LOS}}^{-1} \cdot \mathbf{G}_{\mathrm{R}}^{\mathrm{T}}. \tag{167}$$

Both the HCRB and the AHB are written as a function of the test points $\mathbf{r}_i$'s, which in fact determine the tightness of the bounds in the low SNR régime. As suggested by Abel in [7], the test should be chosen near the location ambiguities of $\mathbf{z}$. Since these points are not known a priori, we propose an estimation method based on the minimisation of the following *location ambiguity* function

$$f_{\text{A-R}}(\hat{\mathbf{z}}) \triangleq \frac{f_{\mathrm{R}}(\hat{\mathbf{z}})}{\|\hat{\mathbf{z}} - \mathbf{z}\|_{\mathrm{F}}^2}, \tag{168}$$

where $\|\hat{\mathbf{z}} - \mathbf{z}\|_{\mathrm{F}}^2$ acts like a *pole* in $\mathbf{z}$ that cancels the *zero* of the WLS objective $f_{\mathrm{R}}(\hat{\mathbf{z}})$ positioned in $\hat{\mathbf{z}} = \mathbf{z}$.

Comparing the above function to the ambiguity function proposed in definition 1 of [128], it results that equation (168) is the ratio between the directed divergence between the distributions of $\tilde{\mathbf{d}}$ obtained with $\hat{\mathbf{z}}$ and the a priori function $e^{-\|\hat{\mathbf{z}}-\mathbf{z}\|_{\mathrm{F}}^2}$, and its upper bound, *i.e.* 1. Therefore, following the procedure in [128], we estimate the location ambiguity as the minimum of $f_{\text{A-R}}(\hat{\mathbf{z}})$, denoted by $\mathbf{z}_{\text{A-R}}$. Using this result, we define an ambiguity region (grid of N_R points around $\mathbf{z}_{\text{A-R}}$) and evaluate the AHB and the HCRB, where for the latter we also include a set of points around $\mathbf{z}$.

4.6 Numerical studies and bound comparisons

The objective of this section is to study the behaviour of the fundamental limits of a range-based positioning in cooperative and non-cooperative (single target) scenarios. The results will be shown with respect to different system parameters, namely, the meshness-ratio m defined in equation (21), the noise $n_{ij} + b_{ij}$ and the percentage of NLOS links, denoted by p_{NLOS}.

For the specific scenario of a non-cooperative positioning, we use the above results to remark that also in a localization problem exists the probability of location-ambiguity and therefore, the well-known problem of large-errors in the low SNR (large noise) regimé [7, 126, 129].

4.6.1 Studies in cooperative positioning

Consider a typical wireless network with $N_{\mathrm{T}} = 10$ target nodes randomly deployed in an area of 14.14×14.14 square meters[10]. Assume that the anchor locations form a regular polygon and for simplicity let $N_{\mathrm{A}} = 4$. Targets are located in the convex-hull formed by the anchors.

We assume that the channel condition of each link ij is in NLOS with probability p_{NLOS} and, such a probability is independent on the distance d_{ij}. The noise standard deviation is considered identical for all links, $\sigma_{ij} = \sigma = 0.3$ meters [130, 131] $\forall ij$, and $c_{ij} = 1$ if $d_{ij} \leq R_{\mathrm{MAX}}$, where R_{MAX} is the maximum connectivity range. To quantify the overall location accuracy of all nodes in the network, we define the PEB as the average CRLB, *i.e.*

$$\overline{\mathrm{PEB}} \triangleq \sqrt{\mathrm{tr}\big(\mathbf{J}_d\big)/N_{\mathrm{T}}}. \tag{169}$$

In Figure 12, we illustrate the comparison between the PEB derived from the LOS ($\overline{\mathrm{PEB}}_{\mathrm{LOS}}$) and the NLOS ($\overline{\mathrm{PEB}}_{\mathrm{NLOS}}$) assumptions as a function of the meshness ratio, which is varied by changing R_{MAX} between 8 and 20 meters. The results show that the larger the amount of cooperation, the larger the redundancy of information and the smaller the effect of bias in distance measurements. In fact, at high meshness-ratio ($m > 0.9$), the network is nearly fully connected, almost all nodes cooperate with each other and the difference between the LOS and NLOS bounds is practically negligible.

[10] The network deployment area is selected to resemble a typical office environment.

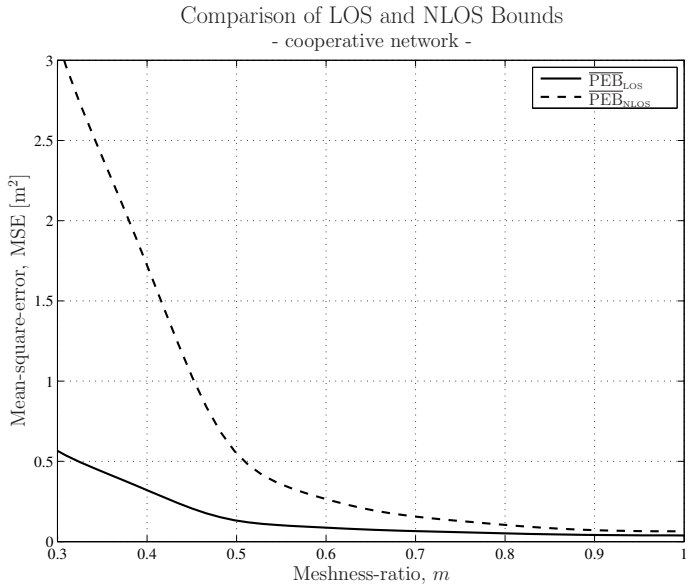

Fig 12. Comparison of the PEB obtained in LOS and NLOS channel conditions as a function of the meshness ratio. The result is shown for regular with $N_{\mathbf{A}} = 4$ anchors and $N_{\mathbf{T}} = 10$ targets.

In Figures 13 and 14 we compare the PEBs as a function of the maximum bias b_{MAX} and the probability of NLOS channel conditions p_{NLOS}, respectively. In these plots, we also show the PEB computed for an incomplete network, where the NLOS links have been removed.

Similarly to the results shown in [92], where the case of non-cooperative positioning was considered, Figures 13 and 14 demonstrate that the PEB obtained by discarding the NLOS measurements is generally higher than that given with the NLOS information. This result is justified by the behaviour of the RII as a function of the noise and bias, as illustrated in Figure 15. The value of ζ_{ij} is always bounded between $1/\sigma_{ij}^2$ and 0, which implies that the information of an NLOS measurement is always less then the one of a LOS data, but larger than a disconnected link. Thus $\mathrm{PEB}_{\mathrm{NLOS}}$ is lower than $\mathrm{PEB}_{\mathrm{LOS}}$ with incomplete information.

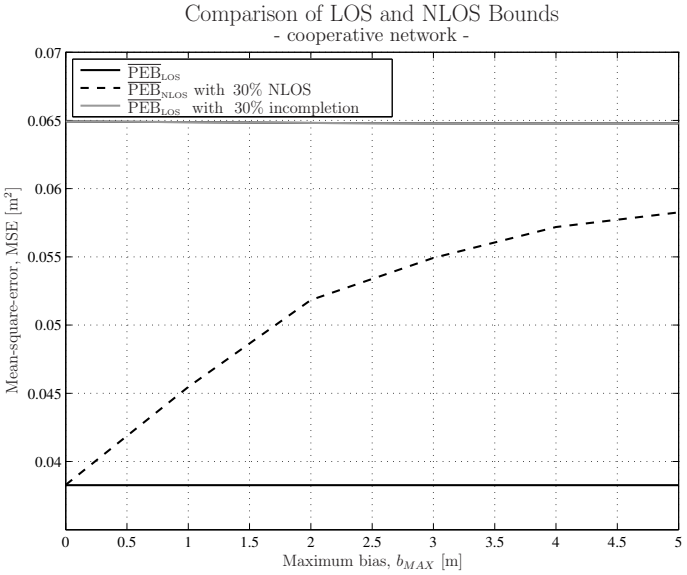

Fig 13. Comparison of the PEB obtained in LOS and NLOS channel conditions as a function of the maximum bias. The result is shown for regular with $N_{\mathbf{A}} = 4$ anchors and $N_{\mathbf{T}} = 10$ targets.

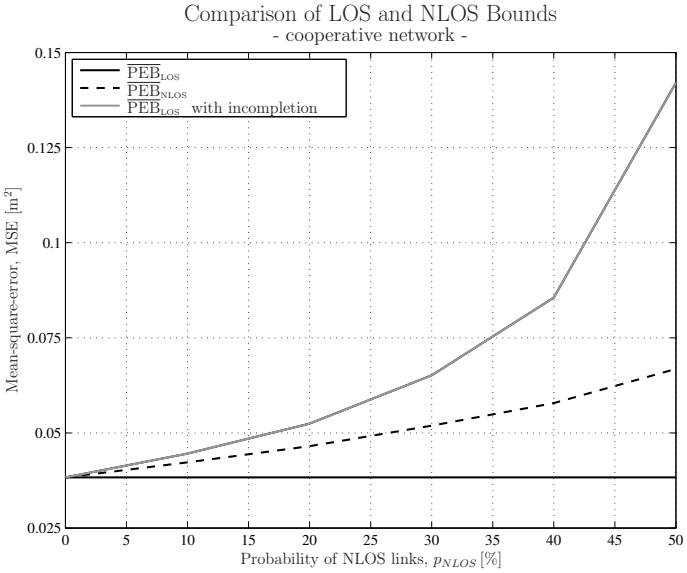

Fig 14. Comparison of the PEB obtained in LOS and NLOS channel conditions as a function of the probability of NLOS. The result is shown for regular with $N_{\mathbf{A}} = 4$ anchors and $N_{\mathbf{T}} = 10$ targets.

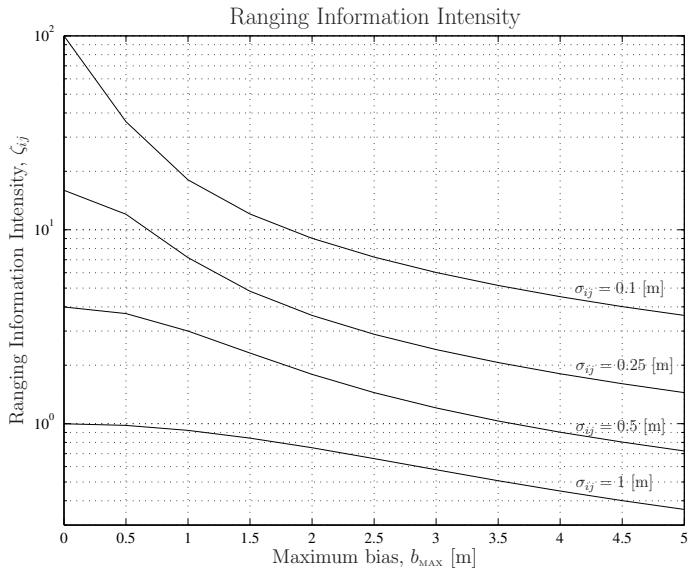

Fig 15. Plot of the RII given by equation (135) **as a function of** b_{MAX} **and** σ_{ij}**.**

4.6.2 Studies in non-cooperative positioning

In this subsection, we consider the case of non-cooperative positioning and investigate the problem of location flip-ambiguity due to the high noise (low SNR) on the distance measurements. For simplicity, it is assumed a ranging error with a zero-mean Gaussian distribution and standard deviation σ.

Figures 16(a) and 16(b) illustrate the location flip-ambiguity phenomenon and the corresponding fundamental limits, respectively. It is noticed that with the considered noise statistics, the ML estimate (marked by "$\times$'s"), which are obtained from a grid-search based minimisation of the log-likelihood function, are grouped in two clusters[11]. The fact that Cluster 2 is not centred in the true target location (marked by "$\bigcirc$") shows the existence of a location ambiguity. The point marked by "$\bullet$" indicates the solution $\mathbf{z}_{\text{A-R}}$ obtained from the optimisation of the ambiguity function $f_{\text{R-A}}$. As expected, such a point is located in the cluster corresponding to the location ambiguities.

[11]Clusters are computed from the *maxclust* function of MATLAB. The ellipses, instead, are derived from the eigenspectrum of the covariance matrices of the ML-samples of each cluster.

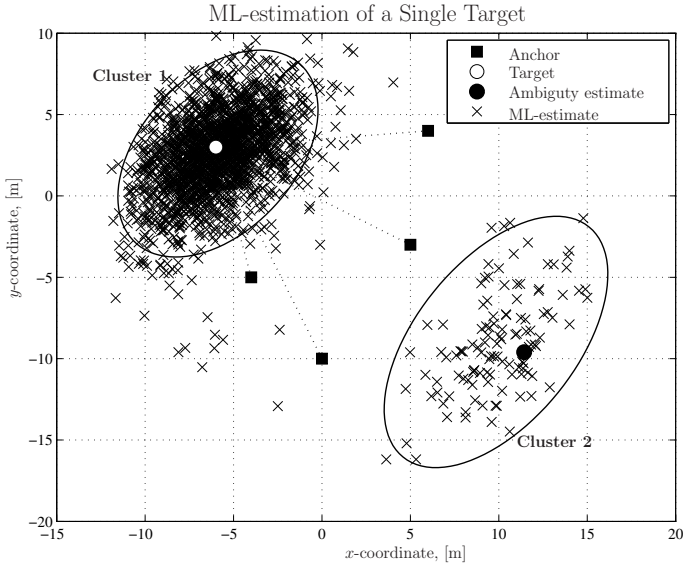

(a) Scatter plot

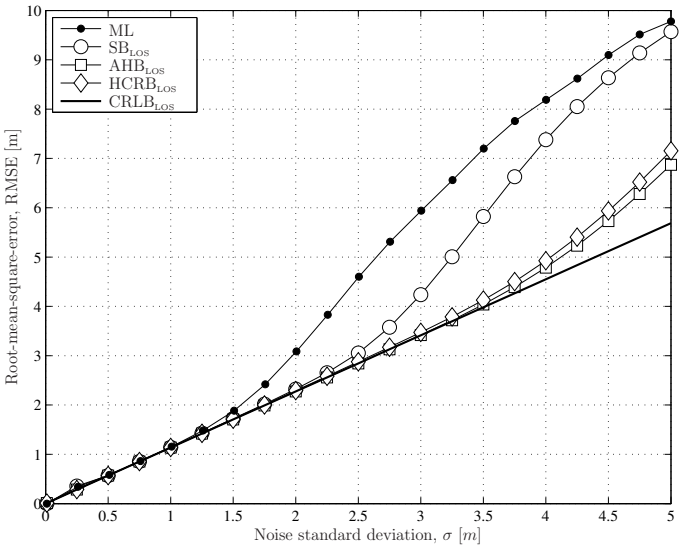

(b) Bounds

Fig 16. Illustration of the location flip-ambiguity problem corresponding to a noise standard deviation $\sigma = 2$ meters.

In Figure 16(b), we compare the RMSE obtained from the ML estimates to the CRLB_{LOS}, the HCRB_{LOS} and the AHB_{LOS} computed from equations (122), (158) and (164), respectively. The test points are derived as suggested in Section 4.5. Specifically, for the HCRB_{LOS} we construct two grids that span symmetrically around $\mathbf{z}$ and $\mathbf{z}_{\text{A-R}}$, respectively. Whereas, for the AHB_{LOS} we consider only a grid around $\mathbf{z}_{\text{A-R}}$.

The comparison shows that the SB [109] can provide a more accurate estimation of the ML-RMSE since it foregoes entirely the use of a prior distribution of the target $\hat{\mathbf{z}}$, replacing it instead by a minimum entropy estimate $L(\hat{\mathbf{z}}|\vec{\mathbf{d}})$. The HCRB and AHB, however, indicate that the location ambiguity problem exists, but in this specific scenario, the noise threshold is not accurately predicted. Better performance can be obtained if the bounds are computed from an optimisation of the bound functions with respect to the test-points.

In Figures 17(a) and 17(b) we show the results obtained with the assumptions of a regular (anchor nodes at the vertexes of a regular polygon) network and the target inside or outside[12] the convex-hull of the anchors, respectively. It can be noticed that the performance of ML estimator deviates from the CRLB only when the noise is large. In fact, all the alternative bounds, namely the SB, the HCRB and the AHB show also similar behaviour to the CRLB. This indicates that with a regular location of the anchors, positioning is less sensitive to the location ambiguity problem despite of the target position. This result suggests that in the design phase of a location system and, in particular, in the planning phase of the anchor locations, it is desirable to deploy the anchors as far as possible to ensure that the target in most likely inside the convex-hull formed by the anchors, and that the shape of such a convex-hull is as close as possible to a regular polygon.

[12]We assume that the target location is within a circle of radius 20 meters and always outside the convex-hull of the anchors.

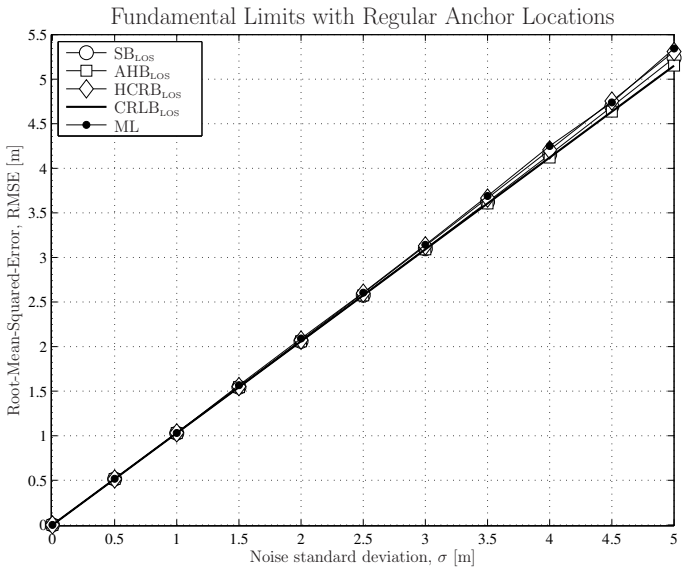

(a) Target inside the convex-hull of the anchors

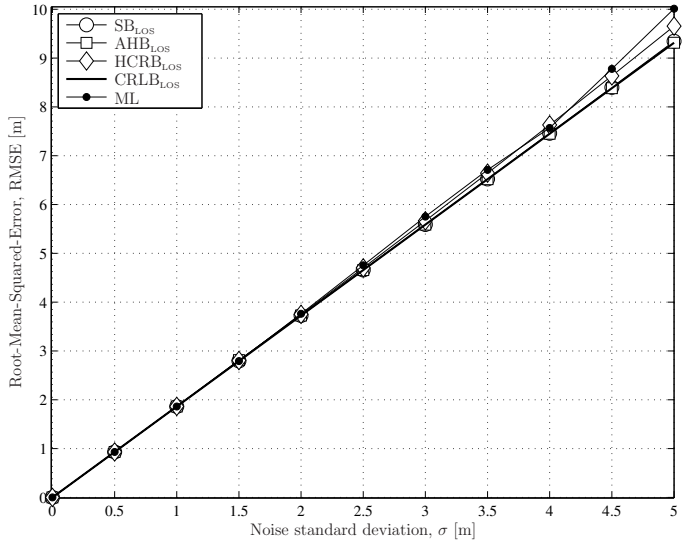

(b) Target outside the convex-hull of the anchors

Fig 17. Comparisons of different bounds and the ML RMSE as a function of the noise standard deviation.

4.7 Summary and discussions

In this chapter, an error analysis of the distance-positioning problem has been provided together with several new results and explicative examples. Theorem T6 is fundamentally important to understand the feasibility of a positioning problem. As mentioned in Section 1.2, the positioning problem is not a mere estimation problem. Localisation is also an Euclidean embedding problem, which is governed by other fundamental limits. The bundle of these two aspects is provided with the proof of consistency.

The results shown in Theorems T7, T8 and Corollaries C2 and C3 are new contributions to the understanding of cooperative positioning and the information-coupling. With the proposed examples, we have shown that the double effect of decoupling. On the one hand, by decoupling the information with the disconnection of a link, the location error increases. On the other hand, the propagation of location uncertainty can be combated by decoupling two or more portions of the networks, for instance, by introducing anchors. This consideration opens an entirely new direction for the design of anchor's deployment strategies that can minimise the average localisation error in the whole network.

To conclude, the proposed numerical studies have also revealed that sufficient cooperation can minimise the average PEB obtained in NLOS scenarios, that NLOS measurements are informative and therefore can not be discarded. Finally, we have observed that the location ambiguity problem can be minimised by deploying the anchors as close as possible to a regular polygon, and that minimum error can be achieved if the target lies in the convex hull of the anchors.

5 Non-cooperative positioning

Non-cooperative positioning refers to a localisation system where target nodes can communicate only with the anchors. The fundamental scenario, therefore, can be simply described by a star-like network topology, as depicted in Figure 18.

Non-cooperative positioning is primarily considered for application scenarios such as cellular and Wi-Fi networks, where a target is typically connected to fixed base-stations (anchors) only. Due to the lack of cooperation with other targets, the amount of redundant information is little and it is difficult to cope with NLOS channel conditions. In Chapter 2, we reviewed the state-of-the-art of the optimisation and mitigation error techniques for non-cooperative positioning, and showed that in LOS and NLOS scenarios the TS-WLS [39] and the C-NLS modified [57] are the best performing algorithm, respectively.

In this chapter, we address the specific problem of NLOS mitigation in a non-cooperative positioning scheme. Starting from an analytical study on the effects of the ranging errors on the WLS objective function $f_R(\vec{\tilde{\mathbf{p}}})$, we derive the original principle of DC and propose two bias-robust positioning algorithms.

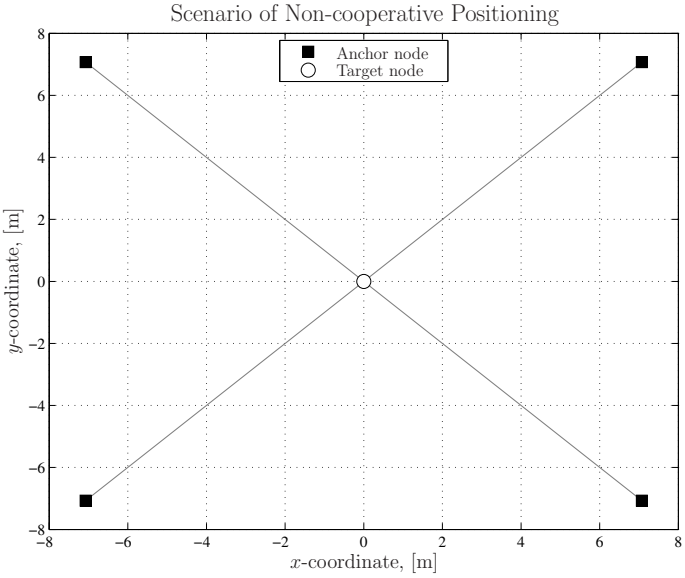

Fig 18. Network model for non-cooperative positioning systems.

5.1 The distance contraction principle

For the sake of clarity, let us simplify the notation by referring to the vector of the anchor's coordinates $\hat{\mathbf{p}}_i$, with $1 \leq i \leq N_{\mathrm{A}}$, by $\mathbf{a}_i$, to the coordinate vector of the target node $\hat{\mathbf{p}}_N$ by $\hat{\mathbf{z}}$ and, to the distance measurements d_{iN} by d_i. Therefore, the WLS objective function $f_R(\vec{\hat{\mathbf{p}}})$ can be written as a function of $\hat{\mathbf{z}}$ only, *i.e.* $f_R(\hat{\mathbf{z}})$, and the gradient and the Hessian are respectively equal to

$$\nabla_{\hat{\mathbf{z}}} f_R(\hat{\mathbf{z}}) = \sum_{i=1}^{N_{\mathrm{A}}} (\mathbf{a}_i - \hat{\mathbf{z}}) \frac{\tilde{d}_i - \hat{d}_i}{\hat{d}_i}, \tag{170}$$

$$\nabla^2_{\hat{\mathbf{z}}} f_R(\hat{\mathbf{z}}) = \mathbf{I}_\eta \sum_{i=1}^{N_{\mathrm{A}}} \frac{\hat{d}_i - \tilde{d}_i}{\hat{d}_i} + \sum_{i=1}^{N_{\mathrm{A}}} \frac{\tilde{d}_i}{\hat{d}_i} \boldsymbol{\Upsilon}_i. \tag{171}$$

The principle of distance contraction is based on the set of Lemmas and Theorems proposed in the following subsections, which will prove that there exists a perturbation vector $\boldsymbol{\rho} \triangleq [\rho_1, \cdots, \rho_{N_{\mathrm{A}}}]$ such that, with $\tilde{d}_i = d_i + \rho_i \; \forall \, i$:

a) The WLS objective function is convex, *i.e.* $\nabla^2_{\hat{\mathbf{z}}} f_R(\hat{\mathbf{z}}) \succeq 0 \, \forall \hat{\mathbf{z}} \in \mathbb{R}^\eta$

b) The global minimum $\hat{\mathbf{z}}^*$ of $f_R(\hat{\mathbf{z}})$ is confined to the true target location $\mathbf{z}$.

5.1.1 Ranging error and function convexity

We start with the analysis of the cost-function $f(\hat{\mathbf{z}})$ and, in particular, seek the conditions for the existence of convexity and local minima. To this end, consider the gradient $\nabla_{\vec{\hat{\mathbf{p}}}}$ and the Hessian $\nabla^2_{\vec{\hat{\mathbf{p}}}}$ of $f(\vec{\hat{\mathbf{p}}})$.

Lemma L5 (Characterization of the convex regions of $f_R(\mathbf{z})$)**.**

Let $\varphi_i \triangleq \tilde{d}_i / \hat{d}_i$. For all $\hat{\mathbf{z}}$ such that $\sum_{i=1}^{N_{\mathrm{A}}} \varphi_i \leq N_{\mathrm{A}}$, the function $f_R(\hat{\mathbf{z}})$ is convex.

Proof. Replace φ_i in equation (171), and re-write the Hessian as

$$\begin{aligned} \nabla^2_{\hat{\mathbf{z}}} f_R(\hat{\mathbf{z}}) &= 2\mathbf{I}_\eta \sum_{i=1}^{N_{\mathrm{A}}} (1 - \varphi_i) + 2 \sum_{i=1}^{N_{\mathrm{A}}} \varphi_i \boldsymbol{\Upsilon}_i \\ &= 2\mathbf{I}_\eta (N_{\mathrm{A}} - \sum_{i=1}^{N_{\mathrm{A}}} \varphi_i) + 2 \sum_{i=1}^{N_{\mathrm{A}}} \varphi_i \boldsymbol{\Upsilon}_i. \end{aligned} \tag{172}$$

From the above, it follows that if $\sum_{i=1}^{N_{\mathrm{A}}} \varphi_i \leq N_{\mathrm{A}}$, then $\nabla^2_{\hat{\mathbf{z}}} f_R(\hat{\mathbf{z}}) \succeq 0$ since $\nabla^2_{\hat{\mathbf{z}}} f_R(\hat{\mathbf{z}})$ is given by the positive sum of psd matrices. □

Lemma L5 shows that $\sum_{i=1}^{N_\mathrm{A}} \varphi_i \leq N_\mathrm{A}$ is a sufficient condition to characterize the local convexity of $f_R(\hat{\mathbf{z}})$. In particular, this result will be utilized as a tool to determine the regions of $\mathrm{dom}(f_R)$ where the WLS objective function is convex, and how they change with imperfect ranging information. Before we address this, let us provide some topological definitions.

Definition D5 (Convex-hull of the anchors)**.**

The convex-hull defined by the anchors, denoted by $\mathcal{C}(\mathbf{P}_\mathrm{A})$, is the set of points $\mathbf{p} \in \mathbb{R}^\eta$ such that

$$\mathcal{C}(\mathbf{P}_\mathrm{A}) \triangleq \left\{ \mathbf{p} = \sum_{i=1}^{N_\mathrm{A}} \omega_i \mathbf{a}_i \;\middle|\; \omega_i \in \mathbb{R},\, \omega_i \geq 0,\, \sum_{i=1}^{N_\mathrm{A}} \omega_i = 1 \right\}. \tag{173}$$

Definition D6 (Enclosed point)**.**

A point $\mathbf{p} \in \mathcal{C}(\mathbf{P}_\mathrm{A})$ is referred to as enclosed.

Now, let us introduce the Lemma on the enclosed set, which establishes the existence of a convex set around the true target location $\mathbf{z}$.

Lemma L6 (Enclosed set)**.**

Let $B \subseteq \mathcal{C}(\mathbf{P}_\mathrm{A})$ be a non-empty sphere $\|\hat{\mathbf{z}} - \vec{\mathbf{o}}\|_\mathrm{F} \leq \delta_B$, where δ_B denotes the radius and $\vec{\mathbf{o}} \in \mathbb{R}^\eta$ denotes the centre point, i.e. the point that is equidistant from the boundaries of the set. If $\mathbf{z} \in \mathcal{C}(\mathbf{P}_\mathrm{A})$ and $\rho_i = 0\,\forall i$ then,

$$\exists \delta_B \geq 0 \mid \vec{\mathbf{o}} = \mathbf{z} \text{ and } \nabla^2_{\hat{\mathbf{z}}} f_R(\hat{\mathbf{z}}) \succeq 0,\ \forall \hat{\mathbf{z}} \in B. \tag{174}$$

Proof. Let $\hat{\mathbf{z}}^*$ be the global minimum of $f_R(\hat{\mathbf{z}})$. Given that $f_R(\hat{\mathbf{z}})$ is a regular function, and convex around $\hat{\mathbf{z}}^*$, $f_R(\hat{\mathbf{z}})$ can be locally approximated at $\hat{\mathbf{z}}^*$ by a quadratic function derived from the Taylor series of $f_R(\hat{\mathbf{z}})$ truncated at the second order [65, pp. 67]. The residual of the approximation is a function of δ_B, therefore it can be arbitrarily small with an infinitesimal δ_B.

Based on this approximation, we prove that $\nabla^2_{\hat{\mathbf{z}}} f_R(\hat{\mathbf{z}}) \succeq 0,\ \forall \hat{\mathbf{z}} \in B$ where B is a non-empty sphere with $\delta_B \geq 0$ and centre $\hat{\mathbf{z}}^*$. Furthermore, since the network is strongly-localisable and ranging information is exact, $\hat{\mathbf{z}}^* = \mathbf{z}$ and the set B can be uniquely determined within the convex hull $\mathcal{C}(\mathbf{P}_\mathrm{A})$. □

Lemma L6 affirms that under the assumption that $\mathbf{z} \in \mathcal{C}(\mathbf{P}_\mathrm{A})$ and $\rho_i = 0\,\forall i$, $\mathbf{z}$ can be enclosed in a convex-set where the function is convex. Our main objective,

however, is to relate the size of the convex set B with the ranging errors. To this end, we utilize the condition of Lemma L5 and show that negative ranging errors preserve the enclosed state of $\mathbf{z}$ and enlarge the radius of the region B.

Lemma L7 (Preservation of the convex regions with negative perturbations)**.** *Let $\hat{\mathbf{z}} \in B$. If $-d_i \leq \rho_i \leq 0 \ \forall i$, then $\nabla^2_{\hat{\mathbf{z}}} f_R(\hat{\mathbf{z}}) \succeq 0$.*

Proof. Replace $\tilde{d}_i$ in equation (230) by $d_i + \rho_i$. The assumption $-d_i \leq \rho_i \leq 0 \ \forall i$ implies $\tilde{d}_i \leq d_i$, and consequently

$$\sum_{i=1}^{N_\mathrm{A}} \frac{\tilde{d}_i}{\hat{d}_i} \leq \sum_{i=1}^{N_\mathrm{A}} \frac{d_i}{\hat{d}_i} N_\mathrm{A}. \tag{175}$$

By Lemma L5, $\nabla^2_{\hat{\mathbf{z}}} f_R(\hat{\mathbf{z}}) \succeq 0 \ \forall \hat{\mathbf{z}} \in B$ and, therefore the size of B is preserved. □

Next, we study how the radius of B is modified with $-d_i \leq \rho_i \leq 0 \ \forall i$.

Theorem T9 (Wider convex regions with negative ranging perturbations)**.**

Let B' be a non-empty sphere with centre $\vec{\mathbf{o}}$ and radius δ'_B. If $\mathbf{z} \in \mathcal{C}(\mathbf{P}_\mathrm{A})$ and $-d_i \leq \rho_i \leq 0 \ \forall i$ then,

$$\exists B' \supseteq B \,|\, \nabla^2_{\hat{\mathbf{z}}} f_R(\hat{\mathbf{z}}) \succeq 0, \ \forall \hat{\mathbf{z}} \in B'. \tag{176}$$

Proof. Let B the convex set obtained with $\rho_i = 0 \ \forall \, i$ and, construct B' as

$$B' \triangleq \{\hat{\mathbf{z}} \mid \|\hat{\mathbf{z}} - \vec{\mathbf{o}}\|_\mathrm{F} \leq \delta'_B \}. \tag{177}$$

where $\vec{\mathbf{o}} = \mathbf{z}$ and $\delta'_B = \varrho_B + \Delta_B$.

Let $\hat{\mathbf{z}}_B$ be a point on the boundary of B and let $\hat{d}_i^B$ denote the distance $\|\hat{\mathbf{z}}_B - \mathbf{a}_i\|_\mathrm{F}$. Using trigonometric rules, $\hat{d}_i^B$ can be written as

$$\hat{d}_i^B = \sqrt{d_i^2 + (\varrho_B + \Delta_B)^2 - 2(\varrho_B + \Delta_B) d_i \cos\theta_{iN\hat{z}_B}}, \tag{178}$$

where $\theta_{iN\hat{z}_B}$ is the angle between the vectors $(\hat{\mathbf{z}}_B - \mathbf{z})$ and $(\mathbf{a}_i - \mathbf{z})$.

The value of $\hat{d}_i^B$ is bounded within $d_i \pm \mathrm{abs}(\varrho_B + \Delta_B)$, thus

$$\sum_{i=1}^{N_\mathrm{A}} \frac{d_i - \mathrm{abs}(\rho_i)}{\hat{d}_i^B} \leq \sum_{i=1}^{N_\mathrm{A}} \frac{d_i - \mathrm{abs}(\rho_i)}{d_i - \mathrm{abs}(\varrho_B + \Delta_B)}, \tag{179}$$

where abs() is the absolute value function.

To ensure that $\nabla^2_{\hat{\mathbf{z}}} f_R(\hat{\mathbf{z}}) \succeq 0,\ \forall \hat{\mathbf{z}} \in B'$, by Lemma L5, it is sufficient that

$$\sum_{i=1}^{N_\mathrm{A}} \frac{d_i - |\rho_i|}{d_i - \mathrm{abs}(\varrho_B + \Delta_B)} \sum_{i=1}^{N_\mathrm{A}} -N_\mathrm{A} \leq 0. \tag{180}$$

Solving the inequality with respect to Δ_B, it is found that

$$0 \leq \mathrm{abs}(\varrho_B + \Delta_B) \leq \min(\{\mathrm{abs}(\rho_i), d_i\}). \tag{181}$$

Imposing the constraint $\Delta_B > 0$, it follows that the radius of B' is defined within ϱ_B and $\min(\{\mathrm{abs}(\rho_i), d_i\})$. □

By Theorem T9, we established that under negative ranging perturbations, or equivalently *contracted* distances, the region B expands. Consequently, the number of local minima of $f_R(\hat{\mathbf{p}})$ may decrease. The next step is to establish the conditions for convexity in the whole function domain.

Corollary C4 (Full convexity with large negative ranging perturbations)**.**
If $\rho_i \leq -d_i\ \forall i$, then $\nabla^2_{\hat{\mathbf{z}}} f_R(\hat{\mathbf{z}}) \succeq 0\ \forall \hat{\mathbf{z}} \in \mathbb{R}^\eta$.

Proof. Replace $\tilde{d}_i$ in equation (171) by $d_i + \rho_i$ and rewrite the Hessian as

$$\begin{aligned} \nabla^2_{\hat{\mathbf{z}}} f_R(\hat{\mathbf{z}}) &= 2\mathbf{I}_\eta \sum_{i=1}^{N_\mathrm{A}} \frac{\hat{d}_i - d_i - \rho_i}{\hat{d}_i} + 2\sum_{i=1}^{N_\mathrm{A}} \frac{d_i + \rho_i}{\hat{d}_i} \hat{\boldsymbol{\Upsilon}}_{iN} \\ &= 2N_\mathrm{A}\mathbf{I}_\eta + 2\sum_{i=1}^{N_\mathrm{A}} \varphi_i^\rho \left(\mathbf{I}_\eta - \hat{\boldsymbol{\Upsilon}}_{iN}\right), \end{aligned} \tag{182}$$

where $\varphi_i^\rho \triangleq -\frac{d_i + \rho_i}{\hat{d}_i} \geq 0$.

Rewrite the difference $\mathbf{I}_\eta - \hat{\boldsymbol{\Upsilon}}_{iN}$ as

$$\mathbf{I}_\eta - \hat{\boldsymbol{\Upsilon}}_{iN} = \begin{bmatrix} \sin^2(\hat{\theta}_{iN}) & -\sin(\theta_i)\cos(\hat{\theta}_{iN}) \\ -\sin(\hat{\theta}_{iN})\cos(\hat{\theta}_{iN}) & \cos^2(\theta_{iN}) \end{bmatrix}. \tag{183}$$

From equation (182), it follows that $\nabla^2_{\hat{\mathbf{z}}} f_R(\hat{\mathbf{z}}) \succeq 0$ since it is the positive sum of psd matrices. □

Corollary C4 achieves the first objective of the distance contraction principle defined in the introduction of Section 5.1. In short, by Theorem T9 we demonstrated that negative errors, or equivalently the condition contracted

distances, increases the size of the convex regions of $f_R(\hat{\mathbf{z}})$, and that if $\rho_i \leq -d_i$ $\forall i$ such regions extend to the whole function domain.

The next subsection is focused on the second objective of the distance contraction principle, that is the confinement of $\hat{\mathbf{z}}^*$ to $\mathbf{z}$.

5.1.2 Ranging perturbation and function global minimum

Consider the first-order condition of a minimum *i.e.* $\nabla_{\hat{\mathbf{z}}} f_R(\hat{\mathbf{z}}) = \mathbf{0}_\eta$. Replace $\tilde{d}_i$ by $d_i + \rho_i$ in equation (170) to obtain

$$\sum_{i=1}^{N_\mathrm{A}} \frac{d_i - \hat{d}_i}{\hat{d}_i}(\mathbf{a}_i - \hat{\mathbf{z}}) = -\sum_{i=1}^{N_\mathrm{A}} \frac{\rho_i}{\hat{d}_i}(\mathbf{a}_i - \hat{\mathbf{z}}). \tag{184}$$

From the above we derive the following Lemma, which provides the conditions for the confinement of $\hat{\mathbf{z}}^*$ in the convex-hull $\mathcal{C}(\mathbf{P}_A)$.

Lemma L8 (Confinement of the WLS minima to the convex-hull of the anchors)**.** *If $\rho_i \leq -d_i \ \forall i$. Then,*

$$\exists | \bar{\mathbf{z}} \in \mathcal{C}(\mathbf{P}_\mathrm{A}) \,|\, \nabla_{\hat{\mathbf{z}}} f_R(\bar{\mathbf{z}}) = \mathbf{0}_\eta. \tag{185}$$

Proof. From equation (184), a minimum of $f_R(\hat{\mathbf{z}})$, denoted by $\bar{\mathbf{z}}$, can be found from the condition

$$\hat{\mathbf{z}} = \sum_{i=1}^{N_\mathrm{A}} \omega_i^\rho \mathbf{a}_i, \tag{186}$$

where

$$\omega_i^\rho \triangleq \frac{(d_i + \rho_i - \hat{d}_i)/\hat{d}_i)}{\sum_{i=1}^{N_\mathrm{A}} (d_i + \rho_i - \hat{d}_i)/\hat{d}_i}. \tag{187}$$

Since $\tilde{d}_i = d_i + \rho_i \leq 0 \, \forall i$ then, $0 \leq \omega_i^\rho \leq 1 \, \forall i$. Therefore, by definition of a convex-hull, $\bar{\mathbf{z}} \in \mathcal{C}(\mathbf{P}_\mathrm{A})$. □

Corollary C5 (Global minimum of the WLS objective with contracted distances)**.** *If $\tilde{d}_i = d_i + \rho_i \leq 0 \, \forall i$, the minimum $\bar{\mathbf{z}}$ is the global minimum of $f_R(\hat{\mathbf{z}})$.*

Proof. By Corollary 4 $f_R(\hat{\mathbf{z}})$ in convex $\forall \hat{\mathbf{z}} \in \mathbb{R}^\eta$. Therefore, $\bar{\mathbf{z}}$ is the global minimum of $f_R(\hat{\mathbf{z}})$, that is $\bar{\mathbf{z}} = \hat{\mathbf{z}}^*$. □

With Lemma L8 and Corollary C5, we demonstrate that contracted distances confine the global minimum of $f_R(\hat{\mathbf{z}})$ in the convex-hull $\mathcal{C}(\mathbf{P}_{\mathrm{A}})$. Now, the last step is to determine when contracted distances will imply the equality $\hat{\mathbf{z}}^* = \mathbf{z}$. To this end, let us introduce two more definitions.

Definition D7 (Null-space function)**.**

Let $\mathcal{N} : \mathbb{R}^{n\times q} \to \mathbb{R}^{q\times(q-r)}$ be a function that computes the orthogonal basis of the null space of a matrix $\mathbf{A} \in \mathbb{R}^{n\times q}$ with column rank $r \leq q$ [91]*.*

Definition D8 (Relative angle matrix)**.**

Let $\boldsymbol{\Omega}$ be the relative angle matrix [67] *defined as*

$$O(\mathbf{P}) \triangleq \boldsymbol{\Omega} = \begin{bmatrix} 1 & \cos(\theta_{1N2}) & \dots & \cos(\theta_{1NN_{\mathrm{A}}}) \\ \cos(\theta_{1N2}) & 1 & \ddots & \cos(\theta_{2NN_{\mathrm{A}}}) \\ \vdots & \ddots & \dots & \vdots \\ \cos(\theta_{1NN_{\mathrm{A}}}) & \cos(\theta_{2NN_{\mathrm{A}}}) & \dots & 1 \end{bmatrix}, \tag{188}$$

where θ_{iNj} is the angle between the vectors $(\mathbf{a}_i - \mathbf{z})$ and $(\mathbf{a}_j - \mathbf{z})$, and $O(\mathbf{P})$ is the relative angle kernel function.

Theorem T10 (Confinement to the true target's location)**.**

If $\mathbf{z} \in \mathcal{C}(\mathbf{P}_{\mathrm{A}})$, $\rho_i \leq -d_i$ and $\boldsymbol{\rho} \in \mathcal{N}(\boldsymbol{\Omega})$, then $\hat{\mathbf{z}}^* = \mathbf{z}$.

Proof. Consider equation (184) and assume that $\hat{\mathbf{z}} = \mathbf{z}$. The left part of equation (184) is 0 since $\frac{d_i - \hat{d}_i}{\hat{d}_i} = 0\,\forall i$. Rewrite equation (184) in a matrix form as

$$\boldsymbol{\rho}^{\mathrm{T}}\boldsymbol{\Xi} = \mathbf{0}_\eta, \tag{189}$$

where $\boldsymbol{\Xi} \in \mathbb{R}^{N_{\mathrm{A}}\times\eta}$ is a matrix with the i-th row-vector given by $[\cos\theta_{iN}, \sin\theta_{iN}]$.

Equation (189) implies that $\boldsymbol{\rho} \in \mathcal{N}(\boldsymbol{\Xi}^{\mathrm{T}})$. Notice, however, that the null-space of $\boldsymbol{\Xi}$ does not change if we consider the matrix product $\boldsymbol{\Xi}\boldsymbol{\Xi}^{\mathrm{T}}$. Now, since the i-th row-vector of $\boldsymbol{\Xi}$ is equal to $[\cos\theta_i, \sin\theta_i]$, it follows that $\boldsymbol{\Xi}\boldsymbol{\Xi}^{\mathrm{T}} = \boldsymbol{\Omega}$. Therefore, the condition $\boldsymbol{\rho} \in \mathcal{N}(\boldsymbol{\Omega})$ implies $\nabla_{\hat{\mathbf{z}}} f_R(\hat{\mathbf{z}})|_{\hat{\mathbf{z}}=\mathbf{z}} = \mathbf{0}_\eta$, which together with the assumptions $\mathbf{z} \in \mathcal{C}(\mathbf{P}_{\mathrm{A}})$ and $\rho_i \leq -d_i$ imply $\hat{\mathbf{z}}^* = \mathbf{z}$. □

In order to exemplify the distance contraction principle exposed above, an illustration is provided in Figure 19. Specifically, Figure 19(a) shows the contour-plot and the convex regions of the WLS objective function (dotted area) obtained with exact ranging. Figures 19(b) and 19(c), instead, illustrate

the variations of the WLS objective function when distances measurements are affected by errors. In particular, the comparison of Figure 19(b) to 19(c), proves that the convex-regions of the function are much wider (almost the whole domain) when $0 < \tilde{d}_i + \rho_i < d_i \, \forall i$. Finally, in the Figure 19(d) it is shown that the contracted distances, computed as in Theorem T10, transform $f_R(\hat{\mathbf{z}})$ into a convex function with the global minimum confined to the true target location.

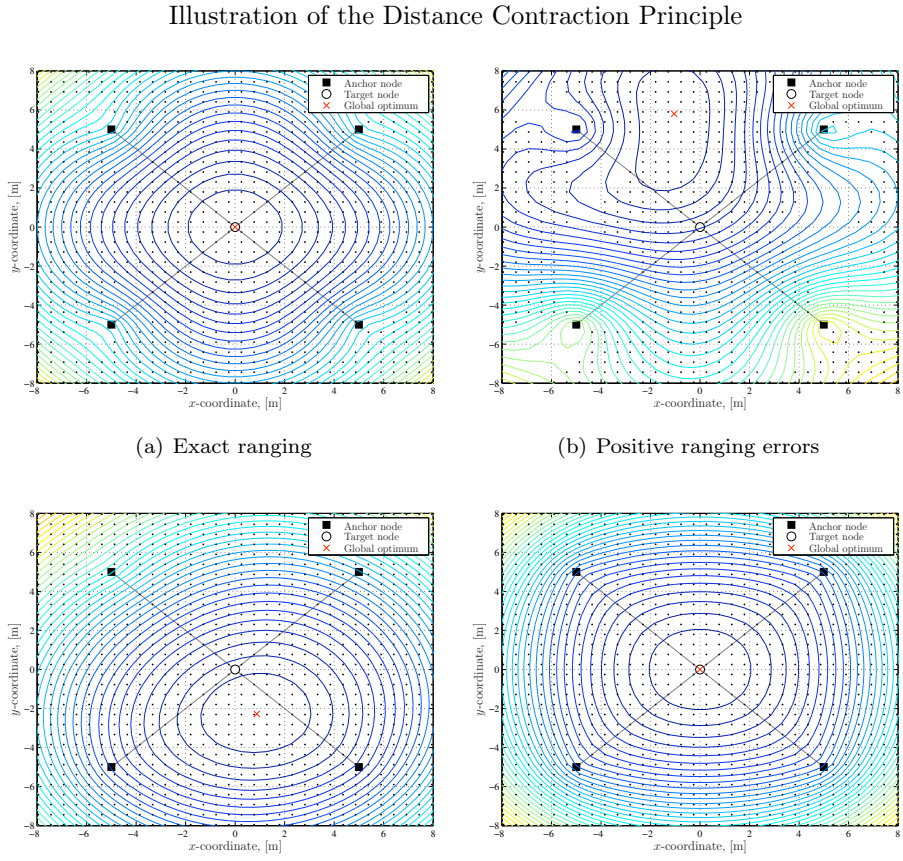

(a) Exact ranging

(b) Positive ranging errors

(c) Negative ranging errors

(d) Contracted distances

Fig 19. Figures a)**,** b)**,** c) **and** d) **illustrate the contour plots of the WLS objective function under** 4 **different types of ranging errors, specifically,** $\boldsymbol{\rho} = \mathbf{0}$**,** $\boldsymbol{\rho} \geq \mathbf{0}$**,** $-\mathbf{d} < \boldsymbol{\rho} < \mathbf{0}$ **and** $\boldsymbol{\rho} \leq \mathbf{0}$ **with** $\boldsymbol{\rho} = \mathcal{N}(\Omega)$**. The global optimum is found via grid-search.**

5.2 Localisation via distance contraction

Based on the DC-principle previously explained, we propose a modified WC and NLS-based optimisation algorithms for non-cooperative positioning in NLOS channel conditions. The original methods are well-known in the literature because of the low-complexity and ease of implementation [25, 32].

The general framework for a DC-based techniques consists of:

1) Estimation of the relative angle kernel $\mathbf{\Omega}$
2) Calculation of the contraction vector $\hat{\boldsymbol{\rho}}$
3) Minimisation of the WLS-objective function with contracted distances.

Assume that $\mathbf{z} \in \mathcal{C}(\mathbf{P}_{\mathrm{A}})$ and that a bias $b_i > 0$ on the ranging of the i-th target-to-anchor distance exist. As shown in Figure 20 the intersection area of the circular traces derived from the measurements defines a convex region, referred to as the *feasibility region*, with $\mathbf{z} \in B_D$ [57, 87, 132].

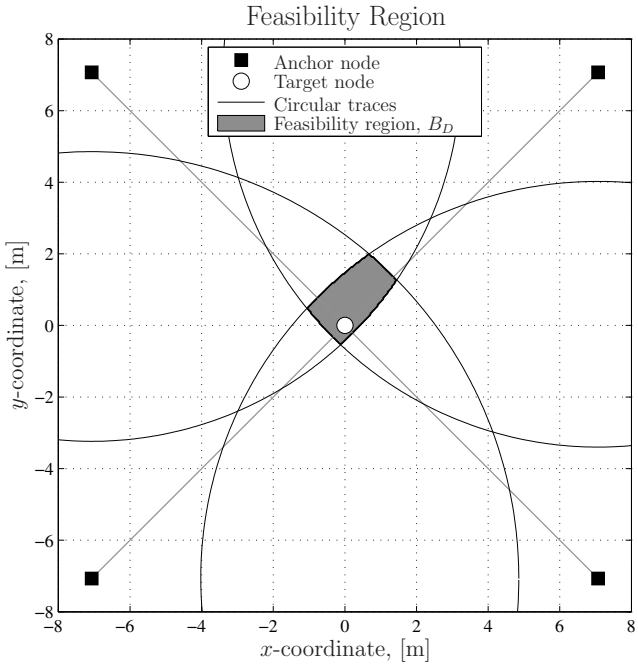

Fig 20. Formation of the feasibility region with biased measurements.

The relative angle kernel can be estimated as $\hat{\mathbf{\Omega}} \triangleq O(\vec{\mathbf{o}}^{B_D})$, where $\vec{\mathbf{o}}^{B_D}$ denotes the centre of B_D, and it can be approximated as

$$\vec{\mathbf{o}}^{B_D} \approx \hat{\vec{\mathbf{o}}}^{B_D} \triangleq \frac{1}{N_v} \sum_{i=1}^{N_v} \mathbf{p}_i^{B_D}, \tag{190}$$

where and N_v are $\mathbf{p}_i^{B_D}$ the number of vertexes and the coordinates of the i-th vertex of B_D, respectively.

If the feasibility region can not be identified (*i.e.*, the intersection of the circular traces is empty), we may relax the constraint $\mathbf{z} \in B_D$ to $\mathbf{z} \in \mathcal{C}(\mathbf{P}_A)$ and compute $\hat{\vec{\mathbf{o}}}^{B_D}$ as a solution to the least square optimisation problem

$$\begin{aligned} \min_{\hat{\mathbf{z}} \in \mathbb{R}^\eta} \quad & \sum_{i=1}^{N_\mathrm{A}} (\tilde{d}_i^2 - \hat{d}_i^2)^2, \\ \text{s.t.} \quad & \hat{\mathbf{z}} \in \mathcal{C}(\mathbf{P}_A). \end{aligned} \tag{191}$$

To simplify the optimisation problem, we rewrite the difference $(\tilde{d}_i^2 - \hat{d}_i^2)$ as

$$\hat{d}_i^2 - \tilde{d}_i^2 = \|\mathbf{a}_1\|_\mathrm{F}^2 + \|\boldsymbol{\omega}^\mathrm{T} \mathbf{P}_A\|_\mathrm{F}^2 - 2\mathbf{a}_i \mathbf{P}_A^\mathrm{T} \boldsymbol{\omega} - \tilde{d}_i^2, \tag{192}$$

where $\hat{\mathbf{z}}$ was replaced by $\hat{\mathbf{z}} = \boldsymbol{\omega}^\mathrm{T} \mathbf{P}_A$.

Consider $\alpha_z \triangleq \|\boldsymbol{\omega}^\mathrm{T} \mathbf{P}_A\|_\mathrm{F}^2$ as an additional variable and rewrite the set of squared distances differences $(\hat{d}_i^2 - \tilde{d}_i^2)$ in a matrix form as $\mathbf{A}_\mathrm{dc} - \mathbf{b}_\mathrm{dc}$ where

$$\mathbf{A}_\mathrm{dc} \triangleq \begin{bmatrix} -\mathbf{a}_1^\mathrm{T} \mathbf{P}_A & 1 \\ \vdots & \vdots \\ -\mathbf{a}_{N_\mathrm{A}}^\mathrm{T} \mathbf{P}_A & 1 \end{bmatrix}, \quad \mathbf{b}_\mathrm{dc} \triangleq \begin{bmatrix} \tilde{d}_1^2 - \|\mathbf{a}_1\|_\mathrm{F}^2 \\ \vdots \\ \tilde{d}_{N_\mathrm{A}}^2 - \|\mathbf{a}_{N_\mathrm{A}}\|_\mathrm{F}^2 \end{bmatrix}. \tag{193}$$

Then, we reformulate equation (191) as a constrained LS problem

$$\begin{aligned} \min_{\hat{\boldsymbol{\omega}}_z \in \mathbb{R}^{N_\mathrm{A}+1}} \quad & \|\mathbf{A}_\mathrm{dc} \hat{\boldsymbol{\omega}}_z - \mathbf{b}_\mathrm{dc}\|_\mathrm{F}^2, \\ \text{s.t.} \quad & 0 \leq \hat{\omega}_i \leq 1 \, \forall i, \\ & \mathbf{1}_{N_\mathrm{A}}^\mathrm{T} \hat{\boldsymbol{\omega}} = 1, \end{aligned} \tag{194}$$

where $\hat{\boldsymbol{\omega}}_z \triangleq [\hat{\boldsymbol{\omega}}; \hat{\alpha}_z]$.

With $\hat{\mathbf{\Omega}}$, we compute the contraction $\hat{\boldsymbol{\rho}}$ as the solution to the quadratic programming optimisation

$$\begin{aligned} \min_{\hat{\boldsymbol{\rho}} \in \mathbb{R}^{N_\mathrm{A}}} \quad & \hat{\boldsymbol{\rho}} \, \hat{\mathbf{\Omega}} \, \hat{\boldsymbol{\rho}}^\mathrm{T}, \\ \text{s.t.} \quad & \tilde{d}_i + \hat{\rho}_i \leq 0 \, \forall i, \end{aligned} \tag{195}$$

where the objective function is derived from the condition $\hat{\boldsymbol{\rho}} \in \mathcal{N}(\hat{\boldsymbol{\Omega}})$ and the constraints from the assumption that $\tilde{d}_i + \hat{\rho}_i <= 0$.

Finally, the estimation of target location is explained in the next subsections.

Weighted centroid method

In the classic WC algorithm described in [32], the estimate of the target location is given by

$$\hat{\mathbf{z}}_{\text{WC}} \triangleq \boldsymbol{\omega}_{\text{WC}} \mathbf{P}_A, \tag{196}$$

where $\boldsymbol{\omega}_{\text{WC}}$ is the weighing vector with elements

$$[\boldsymbol{\omega}_{\text{WC}}]_i \triangleq \left((1/\tilde{d}_i)^q\right) / \left(\sum_{i=1}^{N_{\text{A}}} (1/\tilde{d}_i)^q\right), \tag{197}$$

with $q \geq 1$ (typically $q = 2$).

This approach simply relies on the fact that $\mathbf{z} \in \mathcal{C}(\mathbf{P}_A)$, and on the heuristic that "the longer the measured distance $\tilde{d}_i$, the weaker the dependency on $\mathbf{a}_i$".

On the other hand, from equation (187), it is noticed that ω_i depends on the location of $\mathbf{a}_i$ as well as on the total ranging error ρ_i. Thus, in the proposed WC-DC algorithm the vector $\hat{\mathbf{z}}$ will be simply computed as

$$\hat{\mathbf{z}}_{\text{WC-DC}} \triangleq \boldsymbol{\omega}_{\text{WC-DC}} \mathbf{P}_A. \tag{198}$$

where

$$[\boldsymbol{\omega}_{\text{WC-DC}}]_i \triangleq \hat{\rho}_i / \tilde{d}_i. \tag{199}$$

NLS optimisation

The exact value of the global minimum of the WLS objective function with contracted distances can be computed as the solution to the unconstrained minimization

$$\hat{\mathbf{z}}_{\text{WC-NLS}} \triangleq \arg\min_{\hat{\mathbf{z}}} \sum_{i=1}^{N_{\text{A}}} (\tilde{d}_i + \hat{\rho}_i - \hat{d}_i)^2. \tag{200}$$

The advantage of the contracted distances in a NLS-based minimization is two-fold. First, the convergence of any standard optimisation algorithm [65] is guaranteed since the objective function is convex. Second, there is no need for a constrained optimization to impose $\mathbf{z} \in \mathcal{C}(\mathbf{P}_A)$, since the contracted distances implicitly force such constraints.

5.3 Performance evaluation and comparisons

The objective of this section is to evaluate the performance of the proposed DC-based algorithms in LOS and mixed LOS/NLOS scenarios. The results will be compared to those obtained with state-of-the-art non-cooperative non-parametric localisation techniques, namely, the TS-WLS [39] and the C-NLS with bias compensation, also referred to as the C-NLS *modified* [57] as well as the GLE method [87], which is an efficient and low-complexity technique for both LOS and NLOS scenarios. To verify the optimality, the results will be also compared to the PEB derived in the previous chapter.

In addition to the RMSE given by equation (20), we compute the outage of the location accuracy as

$$\pi_o \triangleq \Pr\left\{\sqrt{\varepsilon_\ell^{(q)}} > \xi_p\right\}, \tag{201}$$

where ξ_p is a pre-defined Quality-of-Location (QoL).

5.3.1 Performance in pure LOS channel conditions

Consider regular networks with $N_{\mathrm{A}} = 4$ anchors and a target deployed with uniform distribution in the convex-hull $\mathcal{C}(\mathbf{P}_A)$. All anchors are connected to the target and each distance is measured once. The ranging error is generated with the model given in equation (25), and we assume the noise standard deviation $\sigma_{ij} = \sigma \, \forall ij$.

In Figure 21(a), we compare the RMSE as a function of the noise-standard deviation σ. All algorithms can provide very similar location accuracies and close to the PEB. This is due to the fact that anchors are well distributed in the space, the target is in the convex-hull $\mathcal{C}(\mathbf{P}_A)$ and the ranging error is small [133]. The outage of the location accuracy is plotted in Figure 21(b) and from this result, it can be noticed that all algorithms can also provide similar QoL. For instance, with an outage of 0.05, all methods can guarantee an approximative QoL $\xi_p \approx \{0.2, 0.6, 2\}$ meters with a ranging error of $\sigma = \{0.1, 0.3, 1\}$ meters, respectively.

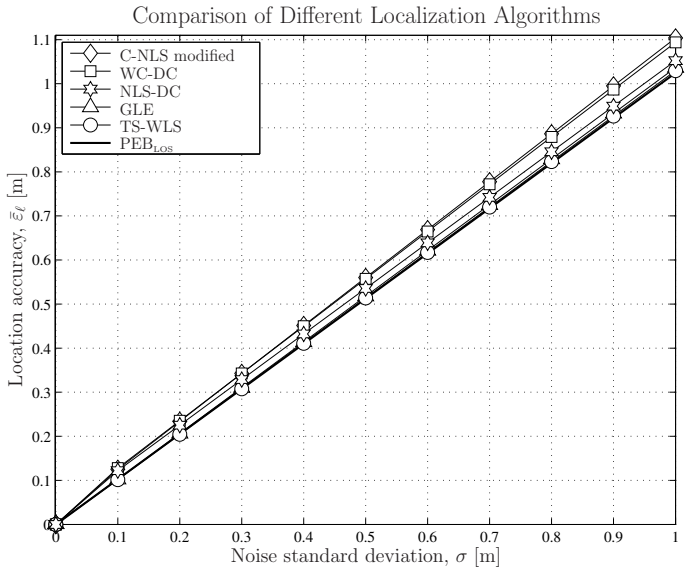

(a) Average location accuracy as a function of σ

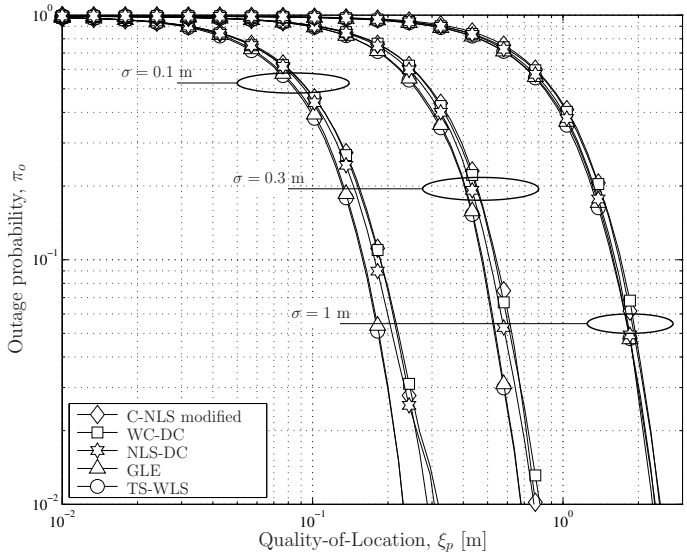

(b) Outage of the location accuracy

Fig 21. Comparison of non-cooperative algorithms for a regular network with $N_{\mathbf{A}} = 4$ anchors and $N_{\mathbf{T}} = 1$ target deployed in 14.14×14.14 squared meters.

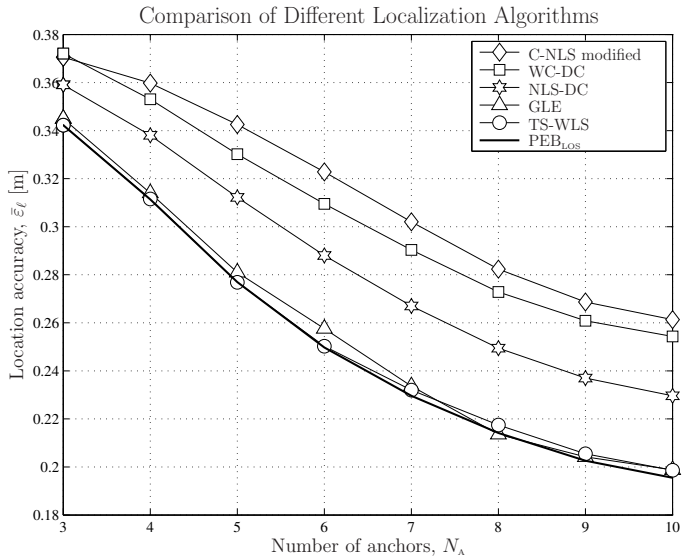

Fig 22. Comparison of different localization algorithms for non-cooperative regular networks. The noise standard deviation is $\sigma = 0.3$ meters. Anchors are equispaced in a circle of radius 10 meters.

Finally in Figure 22, the RMSE comparison is plotted as a function of the number of anchors. Also in this simulation, we assume regular networks and $\mathbf{z} \in \mathcal{C}(\mathbf{P}_A)$. The result shows that the RMSE of each algorithm decreases with the number of anchors. The performance of the TS-WLS and the GLE are the closer to the PEB. The others, however, differ only for a few centimetres.

5.3.2 Performance in mixed LOS/NLOS channel conditions

In this section, we investigate the performance of the aforementioned positioning techniques in the presence of mixed LOS/NLOS channel conditions. To begin with, we consider the case of $p_{\text{NLOS}} = 1$.

In contrast to previous results, both Figures 23(a) and 23(b) show that the WC-DC and NLS-DC algorithms provide the best location accuracy. From Figure 23(b), for example, it is found that with a maximum bias of 3 meters, the proposed DC methods can provide a QoL of 1.6 meters with an outage of 0.05, which is 20% less than the state-of-the-art technique proposed in [57].

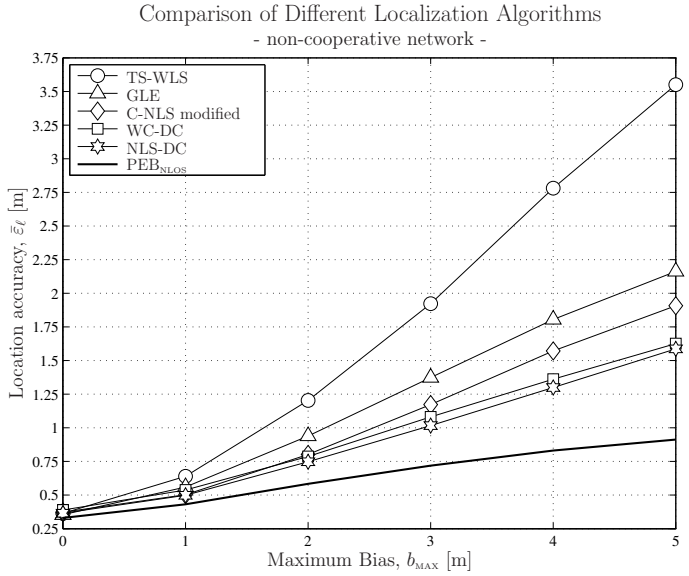

(a) Location accuracy as a function of b_{MAX}

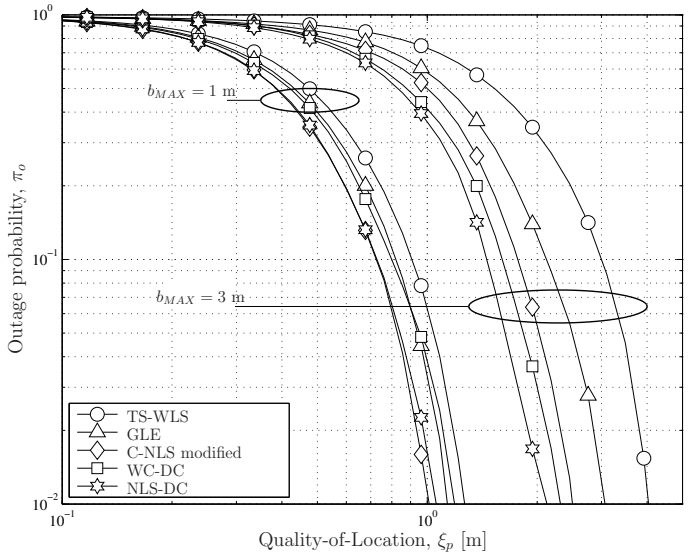

(b) Outage of the location accuracy

Fig 23. Comparison of non-cooperative algorithms for a regular network with $N_{\mathbf{A}} = 4$ anchors and $N_{\mathbf{T}} = 1$ target deployed in 14.14×14.14 squared meters. All links are in NLOS, *i.e.* $p_{\mathbf{NLOS}} = 1$ and, $\sigma_i = 0.3$ meters $\forall\ i$.

None of the algorithms, however, is able to provide a performance comparable to the PEB, which indicates that further improvements can be expected.

In Figure 24, we plot the RMSE as a function of the number of anchors. From this result, it can be noticed that all techniques benefit from the increase of N_{A}. In particular, we notice that the NLS-DC has almost a constant gap with respect to the PEB, which indicates that the algorithm has a behaviour similar to an unbiased estimator. The WC-DC shows a performance that beyond 7 anchors remains quasi-constant, indicating that there is no need of a large number of anchors to increase the accuracy.

Finally, in Figure 25 the algorithms are compared with respect to the probability of NLOS. It is noticed that all techniques but the TS-WLS, whose performance grows with p_{NLOS}, show a peak in mixed LOS/NLOS scenarios, *i.e.* $p_{\mathrm{NLOS}} \neq \{0, 1\}$. The reason is that the NLS-DC, WC-DC, GLE and C-NLS modified algorithms do not use any a priori channel state information. This introduces an uncertainty, which is non-uniform when $p_{\mathrm{NLOS}} \neq \{0, 1\}$, that penalises the performance of the algorithms.

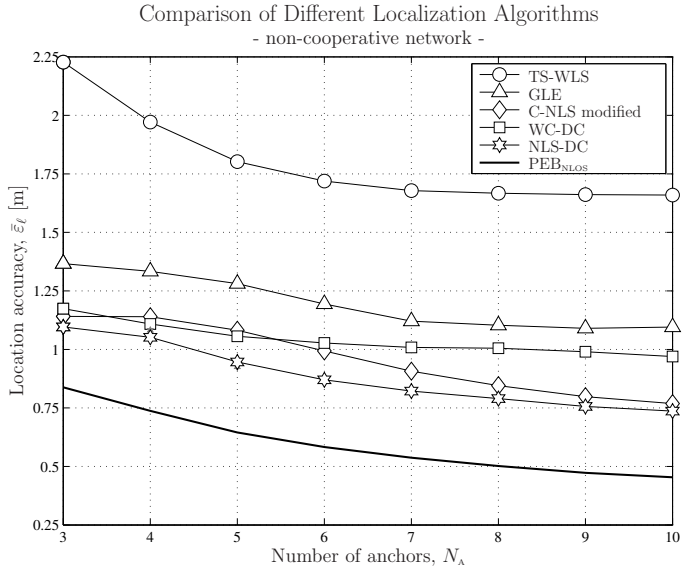

Fig 24. Comparison of non-cooperative algorithms for a regular network with $N_{\mathbf{A}} = 4$ anchors and $N_{\mathbf{T}} = 1$ target deployed in 14.14×14.14 squared meters. All links are in NLOS, *i.e.* $p_{\mathbf{NLOS}} = 1$, $\sigma_i = 0.3$ meters and $b_i \in (0, 3)$ meters $\forall\, i$. Anchors are equispaced in a circle of radius 10 meters.

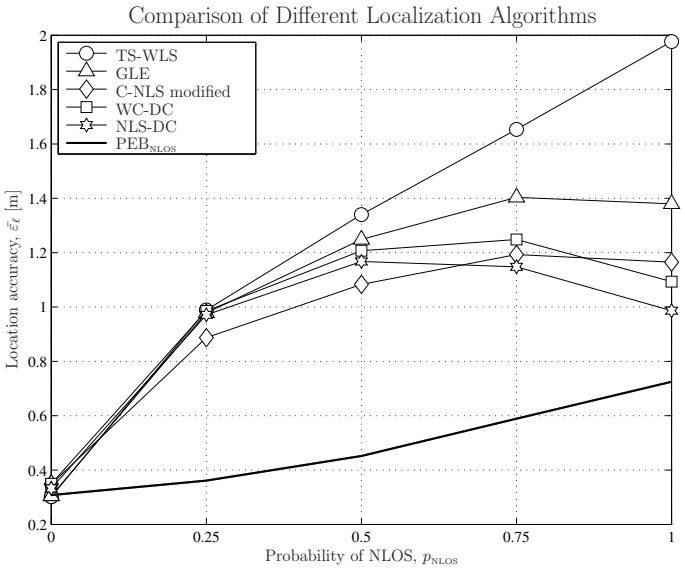

Fig 25. Comparison of non-cooperative algorithms for a regular network with $N_{\mathbf{A}}$ anchors and $N_{\mathbf{T}} = 1$ target deployed in 14.14×14.14 squared meters. $\sigma_i = 0.3$ and $b_i \in (0, 3)$ meters $\forall\, i$.

5.4 Summary and discussions

In this chapter we focused on the development of ToA-based non-cooperative positioning techniques. Starting with the assumptions that no a priori information on the channel state as well on the ranging model are available, we have addressed the problem as a WLS optimization problem.

Our main contribution is the DC principle explained in Section 5.1. Thereby we have shown that if the target node lies within the convex-hull formed by the anchors, the target-to-anchor distance estimates $d_i + \rho_i$, $\forall i$ are *negative* and the vector $\boldsymbol{\rho}$ lies in the null subspace of the relative angle matrix $\boldsymbol{\Omega}$, then: 1) the associated least-square objective is a convex function, and 2) its global minimum coincides with the true target location. Based on this principle, we proposed two robust algorithms, namely the WC-DC and the NLS-DC, which can provide an location error close to the PEB in LOS scenarios, and better performance than the state-of-the-art non-parametric localisation method, namely the C-NLS modified algorithm [57].

6 Cooperative positioning

Cooperative positioning refers to a localisation system where all nodes cooperate with each other in order to infer their locations by communicating and exchanging location-related information, *e.g.* ranging and location estimates. Typically, cooperative localisation techniques are considered for ad-hoc and sensor network application scenarios, where in fact, nodes can communicate either via a direct link or through multi-hop connections. Examples are ad-hoc networks of devices worn by fire-fighters to optimise rescuing operations; smart-tag networks deployed in warehouses and hospitals to enable items and equipment to be located and sensor networks deployed in the wild, where knowledge of node locations can provide topological information additional to sensed data.

As depicted in Figure 26, these networks can be modelled with a mesh topology, where each node is connected to many others within the coverage area. Cooperative positioning algorithms can be more accurate and also more sophisticated than those utilised for non-cooperative positioning. In fact, these methods must handle a larger number of variables, a more complicated objective function, and multiple minima due to the partial network connectivity.

All of these challenges were extensively discussed throughout Chapters 1, 2, 3 and 4, and, specifically, in Chapter 2 it was shown that the state-of-the-art of non-parametric non-Bayesian methods are either too complex, not optimal, and yet dependent on a priori information to handle NLOS scenarios. To achieve optimality, a global optimisation algorithm based on the WLS objective function with *non-squared* distances is needed. To minimise the computational complexity, the optimisation methods should be designed with lightweight techniques, such as the BFGS algorithm. Finally, to handle bias and noise ranging errors non parametric weighing strategies are required.

Therefore, in this chapter we propose:

a) A lightweight global optimisation algorithm based on the combination of Global Distance Continuation (GDC) method and BFGS numeric optimisation

b) A robust non-parametric weighing strategy based on small scale statistics and statistical-geometry.

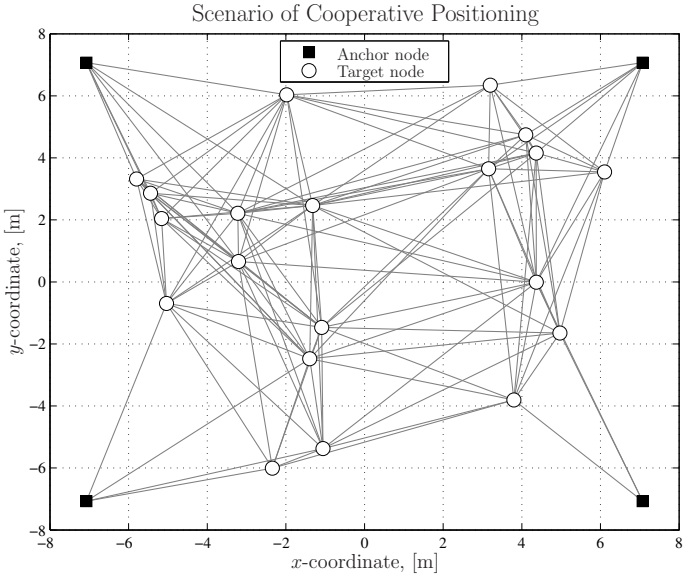

Fig 26. Network model for cooperative positioning systems.

6.1 Optimisation strategy in cooperative positioning

In Section 3.2 we have shown that the WLS objective function is not convex and, in Chapter 2, we reviewed several optimisation techniques that are proposed to minimise the objective function either with the aid of reliable initial estimates [82, 134–136] or relying on global optimization methods [68, 69, 71, 73]. Amongst all those methods, the SR-GDC algorithm proposed in [71], which is fundamentally an application of global smoothing and numerical continuation methods [137], provided the best compromise between complexity and performance.

The main characteristic of a GDC method is the fact that the solution of the localisation problem is found by minimising smoothed WLS-objectives, each obtained from the convolution of the original WLS-objective with a different Gaussian kernel. Since the first smoothed WLS-objective can always be made convex, this technique eliminates any sensitivity to initial estimates. However, in the form developed in [71], the algorithm was derived from a sub-optimal formulation of the localisation problem based on *squared distances*.

In the following subsections, we return to the principle of the GDC method for a distance-based localisation problem and propose a variation of the SR-GDC that can be applied to the WLS minimisation problem without squared distances. This new algorithm, which will be referred to as R-GDC, is a method to obtain ML-solutions for both the single target and network localisation problems (like the LM-WLS and the SMACOF), with insensitivity to initial estimates (like the convex SDP and the SR-GDC), and at very low complexity (like the SMACOF).

6.1.1 Global distance continuation principle

The principle of a GDC method relies on the following definitions and theorem.

Definition D9 (Gaussian kernel)**.**
*The **Gaussian kernel** is defined as*

$$g(u;\lambda) \triangleq e^{-u^2/\lambda^2}. \tag{202}$$

Definition D10 (Smooth function)**.**
*Consider a variable $\boldsymbol{z} \in \mathbb{R}^n$ and a multivariate continuous function $f : \mathbb{R}^n \to \mathbb{R}$. The smoothed version (or **smoothed function**) of $f(\boldsymbol{z})$, denoted $\langle f \rangle_\lambda(\boldsymbol{z})$, is defined as*

$$\langle f \rangle_\lambda(\boldsymbol{z}) \triangleq \frac{1}{\pi^{n/2}\lambda^n} \int_{\mathbb{R}^n} f(\boldsymbol{u}) \cdot \exp\left(-\frac{\|\boldsymbol{z}-\boldsymbol{u}\|_{\mathrm{F}}^2}{\lambda^2} \right) \mathrm{d}\boldsymbol{u}, \tag{203}$$

where $\lambda \in \mathbb{R}^+$ is a parameter that controls the degree of smoothing ($\lambda \gg 0$ strong smoothing).

Theorem T11 (Continuation Principle [71])**.**
Let $\mathcal{L}_\lambda^K = \{\lambda^{(k)}\}$ with $\{1 \leq k \leq K\}$ be any decreasing sequence of λ's converging to zero, i.e. $\lambda^{(K)} = 0$. If $\boldsymbol{z}^{(k)}$ is a global minimiser of $\langle f \rangle_{\lambda^{(k)}}(\boldsymbol{z})$ and $\{\boldsymbol{z}^{(k)}\}$ converges to $\boldsymbol{z}^*$, then $\boldsymbol{z}^*$ is the global minimum of $f(\boldsymbol{z})$.

Proof. See [71]. □

In light of the above, a numeric optimisation based on the continuation principle can be concisely described in three steps: *smoothing*, *minimisation* and *continuation*. In the smoothing step the entire objective is transformed into a function with a higher degree of differentiability (smoothed), obtained by means of a convolution with a Gaussian kernel. In the minimisation step each of

these smoothed functions is minimised using a standard optimisation algorithm, *e.g.* the BFGS method [65]. Finally, the continuation refers to the process of tracing the sought minimum, which in practice is performed by initialising the minimisation of the next smoothed objective with the latest solution.

In Figure 27, we illustrate the idea of a numeric minimisation performed with the continuation principle. Specifically, we consider the minimisation of a non-convex object function given by the Gaussian mixture

$$g_m(x) \triangleq \sum_{i=1}^{I_g} A_{gi} g_{mi}(x; \mu^{gi}, \sigma_{gi}), \tag{204}$$

where

$$g_{mi}(x; \mu_{gi}, \sigma_{gi}) \triangleq \frac{A_{gi}}{\sqrt{2\pi\sigma_{gi}^2}} e^{-\frac{(x-\mu_{gi})^2}{2\sigma_{gi}^2}}. \tag{205}$$

and $I_g = 3$. The gray lines illustrate the smoothed functions $\langle g_m \rangle_\lambda(x)$ computed for a decreasing values of the smoothing parameter λ. The marker "○" indicates the result of the k-th iteration, thus the continuation principle.

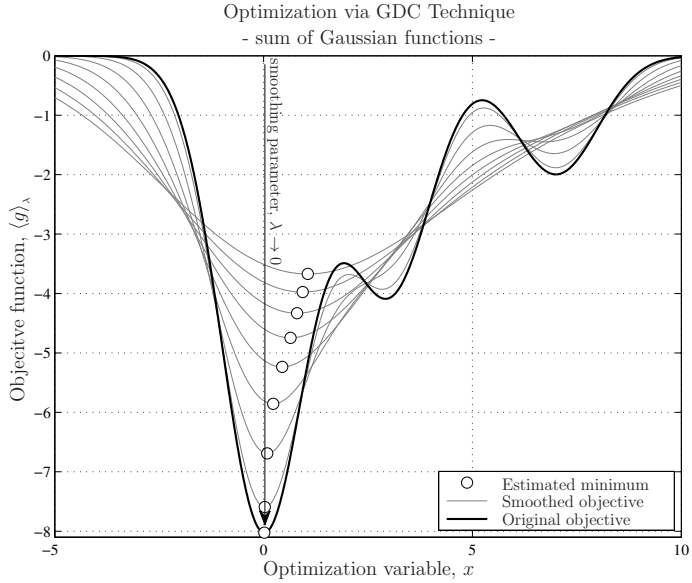

Fig 27. Illustration of the GDC method with the optimisation of a Gaussian mixture function $g_m(x)$ with $A_{gi} = \{-20, -10, -5\}$, $\mu_{gi} = \{0, 3, 7\}$ and $\sigma_{gi} = 1\ \forall i$.

As previously discussed, the advantage of a GDC-based cooperative positioning algorithm is two-fold. First, if the first smoothed version is convex, then the continuation principle ensures insensitivity to initial estimates, which is a desirable requirement for the minimisation of complexity and location errors especially in distributed approaches. Second, if the sequence of smoothing parameters $\mathcal{L}_{\lambda}^{K}$ is properly selected, low-complexity and standard optimisation techniques, like the BFGS method, are sufficient to guarantee the numeric convergence at each minimisation step.

However, in order to apply the GDC method to the ML network localisation problem, two main challenges are met: a closed-form expression for the smoothed range-WLS objective $\langle f_{\mathrm{R}} \rangle_{\lambda}(\vec{\mathbf{p}})$, along with its Gradient and Hessian, needs to be derived; a least upper bound, or *supremum* on the initial smoothing parameter $\lambda^{(1)}$ needs to be found. The first challenge goes to the implementation of the numeric optimisation method and by product, to the overall complexity of the algorithm itself. The second, instead, goes to the applicability of the continuation principle and its usage for eliminating the sensitivity to initial estimates.

In the following subsections these objectives are addressed in details.

6.1.2 Smoothed WLS-function, gradient and Hessian

Consider the WLS objective function $f_{\mathrm{R}}(\vec{\mathbf{p}})$ given in equation (26), which we rewrite in the next equation as

$$f_{\mathrm{R}}(\vec{\mathbf{p}}) = \sum_{ij \in E} w_{ij}^{2} (\tilde{d}_{ij}^{2} - \hat{d}_{ij}^{2})^{2}. \tag{206}$$

To simplify the derivation of the following results, assume $\eta = 2$ (two-dimensional networks) and let x and y refers to the 1-st and 2-nd element of a coordinate vector $\mathbf{p}$, *e.g* $\mathbf{p}_i = [p_i^x, p_i^y]$.

Theorem T12 (Smoothed ML Objective)**.**

The smoothed version of the ML objective defined in equation (26) *is*

$$\langle f_{\mathrm{R}} \rangle_{\lambda}(\vec{\mathbf{p}}) = \sum_{ij \in E} w_{ij}^{2} \left(\lambda^{2} + \tilde{d}_{ij}^{2} + \hat{d}_{ij}^{2} - \lambda \sqrt{\pi} \tilde{d}_{ij} \, {}_1F_1 \left(\frac{3}{2}; 1; \frac{\hat{d}_{ij}^{2}}{\lambda^{2}} \right) \exp \left(\frac{-\hat{d}_{ij}^{2}}{\lambda^{2}} \right) \right), \tag{207}$$

where $\mathscr{E}(a)$ *is the gamma function and* ${}_1F_1(a; b; c)$ *is the confluent hyper-geometric function [138].*

Proof. Apply equation (203) to the objective function in equation (206)

$$\begin{aligned}\langle f_{\mathrm{R}}\rangle_\lambda(\vec{\hat{\mathbf{p}}}) &= \frac{1}{\pi}\int_{\mathbb{R}^\eta}\sum_{ij\in E} w_{ij}^2\left(\tilde{d}_{ij} - \|\hat{\mathbf{p}}_i-\hat{\mathbf{p}}_j+\lambda\mathbf{u}\|_{\mathrm{F}}\right)^2 \exp(\,-\|\mathbf{u}\|_{\mathrm{F}}^2\,)\;\mathrm{d}\mathbf{u}\\ &= \frac{1}{\pi}\sum_{ij\in E} w_{ij}^2(\mathcal{I}_1+\mathcal{I}_2-2\tilde{d}_{ij}\mathcal{I}_3),\end{aligned} \tag{208}$$

where $\mathbf{u} \triangleq [u^x, u^y]$ and

$$\mathcal{I}_1 \triangleq \int_{-\infty}^{+\infty}\int_{-\infty}^{+\infty} \tilde{d}_{ij}^2 \exp\left(-\bar{u}^2\right)\,\mathrm{d}u^x\,\mathrm{d}u^y, \tag{209}$$

$$\mathcal{I}_2 \triangleq \int_{-\infty}^{+\infty}\int_{-\infty}^{+\infty}\left((\hat{\Delta}_{ij}^x+\lambda u^x)^2+(\hat{\Delta}_{ij}^y+\lambda u^y)^2\right)\exp\left(-\bar{u}^2\right)\,\mathrm{d}u^x\,\mathrm{d}u^y, \tag{210}$$

$$\mathcal{I}_3 \triangleq \int_{-\infty}^{+\infty}\int_{-\infty}^{+\infty}\sqrt{(\hat{\Delta}_{ij}^x+\lambda u^x)^2+(\hat{\Delta}_{ij}^y+\lambda u^y)^2}\,\exp\left(-\bar{u}^2\right)\,\mathrm{d}u^x\,\mathrm{d}u^y, \tag{211}$$

in which $\bar{u}^2 \triangleq (u^x)^2 + (u^y)^2$, $\hat{\mathbf{p}}_i - \hat{\mathbf{p}}_j = [\hat{\Delta}_{ij}^x, \hat{\Delta}_{ij}^y]$ with $\hat{\Delta}_{ij}^x \triangleq \hat{p}_i^x - \hat{p}_j^x$ and $\hat{\Delta}_{ij}^y \triangleq \hat{p}_i^y - \hat{p}_j^y$.

In the remainder of this proof the subscript $_{ij}$ is temporarily omitted for notational convenience.

The integrals $\mathcal{I}_1$ and $\mathcal{I}_2$ shown above admit the following trivial solutions [71]

$$\mathcal{I}_1 = \pi\tilde{d}^2, \tag{212}$$

$$\mathcal{I}_2 = \pi(\hat{d}^2 + \lambda^2). \tag{213}$$

In turn, $\mathcal{I}_3$ can be solved as follows. First, consider the change of variables

$$\hat{\Delta}^x + \lambda u^x = \varrho\cos\phi, \tag{214}$$

$$\hat{\Delta}^y + \lambda u^y = \varrho\sin\phi. \tag{215}$$

The integral $\mathcal{I}_3$ can then be rewritten as

$$\begin{aligned}\mathcal{I}_3 &= \frac{1}{\lambda^2}\int_0^{+\infty}\int_0^{2\pi}\varrho^2\exp\left(\frac{-\varrho^2-\hat{d}^2+2\varrho(\hat{\Delta}^x\cos\phi+\hat{\Delta}^y\sin\phi)}{\lambda^2}\right)\mathrm{d}\varrho\,\mathrm{d}\phi \\ &= \frac{1}{\lambda^2}\exp\left(\frac{-\hat{d}^2}{\lambda^2}\right)\int_0^{+\infty}\varrho^2\exp\left(\frac{-\varrho^2}{\lambda^2}\right)\mathrm{d}\varrho\underbrace{\int_0^{2\pi}\exp\left(\frac{2\varrho(\hat{\Delta}^x\cos\phi+\hat{\Delta}^y\sin\phi)}{\lambda^2}\right)\mathrm{d}\phi}_{\mathcal{I}_4}.\end{aligned} \tag{216}$$

Choosing $\{a=0, p=0, q=0, b=\frac{-2\varrho\hat{\Delta}^x}{\lambda^2}, c=\frac{-2\varrho\hat{\Delta}^y}{\lambda^2}\}$ and performing the change of variables $x=\phi+\pi$ in [139, Eq. $3.338-4.^6$, pp. 336], yields the following closed-form solution for $\mathcal{I}_4$

$$\mathcal{I}_4 \triangleq \int_0^{2\pi} \exp\left(\frac{2\varrho(\hat{\Delta}^x\cos\phi+\hat{\Delta}^y\sin\phi)}{\lambda^2}\right)\mathrm{d}\phi = I_0\left(\frac{2\varrho\hat{d}}{\lambda^2}\right), \tag{217}$$

where $I_0(\cdot)$ is the modified Bessel function of the first kind and 0-th order.

Using equation (217) into equation (216) yields

$$\mathcal{I}_3 = \pi\int_0^{+\infty} \frac{\varrho^2}{\lambda^2/2}\exp\left(-(\varrho^2+\hat{d}^2)/\lambda^2\right) I_0\left(\frac{\varrho\hat{d}}{\lambda^2/2}\right)\mathrm{d}\varrho, \tag{218}$$

It is recognized that the integral above is the first moment of a Rice distribution (see [140, eq. (2.1-140), pp.46] with $\{\sigma^2=\lambda^2/2, s=\hat{d}, r=\varrho\}$), such that the closed-form of $\mathcal{I}_3$ is

$$\mathcal{I}_3 = \pi\lambda\mathscr{E}\left(\frac{3}{2}\right)\,{}_1F_1\left(\frac{3}{2};1;\frac{\hat{d}^2}{\lambda^2}\right)\exp\left(\frac{-\hat{d}^2}{\lambda^2}\right). \tag{219}$$

Substituting equations (212), (213) and (219) into equation (208) finally yields equation (207). □

Since the GDC method requires repeated optimisation of various smoothed objectives $\langle f_{\mathrm{R}}\rangle_\lambda(\vec{\mathbf{p}})$ with decreasing $\lambda^{(k)}$, the complexity of evaluating equation (207) is of crucial importance. Indeed, as $\lambda\to 0$, the confluent hyperbolic function increases boundlessly, while the exponential term vanishes. However this issue can be circumvented by using the alternative expressions [138, eq. 13.1.2, pp. 504]

$${}_1F_1\left(\frac{3}{2};1;s\right) = 1+\sum_{q=1}^{+\infty}\left(s^q\cdot\prod_{t=1}^{q}\left(\frac{1}{2t^2}+\frac{1}{t}\right)\right), \tag{220}$$

and [138, eq. 13.5.1, pp. 508]

$$\begin{aligned}{}_1F_1\left(\frac{3}{2};1;s\right) &= \frac{2e^s}{\sqrt{\pi}}\sum_{p=0}^{P-1}\frac{s^{\frac{1}{2}-p}}{p!}\prod_{t=0}^{p-1}\left(t-\frac{1}{2}\right)^2 \qquad (221)\\ &= \frac{s^{-3/2}}{2\sqrt{\pi}}\sum_{q=0}^{Q-1}\frac{(-s)^{-q}}{q!}\prod_{t=0}^{q-1}\left(\frac{3}{2}+t\right)^2+\mathcal{O}(|s|^{-Q})+\mathcal{O}(|s|^{-P}).\end{aligned}$$

Notice that the product in equation (220) decreases fast with t (and therefore q), such that the series convergences quickly for *small* s. In contrast, the residues $\mathcal{O}(|s|^{-Q})$ and $\mathcal{O}(|s|^{-P})$ in equation (221) decrease geometrically with Q and P, respectively (see [138, eq. 13.5.3-4, pp.508]), such that the series converges quickly for *large* s. Therefore, using these two expressions with $s \triangleq \frac{\hat{d}^2}{\lambda^2}$, equation (207) can be evaluated efficiently for any values of $\hat{d}^2$ and λ^2.

In order to perform numeric optimisation of the objective in theorem T12, however, closed-forms of the Gradient and Hessian of $\langle f_{\mathrm{R}} \rangle_\lambda(\vec{\hat{\mathbf{p}}})$ are also required. Thus, the following results are in order.

Lemma L9 (Gradient of the Smoothed ML Objective)**.**

The closed-form of the gradient of the smoothed objective $\langle f_{\mathrm{R}} \rangle_\lambda(\vec{\hat{\mathbf{p}}})$*, denoted by* $\nabla_{\vec{\hat{\mathbf{p}}}} \langle f_{\mathrm{R}} \rangle_\lambda(\vec{\hat{\mathbf{p}}})$*, is*

$$\nabla_{\vec{\hat{\mathbf{p}}}} \langle f_{\mathrm{R}} \rangle_\lambda(\vec{\hat{\mathbf{p}}}) \triangleq \sum_{ij \in E} w_{ij}^2 \cdot \left(2 - \frac{\sqrt{\pi}\tilde{d}_{ij}}{\lambda} e^{\frac{-\hat{d}_i^2}{\lambda^2}} {}_1F_1\left(\frac{3}{2}; 2; \frac{\hat{d}_i^2}{\lambda^2} \right) \right) \times \left(\mathbf{e}_{ij} \otimes (\vec{\hat{\mathbf{p}}}_j - \vec{\hat{\mathbf{p}}}_i) \right),$$

where $\otimes$ *indicates the Kronecker product and* $\mathbf{e}_{ij} \in \mathbb{R}^N$ *are row-vectors with the* i*-th and the* j*-th element equal to* 1 *and* -1 *respectively.*

Proof. Define

$$f_{ij}^{\mathrm{R}}(\vec{\hat{\mathbf{p}}}; \lambda) \triangleq \lambda^2 + \tilde{d}_{ij}^2 + \hat{d}_{ij}^2 - \lambda\sqrt{\pi}\tilde{d}_{ij} \, {}_1F_1\left(\tfrac{3}{2}, 1, \tfrac{\hat{d}_{ij}^2}{\lambda^2} \right) \exp\left(\tfrac{-\hat{d}_{ij}^2}{\lambda^2} \right), \tag{222}$$

such that $\langle f_{\mathrm{R}} \rangle_\lambda(\vec{\hat{\mathbf{p}}}) = \sum_{ij \in E} w_{ij}^2 f_{ij}^{\mathrm{R}}(\vec{\hat{\mathbf{p}}}; \lambda)$ and the gradient $\nabla_{\vec{\hat{\mathbf{p}}}} \langle f_{\mathrm{R}} \rangle_\lambda(\vec{\hat{\mathbf{p}}})$ can be written concisely as

$$\nabla_{\vec{\hat{\mathbf{p}}}} \langle f_{\mathrm{R}} \rangle_\lambda(\vec{\hat{\mathbf{p}}}) \triangleq \sum_{ij \in E} w_{ij}^2 \nabla_{\vec{\hat{\mathbf{p}}}} f_{ij}^{\mathrm{R}}(\vec{\hat{\mathbf{p}}}; \lambda). \tag{223}$$

To derive a closed-form expression for $\nabla_{\vec{\hat{\mathbf{p}}}} f_{ij}^{\mathrm{R}}(\vec{\hat{\mathbf{p}}}; \lambda)$, consider the representation of $f_{ij}^{\mathrm{R}}(\vec{\hat{\mathbf{p}}}; \lambda)$ as a composite function $h(g(\vec{\hat{\mathbf{p}}}); \lambda)$, with $h : \mathbb{R} \to \mathbb{R}$, $g : \mathbb{R}^{N\eta} \to \mathbb{R}$, so that each element of $\nabla_{\vec{\hat{\mathbf{p}}}} f_{ij}^{\mathrm{R}}(\vec{\hat{\mathbf{p}}}; \lambda)$ can be obtained via the chain rule

$$\frac{\partial h(g(\vec{\hat{\mathbf{p}}}); \lambda)}{\partial \hat{p}_i^n} = \frac{\mathrm{d}h(u; \lambda)}{\mathrm{d}u} \frac{\partial g(\vec{\hat{\mathbf{p}}})}{\partial \hat{p}_i^n}, \tag{224}$$

where $u = g(\vec{\hat{\mathbf{p}}})$.

From equation (224), it is obtained that the gradient of $f_{ij}^{\mathrm{R}}(\hat{d}_{ij};\lambda)$ is given by a scalar corresponding to the term $\frac{\mathrm{d}h(u;\lambda)}{\mathrm{d}u}$, multiplied by the vector $[\frac{\partial g(\vec{\mathbf{p}})}{\partial \hat{p}_1^1},\cdots,\frac{\partial g(\vec{\mathbf{p}})}{\partial \hat{p}_N^2}]$. Specifically

$$\nabla_{\vec{\mathbf{p}}} f_{ij}^{\mathrm{R}}(\hat{d}_{ij};\lambda) = S_1(\hat{d}_{ij}^2;\lambda)\nabla_{\vec{\mathbf{p}}}(\hat{d}_{ij}^2), \tag{225}$$

where, from $g_{ij}(\vec{\hat{\mathbf{p}}}) = \hat{d}_{ij}^2$ we obtain

$$\nabla_{\vec{\mathbf{p}}}(\hat{d}_{ij}^2) \triangleq \left[\frac{\partial \hat{d}_{ij}^2}{\partial \hat{p}_1^1},\cdots,\frac{\partial \hat{d}_{ij}^2}{\partial \hat{p}_N^2}\right] = 2\mathbf{e}_{ij}\otimes(\vec{\hat{\mathbf{p}}}_i - \vec{\hat{\mathbf{p}}}_j), \tag{226}$$

while from $h = f_{ij}^{\mathrm{R}}(u;\lambda)$ we have

$$S_1(u;\lambda) \triangleq \frac{\mathrm{d}f_{ij}^{\mathrm{R}}(u;\lambda)}{\mathrm{d}u} = 1 + \frac{\sqrt{\pi}\tilde{d}_{ij}}{\lambda}\exp\left(\tfrac{-u}{\lambda^2}\right)\left({}_1F_1\left(\tfrac{3}{2},1,\tfrac{u}{\lambda^2}\right) - \frac{\mathrm{d}}{\mathrm{d}u}\,{}_1F_1\left(\tfrac{3}{2},1,\tfrac{u}{\lambda^2}\right)\right), \tag{227}$$

where for simplicity we commit a slight abuse of notation by omitting the sub-index ij in S_1.

Equation (227) can be simplified utilising the recurrence formula [138, pp.508, 13.5.1]

$$\frac{(b-a)}{b}\,{}_1F_1\left(a;b+1;u\right) = {}_1F_1\left(a;b;u\right) - \frac{\mathrm{d}}{\mathrm{d}u}\,{}_1F_1\left(a;b;u\right), \tag{228}$$

such that

$$S_1(u;\lambda) = 1 - \frac{\sqrt{\pi}\tilde{d}_{ij}}{2\lambda}\exp\left(\frac{-u}{\lambda^2}\right){}_1F_1\left(\frac{3}{2};2;\frac{u}{\lambda^2}\right). \tag{229}$$

Substituting equations (226) and (229) into (225), and the result into equation (223) yields (222). □

Lemma L10 (Hessian of the Smoothed ML Objective)**.**

The Hessian of $\langle f_{\mathrm{R}}\rangle_\lambda(\vec{\hat{\mathbf{p}}})$*, denoted by* $\nabla^2_{\vec{\hat{\mathbf{p}}}}\langle f_{\mathrm{R}}\rangle_\lambda(\vec{\hat{\mathbf{p}}})$*, is*

$$\nabla^2_{\vec{\hat{\mathbf{p}}}}\langle f_{\mathrm{R}}\rangle_\lambda(\vec{\hat{\mathbf{p}}}) = \sum_{ij\in E} w_{ij}^2\cdot\Big(S_1(\hat{d}_{ij}^2;\lambda)\nabla^2_{\vec{\hat{\mathbf{p}}}}(\hat{d}_{ij}^2) + S_2(\hat{d}_{ij}^2;\lambda)\nabla^{\mathrm{T}}_{\vec{\hat{\mathbf{p}}}}(\hat{d}_{ij}^2)\nabla_{\vec{\hat{\mathbf{p}}}}(\hat{d}_{ij}^2)\Big),$$

where $\nabla^2_{\vec{\hat{\mathbf{p}}}}(\hat{d}_{ij}^2) \in \mathbb{R}^{\eta N_{\mathrm{T}}\times\eta N_{\mathrm{T}}}$ *and it is given by*

$$\nabla^2_{\vec{\hat{\mathbf{p}}}}(\hat{d}_{ij}^2) = 2(\mathbf{e}_{ij}\otimes\mathbf{I}_\eta)^{\mathrm{T}}(\mathbf{e}_{ij}\otimes\mathbf{I}_\eta), \tag{230}$$

and

$$S_2(\hat{d}_{ij}^2;\lambda) = \frac{\tilde{d}_{ij}\sqrt{\pi}}{8\lambda^3}\exp\left(\frac{-\hat{d}_{ij}^2}{\lambda^2}\right){}_1F_1\left(\frac{3}{2};3;\frac{\hat{d}_{ij}^2}{\lambda^2}\right). \tag{231}$$

Proof. Proceeding as in the proof of Lemma 9, the Hessian of $\langle f_{\mathrm{R}} \rangle_{\lambda}(\vec{\hat{\mathbf{p}}})$ can be written as

$$\nabla^2_{\vec{\hat{\mathbf{p}}}} \langle f_{\mathrm{R}} \rangle_{\lambda}(\vec{\hat{\mathbf{p}}}) \triangleq \sum_{ij \in E} w_{ij}^2 \nabla^2_{\vec{\hat{\mathbf{p}}}} f_{ij}^{\mathrm{R}}(\vec{\hat{\mathbf{p}}}; \lambda), \tag{232}$$

where kq-th element of $\nabla^2_{\vec{\hat{\mathbf{p}}}} f_{ij}^{\mathrm{R}}(\hat{d}_{ij}^2; \lambda)$ is obtained from the chain rule

$$\frac{\partial^2 h(g(\vec{\hat{\mathbf{p}}}))}{\partial \hat{p}_i^n \partial \hat{p}_j^q} = \frac{\mathrm{d}h(u)}{\mathrm{d}u} \frac{\partial^2 g(\vec{\hat{\mathbf{p}}})}{\partial \hat{p}_i^n \partial \hat{p}_j^q} + \frac{\mathrm{d}^2 h(u)}{\mathrm{d}^2 u} \frac{\partial g(\vec{\hat{\mathbf{p}}})}{\partial \hat{p}_i^n} \frac{\partial g(\vec{\hat{\mathbf{p}}})}{\partial \hat{p}_j^q}. \tag{233}$$

From equation (233) it can be seen that the Hessian of $f_{ij}^{\mathrm{R}}(\hat{d}_{ij}^2; \lambda)$ is a sum of two matrices, the first given by $\nabla^2_{\vec{\hat{\mathbf{p}}}} \hat{d}_{ij}^2 \in \mathbb{R}^{N\eta \times N\eta}$, multiplied by the scalar $S_1(u; \lambda)$ found in equation (229); and the second given by the cross-product of the vector $\nabla_{\vec{\hat{\mathbf{p}}}} \hat{d}_{ij}^2$ described in equation (226), multiplied by another scalar corresponding to the term $\frac{\mathrm{d}^2 h(u)}{\mathrm{d}^2 u}$. Specifically

$$\nabla^2_{\vec{\hat{\mathbf{p}}}} f_{ij}^{\mathrm{R}}(\hat{d}_{ij}; \lambda) = S_1(\hat{d}_{ij}^2; \lambda) \nabla^2_{\vec{\hat{\mathbf{p}}}} (\hat{d}_{ij}^2) + S_2(\hat{d}_{ij}^2; \lambda) \nabla^{\mathrm{T}}_{\vec{\hat{\mathbf{p}}}} (\hat{d}_{ij}^2) \nabla_{\vec{\hat{\mathbf{p}}}} (\hat{d}_{ij}^2), \tag{234}$$

with

$$\nabla^2_{\vec{\hat{\mathbf{p}}}} \hat{d}_{ij}^2 = 2(\mathbf{e}_{ij} \otimes \mathbf{I}_{\eta})^{\mathrm{T}} (\mathbf{e}_{ij} \otimes \mathbf{I}_{\eta}), \tag{235}$$

and

$$\begin{aligned} S_2(u; \lambda) \triangleq \frac{\mathrm{d}^2 f_{ij}^{\mathrm{R}}(u; \lambda)}{\mathrm{d}u^2} &= \frac{\tilde{d}_{ij} \sqrt{\pi}}{2\lambda^3} \exp\left(\frac{-u}{\lambda^2}\right) \left(\frac{\mathrm{d}}{\mathrm{d}u} {}_1F_1\left(\frac{3}{2}; 2; \frac{u}{\lambda^2}\right) - {}_1F_1\left(\frac{3}{2}; 2; \frac{u}{\lambda^2}\right) \right) \\ &= \frac{\tilde{d}_{ij} \sqrt{\pi}}{8\lambda^3} \exp\left(\frac{-u}{\lambda^2}\right) {}_1F_1\left(\frac{3}{2}; 3; \frac{u}{\lambda^2}\right), \end{aligned} \tag{236}$$

where we again omit the sub-index ij in S_2 for simplicity and employed the recursive relation of equation (228) [138, pp.508, 13.5.1] in the last equality.

Substituting equations (226), (229), (235) and (236) into equation (234) and the result into (232) finally yields equation (230). □

To conclude this subsection, we remark that also in equations (222) and (230), all partial derivatives (including those of the second order) with respect to $\hat{p}_i^n$ with $1 \leq i \leq N_{\mathrm{A}}$ are 0, since they refer to the location of an anchor. Therefore, similarly to the gradient and Hessian of the WLS objective function given in equations (31) and (36), $\nabla^2_{\vec{\hat{\mathbf{p}}}} \langle f_{\mathrm{R}} \rangle_{\lambda}(\vec{\hat{\mathbf{p}}})$ and $\nabla^2_{\vec{\hat{\mathbf{p}}}} \langle f_{\mathrm{R}} \rangle_{\lambda}(\vec{\hat{\mathbf{p}}})$ can be replaced by the compact matrices $\nabla^2_{\vec{\hat{\mathbf{z}}}} \langle f_{\mathrm{R}} \rangle_{\lambda}(\vec{\hat{\mathbf{z}}}) \in \mathbb{R}^{N_{\mathrm{T}}\eta}$ and $\nabla^2_{\vec{\hat{\mathbf{z}}}} \langle f_{\mathrm{R}} \rangle_{\lambda}(\vec{\hat{\mathbf{z}}}) \in \mathbb{R}^{N_{\mathrm{T}}\eta \times N_{\mathrm{T}}\eta}$.

6.1.3 The initial smoothing parameter $\lambda^{(1)}$

In this subsection we address the derivation of the least upper bound on the set of smoothing parameters that ensure $\nabla^2_{\vec{\hat{\mathbf{p}}}}\langle f_{\mathrm{R}}\rangle_\lambda(\vec{\hat{\mathbf{p}}}) \succeq 0$, $\forall\, \vec{\hat{\mathbf{p}}} \in \mathbb{R}^{\eta N}$. To this end, we introduce the following definitions.

Definition D11 (Set of Convexizing Smoothing Parameters)**.**

The set of ***convexizing smoothing parameters*** *is defined by*

$$\mathscr{L} \triangleq \{\lambda | \nabla^2_{\vec{\hat{\mathbf{p}}}}\langle f_{\mathrm{R}}\rangle_\lambda(\vec{\hat{\mathbf{p}}}) \succeq 0,\, \forall\, \vec{\hat{\mathbf{p}}} \in \mathbb{R}^{N_{\mathrm{T}}\times\eta}\}. \tag{237}$$

Definition D12 (Critical Smoothing Parameter λ^*)**.**

Let $\lambda^* \in \mathscr{L}$ be a smoothing parameter such that

$$\nexists \lambda < \lambda^* | \nabla^2_{\vec{\hat{\mathbf{p}}}}\langle f_{\mathrm{R}}\rangle_{\lambda^*}(\vec{\hat{\mathbf{p}}}) \succeq 0,\, \forall\, \vec{\hat{\mathbf{p}}} \in \mathbb{R}^{N_{\mathrm{T}}\times\eta}. \tag{238}$$

The parameter λ^*, which can alternatively be defined as $\lambda^* \triangleq \inf\{\mathscr{L}\}$, will hereafter be referred to as the ***critical smoothing parameter****.*

A closed-form and simple expression for the critical smoothing parameter λ^* is hard to determine. However, the GDC method requires that various smoothed objectives $\langle f_{\mathrm{R}}\rangle_{\lambda^{(k)}}(\vec{\hat{\mathbf{p}}})$ be minimized with decreasing smoothing parameters $\lambda^{(1)} > \cdots > \lambda^{(k)} > \cdots > \lambda^{(K)} = 0$, such that the first smoothed objective $\langle f_{\mathrm{R}}\rangle_{\lambda^{(1)}}(\vec{\hat{\mathbf{p}}})$ is convex and the last $\langle f_{\mathrm{R}}\rangle_{\lambda^{(K)}}(\vec{\hat{\mathbf{p}}}) = f_{\mathrm{R}}(\vec{\hat{\mathbf{p}}})$. Referring to Definition D11 and to the set $\mathcal{L}^K_\lambda \triangleq \{\lambda^{(k)}\}$ defined in Theorem T11, it is sufficient and necessary that $\lambda^{(1)} \in \mathscr{L} \Longrightarrow \lambda^{(1)} \geq \lambda^*$, such that $\lambda^{(1)}$ can be referred to as a *majoriser* of λ^*. In the sequel, a simple closed-form expression for a *majoriser* of λ^* is derived. To start, consider the following auxiliary result.

Lemma L11 (Properties of $S_3(a,b,u)$)**.**

Define the auxiliary function $S_3(a,b,u) \triangleq \exp(-u)\cdot {}_1F_1(a;b;u)$, where $(a,b,u) > 0$. This function has the following properties:

i) Monotonicity: $\mathrm{sign}(\frac{\mathrm{d}}{\mathrm{d}u}S_3(a,b,u)) = \mathrm{sign}(a-b)$

ii) Confinement: $0 \leq S_3(a,b,u) \leq 1$ *for* $a < b$.

Proof. In order to prove the first property, we study the derivative of $S_3(a,b,u)$. Invoking the recurrence relation of equation (228), we obtain

$$\frac{\partial S_3(a,b,u)}{\partial u} = \frac{(a-b)}{b}\exp(-u)\cdot {}_1F_1\left(a;b+1;u\right). \tag{239}$$

Since $\exp(-u)\cdot{}_1F_1(a;b+1;u)$ is always positive, equation (239) implicates in property *i*. Finally, recognise [138, pp.514] that $S_3(a,b,0) = {}_1F_1(a;b+1;0) = 1$ and that $\exp(-u){}_1F_1(a;b+1;u)$ is always positive, such that $\lim\limits_{u\to\infty} S_3(a,b,u) = 0^+$ for $a < b$. □

Theorem T13 (Initial Smoothing Parameter: Single Target)**.**

Let $\{\tilde{d}_{it}\}$ *be the set of ranging measurement between the anchors* $\{\mathbf{a}_i\}$ *and a single target. Then*

$$\left\{\lambda \geq \frac{\sqrt{\pi}}{2}\frac{\sum_{i=1}^{N_\mathrm{A}} w_{it}^2\tilde{d}_{it}}{\sum_{i=1}^{N_\mathrm{A}} w_{it}^2} \triangleq \lambda_\mathrm{S}^*\right\} \Longrightarrow \left\{\nabla^2_{\vec{\hat{\mathbf{p}}}}\langle f_\mathrm{R}\rangle_\lambda(\vec{\hat{\mathbf{p}}}) \succeq 0,\, \forall\, \vec{\hat{\mathbf{p}}} \in \mathbb{R}^{\eta N_\mathrm{T}}\right\}. \tag{240}$$

Proof. Invoking equation (230), and noticing that in the source localisation case $\nabla^\mathrm{T}_{\hat{\mathbf{z}}}(\hat{d}^2_{it})\nabla_{\hat{\mathbf{z}}}(\hat{d}^2_{it})$ and $\nabla^2_{\vec{\hat{\mathbf{p}}}}(\hat{d}^2_{it})$ reduce to $\frac{4}{\hat{d}^2_{it}}\hat{\boldsymbol{\Upsilon}}_{it}$ and $2\mathbf{I}_\eta$, as can be found by setting $\mathbf{e}_{it} = 1$ in equations (235) and (226), respectively, we obtain

$$\nabla^2_{\vec{\hat{\mathbf{p}}}}\langle f_\mathrm{R}\rangle_\lambda(\vec{\hat{\mathbf{p}}}) \succeq \underbrace{\left(2\sum_{i=1}^{N_\mathrm{A}} w_{it}^2\left(1-\tfrac{\sqrt{\pi}}{2\lambda}\tilde{d}_{it}\right)\right)\mathbf{I}_\eta}_{\boldsymbol{\aleph}} + \underbrace{\sum_{i=1}^{N_\mathrm{A}}\frac{4w_{it}^2}{\hat{d}^2_{it}}S_2(\hat{d}^2_{it};\lambda)\cdot\hat{\boldsymbol{\Upsilon}}_{it}}_{\bar{\boldsymbol{\Upsilon}}}, \tag{241}$$

where $\hat{\boldsymbol{\Upsilon}}_{it}$ are as in equation (47) for $\eta = 2$ and can be found in [141] for $\eta = 3$, and the inequality results from the minorisation of $S_1(\hat{d}^2_{it};\lambda)$ by $\left(1-\frac{\sqrt{\pi}}{2\lambda}\tilde{d}_{it}\right)$ in light of Lemma L11 and equation (229).

Next, invoke the Wenyl bounds [142, eq. (2.3)], which yields

$$\mathscr{E}_1(\boldsymbol{\aleph}+\bar{\boldsymbol{\Upsilon}}) \geq \mathscr{E}(\boldsymbol{\aleph}) + \mathscr{E}_1(\bar{\boldsymbol{\Upsilon}}), \tag{242}$$

where $\mathscr{E}_k(\cdot)$ denote the k-th smallest eigenvalue of a matrix and $\mathscr{E}(\boldsymbol{\aleph}) \triangleq \mathscr{E}_1(\boldsymbol{\aleph}) = \cdots = \mathscr{E}_\eta(\boldsymbol{\aleph})$, since $\boldsymbol{\aleph}$ has a single eigenvalue of multiplicity η.

Finally, notice that in order for inequality (241) to hold it is sufficient it that $\mathscr{E}_1(\boldsymbol{\aleph}+\bar{\boldsymbol{\Upsilon}})$ is non-negative, which under the fact that $\bar{\boldsymbol{\Upsilon}}$ is positive semi-definite, *i.e.* $\mathscr{E}_1(\bar{\boldsymbol{\Upsilon}}) \geq 0$, is equivalent to

$$\sum_{i=1}^{N_\mathrm{A}} w_{it}^2\left(1-\frac{\sqrt{\pi}\tilde{d}_{it}}{2\lambda}\right) \geq 0, \tag{243a}$$

$$\lambda \geq \frac{\sqrt{\pi}}{2}\cdot\frac{\sum_{i=1}^{N_\mathrm{A}} w_{it}^2\tilde{d}_{it}}{\sum_{i=1}^{N_\mathrm{A}} w_{it}^2} \triangleq \lambda_\mathrm{S}^*, \tag{243b}$$

□

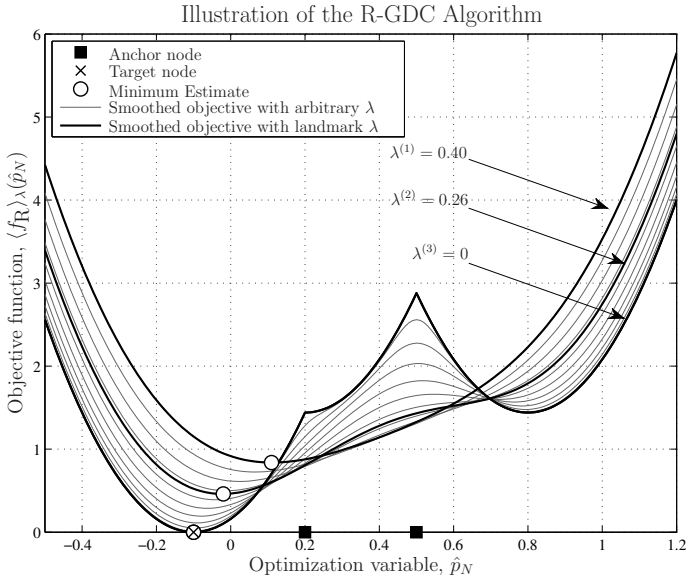

Fig 28. Illustration of the R-GDC method with the example of a single-target localisation in $\eta = 1$. The marker "$\bigcirc$" indicates the result of the k-th iteration. [9, ©IEEE 2011].

In addition to an analytical and simple expression for the majoriser of λ^*, which can be used as the initial smoothing parameter in the R-GDC algorithm, Theorem T13 also hints on a strategy to select the remaining $\lambda^{(k)}$'s. To elaborate, let $\{\tilde{d}_{it}\}$ be ordered without loss of generality so that $\tilde{d}_{1t} \geq \cdots \geq \tilde{d}_{N_\mathrm{A}t}$. Then, a set $\mathcal{L}_\lambda^\mathrm{K} = \{\lambda^{(k)}\}$ of $K = N_\mathrm{A} + 1$ "landmark" smoothing parameters are

$$\lambda_\mathrm{S}^* \geq \cdots \geq \frac{\sqrt{\pi}}{2} \frac{\sum_{i=k}^{N_\mathrm{A}} w_{it}^2 \tilde{d}_{it}}{\sum_{i=k}^{N_\mathrm{A}} w_{it}^2} \geq \cdots \geq \frac{\sqrt{\pi}}{2} \tilde{d}_{1t} \geq 0, \tag{244}$$

such that

$$\lambda^{(k)} \triangleq \frac{\sqrt{\pi}}{2} \frac{\sum_{i=k}^{N_\mathrm{A}} w_{it}^2 \tilde{d}_{it}}{\sum_{i=k}^{N_\mathrm{A}} w_{it}^2}, \tag{245}$$

with $1 \leq k \leq N_\mathrm{A}$ and $\lambda^{(K)} = 0$.

The sequence shown above is monotonically descending, involves less information to be evaluated as k increases and, as can be inferred form the proof of Theorem T13, leads to successively less smooth objectives $\langle f_\mathrm{R} \rangle_{\lambda^{(k)}}(\vec{\hat{\mathbf{p}}})$, as desired. Obviously, arbitrarily many additional smoothing parameters can be selected in between the ones given above as well, although exhaustively numerical tests have consistently shown that to be typically unnecessary (see Section 6.3.1).

An illustration of the effect of choosing the aforementioned landmark smoothing parameters is shown in Figure 28.

The result refers to a scenario with $N_{\mathrm{A}} = 2$ anchors – marked by dark squares –, one target and exact distances. The curves illustrate various versions of the smoothed objectives $\langle f_{\mathrm{R}} \rangle_{\lambda}(\vec{\tilde{\mathbf{p}}})$ derived from different smoothing parameters, including those given in the sequence (244) (bold lines) as well as others assuming intermediary values (grey lines). The minima of corresponding objectives are marked with a "$\bigcirc$," while the actual target location is marked with a "$\times$," which coincides with the last "$\bigcirc$" obtained at the last round of the R-GDC algorithm. It can be observed that the landmark smoothing parameters captures the progressively less smooth behaviour of $\langle f_{\mathrm{R}} \rangle_{\lambda}(\vec{\tilde{\mathbf{p}}})$, allowing for the global minimum of $f_{\mathrm{R}}(\vec{\tilde{\mathbf{p}}})$ to be attained with a small number of R-GDC continuations.

Theorem T14 (Initial Smoothing Parameter: Multiple Targets)**.**

$$\{\lambda \geq \tfrac{\sqrt{\pi}}{2} \max_{ij \in E_T} \tilde{d}_{ij}\} \Longrightarrow \{\nabla^2_{\vec{\tilde{\mathbf{p}}}} \langle f_{\mathrm{R}} \rangle_{\lambda}(\vec{\tilde{\mathbf{p}}}) \succeq 0,\, \forall\, \vec{\tilde{\mathbf{p}}} \in \mathbb{R}^{\eta N_{\mathrm{T}}}\}, \tag{246}$$

where E_T denotes the set of all links connected to the targets.

Proof. Recall from equation (232) that the Hessian matrix of $\langle f_{\mathrm{R}} \rangle_{\lambda}(\vec{\tilde{\mathbf{p}}})$ is given by a positive sum of the matrices $\nabla^2_{\vec{\tilde{\mathbf{p}}}} f^{\mathrm{R}}_{ij}(\hat{d}_{ij}; \lambda)$, such that a sufficient condition for $\nabla^2_{\vec{\tilde{p}}} \langle f_{\mathrm{R}} \rangle_{\lambda}(\vec{\tilde{\mathbf{p}}}) \succeq 0$ is that $\nabla^2_{\vec{\tilde{\mathbf{p}}}} f^{\mathrm{R}}_{ij}(\hat{d}_{ij}; \lambda) \succeq 0,\ \forall ij$. Next, invoke equation (234) and notice that the matrices $\nabla^{\mathrm{T}}_{\vec{\tilde{\mathbf{p}}}} \hat{d}^2_{ij} \nabla_{\vec{\tilde{\mathbf{p}}}} \hat{d}^2_{ij}$ and $\nabla^2_{\vec{\tilde{\mathbf{p}}}} \hat{d}^2_{ij}$ are positive semi-definite since the first is the Gramian of the gradient vector $\nabla_{\vec{\tilde{\mathbf{p}}}} \hat{d}^2_{ij}$ and the second is the Hessian of a norm function [62].

Therefore a sufficient condition to ensure that $\nabla^2_{\vec{\tilde{\mathbf{p}}}} f^{\mathrm{R}}_{ij}(\hat{d}_{ij}; \lambda) \succeq 0$ is that the functions $S_1(u; \lambda)$ and $S_2(u; \lambda)$ given in equations (229) and (236), respectively, are both positive for any u. In order to prove that $S_1(u; \lambda)$ is positive consider the following inequalities

$$1 \geq \frac{\sqrt{\pi}\tilde{d}_{ij}}{2\lambda} \exp\left(\frac{-u}{\lambda^2}\right) {}_1F_1\left(\frac{3}{2}; 2; \frac{u}{\lambda^2}\right), \tag{247a}$$

$$\lambda \geq \frac{\sqrt{\pi}\tilde{d}_{ij}}{2} \exp\left(\frac{-u}{\lambda^2}\right) {}_1F_1\left(\frac{3}{2}; 2; \frac{u}{\lambda^2}\right) \geq \tfrac{\sqrt{\pi}\tilde{d}_{ij}}{2}, \tag{247b}$$

where the last inequality holds due to Lemma L11 *ii*).

As for $S_2(u; \lambda)$, referring to equation (236), it is clear that $S_2(u; \lambda)$ is positive since it is a product of positive terms, namely, the exponential function, the

Hypergeometric function with parameters $a = 3/2, b = 3$ (see [138, pp.514]) and the coefficient $\sqrt{\pi}(8\lambda^3)^{-1}\tilde{d}_{ij}$, which is positive since negative distance measurements $\tilde{d}_{ij}$ are discarded due to the physical impossibility of $d_{ij} < 0$. Finally, since the last inequality of (247) must hold for all ij, the implication (246) requires that

$$\lambda \geq \tfrac{\sqrt{\pi}}{2} \max_{ij \in E} \tilde{d}_{ij} \triangleq \lambda_{\mathrm{N}}^{*}. \tag{248}$$

□

Notice that the majoriser given in equation (248) is also a majoriser of the critical smoothing parameter for the source localisation case. In other words, if the expression in equation (248) is used for a set of distance measurements $\{\tilde{d}_{it}\}$ associated to a single target, we have $\lambda_{\mathrm{N}}^{*} \geq \lambda_{\mathrm{S}}^{*} \geq \lambda^{*}$. Based on Theorem T14, the set of λ can be defined as $\mathcal{L}_{\lambda}^{\mathrm{K}} \triangleq \{\frac{K-k+1}{K}\lambda_{\mathrm{N}}^{*}\}$ with $1 \leq k \leq K+1$.

6.2 Weighing strategy in cooperative positioning

In Chapter 2 we have shown different weighing mechanisms [69, 79–82], which typically resort to heuristics and/or exterior information related to the measurements. However, we recognise that all methods follow the rule-of-thumb of assigning weight $w_{ij} \to 0$ when $\tilde{d}_{ij}$ is to be neglected (with equality if d_{ij} is not measured at all), and $w_{ij} \gg 0$ when $\tilde{d}_{ij}$ is to be relied upon (the more so, the larger w_{ij}). Based on this general idea, we propose a more concrete weighing strategy that does not rely on any assumptions on the ranging model or relationship between ranging error and real distance, and attempts to quantify the reliability of the data. The principle of this strategy is described as follows.

6.2.1 Weighing strategy principle

Let $\tilde{d}_{ij}^{(k)}$ be the k-th measurement of the distance d_{ij}, and let $\bar{d}_{ij}$ be the sample mean of the set $\{\tilde{d}_{ij}^{(k)}\}$ given by

$$\bar{d}_{ij} \triangleq \frac{1}{K_{ij}} \sum_{k=1}^{K_{ij}} \tilde{d}_{ij}^{(k)}. \tag{249}$$

Under the assumption of LOS channel conditions, $\tilde{d}_{ij}^{(k)} = d_{ij} + n_{ij}$ with n_{ij} as a zero-mean Gaussian random variable, it is known that $\bar{d}_{ij}$ is an unbiased estimate of d_{ij} [45], thus the WLS optimisation problem given in equation (28),

can be reformulated as the constrained feasibility problem [143]

$$\begin{aligned} &\text{find} \quad \hat{\mathbf{P}} \\ &\text{s.t.} \quad \bar{d}_{ij} - \epsilon \leq \|\hat{\mathbf{p}}_i - \hat{\mathbf{p}}_j\|_2 \leq \bar{d}_{ij} + \epsilon, \forall ij \in E \\ &\qquad \hat{\mathbf{p}}_i = \mathbf{a}_i \; \forall i = 1, \ldots, N_{\mathrm{A}}. \end{aligned} \tag{250}$$

Employing the terminology used in [143], the solution of (250) is referred to as ϵ-*optimal*, meaning that if a solution $\hat{\mathbf{P}}^*$ to the problem (250) exists, then it is locally true to the observed distances $\bar{d}_{ij}$ within the error ϵ.

We remark, however, that the localisation error $\|\mathbf{P} - \hat{\mathbf{P}}^*\|_{\mathrm{F}}$ obtained from the solution of (250) depends on the quality of the set of distance estimates $\bar{d}_{ij}$'s. In other words, the more accurate are $\bar{d}_{ij}$'s, as estimates of d_{ij}'s, the more reliable is $\hat{\mathbf{P}}^*$, as an estimate of $\mathbf{P}$.

Given a solution $\hat{\mathbf{P}}^*$ of (250) and a confidence bound γ on the distance $\bar{d}_{ij}$, we can determine a confidence region

$$d_{ij} - \epsilon - \gamma \leq \hat{d}_{ij} \leq d_{ij} + \epsilon + \gamma, \tag{251}$$

which holds with a probability

$$\Pr\{d_{ij} - \gamma \leq \bar{d}_{ij} \leq d_{ij} + \gamma\}, \tag{252}$$

since $|\hat{d}_{ij} - \bar{d}_{ij}| \leq \epsilon$ is ensured by the constraints of the formulation itself, as shown in equation (250).

Notice that equation (252) is equivalent to

$$\Pr\{\bar{d}_{ij} - \gamma \leq d_{ij} \leq \bar{d}_{ij} + \gamma\}, \tag{253}$$

which is the *confidence* that the true distance d_{ij} is in the vicinity (confidence bound) γ of the observation $\bar{d}_{ij}$.

This constrained formulation of the network localisation problem (250) shows that, in the absence of a control mechanism on each term $\left(\bar{d}_{ij} - \|\hat{\mathbf{p}}_i - \hat{\mathbf{p}}_j\|_{\mathrm{F}}\right)^2$, the conditions given by equation (251) happen with probability (252) due to the statistics of $\bar{d}_{ij}$. This indicates that under the formulation given in equation (28), the likelihood of satisfying the conditions defined in equation (251) can be increased by matching the *concern* over the term $\left(\bar{d}_{ij} - \|\hat{\mathbf{p}}_i - \hat{\mathbf{p}}_j\|_{\mathrm{F}}\right)^2$ to the probability (or *confidence* over $\bar{d}_{ij}$) as given by equation (252). And under the assumption that $\bar{d}_{ij}$ is an unbiased estimator of d_{ij} – which is true *only* in LOS

conditions ($b_{ij} = 0$) – the probability given by equation (252) is a valid measure of the reliability of $\bar{d}_{ij}$ to estimate d_{ij}.

In light of the above, we define

$$w_{ij} \triangleq \Pr\{-\gamma \leq \varepsilon_{ij} \leq \gamma\} \cdot \mathcal{P}_{ij}, \tag{254}$$

where γ is the confidence bound of the observation $\bar{d}_{ij}$ around the true distance d_{ij}, $\mathcal{P}_{ij}$ is a penalty imposed over the LOS assumption and $\delta_{ij} \triangleq d_{ij} - \bar{d}_{ij}$.

For convenience, we shall hereafter use w_{ij}^{D} in reference to the probability in equation (255), such that $w_{ij} = w_{ij}^{\mathrm{D}} \cdot \mathcal{P}_{ij}$. The weights w_{ij}^{D} and $\mathcal{P}_{ij}$ will also be dubbed the dispersion (confidence) weights and penalty weights, respectively.

6.2.2 Dispersion weight

The dispersion weight is mathematically formulated as

$$w_{ij}^{\mathrm{D}} \triangleq \Pr\{-\gamma \leq \delta_{ij} \leq \gamma\}, \tag{255}$$

which, under the assumptions that $\rho_{ij} = 0$ (LOS channel conditions), and $\tilde{d}_{ij}^{(k)}$ are independent, can be rewritten in the form

$$w_{ij}^{\mathrm{D}} = 2 \cdot \Pr\{\delta_{ij} \leq \gamma\} - 1, \tag{256}$$

where we used the symmetric properties of the Gaussian error assumption.

By means of small scale statistics w_{ij}^{D} can be computed as [144]

$$w_{ij}^{\mathrm{D}} = \mathcal{W}_d(\hat{\sigma}_{ij}, K_{ij}; \gamma) \triangleq -1 + 2 \cdot \int_{-\infty}^{t_{ij}} f_{\mathrm{T}}(t; K_{ij} - 1)\, dt, \tag{257}$$

$$t_{ij} \triangleq \gamma \cdot \sqrt{K_{ij}/\hat{\sigma}_{ij}^2}, \tag{258}$$

where $f_{\mathrm{T}}(t; n)$ is the T-distribution of n degree of freedom and t_{ij} is the *t-score*.

As emphasised by the notation, w_{ij}^{D} is a function of the sample variance $\hat{\sigma}_{ij}^2$ and the number of samples K_{ij}, as well as the confidence bound γ, to be specified below. Since $\hat{\sigma}_{ij}^2$ and K_{ij} carry different information about the true value of d_{ij}, it is not surprising that both these parameters impact on the weight w_{ij}^{D}. In fact, the plots of $\mathcal{W}_d(\hat{\sigma}_{ij}, K_{ij}; \gamma)$ illustrated in Figures 29(a) and 29(b), show that w_{ij}^{L} grows with the inverse of $\hat{\sigma}_{ij}^2$ (for fixed K_{ij}), and with K_{ij} (for fixed $\hat{\sigma}_{ij}^2$). This is in accordance with the rule-of-thumb of assigning weight $w_{ij}^{\mathrm{D}} \to 0$ when $\bar{d}_{ij}$ is to be neglected (with equality if d_{ij} is not measured at all),

and $w_{ij}^{\mathrm{D}} \gg 0$ when $\bar{d}_{ij}$ is to be relied upon (the more so, the larger w_{ij}^{D}) since, $\hat{\sigma}_{ij}^2$ is proportional to the uncertainty of $\bar{d}_{ij}$, as a measure of d_{ij}, while K_{ij} relates to the quality of $\bar{d}_{ij}$ and $\hat{\sigma}_{ij}^2$ as measures of d_{ij} and its dispersion, respectively.

Unlike $\hat{\sigma}_{ij}^2$ and K_{ij}, which are obtained in the process of measuring inter-node distances, the confidence bound γ is a free choice parameter that allows for fine-tuning the relative values of w_{ij}^{D}.

The mechanism to find the optimum γ is given by the following optimisation problem based on the *diversity index* or *entropy* metric

$$\gamma_{\mathrm{opt}} = \arg \max_{\gamma \in \mathbb{R}^+} \ \mathcal{H}(\gamma), \tag{259}$$

where

$$\mathcal{H}(\gamma) = -\sum_{k=K_{\mathrm{MIN}}}^{K_{\mathrm{MAX}}} \int_{\sigma_{\mathrm{MIN}}}^{\sigma_{\mathrm{MAX}}} \mathcal{W}_d(s,k;\gamma) \cdot \ln\left(\mathcal{W}_d(s,k;\gamma)\right)\, ds, \tag{260}$$

where $K_{\mathrm{MIN}}, K_{\mathrm{MAX}}, \sigma_{\mathrm{MIN}}$ and σ_{MAX} are the minimum and the maximum number of observable samples and the minimum and the maximum typical ranging error, respectively. It is imperative, therefore, to find a mechanism to optimise γ, which is the topic of the next subsection.

Derivation of the ergodic confidence bound

We seek a mechanism to select an optimum γ, that results in a characterisation of equation (257) for a broad ensemble of networks. In other words, we are interested in the derivation of an ergodic[13] optimum γ, relying only on weak assumptions on the design and technological characteristics of the network.

In the pursuit of such a mechanism, we recognize an analogy between our problem and the one of characterising a population by categorising its individuals, which is the subject of Categorical Data Analysis [145]. Since K_{ij} and $\hat{\sigma}_{ij}^2$ carry different information about the estimate of the distance d_{ij}, these parameters can be used to categorise $\bar{d}_{ij}$, while w_{ij}^{D} can be seen as the metric – to be fine-tuned – that distinguishes $\bar{d}_{ij}$ from all other distance estimates whose admissible categorical values $(K_{q\ell}, \hat{\sigma}_{q\ell}^2)$ lie within a region $\mathscr{W}$. In our context, the problem of finding an ergodic optimum γ is equivalent to finding the metric formula that best distinguishes individuals of the population $\mathscr{W}$.

[13] Ergodic here refers to the fact that the statistics of $\tilde{d}_{ij}^{(k)}$ for a fixed (i,j) over many network realisations is the same as the statistics of $\tilde{d}_{ij}^{(k)}$ for a fixed k over all (i,j) of a given realisation.

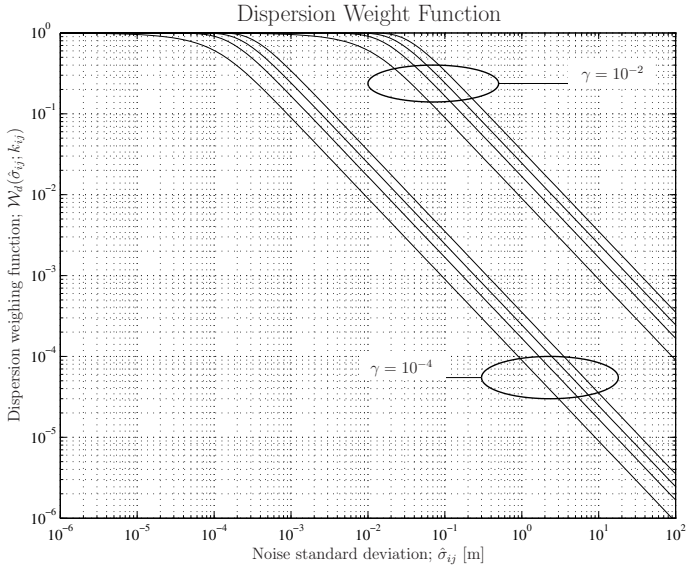

(a) Dispersion weight as functions of $\hat{\sigma}_{ij}$

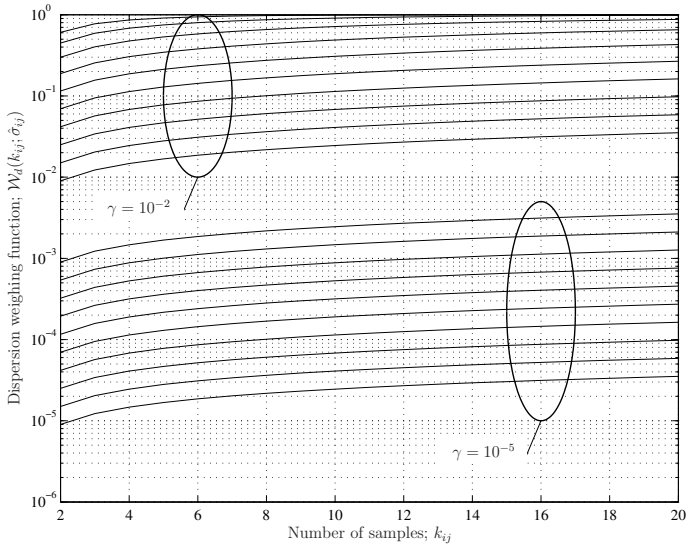

(b) Dispersion weight as functions of K_{ij}

Fig 29. Family of dispersion weight functions. [8, ©IEEE 2009].

A well-known tool of categorical data analysis often employed to solve similar problems is maximum diversity sampling [146], which establishes that the optimum way to characterise an entire population given a limited categorical sample size, is to purposefully select individuals that are maximally distinct. To draw an analogy, if one wishes to find out the political views of a given population by interviewing a limited number of individuals, then best results are achieved by interviewing as distinct individuals as possible (the old, the young, the rich, the poor, etc.). Brought to our context, this result indicates that the right criterion to fine-tune the weight function w_{ij}^{D} is to select the parameter γ that maximises, across the population $\mathscr{W}$, the diversity of the estimates $\bar{d}_{ij}$ as measured by their weights w_{ij}^{D}. A well-known metric of the diversity of a categorical population $\mathscr{W}$ with individual relevance measured by the occurrence $p_{\mathrm{W}}(w)$ of each category w is

$$\mathcal{H} = -\sum_{\mathscr{W}} p_{\mathrm{Z}}(w) \cdot \ln p_{\mathrm{Z}}(w). \tag{261}$$

This metric is known in the categorical data analysis [145] and in the communication theory [147] literatures as the *diversity index* and the *entropy* of $\mathscr{W}$, respectively. These two terms will therefore be hereafter used interchangeably.

Notice, however, that while entropy is commonly defined over probabilistic measures, the diversity index is also applied to non-probabilistic measures [148], which is the case at hand since, in general, $\int_{\mathscr{W}} \mathcal{W}_d(s,k;\gamma) \neq 1$. In our context, this leads to $p_{\mathrm{Z}}(z) = \mathcal{W}_d(s,k;\gamma)$ and $\mathscr{W} = [K_{\mathrm{MIN}}, K_{\mathrm{MAX}}] \times [\sigma_{\mathrm{MIN}}, \sigma_{\mathrm{MAX}}]$, where $(K_{\mathrm{MIN}}, K_{\mathrm{MAX}})$ and $(\sigma_{\mathrm{MIN}}, \sigma_{\mathrm{MAX}})$ are the pairs of minimum/maximum numbers of samples and noise standard deviation admitted by the system, respectively. From the preceding arguments and equations (257) and (261), we conclude that the optimisation criterion[14] for γ is to *maximise*

$$\mathcal{H}(\gamma) = -\sum_{k=K_{\mathrm{MIN}}}^{K_{\mathrm{MAX}}} \int_{\sigma_{\mathrm{MIN}}}^{\sigma_{\mathrm{MAX}}} \mathcal{W}_d(s,k;\gamma) \cdot \ln\left(\mathcal{W}_d(s,k;\gamma)\right)\, ds, \tag{262}$$

where the dependence of $\mathcal{H}$ on γ is made explicit for clarity.

[14] While equation (262) is the appropriate expression for an *ergodic* optimization of γ, $\mathcal{H}(\gamma) = -\sum_i \sum_j \mathcal{W}_d(\hat{\sigma}_{ij}, K_{ij};\gamma) \cdot \ln(\mathcal{W}_d(\hat{\sigma}_{ij}, K_{ij};\gamma))$ can be used for an adaptive optimisation specific to a particular network realisation. In the case of large scale networks, however, the two formulations are equivalent since data evenly span the range $[K_{\min}, K_{\max}] \times [\sigma_{\min}, \sigma_{\max}]$.

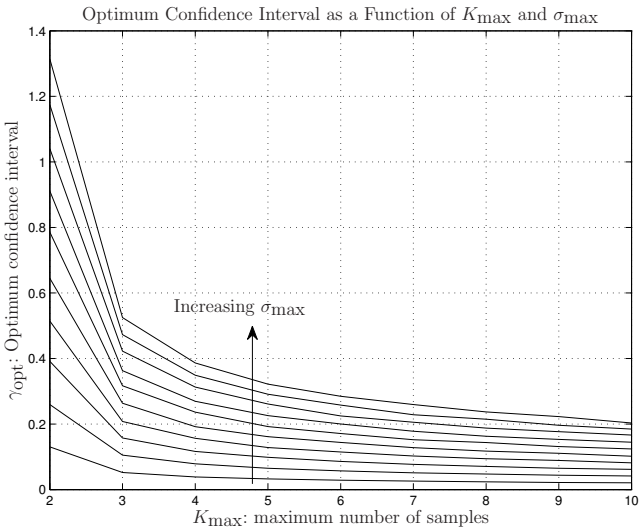

Fig 30. Variations of the optimal confidence bound as a function of the maximum number of samples K_{MAX} and parameterised by the noise standard deviation σ_{MAX}.

Thus,

$$\gamma_{\text{opt}} \triangleq \arg\max_{\gamma \in \mathbb{R}^+} \ \mathcal{H}(\gamma). \tag{263}$$

Due to the monotonicity of $\mathcal{W}_d(s,k;\gamma)$ and the convexity of the entropy function, this optimisation problem can be easily solved via standard optimisation techniques [65]. For the sake of completeness, in Figure 30 we illustrate γ_{opt} as function of K_{MAX} and σ_{MAX}.

Validation of optimum confidence bound

To validate the proposed weight optimisation mechanism, we compare the RMSE of a WLS-based positioning which utilises the dispersion weight against those obtained with alternative strategies[15], namely, the connectivity-based ($w_{ij} = 1$ if $c_{ij} = 1$, and $w_{ij} = 0$ otherwise) weight, the inverse-distance based [69] and the LOESS-based [82] methods. The results illustrated in Figure 31 are

[15]The result obtained with inverse-variance weighing strategy [79, 80] that leads to the CRLB will be omitted since, the exact knowledge of σ_{ij}^2 at each link is infeasible with the assumptions that only few ranging samples can be measured.

obtained with the R-GDC method and, refer to regular networks with $N_{\mathrm{A}} = 4$ anchors equispaced in a circle of radius 10 meters, and $N_{\mathrm{T}} = 10$ targets, meshness ratio $m = 1$, zero-mean ranging error ($b_{ij} = 0$), $\sigma_{ij} \in (0.01, 0.3)$ meters and $K_{ij} \sim \mathcal{U}(2, 5)$.

An important outcome of this investigation is that the dispersion weight function with the confidence bound computed as prescribed by equation (263), yields in fact the best weighing strategy, outperforming all the alternative approaches. Interestingly, this turns out to be true even when the confidence bound deviates within a certain range from γ_{opt}, which indicates that the overall mechanism is robust to numerical approximations or errors. As shown in Figure 32, the difference between the inverse-variance weighing strategy and the PEB with the increase of the number of samples[16].

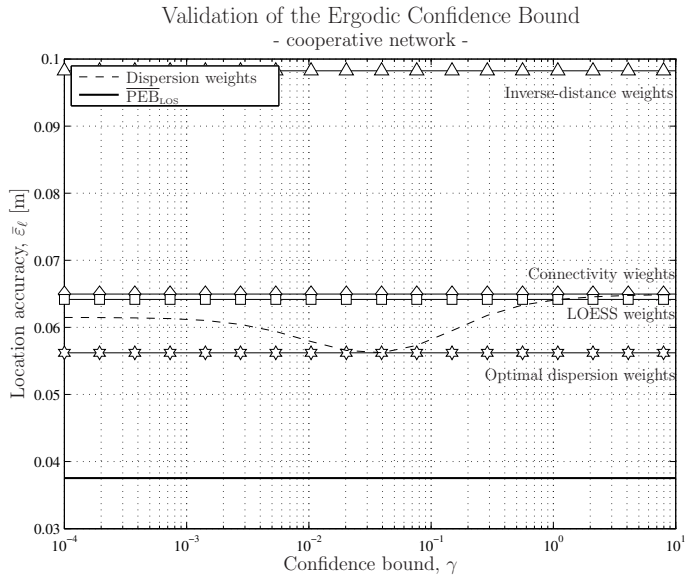

Fig 31. Validation of the ergodic bound and comparison to different weighing strategies. It is assumed a regular network with of $N_{\mathbf{A}} = 4$ and $N_{\mathbf{T}} = 10$, full connectivity, *i.e.* $m = 1$**,** $\sigma_{ij} \in (0.01, 0.3)$ **meters and** $K_{ij} \in (2, 5)$**.**

[16]The convergence is guaranteed by the fact that for $K_{ij} \to \infty$, $\bar{d}_{ij} \to d_{ij}$.

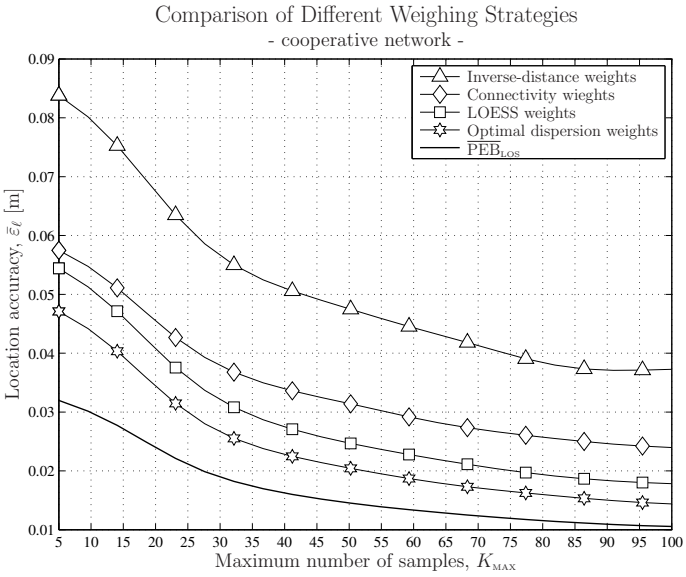

Fig 32. Comparison of different weighing strategies for the localisation of a regular network with of $N_{\mathbf{A}} = 4$ and $N_{\mathbf{T}} = 10$. It is assumed a full connectivity, $i.e.$ $m = 1$, $\sigma_{ij} \in (0.01, 0.3)$ meters and $K_{ij} \in (2, K_{\mathbf{MAX}})$.

6.2.3 Penalty weight

The second term of the proposed weight given in equation (255) is represented by the penalty weight $\mathcal{P}_{ij}$. As mentioned in the introduction of this section, $\mathcal{P}_{ij}$ is a corrective factor that penalises the hypothesis that link ij is in LOS channel conditions, as implied in the formulation of the dispersion weighing function $\mathcal{W}_d(s, k; \gamma)$ given by equation (257).

To be specific, if $\mathcal{P}_{ij} \to 1$ then it is considered that $\bar{d}_{ij}$ is obtained from ranging samples without bias error (as assumed and required when computing w_{ij}^{D}). Conversely, if $\mathcal{P}_{ij} \to 0$ then it will be assumed that the samples $\tilde{d}_{ij}^{(k)}$ are likely to be affected by a bias (NLOS channel assumption).

With scarce distance information ($K_{ij} \to 1$), little can be done to infer whether the link ij is in LOS or NLOS from $\{\tilde{d}_{ij}^{(k)}\}$ alone. In order to circumvent this problem, we observe that the risk of the LOS assumption can be inferred from geometric properties of 3-node cliques.

In other words, in large-scale networks with power-constrained devices, where connectivity depends on the radio range $R_{\max}$ and ranging information is scarce, the likelihood that 3-node cliques form obtuse triangles is small since the connected nodes are typically "close" to each other. If we assume that the bias error due to NLOS condition is positive, its effect onto a set of distance measurements $\{\tilde{d}_{ij}^{(k)}\}$ is to increase the likelihood that an obtuse triangle is *observed*, despite the fact that the true locations of the 3-connected nodes i, j and q do not form an obtuse triangle. Therefore, the risk associated with the LOS assumption over a link ij can be inferred based on the likelihood that the observations indicate the formation of an obtuse triangle, with the strength of this relationship inversely proportional to R_{MAX}.

Incidentally, a similar idea to the one summarised above has been put forward in [149], although several differences between the material thereby and our own contributions exist. To cite a few, the work in [149] is focused on 4-node cliques, does not elaborate into concrete algorithms, suggests the application of the idea only in the form of a potential tool for binary (hard-decision) LOS/NLOS identification and, of course, does not develop or hint to associated weighing strategies. Our approach instead exploits the properties of a simpler cliques (3 node only), translates into LOS/NLOS non parametric soft-identification method as well as weighing strategy.

Computation of the penalty weights

Consider a network realization $\mathbf{P}$, represented by the graph $G = \mathcal{G}(V, E, \bar{\mathbf{D}})$, where V, E and $\bar{\mathbf{D}}$ are the sets of vertices, of links and weights, respectively. Focus on a 3-cliques (v_i^G, v_j^G, v_q^G) of G, and define two hypothesis H_0 and H_1 as:

$$\begin{cases} H_0 : \text{the clique}(v_i^G, v_j^G, v_q^G) \text{ forms a triangle,} \\ H_1 : \text{the clique}(v_i^G, v_j^G, v_q^G) \text{ does not forms a triangle.} \end{cases} \tag{264}$$

Based on the 4-th property of the EDM, namely the triangle inequality

$$d_{ij} - d_{iq} - d_{jq} \leq 0, \tag{265}$$

the hypothesis H_0 can be tested from the sets of measurements $\{\tilde{d}_{ij}^{(k)}\}$, $\{\tilde{d}_{iq,k}\}$ and $\{\tilde{d}_{jq,k}\}$ by testing

$$\bar{\mu}_{ijq} \underset{H_0}{\overset{H_1}{\gtrless}} 0, \tag{266}$$

where $\bar{\mu}_{ijq}$ is the sample mean of the variable

$$\tilde{\mu}_{ijq} = \tilde{d}_{ij} - \tilde{d}_{iq} - \tilde{d}_{jq}, \tag{267}$$

defined for all $C_{ijq} = K_{ij} \cdot K_{iq} \cdot K_{jq}$ arranges of estimates taken from the sets $\{\tilde{d}_{ij}^{(k)}\}$, $\{\tilde{d}_{iq}^{(k)}\}$ and $\{\tilde{d}_{jq}^{(k)}\}$, such that $\{ij, iq, jq\} \in E$.

This test belongs to the class of the hypothesis test method with one-side rejection region, where the critical value is given by

$$\varkappa_{ijq} \triangleq \frac{\bar{\mu}_{ijq} - 0}{\hat{\sigma}_{\mu_{ijq}} / \sqrt{C_{ijq}}}, \tag{268}$$

where $\hat{\sigma}_{\mu_{ijq}}$ is the sample-standard deviation of the variable $\tilde{\mu}_{ijq}$. The confidence that the 3-tuple (v_i^G, v_j^G, v_q^G) forms a triangle, given the observations $\{\tilde{d}_{ij}^{(k)}\}$, $\{\tilde{d}_{iq}^{(k)}\}$ and $\{\tilde{d}_{jq}^{(k)}\}$, is therefore expressed by the probability

$$p_{ijq} = 1 - \Pr\{z \leq \varkappa_{ijq}\} = Q(\varkappa_{ijq}). \tag{269}$$

Since the link ij forms a distinct triangle with each v_q^G, the penalty $\mathcal{P}_{ij}$ can be defined as

$$\mathcal{P}_{ij} \triangleq \min_q p_{ijq} \quad \forall \left(e_{ij}^G, e_{iq}^G, e_{jq}^G\right) \in E, \tag{270}$$

which ensures that the most conservative decision on the penalty over the LOS assumption onto the link ij is taken.

As mentioned above, a by-product of the penalty weights $\mathcal{P}_{ij}$ calculation is a non-parametric geometric mechanism for LOS/NLOS channel identification that relies on few distance observations and exploits the relationship of not only a pair, but a 3-tuple of nodes. This differs from the majority of LOS/NLOS identification methods found in the literature (see [21, Sec. IV]) which apply to each link separately, require large numbers of samples and assume the knowledge of either the ranging error distribution [150], or other physical layer parameters such as the delay-spread of the channel [81].

Specifically, compare $\mathcal{P}_{ij}$ to a pre-defined threshold ξ_H. If $(\mathcal{P}_{ij} \geq \xi_H)$, then the link ij is recognised as being in LOS and, conversely, if $(\mathcal{P}_{ij} < \xi_H)$, the link ij is considered to be in NLOS.

To assert the performance of proposed LOS/NLOS identification algorithm we evaluate the probability of NLOS miss-detection $\mathrm{P_{MD}}$ (*i.e.* misinterpreting a NLOS as LOS) and the probability of NLOS false-alarm $\mathrm{P_{FA}}$ (*i.e.* misinterpreting

a LOS as NLOS), respectively given by

$$\mathrm{P_{MD}}(b_{ij};\theta^*_{ij}) \triangleq \Pr\{\mathcal{P}_{ij} \geq \xi_H | b_{ij} \neq 0\}, \tag{271}$$

$$\mathrm{P_{FA}}(\sigma_{ij};\theta^*_{ij}) \triangleq \Pr\{\mathcal{P}_{ij} < \xi_H | b_{ij} = 0\}, \tag{272}$$

where the characteristic angle θ^*_{ij} is the angle that faces the edge ij for which the penalty weight $\mathcal{P}_{ij}$ is computed.

In Figures 33(a) and 33(b), the results obtained with a network of $N_\mathrm{A} = 4$, $N_\mathrm{T} = 10$, uneven noise $\sigma_{ij} \sim \mathcal{U}(0.01, 0.3)$ meters, 30% of NLOS links with uneven bias $b_{ij} \sim \mathcal{U}(0.5, 3)$ meters and $K_{ij} \sim \mathcal{U}(2, 5)$ are illustrated. Specifically, in Figure 33(a) it is shown that the LOS/NLOS identification algorithm misses the NLOS detection when both θ^*_{ij} and b_{ij} are relatively small, which corresponds to the situation of a link ij that is part of acute triangles and affected by a little error. While a small bias is typically ineffective to the localisation system, the dominant presence of acute triangles and NLOS miss-detection can introduce large error on the final node location accuracy. Therefore, to minimise the location error due to a miss-detection of the bias, it is necessary to either take a large ξ_H or increase the occurrence of obtuse triangles by rising the density of the nodes in the network.

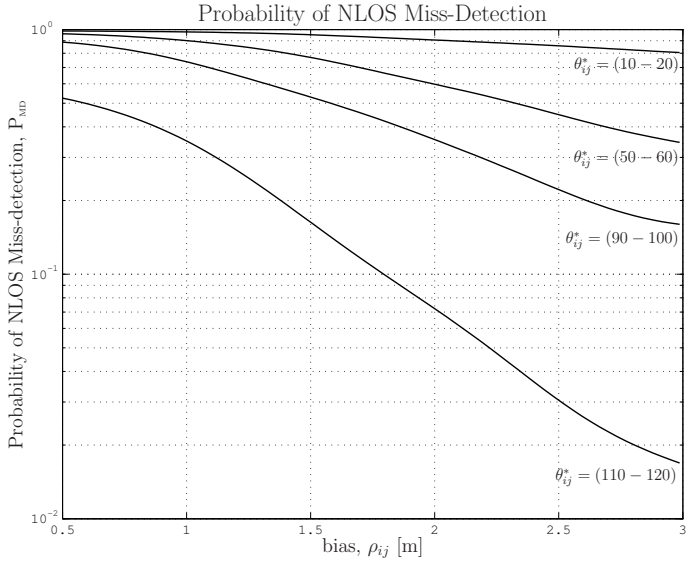

(a) Probability of NLOS miss-detection: $\mathrm{P_{MD}}$

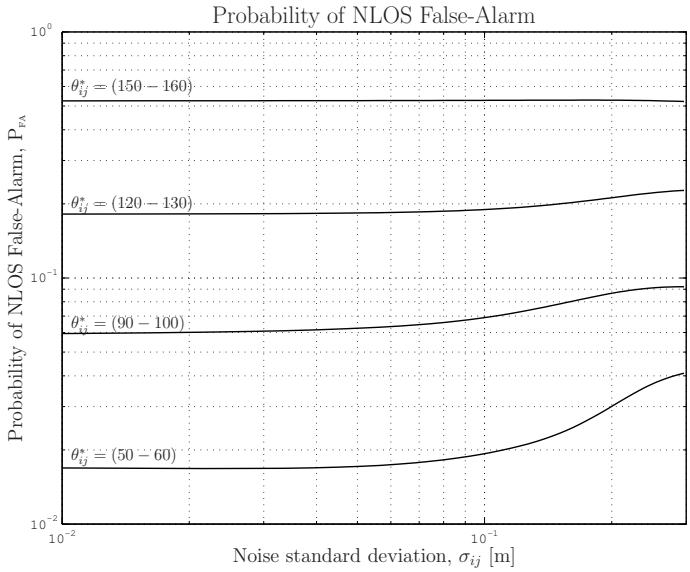

(b) Probability of NLOS false-alarm: P_{FA}

Fig 33. Probability of NLOS miss-detection and false-alarm. Network of $N_{\mathbf{A}} = 4$, $N_{\mathbf{T}} = 10$, uneven noise $\sigma_{ij} \sim \mathcal{U}(0.01, 0.3)$ meters, 30% of NLOS links with uneven bias $b_{ij} \sim \mathcal{U}(0.5, 3)$ meters and $K_{ij} \sim \mathcal{U}(2, 5)$.

In Figure 33(b), instead, we show that the P_{FA} increases when θ_{ij}^{*} is larger (obtuse triangle). Therefore, to minimize the P_{FA} it is necessary to either take a low ξ_H or decrease the occurrence of obtuse triangles.

To achieve a trade-off between P_{MD} and P_{FA} we experienced that $\xi_H = 0.45$ is sufficient to yield a more selective LOS/NLOS decision and avoids false-alarms due to the presence of obtuse triangles and large noise.

6.3 Performance evaluation and comparison

In this section, we evaluate and compare the performance of the proposed cooperative localisation algorithm (R-GDC with the dispersion-penalty weight) against a SMACOF [59], a LM-WLS [65] and an SDP [69] based positioning algorithms. To efficiently implement the SMACOF algorithm, we utilise the Guttman-transform which provides a closed-form expression for the minimum

at the k-th iteration [59]. The LM-WLS algorithm can be implemented with a subspace trust-region method with pre-computed Jacobians [65]. To minimise this sensitivity, we utilise the combination of the Nyström and shortest-path completion algorithms [151]. Hereafter, the random and the Nyström-based initialisation will be distinguished by labelling the name of the algorithm with a " $*$ " when the latter is used. The SDP based optimisation is coded with the `cvx` MATLAB package provided by Standford University.

The study will be divided in two parts. In the first one, the R-GDC technique will be compared to the alternative optimisation methods from a mere minimisation perspective. In this regard, we assume LOS conditions, optimal weighing strategy (inverse of the variance) and we evaluate the localisation accuracy, the minimisation effectiveness defined in the next section), and the computational complexity. In the second part, we compare the proposed dispersion-penalty with the alternatives LOESS, inverse-distance and connectivity-based methods.

6.3.1 Comparison of the optimisation methods

Consider a network with $N_{\mathrm{A}} = 4$ anchors equispaced in a circle of radius 10 meters and $N_{\mathrm{T}} = 10$ targets deployed in the convex-hull of the anchors. Without loss of generality, assume $\sigma_{ij} = \sigma \ \forall \ ij$ and let $c_{ij} = 1$ if $d_{ij} \leq R_{\mathrm{MAX}}$.

Location accuracy

In Figure 34(a), we compare the location accuracy obtained with the aforementioned algorithms as a function of the noise standard deviation σ while $m = 1$ (full connectivity). The location accuracy obtained with the SMACOF* slightly deviates from those obtained with the R-GDC, the SDP and the LM-WLS*, which in turn achieve the performance of an ideal unbiased estimator. In Figure 34(b), the location accuracy obtained with the same algorithms is plotted as a function of the meshness ratio m while $\sigma = 0.3$ meters. In this case, the advantage of the R-GDC with respect to the SMACOF* and the LM-WLS* algorithms is clearly demonstrated. At low meshness ratio (scarce connectivity), the R-GDC provides a better localization accuracy and it almost achieves the performance of the SDP. This is an indication that the R-GDC performs a better minimisation than the LM-WLS and the SMACOF, and it proves a good

robustness to the local minima problem. The gap between the SDP and the bound is probably a consequence of the non localisability of the network. Indeed, these tests were performed only with the assumptions that the node-degree[17] is larger than three, which is not a sufficient condition for localisability.

Minimisation effectiveness

To further investigate the performance of the minimisation algorithms from a mere optimisation perspective, we define two new metrics, namely the minimisation effectiveness and the minimisation deviation.

Definition D13 (Minimisation Effectiveness)**.**

*The **minimisation effectiveness** of the ℓ-th algorithm over the set of L alternatives is defined as*

$$\Pi(\ell) \triangleq \Pr\{f_{\mathrm{R}}(\vec{\hat{\mathbf{p}}}^{*}_{\ell}; \vec{\tilde{\mathbf{d}}}) = \min_{\forall\, q} f_{\mathrm{R}}(\vec{\hat{\mathbf{p}}}^{*}_{q}; \vec{\tilde{\mathbf{d}}})\}, \tag{273}$$

where $\hat{\mathbf{p}}^{*}_{\ell}$ is the solution provided by the ℓ algorithm, $f_{\mathrm{R}}(\vec{\hat{\mathbf{p}}}^{*}_{q}; \vec{\tilde{\mathbf{d}}})$ makes explicit the dependence of $f_{\mathrm{R}}(\vec{\hat{\mathbf{p}}}^{*}_{q})$, with the ranging $\vec{\tilde{\mathbf{d}}}$.

Definition D14 (Minimiser Deviation)**.**

*The **minimiser deviation** of the ℓ-th algorithm over the set of L alternatives is defined as*

$$\mathscr{S}(\ell) \triangleq \mathrm{E}_{\tilde{\mathbf{D}}}\left[f_{\mathrm{R}}(\vec{\hat{\mathbf{p}}}^{*}_{\ell}; \vec{\tilde{\mathbf{d}}}) - \min_{\forall\, q} f_{\mathrm{R}}(\vec{\hat{\mathbf{p}}}^{*}_{q}; \vec{\tilde{\mathbf{d}}})\right]. \tag{274}$$

In plain words, the *minimisation effectiveness* of a given algorithm is the likelihood that *it* is the best minimiser *amongst the methods compared*; while the *minimiser deviation*, quantifies the average error of the objective at the solution attained by each algorithm with respect to the that attained by the best minimiser.

[17] In graph theory, the node-degree of the i-th node is equal to the number of connections departing and arriving at that node.

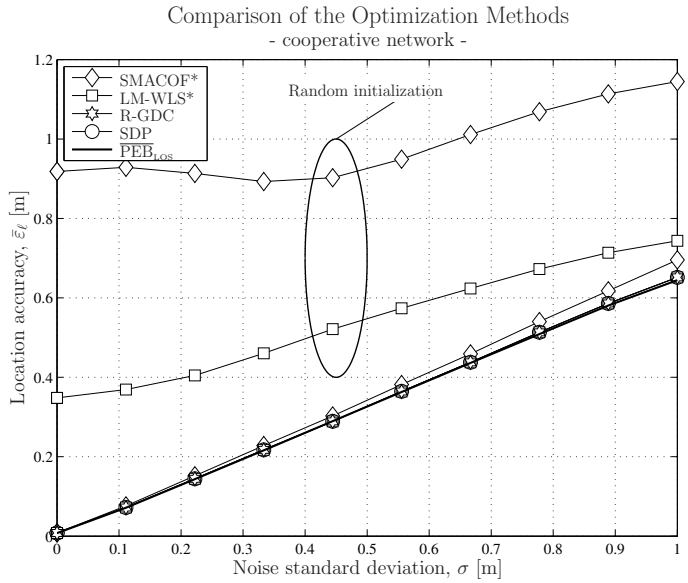

(a) RMSE as a function of the noise with $m = 1$

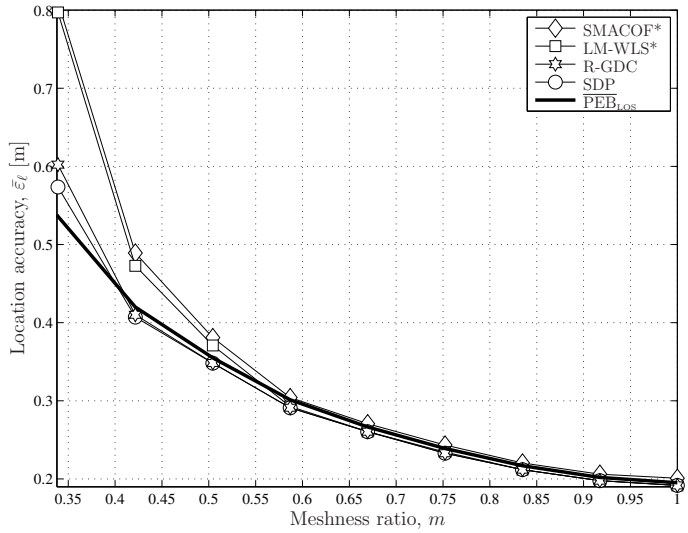

(b) RMSE as a function of the meshness with $\sigma_{ij} = \sigma = 0.3$ meters.

Fig 34. Comparison of the optimisation algorithms for cooperative positioning in LOS scenarios. The network consists of $N_{\mathbf{A}} = 4$ anchors, $N_{\mathbf{T}} = 10$ targets and it is deployed in a square of 14.14×14.14 square meters.

The result for a multi-target scenario is offered in Figure 35, where the ring chart shows that the minimisation effectiveness of the R-GDC method is generally superior to those observed with the alternative optimisation techniques, especially for high meshenss ratio. The accompanying Table 1 indeed reveals that the minimiser deviation of the R-GDC algorithm is typically at the order of 10^{-5}, similar to that of the SDP, and one order smaller than those obtained with the LM-WLS* and SMACOF*. The failures of the R-GDC methods are probably a consequence of the lack of consistency in the estimation problem. Indeed, at low mesheness ratio, the network is rarely strongly-localisable and therefore, minima with a similar value to the global one can occur.

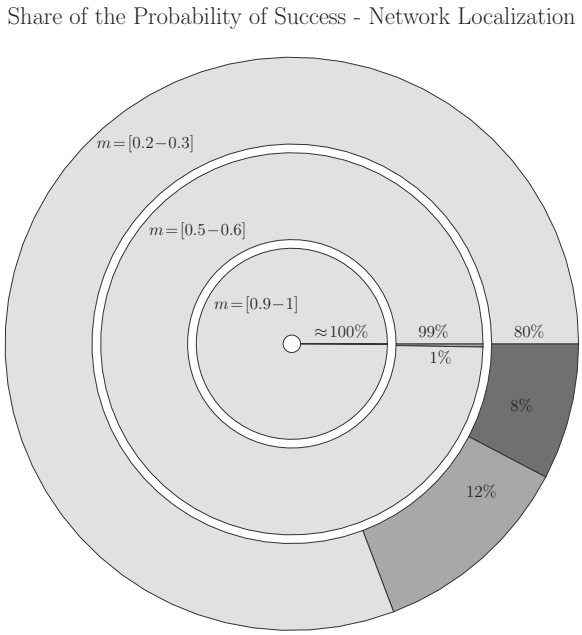

Fig 35. Comparison of the minimisation effectiveness $\Pi(\ell)$ of various localisation algorithms in networks with $N_{\mathbf{A}} = 4$ anchors and $N_{\mathbf{T}} = 10$ under various values of meshness ratios $m \in [0, 1]$ and $\sigma_{ij} = \sigma = 0.3$ meters. All minimisation techniques operate under the same tolerances of 10^{-8} on the variations of the estimates and the objective function.

Table 1. Average minimiser deviation for network localisation.

m	SMACOF*	LM-WLS*	SDP	R-GDC
(0.2,0.3)	1.6e-01	1.3e-01	3.2e-03	2.3e-02
(0.3,0.4)	2.2e-01	1.9e-01	4.1e-03	4.9e-03
(0.4,0.5)	7.6e-02	3.1e-02	1.2e-03	8.5e-05
(0.5,0.6)	5.5e-02	7.3e-03	1.6e-04	7.1e-06
(0.6,0.7)	6.5e-02	1.7e-08	1.6e-09	0
(0.7,0.8)	7.5e-02	4.3e-04	1.3e-09	0
(0.8,0.9)	9.2e-02	8.6e-09	6.9e-10	0
(0.9,1)	1.1e-01	8.6e-09	8.5e-08	8.5e-08

Computational complexity and convergence

The next performance comparison addresses the computational complexity of the algorithms and the rate of convergence. To this end, we calculate the average algorithm complexity $\mathcal{O}(N_V^{\varphi})$, and we use the average complexity exponent.

$$\varphi \triangleq \log_{N_V}(\mathrm{E}_{\tilde{\mathbf{D}},\mathbf{Z}}\big[\mathcal{C}(N_V)\big]), \tag{275}$$

as the metric for comparison, where the subscripts $\tilde{\mathbf{D}}$ and $\mathbf{Z}$ indicate the expectations over the random processes of the ranging and networks, respectively.

The complexity of the SMACOF* and LM-WLS* algorithms, instead, can be estimated as follows[18]

$$\mathcal{C}_{\mathrm{SMACOF}} \approx N^3 + t\left(N^2(2\eta+\tfrac{1}{2}) - N(\eta+\tfrac{1}{2})\right) \approx \mathcal{O}(N^3), \tag{276}$$

$$\begin{aligned}\mathcal{C}_{\mathrm{LM}} &\approx t\left(\tfrac{N_V^3}{\eta^2} + (\tfrac{N_V^2}{\eta^2} + \tfrac{N_V}{\eta})(2N_{\mathrm{A}}-1) + N_V\right) + r(t)\left(N_V^3 + \tfrac{N}{2}(N-1)\right), \\ &\approx \mathcal{O}(C_L N_V^3),\end{aligned} \tag{277}$$

$$\begin{aligned}\mathcal{C}_{\text{R-GDC}} &\approx \frac{1}{2}\sum_{k=1}^{K} t_k\left((N^2-N)C_2 + 16N_V^2 - 2N_V\right) + r(t_k)(N^2-N)C_1, \\ &\approx \mathcal{O}(C_R N_V^2),\end{aligned} \tag{278}$$

where t and $r(t)$ refer to the number of iterations of the main and inner loops of the optimisations, the subscript $_k$ refers to the k-th minimisation of the

[18] In [69] , it is shown that for large scale networks the computational complexity of the SDP algorithm based on an interior-point minimisation method grows as $\mathcal{O}(N_V^6)$ which is way above the results obtained with the alternative algorithms.

R-GDC method with $\lambda^{(k)}$, C_1 and C_2 are the costs for the calculation of the Hypergeometric functions of equations (207) and (222), and C_L and C_R are cumulative values that account for all iterations. Derivation details are given in the Appendix A1. Notice that the complexity of the algorithms of interest depends not only on their structure, which is mostly related to the number of variables N_V, but also on conditions such as noise and robustness to initial estimates, which in turn are captured by the number of iterations t. Due to these factors, the computational complexity of the R-GDC algorithm is rarely $\mathcal{O}(N_V^2)$, nevertheless, it is inferior to the LM-WLS method. Indeed, in Figure 36, the results show that for large networks[19] the LM-WLS requires approximately $\mathcal{O}(N_V^4)$ operations, whereas the R-GDC $\mathcal{O}(N_V^{3.5})$ and SMACOF* $\mathcal{O}(N_V^3)$.

In Figure 37, we illustrate the localisation error achieved with the R-GDC algorithm in a large scale network set-up, *i.e.* $N_{\mathrm{T}} = 50$, $N_{\mathrm{T}} = 100$ and $N_{\mathrm{T}} = 200$ target nodes.

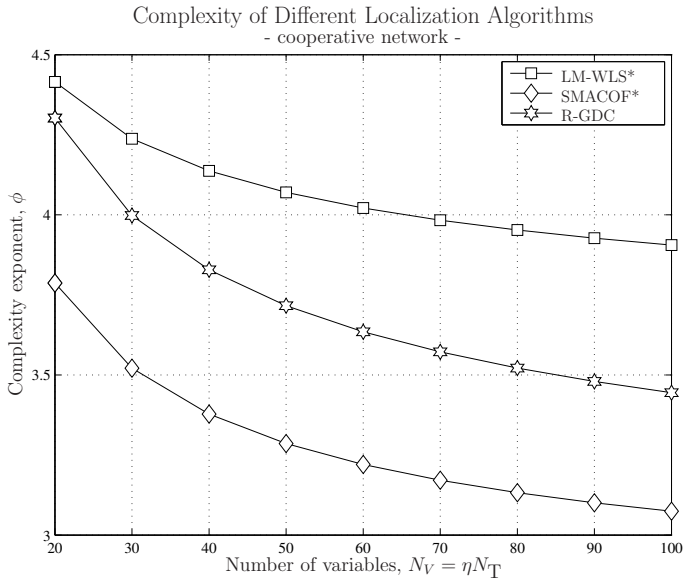

Fig 36. Comparison of algorithm complexity as a function of N_V. All algorithms operate under the same maximum number of iterations $T_{\mathsf{MAX}} = 51$, tolerances of 10^{-8} on the variations of objective function and the estimates. [9, ©IEEE 2011].

[19] To ensure that for any network size, the optimisation problem starts with the same assumptions, we consider a fully connected network, *i.e.* $m = 1$.

The results show that the R-GDC algorithm can achieve the PEB along a wide range of meshness ratio[20], hence offering a good scalability property.

Finally, with $T_{\mathrm{MAX}} = 51$, $\chi_Z = 10^{-8}$ and $\chi_F = 10^{-8}$, the convergence behaviour of the R-GDC, SMACOF, LM-WLS, SMACOF* and LM-WLS* algorithms are shown in Figure 38. Notice that the stair-case convergence behaviour of the R-GDC (in terms of objective minimisation) seen in Figure 38(a) is consistent with the strategy of the algorithm. This is in fact another desirable feature of the method since it indicates that further gains in complexity reduction can be achieved by relaxing the continuation principle (see Theorem T11) down to a few iterations *per* smoothed objective. Indeed, in Figure 38(b) it is shown that the R-GDC outperforms the alternatives (in terms of localisation accuracy) already after as few as 9 iterations. Based on this and the other results, it can be safely be stated that the proposed R-GDC algorithm exhibits superior performance to that of the SDP, with complexity inferior to that of the classic LM-WLS, and comparable to that of the SMACOF.

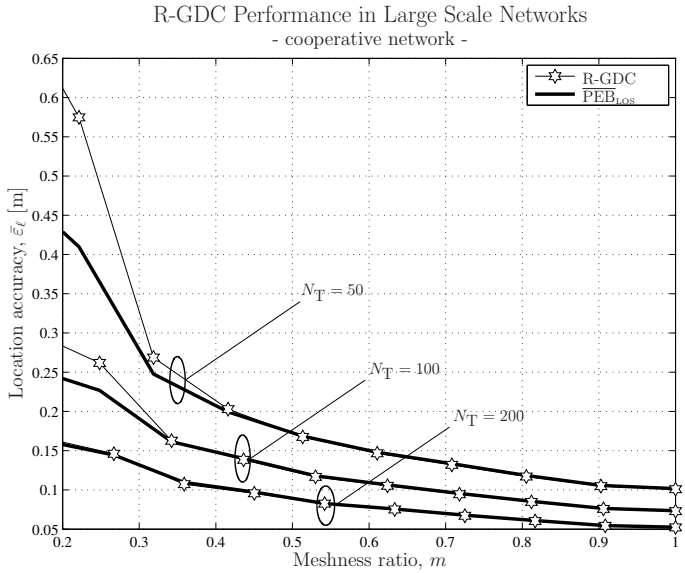

Fig 37. Performance of the R-GDC algorithm with large-scale networks in LOS scenarios and $\sigma = 0.3$ meters. The networks consist of $N_{\mathbf{A}} = 4$ anchors, and are deployed in a square of 14.14×14.14 square meters.

[20]The divergence of the R-GDC performance at low meshness ratio is a consequence of the non-localisability of the network.

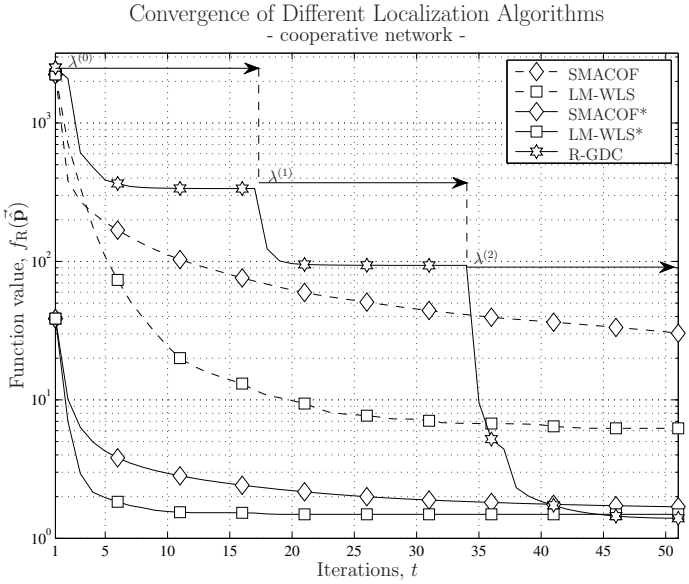

(a) Function value vs Iterations

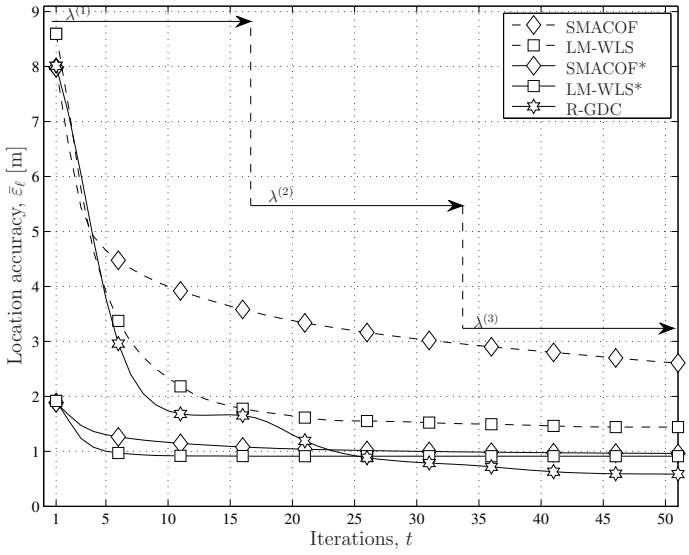

(b) RMSE vs Iterations

Fig 38. Convergence of R-GDC, SMACOF, LM-WLS, SMACOF* and LM-WLS* algorithms with $m < 0.4$. All algorithms operate under the same conditions, $i.e.$, $T_{\mathbf{MAX}} = 51$, $\chi_Z = 10^{-8}$ and $\chi_F = 10^{-8}$ R-GDC performs $K = 3$ iterations. [9, ©IEEE 2011].

Distributed versus centralised approach

In this section we address the distributed implementation of the R-GDC algorithm. Similar to the distributed SMACOF [82], the ML [97] and the barycentric-coordinate [152, 153] methods, each node estimates its own location by cooperating with its neighbours and performing calculations locally.

Specifically, the i-th target starts with a random guess of its location, performs ranging to the neighbour nodes (connected nodes) and requests their current location estimates. From this information it constructs the *local* smoothed objective function

$$\langle f_{\mathrm{R}}^{i}\rangle_{\lambda_i}(\hat{\mathbf{p}}_i) \triangleq \sum_{ij\in E_i} w_{ij}^2\left(\lambda_i^2+\tilde{d}_{ij}^2+\hat{d}_{ij}^2-\lambda_i\sqrt{\pi}\tilde{d}_{ij}\,{}_1F_1\left(\tfrac{3}{2};1;\tfrac{\tilde{d}_{ij}^2}{\lambda_i^2}\right)\exp\left(\tfrac{-\tilde{d}_{ij}^2}{\lambda_i^2}\right)\right), \quad (279)$$

where $\hat{\mathbf{p}}_j$ is not considered a variable, $E_i \triangleq \{ij|c_{ij}=1\}$ and λ_i is the *local* smoothing parameter derived from $\{\tilde{d}_{ij}\}$ with $ij \in E_i$.

Then, it updates its own locations by computing

$$\hat{\mathbf{p}}_i^{new} \triangleq \hat{\mathbf{p}}_i + \alpha_s \boldsymbol{\delta}_{pi}, \quad (280)$$

where ${}_i$ refers to the i-th node, α_s is the step-size obtained with a backtracing method [65] and $\boldsymbol{\delta}_{pi}$ is the descending direction computed from $\nabla_{\hat{\mathbf{p}}_i}\langle f_{\mathrm{R}}^{i}\rangle_{\lambda_i}(\hat{\mathbf{p}}_i)$.

The result is transmitted to the neighbour nodes, and iteratively, each node repeats the update and dissemination procedures until the total number of transmissions or the difference $\|\hat{\mathbf{p}}_i^{new}-\hat{\mathbf{p}}_i\|_F$ is less than a given threshold.

From a systemic perspective, the SMACOF [82], ML [97] and barycentric [152, 153] methods are more efficient than the R-GDC since, their convergence time is shorter and less transmissions are needed to achieve a solution. However, the proposed R-GDC offers a substantial advantage in terms of performance since it exploits the smoothing-continuation method to minimise the local minima problem. In practice, the nodes can select a random initial guess without compromising the location accuracy. Furthermore, there are no assumptions on the network topology and geometry that imply the applicability of the algorithm. In fact, the distributed R-GDC works on random networks, where node are not necessarily confined in the convex-hull of the anchors as, for instance, required by the algorithms [152, 153]. In Figures 39(a) and 39(b) we compare the performance obtained with the centralised and the distributed implementation of the R-GDC algorithm. Both methods can provide location accuracies that are close to the PEB despite of the noise and meshness ratio.

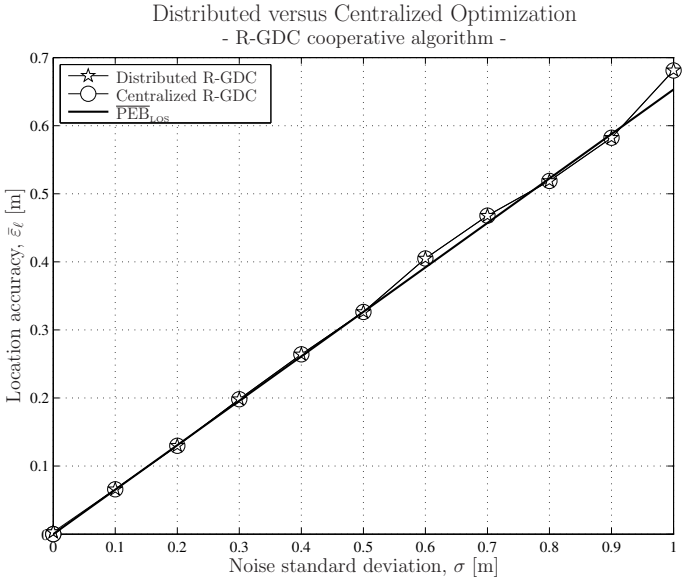

(a) RMSE as a function of the noise

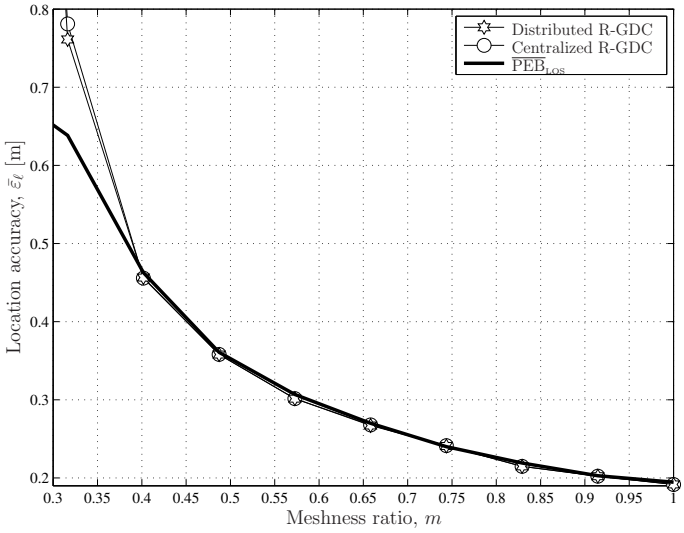

(b) RMSE as a function of the meshness

Fig 39. Comparison of the distributed optimisation algorithms for cooperative positioning in LOS scenarios. The network consists of $N_{\mathbf{A}} = 4$ anchors, $N_{\mathbf{T}} = 10$ targets and it is deployed in a square of 14.14×14.14 square meters.

6.3.2 Comparison of the weighing strategies

Consider the same type of network with N_{A} anchors and $N_{\mathrm{T}} = 20$ targets deployed in the convex-hull of the anchors. Assume a scenario with mix LOS and NLOS channel conditions, where the noise standard deviation σ_{ij}, the bias b_{ij} the number of ranging samples K_{ij} are random variables chosen with uniform distribution in the interval $(0.01, 0.3)$ meters, $(0, b_{\mathrm{MAX}})$ meters and $(2, 5)$, respectively. A connected link ij is in NLOS with a probability p_{NLOS} and such a probability is independent from the value of the true distance d_{ij}.

Amongst all optimisation methods, we focus on the proposed R-GDC algorithm and compare the localisation accuracy obtained with the proposed dispersion-penalty ($w_{ij}^2 = w_{ij}^D \mathcal{P}_{ij}$) weighing strategy to the alternative techniques, namely, the connectivity-based ($w_{ij}^2 = c_{ij}$), the LOESS-based and the inverse-distance based weighing methods. The performances are measured by the location accuracy $\bar{\varepsilon}_\ell$, and studied as a function of the meshness ratio m, the number of anchors N_{A} , the number of targets N_{T}, the maxim bias b_{MAX} and probability of NLOS p_{NLOS}. Furthermore, the results are also compared with the PEB computed as in equation (131).

In Figure 40 the comparison of the aforementioned methods is illustrated as a function of the meshness ratio. The result shows that the proposed dispersion-penalty weighing strategy provides a lower location accuracy than those obtained with any other alternative. The fact that a significant gap between the average PEB and the performance of the R-GDC algorithm exists is an indication that the bias problem is not totally eliminated. To further improve the performance, it is necessary to employ a technique that compensates the bias terms, which on the other hand will increase geometrically the computational complexity of the algorithm especially for very large scale networks.

Next, in Figure 41 we illustrate the RMSE performance obtained with the different weighing strategies with respect to the number of anchors. The number of targets, the probability of NLOS, the maximum bias and the meshness ratio are fixed parameters with values, $N_{\mathrm{T}} = 20$, $p_{\mathrm{NLOS}} = 0.3$, $b_{\mathrm{MAX}} = 3$ meters and $m = 1$, respectively. The result shows that with all weighing strategies the localisation error computed via the R-GDC optimisation algorithm decreases with the increase of the number of anchors. The reason is related to the fact that the amount of information in the network increases with N_{A} (see Chapter 4).

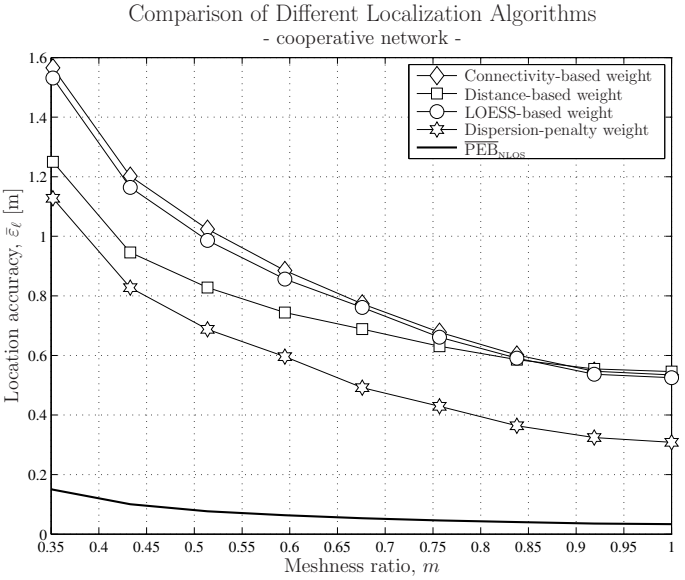

Fig 40. Performance of different weighing strategies as a function of m.The network is deployed in 14.14×14.14 squared meters. $N_{\mathbf{A}} = 4$, $N_{\mathbf{T}} = 20$, $\sigma_{ij} = (0.01, 0.3)$ meters, $b_{ij} = (0, 3)$ meters and $p_{\mathbf{NLOS}} = 0.3$.

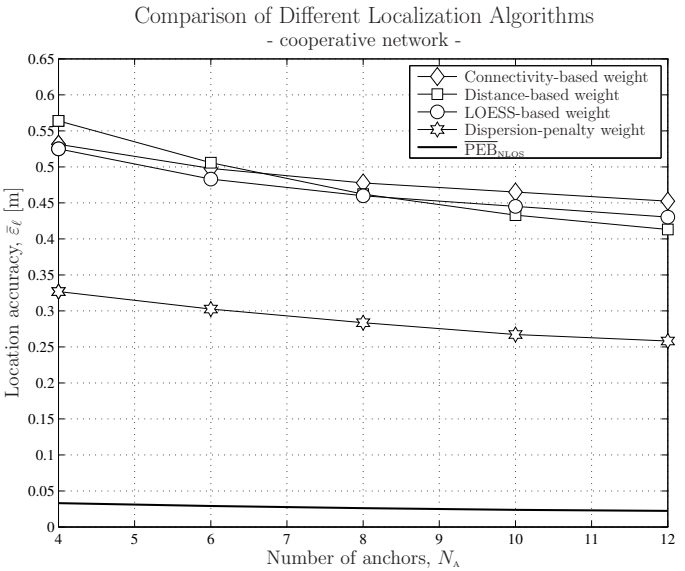

Fig 41. Performance of different weighing strategies as a function of $N_{\mathbf{A}}$.The network is deployed in 14.14×14.14 squared meters. $m = 1$, $N_{\mathbf{T}} = 20$, $\sigma_{ij} = (0.01, 0.3)$ meters, $b_{ij} = (0, 3)$ meters and $p_{\mathbf{NLOS}} = 0.3$.

Thus, the performance of any positioning algorithm improves consequently. Nevertheless, it is noticed that the proposed dispersion-penalty weighing strategy provides still the best performance with a gain of approximately 10 centimetres.

In Figure 42 we show the localisation accuracy as a function of the maximum bias. Also in this case the proposed weighing strategy outperforms the alternatives, especially when the amount of bias increases. This proves the geometric based principle that grounds the penalty weight is more effective when the bias and the connectivity is large.

The next result shows the behaviour of the location accuracy as a function of the number of targets, while the number of anchors, the probability of NLOS and the meshness ratio are fixed parameters with values $N_{\mathrm{A}} = 4$, $p_{\mathrm{NLOS}} = 0.3$ and $m = 1$, respectively. Similar to the previous study, also the plot illustrated in Figure 43 shows that the location accuracy improves with the increase of the number of nodes despite of the weighing strategy.

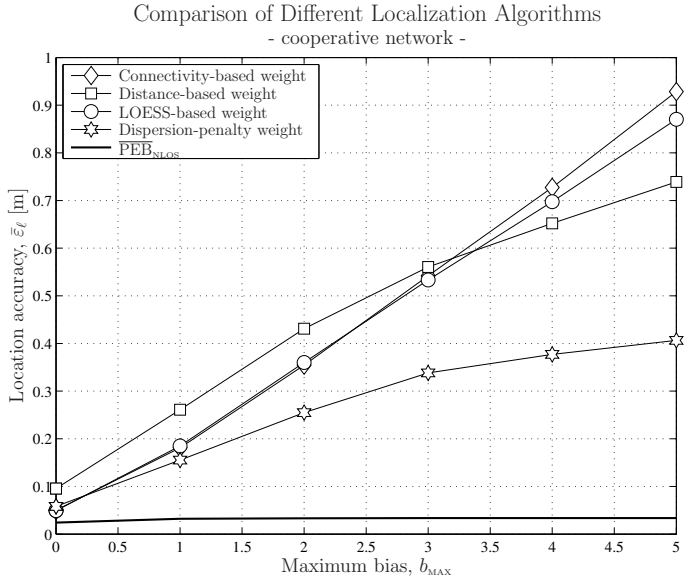

Fig 42. Performance of different weighing strategies as a function of b_{MAX}. The network is deployed in 14.14×14.14 squared meters. $N_{\mathsf{A}} = 4$, $N_{\mathsf{T}} = 20$, $m = 1$, $\sigma_{ij} = (0.01, 0.3)$ meters, $b_{ij} = (0, b_{\mathsf{MAX}})$ meters and $p_{\mathsf{NLOS}} = 0.3$.

In particular it can be noticed that by increasing N_{T}, the location accuracy obtained with the proposed dispersion-penalty weighing technique decreases faster than those provided by the alternative methods. This is due to the fact that by increasing N_{T}, the node density grows, the probability of NLOS miss-detection decreases, and the penalty weight becomes more and more effective. Therefore, the penalty $\mathcal{P}_{ij}$ is generally less than one and the higher the node density, larger is the likelihood that the NLOS is correctly detected from the proposed geometric test.

Finally, in Figure 44 we compare the performance of the different weighing strategies as a function of the probability p_{NLOS} ($p_{\mathrm{NLOS}} = 0$ and $p_{\mathrm{NLOS}} = 1$ indicate that all links in the network are in LOS and NLOS channel conditions, respectively). In this simulation, we consider $N_{\mathrm{A}} = 4$, $N_{\mathrm{T}} = 20$ and $m = 1$.

We observe that above a certain p_{NLOS}, that in this simulation is about 0.45, the usage of the proposed weights in no longer advantageous with respect to the alternatives.

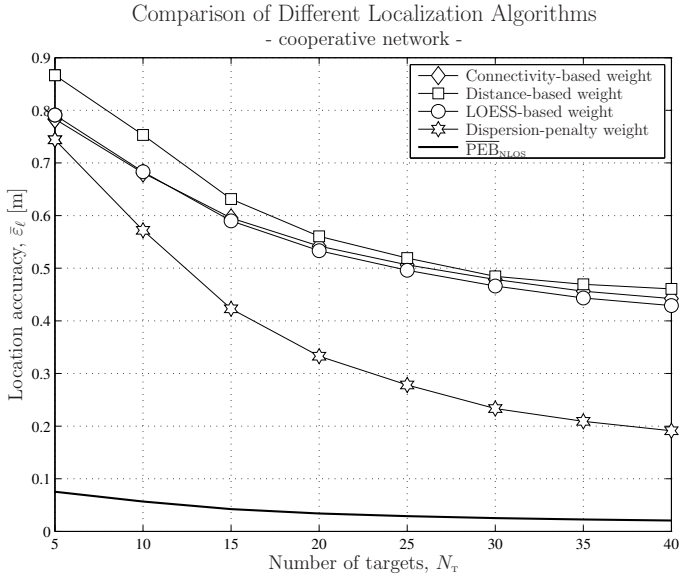

Fig 43. Performance of different weighing strategies as a function of N_{T}.The network is deployed in 14.14×14.14 squared meters. $N_{\mathrm{A}} = 4$, $m = 1$, $\sigma_{ij} = (0.01, 0.3)$ meters, $b_{ij} = (0, 3)$ meters and $p_{\mathrm{NLOS}} = 0.3$.

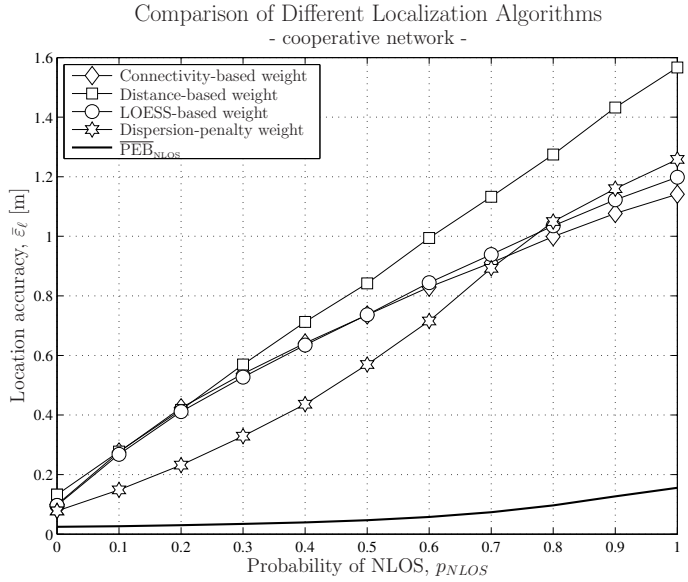

Fig 44. Performance of different weighing strategies as a function of p_{NLOS}.

The reason is that by increasing the number of NLOS links, more and more affected by a bias error. Since the penalty weight is based on a geometric property (triangle inequality), the test of equation (264) is likely to be unaffected by the variations of the length of the edges if a positive error is added to all distances. Consequently, the confidence that a triangle can be formed with the distance measurements of a 3-clique nodes is higher, and in turn the NLOS error is miss-detected.

6.4 Summary and discussions

In this chapter, we proposed a centralized cooperative positioning algorithm based on a WLS optimisation. The contributions have addressed two fundamental parts of this type of positioning methods, namely, the development of a robust global minimisation technique and a non-parametric weighing strategy to mitigate the effects of the ranging errors.

Unlike preceding methods, the proposed optimisation algorithm, dubbed the Range-Global Distance Continuation (R-GDC), holds true to a ML principle by

adhering to the formulation directly derived form the likelihood function and by yielding, given an observation, the same result despite of initialisation. The R-GDC method is shown via extensive comparison to outperform the best and most popular alternatives, in particular the SDP, the NLS and the SMACOF techniques, while exhibiting a computational complexity comparable to that of the SMACOF algorithm, which is widely known for its efficiency.

The combination of this optimization scheme with an effective weighing strategy, such as the proposed dispersion-penalty method, has also demonstrated that sufficient accurate location estimates can be obtained in mixed LOS/NLOS environments without prior knowledge of error statistics. Specifically, the proposed weighing strategy is derived with the approach that the disturbances on distance estimates due to noise and bias can be addressed separately. We first employ smalls scale statistics to mathematise the concept of weighing with basis on the reliability of ranging samples, which is commonly invoked in the literature [51, 58, 68, 78, 82, 135, 154], but had not been previously formalised. This yields a family of *dispersion weighing* functions, parameterised by a confidence bound of choice, which is then optimised under a maximum entropy criterion. Then, we extend the strategy so as to handle the possibility of NLOS conditions, via the introduction of a penalty onto the LOS assumption. These *penalty weights* would, in principle, require LOS/NLOS identification, which can be difficult to perform either because of scarce ranging information or because the devices cannot support this feature.

In order to circumvent this problem, we exploited the assumptions that biases are positive and that connectivity depends on the radio range $R_{\max}$ to establish a connection between the risk of the LOS assumption over a link ij and the geometry of 3-node cliques. This led to a hypothesis-theoretical method to quantify the penalty and to perform LOS/NLOS identification.

7 Positioning in a realistic environment

In this chapter we offer the results of a positioning experiment performed at the Centre for Wireless Communications of the University of Oulu. We validate the performance of the proposed non-cooperative and cooperative algorithms and, compare the results with the state-of-the-art techniques. The test is conducted with UWB devices, namely the TimeDomain PulseOn 210.

7.1 Wireless network set-up

In Figure 45 we illustrate the floor-map of a section of the Centrer for Wireless Communication offices located at the 4-th floor of the TF wing of the University of Oulu. The overall size of the environment is about 10.0×10.0 square meters and it consists of a corridor of size 1.0×10.0 square meters, four offices of different size and an electronic laboratory (eLAB).

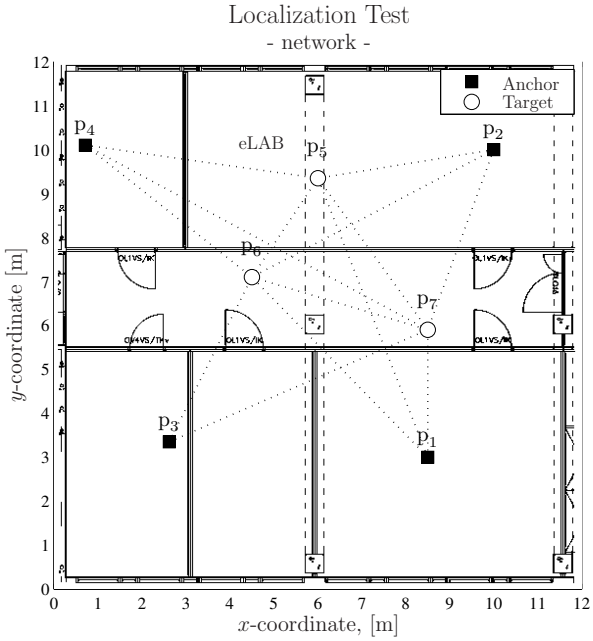

Fig 45. Floor map of a section of the Centre for Wireless Communication's offices in the TF wing of the University of Oulu.

Each office-room is equipped with wooden furniture (shelves, desks) and computers. The laboratory, instead, is equipped of electronic instruments, metallic shelves, wooden desks and computers.

We interconnect $N = 7$ the devices, of which four devices are considered anchors and the remaining targets. The nodes are deployed as illustrated in Figure 45, in which we adopt a relative reference system to assign a numerical value to the nodes' coordinates. Coherently with the notation adopted in this thesis, the vector-coordinate of the i-th node is denoted by $\mathbf{p}_i$ where $1 \leq i \leq 4$ and $5 \leq i \leq 7$ refers to the indexes of anchors and targets, respectively.

7.2 Ranging measurements

The TimeDomain PulseOn 210 devices are able to perform ranging using a 2-way protocol and a threshold-based algorithm for the estimation of the direct path. Details are provided in [155] and reference therein. Briefly, the 2-way ranging protocol consists of exchanging time-stamp information between the transmitter and the receiver. The transmitter measures the time elapsed between the transmission of its ranging request packet and the reception of the ranging response packet, hereafter denoted by δ_{Tx-Rx}.

The time estimation, however, is also affected by other errors:

a) ϵ_{te}, the time spent by the circuits to generate and send the waveform to the antenna as well as to receive and forward the signal to the internal logic

b) ϵ_{tl}, the time necessary to the leading-edge algorithm to estimate the first path

c) ϵ_{ts}, the time spent for the synchronisation.

Then, the estimate of time-of-flight performed by the device is given by:

$$\tilde{d} = 1.5 \cdot 10^{-4} \cdot (\delta_{TX-RX} - \epsilon_{te}^{TX} - \epsilon_{te}^{RX} - \epsilon_{tl}^{TX} - \epsilon_{tl}^{RX} - \epsilon_{ts}), \tag{281}$$

where the superscripts ^{TX} and ^{RX}, indicates that the time is measured at transmitter and the receiver, respectively.

Utilising this built-in ranging functionality, 1000 measurements were collected for each measurable distance. Upon the elimination of those measurements with negative value, it was found that the distribution of the distance measurement can be approximated with a mixture of N_G Gaussian distributions where N_G is at most equal to five. Each Gaussian function can be associate to a cluster of

arrival paths, as indeed, shown other research articles [93, 94, 130, 156]. In Table 2, we provide the numerical values of the mean μ_{gi}, the standard deviation σ_{gi} and the mixture coefficient A_{gi} associated to each cluster. The data reveals that most of the measurements are affected by a bias (in average 0.5 meter), and in some cases, such as the links 37, with a value above two meters. Considering the nature of the environment as well as the location of nodes, the NLOS channel conditions are due to the blockage of the direct path because of the walls (*e.g.* the link 45) as well as by the strong multi path reflections that occurs in a corridor environment (*e.g.* the link 37).

7.3 Experimental results

We utilise the database of ranging information to test off-line non-cooperative and cooperative algorithms. The estimation of the nodes is performed under the assumptions that ranging statistics are unknown, that the number of ranging samples are given by the random variable K_{ij}, with $K_{ij} \sim \mathcal{U}(2, 5)$. From the set of measurements $\{\tilde{d}_{ij}^{(k)}\}$, we compute the sample mean $\bar{d}_{ij}$, which will be utilised in the WLS objective function instead of $\tilde{d}_{ij}$, and the weight w_{ij}. To compare the performance of the positioning algorithms, we measure the location accuracy (RMSE) relative to each node location and, to quantify the dispersion of the estimates, we utilise the Circular Error Probability (CEP) metric, which is defined as the radius of a circle centred at the true node location, whose boundary includes a specified percentage (*e.g.* 50%) of the estimate population.

In the first test, we compare the performance of the proposed NLS-DC and WC-DC positioning techniques to those obtained with the C-NLS modified algorithm [57]. Since the methods are non-cooperative, only the anchor-to-target ranging is considered available to the algorithms.

In Figure 46, we illustrate the scatter plot of the location estimates obtained with each method. It can be noticed that the positions of the 5-th and 7-th targets are estimated with a sufficient accuracy and the estimates are uniformly spread within a circle of approximately 0.4 meters. The cloud of estimates of the 6-th node location, instead, is approximately centred at the true target position but, the distribution of the points is stretched towards the location $\mathbf{p}_3$. This indicates that $\tilde{d}_{16}$ and $\tilde{d}_{26}$ are mainly affected by a bias error. In fact, from the Table 2 we can observe that $b_{16} = 0.78$ and $b_{26} = 0.26$ meters.

Table 2. Ranging statistics based on a Gaussian mixture model.

Link		Cluster 1			Cluster 2			Cluster 3			Cluster 4			Cluster 5		
i-th node	j-th node	A_{g1}	μ_{g1}	σ_{g1}	A_{g2}	μ_{g2}	σ_{g2}	A_{g3}	μ_{g3}	σ_{g3}	A_{g4}	μ_{g4}	σ_{g4}	A_{g5}	μ_{g5}	σ_{g5}
1	5	0.04	0.17	0.03	0.88	0.45	0.09	0.02	0.73	0.02	0.05	0.90	0.03	-	-	-
1	6	1.00	0.78	0.19	-	-	-	-	-	-	-	-	-	-	-	-
1	7	1.00	0.00	0.02	-	-	-	-	-	-	-	-	-	-	-	-
2	5	0.96	-0.03	0.005	0.01	-0.02	0.001	0.02	0.01	0.005	-	-	-	-	-	-
2	6	1.00	0.27	0.37	-	-	-	-	-	-	-	-	-	-	-	-
2	7	1.00	0.49	0.15	-	-	-	-	-	-	-	-	-	-	-	-
3	5	-	-	-	-	-	-	-	-	-	-	-	-	-	-	-
3	6	1.00	0.11	0.02	-	-	-	-	-	-	-	-	-	-	-	-
3	7	0.02	1.29	0.06	0.98	2.03	0.09	-	-	-	-	-	-	-	-	-
4	5	1.00	0.51	0.10	-	-	-	-	-	-	-	-	-	-	-	
4	6	1.00	0.22	0.06	-	-	-	-	-	-	-	-	-	-	-	-
4	7	1.00	0.62	0.05	-	-	-	-	-	-	-	-	-	-	-	-
5	6	1.00	0.44	0.07	-	-	-	-	-	-	-	-	-	-	-	-
5	7	1.00	0.12	0.04	-	-	-	-	-	-	-	-	-	-	-	-
6	7	0.01	-0.09	0.004	0.05	-0.08	0.002	0.88	-0.05	0.09	0.03	-0.02	0.003	0.02	-0.01	0.003

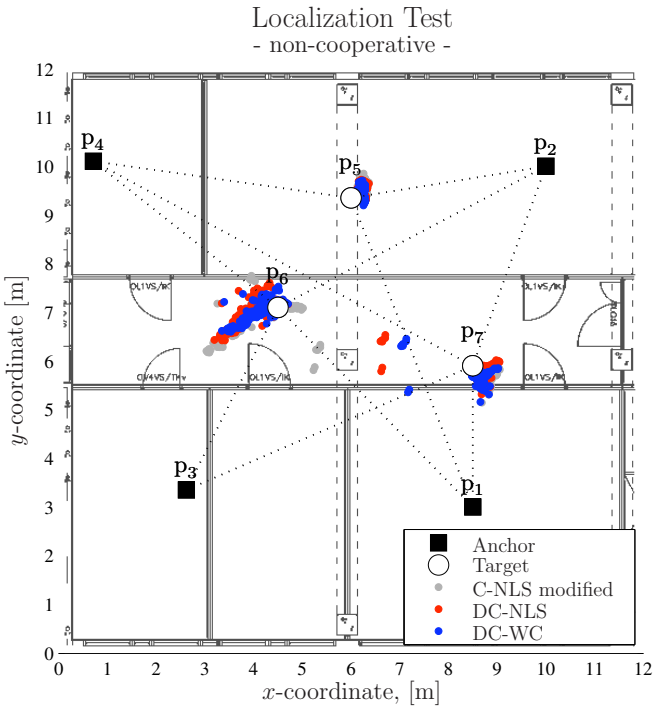

Fig 46. Scatter plot of a positioning test with non-cooperative methods utilising 11 **UWB wireless devices.**

Table 4. Numeric results of the non-cooperative positioning test.

Target	DC-NLS	DC-WC	C-NLS modified
Location Accuracy (RMSE) [m]			
5	0.30	0.28	0.36
6	0.28	0.22	0.31
7	0.30	0.31	0.46
Circular Error Probability (CEP) 50% [m]			
5	0.27	0.26	0.32
6	0.18	0.13	0.20
7	0.27	0.29	0.40
Circular Error Probability (CEP) 95% [m]			
5	0.37	0.35	0.46
6	0.53	0.42	0.52
7	0.32	0.33	0.44

Comparing the numeric values of the RMSE and the CEP, which are provided in Table 4, it is shown that the proposed DC methods are generally more accurate than the alternative. The average location accuracy is 0.28 meters, which is 25% smaller than that obtained with the C-NLS algorithm. Furthermore, comparing the CEP-50 and CEP-95 figures, it can be noticed that the dispersion of the location estimates is typically smaller for the DC methods.

Next, we perform a positioning test with cooperative algorithms, namely the proposed R-GDC technique with the dispersion-penalty weights, the SDP-based method with the connectivity and the LOESS based weighing mechanisms. For the sake of clarity, these methods will be referred to as R-GDC - DP, SDP - C and SDP - LOESS, respectively.

For the optimisation of ergodic confidence bound γ_{opt}, we utilize the adaptive expression

$$\gamma_{\text{opt}} \approx \hat{\gamma}_{\text{opt}} \triangleq \arg \min_{\gamma \in \mathbb{R}^+} \sum_i \sum_j \mathcal{W}_d(\hat{\sigma}_{ij}, K_{ij}; \gamma) \cdot \ln(\mathcal{W}_d(\hat{\sigma}_{ij}, K_{ij}; \gamma)), \qquad (282)$$

where $\hat{\sigma}_{ij}$ is the measured sample standard deviation of the noise.

The scatter plot illustrated in Figure 47 shows that the estimates obtained with the proposed R-GDC - DP are in general less biased than those computed with the SDP methods, however, they are affected by a large dispersion. In fact, by comparing the numerical values of the RMSE shown in Table 5, the location accuracy obtained with the R-GDC is 8 centimetres smaller than those given by the alternative methods. The CEP-95 instead shows that the dispersion of estimates is larger, especially for the 6-th node.

This result is due to the fact that network is small and the number of connections are not sufficient to distinguish LOS and NLOS links with the proposed geometric test. To verify this argument we repeat the cooperative positioning test described above with a network of $N_{\text{T}} = 9$ targets.

In this scenario, the ratio between LOS and NLOS links is lower, and as explained before, the scatter plot illustrated in Figure 48 shows that the R-GDC method provides the most accurate estimates and with the least dispersion. For instance, in Table 6 it is shown that the RMSE, CEP-50 and CEP-95 of the R-GDC-DP with respect to the SDP-LOESS are 13%, 35% and 20% smaller.

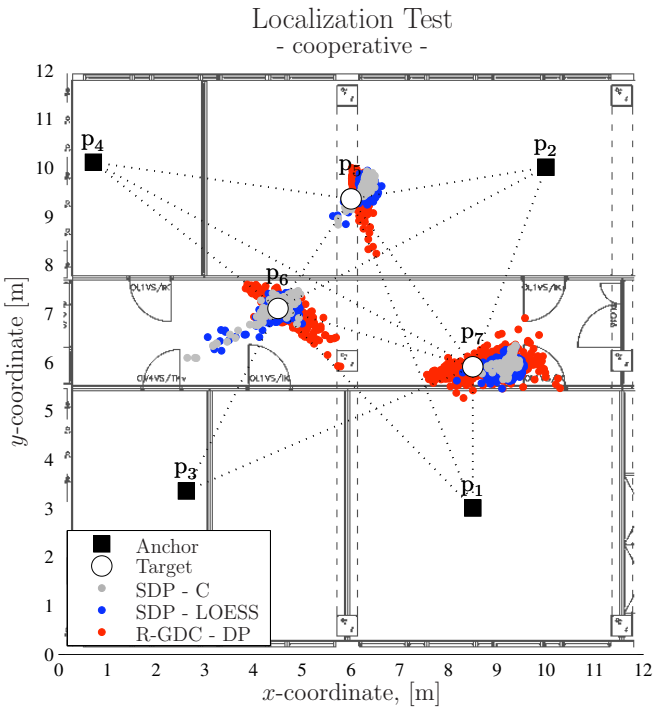

Fig 47. Scatter plot of a positioning test with cooperative methods utilising 7 UWB wireless devices.

Table 5. Numeric results of the cooperative positioning test with 7 devices.

Target	R-GDC - DP	SDP - LOESS	SDP - C
Location Accuracy (RMSE) [m]			
5	0.35	0.44	0.49
6	0.33	0.21	0.21
7	0.48	0.66	0.79
Circular Error Probability (CEP) 50% [m]			
5	0.34	0.43	0.49
6	0.20	0.15	0.14
7	0.34	0.64	0.80
Circular Error Probability (CEP) 95% [m]			
5	0.48	0.56	0.57
6	0.63	0.32	0.28
7	0.92	0.90	0.85

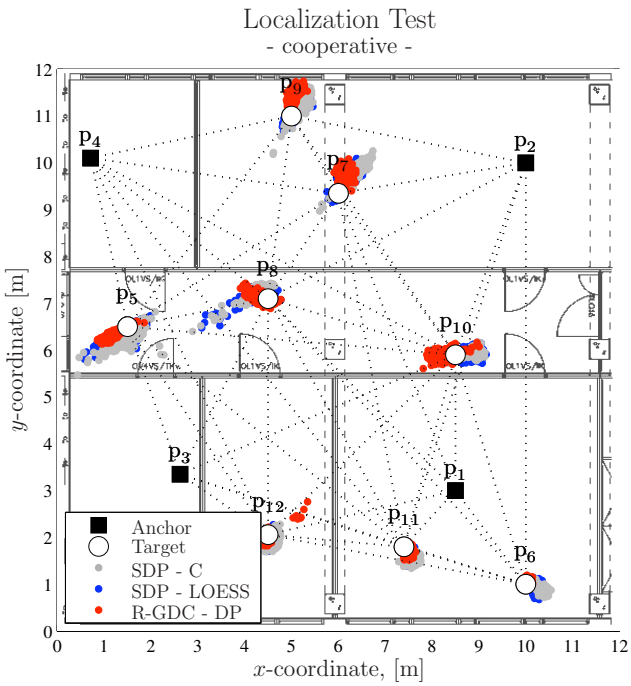

Fig 48. Scatter plot of a positioning test with cooperative methods utilising 13 UWB wireless devices.

Table 6. Numeric results of the cooperative positioning test with 13 devices.

Metric	R-GDC - DP	SDP - LOESS	SDP - C
RMSE [m]	0.29	0.33	0.40
CEP-50 [m]	0.16	0.27	0.37
CEP-95 [m]	0.46	0.56	0.63

7.4 Summary and discussions

In this chapter we described and show the results of non-cooperative and cooperative positioning experiments performed at the University of Oulu with commercial UWB devices. The network was deployed in an environment characterised by LOS and NLOS radio propagation channels.

A measurement campaign for the characterization of the ranging statistics was carried on, and the results revealed that the distance measurements were affected by bias. Moreover, it was verified that the arrival paths are governed by a modified Saleh-Valenzuela model.

The results of the positioning tests showed that the proposed DC-based non-cooperative and the R-GDC - DP cooperative techniques provide the best results with respect to the proposed alternatives.

8 Conclusions and future work

In a broad sense, the aim of the thesis was to study distance-based positioning techniques for wireless networks. We assumed scarce ranging information, unknown statistics and focused on a non-Bayesian non-parametric approach, namely a WLS optimisation problem.

The thesis comprises several theoretical and algorithmic contributions, and amongst all of them, we highlight the studies of cooperative networks. Specifically, the error analysis shown in Chapter 4 revealed important insights into the nature of the node uncertainty and the effect of coupling between cooperative nodes. The derivation of the equivocation matrix, which in a general sense can be considered the uncertainty due to cooperation with other target nodes, gave us a tool to understand the impact of inserting a measurement link or a new anchor.

Chapter 6 was fully dedicated to the development of a low-complexity and scalable cooperative positioning algorithm. We showed that the non-convex optimisation problem used in the maximum likelihood formulation of positioning can be effectively solved via continuation methods. Several quantities, including Gradient, Hessian, smoothing parameter bounds and weights were derived in closed-form so as to minimise the overall computational complexity, which was shown as $\mathcal{O}(C_R N^2)$.

In addition to the above, the thesis includes other relevant contributions. In Chapters 3 and 4 we derived

1) The closed-form expression of the WLS gradient and Hessian

2) The equivalence between the WLS and the ML estimator

3) The consistency of a ML estimator

4) A hybrid-bound for the MSE in low SNR régime.

These results can be generally utilised in both theoretical and algorithmic studies related to positioning. For instance, novel Newton based optimisation methods can benefit from the closed-form expression of the WLS gradient and Hessian, whereas new analytical studies can exploit the results in 2)-4).

In Chapters 5 and 6, we proposed:

5) The DC principle for non-cooperative positioning

6) The WC-DC algorithm that is very-low complexity and robust to bias errors

7) The NLS-DC algorithm that has the best performance amongst all tested non-cooperative techniques in NLOS scenarios

8) Dispersion weight that captures the effect of noise under the assumption of bias-free samples

9) A geometric-based bias detection.

Finally, in Chapter 7 we offered the results of a non-cooperative and a cooperative positioning test performed at the Centre for Wireless Communications and demonstrated that:

10) The DC-based algorithms provide an average accuracy of 0.3 meters

11) The R-GDC with the dispersion-penalty weight component provides an average accuracy of 0.27 meters in a large network.

Based on these results, several directions can be followed for future analysis, design and development works. For instance, the proposed CRLB offers a general framework for studying the fundamental limits to the MSE of a distance-based positioning estimator in realistic environments. In fact, the novel expressions are derived for generic ranging error distributions, which can be empirically obtained from measurement campaigns. This provides more flexibility and correctness to the analysis of a positioning problem in a realistic environment.

Based on the study of the information coupling, novel analysis and design strategies can be developed. For instance, we showed that anchors can be strategically placed in the network in order to decouple the information and, therefore, minimise the average location accuracy of all nodes. This result can be used to develop planning methods that determine a priori, where and how many anchors are needed to guarantee a minimum location error.

Yet another future work is envisioned on the basis of the DC principle. In the thesis we proposed an application to non-cooperative networks with the assumptions that the target is inside the convex-hull of the anchors. Although many application scenarios can be related to this system model, the proposed DC

principle is not general yet. Therefore, the first step is to relax the assumption on the location of the target, and following, to develop a generalised technique to cooperative positioning. Incidentally, in [157] WC-DC like algorithm was proposed, which links to the DC principle with the fact that the target location is computed as the weighted average of the anchor nodes, with the weights derived from null-space of a matrix related to the angle kernel. DC-based cooperative positioning can instead exploit recent results on POCS-based localisation methods [83, 158], from which the initial points used to derive the angle-kernel and the contraction vector can be obtained.

Finally, we conclude with a farther vision of the follow-up work. As mentioned in the introduction of thesis, positioning can be intended also as semantic localisation, *e.g.* "I am at home", "I am in the office", etc. In this case, the objective is to determine not coordinates but pre-defined "location-profiles" from heterogeneous and not necessarily physical measurements. The author foresees that such a problem can be addressed with a localisation method defined on a lattice, where each node is associated to a location-profile and defined in a multidimensional space. In this regard, the algorithms can be formulated as integer programming problems, where GDC methods can be applied [71].

References

1. Commission FC (1994) Notice of proposed rule-making, Docket no. 94-102. Technical report.
2. ITU (2011). The world in 2011: ICT facts and figures.
3. Malm A (2011) Mobile location-based services. Technical Report 6th edition, Berg Insight AB.
4. Hilton S (2010) Machine-to-machine device connections: worldwide forecast 2010–2020. Technical report, Analysis Mason.
5. Sahinoglu Z, Gezici S & Güvenc I (2011) Ultra-wideband Positioning Systems: Theoretical Limits, Ranging Algorithms, and Protocols. Cambridge University Press.
6. Stoica P & Sharman K (1990) Maximum likelihood methods for direction-of-arrival estimation. IEEE Transactions on Acoustics, Speech and Signal Processing 38(7): 1132–1143.
7. Abel JS (1993) A bound on the mean-square-estimate error. IEEE Transactions on Information Theory 39(5): 1675–1680.
8. Destino G & Abreu G (2009) Weighing strategy for network localisation under scarce ranging information. IEEE Transactions on Wireless Communications 8(7): 3668 – 3678.
9. Destino G & Abreu G (2011) On the maximum likelihood solution of source and network localisation. IEEE Transactions on Signal Processing 59(10): 4954–4970.
10. Destino G & Abreu G (2006) Sensor localization from WLS optimization with closed-form Gradient and Hessian. In: Proc. IEEE 49th Annual Globecom Conference, pp. 1–6.
11. Destino G & Abreu G (2008) Optimised confidence weights for localization algorithms with scarce information. In: Proc. IEEE International Conference on Ultra-Wideband, volume 3, pp. 81–84.
12. Destino G, Saaloranta J & Abreu G (2008) Sensor localization in realistic environment using ultra-wideband radio. In: Proc. 11th International Symposium on Wireless Personal Multimedia Communications.
13. Destino G & Abreu G (2009) Solving the source localization problem via global distance continuation. In: Proc. IEEE International Conference on Communications, pp. 1–6.

14. Destino G & Abreu G (2009) Reformulating the least-square source localization problem with contracted distances. In: Proc. IEEE 43th Asilomar Conference on Signals, Systems and Computers, pp. 307 – 311.
15. Destino G & G A (2010) Improving source localization in NLOS conditions via ranging contraction. In: Proc. IEEE 7th Workshop on Positioning, Navigation and Communication, pp. 56–61.
16. Rabbat M & Nowak R (2004) Distributed optimization in sensor networks. In: Proc. IEEE 3rd International Symposium on Information Processing in Sensor Networks, pp. 20–27.
17. Liu J, Zhang Y & Zhao F (2006) Robust distributed node localization with error management. In: Proc. ACM 7th International Symposium on Mobile Ad Hoc Networking and Computing (MobiHoc), pp. 250–261.
18. Saleh AAM & Valenzuela R (1987) A statistical model for indoor multipath propagation. IEEE Journal on Selected Areas in Communications 5(2): 128–137.
19. Hashemi H (1993) The indoor radio propagation channel. IEEE Proceedings 81(7): 943–968.
20. Cassioli D, Win MZ & Molisch AF (2002) The ultra-wide bandwidth indoor channel: from statistical model to simulations. IEEE Journal on Selected Areas in Communications 20(6): 1247–1257.
21. Mao G, Fidan B & Anderson BDO (2007) Wireless sensor network localization techniques. Computer Networks: The International Journal of Computer and Telecommunication Networking 51(10): 2529–2553.
22. Jin Y, Soh WS & Wong WC (2010) Localization with channel impulse response based fingerprint and non-parametric regression. IEEE Transactions on Wireless Communications 9(3): 1120–1127.
23. Kaplan E & Hegarty C (2006) Understanding GPS: Principles and Applications. Artech House, 2nd edition.
24. Güvenc I & Chong CC (2009) A survey on TOA based wireless localization and NLOS mitigation techniques. IEEE Communications Surveys and Tutorials 11(3): 107–124.
25. Liu H, Darabi H, Banerjee P & Liu J (2007) Survey of wireless indoor positioning techniques ans systems. IEEE Transactions on Systems, Man and Cybernetics-Part C: Applications and Reviews 37(6): 1067–1080.
26. Huhtiniemi A & Vanhatupa T (2010) The positioning algorithm of a high-performance Wi-Fi RTLS. In: International Conference on Ubiquitous Positioning, Indoor Navigation and Location-Based Service.

27. Niculescu D & Nath B (2003) Ad hoc positioning (APS) using AOA. In: Proc. IEEE 22nd Conference of Computer and Communications, volume 3, pp. 1734 – 1743.
28. Brunato M & Battiti R (2005) Statistical learning theory for location fingerprinting in wireless LANs. Elsevier Journal on Computer Networks 47(6): 825–845.
29. Taylor JD (2000) Ultra-wideband Radar Technology. CRC Press.
30. Opperman I, Zeisberg S, Jondral F, Rinaldi N, Kardo-Sysoev A, Simic D & Brankovic V (2004) UWB low data rate communications with localization and tracking approach (LDR-LT), applications and challenges. In: Proc. IST Mobile & Wireless Communications Summit. Lyon, France.
31. EUWB (2011) Ultra-wideband: Past, present and future. Technical report, FP7 European Integrated Project.
32. Blumenthal J, Grossmann R, Golatowski F & Timmermann D (2007) Weighted centroid localization in zigbee-based sensor networks. In: IEEE International Symposium on Intelligent Signal Processing, pp. 1–6.
33. Steiner C & Wittneben A (2011) Efficient training phase for ultra wide band-based location fingerprinting systems. IEEE Transactions on Signal Processing 59(12): 6021–6032.
34. Erguizian C, Despins C & Affes S (2006) Geolocation in mines with an impulse response fingerprinting technique and neural networks. IEEE Transactions on Wireless Commununications 5(3): 603–611.
35. Fang SH & Wang CH (2011) A dynamic hybrid projection approach for improved wi-fi location fingerprinting. IEEE Transactions on Vehicular Technology 60(3): 1037–1044.
36. Wigren T (2011) A polygon to ellipse transformation enabling fingerprinting and emergency localization in GSM. IEEE Transactions on Vehicular Technology 60(4): 1971–1976.
37. Triki M, Slock D, Rigal V & Francois P (2006) Mobile terminal positioning via power delay profile fingerprinting: Reproducible validation simulations. In: Proc. IEEE 64th Vehicular Technology Conference, pp. 1–5.
38. Stansfield R (1947) Statistical theory of d.f. fixing. IEEE Journal of the Institution of Electrical Engineers - Part IIIA: Radiocommunication 94(15): 762–770.
39. Foy W (1976) Position-location solutions by taylor-series estimation. IEEE Transactions on Aereospace and Electronic Systems AES-12(2): 187–194.
40. Torrieri DJ (1984) Statistical theory of passive location systems. IEEE Transactions on Aereospace and Electronic Systems 20(2): 183–198.

41. Pages-Zamora A, Vidal J & Brooks D (2002) Closed-form solution for positioning based on angle of arrival measurements. In: Proc. IEEE 13th International Symposium on Personal, Indoor and Mobile Radio Communications, volume 4, pp. 1522–1526.
42. Madigan D, Einahrawy E, Martin R, Ju WH, Krishnan P & Krishnakumar A (2005) Bayesian indoor positioning systems. In: Proc. 24th IEEE International Conference on Computer Communications, volume 2, pp. 1217–1227.
43. Rong P & Sichitiu M (2006) Angle of arrival localization for wireless sensor networks. In: Proc. IEEE 3rd Annual Communications Society on Sensor and Ad Hoc Communications and Networks, pp. 374–382.
44. Biswas P, Aghajan H & Ye Y (2005) Semi-definite programming algorithms for sensor network localization using angle information. In: Proc. IEEE 39th Asilomar Conference on Signal, Systems and Computers, pp. 220–224.
45. Kay SM (1993) Fundamentals of Statistical Signal Processing: Estimation Theory, volume I. Prentice Hall Signal Processing Series, Englewood Cliffs, New Jersey.
46. Wymeersch H, Lien J & Win M (2009) Cooperative localization in wireless networks. IEEE Proceedings 97(2): 427–450.
47. Yiu-Tong C, Chin HHY & Pak-chung C (2206) Exact and approximate maximum likelihood localization algorithms. IEEE Transactions on Vehicular Technology 55(1): 10–16.
48. Chan YT & Ho KC (1994) A simple and efficient estimator for hyperbolic location. IEEE Transactions on Signal Processing 42(8): 1905–1915.
49. Beck A, Stoica P & Li J (2008) Exact and approximate solutions for source localization problems. IEEE Transactions on Signal Processing 56(5): 1770–1778.
50. Spirito M (2001) On the accuracy of cellular mobile station location estimation. IEEE Transactions on Vehicular Technology 50(3).
51. Patwari N, Dea RJO & Wang Y (2003) Relative location estimation in wireless sensor networks. IEEE Transactions on Signal Processing 51(8): 2137–2148.
52. Yihong Q, Suda H & Kobayashi H (2004) On time-of-arrival positioning in a multipath environment. In: Proc. IEEE 60th Vehicular Technology Conference (VTC'04 Fall), volume 5, pp. 3540– 3544.
53. Gezici S, Tian Z, Giannakis G, Kobayashi H, Molisch A, Poor H & Sahinoglu Z (2005) Localization via ultra-wide band radios: a look at positioning aspects for future sensor networks. IEEE Signal Processing Magazine 22(4): 70–84.
54. So AMC & Ye Y (2005) Theory of semi-definite programming for sensor network localization. In: Proc. ACM-SIAM 16th Annual Symposium on Discrete Algorithms, pp. 405 – 414.

55. Al-Homidan S & Wolkowicz H (2005) Approximate and exact completion problems for euclidean distance matrices using semi-definite programming. Linear Algebra and Its Applications 406(1-3): 109–141.
56. Weiss AJ & Picard JS (2008) Network localization with biased range measurements. IEEE Transactions on Wireless Communications 7(1): 298–304.
57. Yu K & Guo Y (2008) Improved positioning algorithms for non-line-of-sight environments. IEEE Transactions on Vehicular Technology 57(4): 2342–2353.
58. Guvenc I, Gezici S, Watanabe F & Inamura H (2008) Enhancements to linear least squares localization through reference selection and ML estimation. In: Proc. IEEE Wireless Communications and Networking Conference, pp. 284–289.
59. Cox TF & Cox MAA (2000) Multidimensional Scaling. Chapman & Hall/CRC, 2 edition.
60. Groenen P & van de Velden M (2004) Multidimensional scaling. Technical Report EI 2004-15, Econometric Institute.
61. Groenen P & Heiser W (1994) The tunnelling method for global optimization in multidimensional scaling. Psychometrika 61(3): 529–550.
62. Boyd S & Vandenberghe L (2004) Convex Optimization. Cambridge University Press.
63. Hendrickson B (1992) Conditions for unique graph realization. SIAM Journal on Computing 21(1): 65–84.
64. Groenen P, Heiser W & Meulman J (1997) Global optimization in least-squares multidimensional scaling by distance smoothing. Journal of Classification 16: 225–254.
65. Nocedal J & Wright S (2006) Numerical Optimization. Springer.
66. Shang Y, Ruml W, Zhang Y & Fromherz MPJ (2003) Localization from mere connectivity. In: Proc. ACM 4th International Symposium on Mobile Ad-Hoc Networking and Computing, pp. 201 – 212. Annapolis, Maryland, U.S.A.
67. Dattorro J (2005) Convex Optimization and Euclidean Distance Geometry. Meboo Publishing.
68. Biswas P, Liang TC, Toh KC, Wang TC & Ye Y (2006) Semi-definite programming approaches for sensor network localization with noisy distance measurements. IEEE Transactions on Automation Science and Engineering 3(4): 360–371.
69. Biswas P, Liang TC, Toh KC & Wang TC (2006) Semi-definite programming based algorithms for sensor network localization with noisy distance measurements. ACM Transactions on Sensor Networks 2(2): 188–220.
70. Addis B, Locatelli M & Schoen F (2005) Local optima smoothing for global optimization. Optimization Methods and Software 20(4-5): 417–437.

71. More J & Wu Z (1997) Global continuation for distance geometry problems. SIAM Journal on Optimization 7: 814–836.
72. Larsson E & Danev D (2010) Accuracy comparison of LS and squared-range LS for source localization. IEEE Transactions on Signal Processing 58(2): 916–923.
73. Kannan AA, Guoqiang M & Vucetic B (2005) Simulated annealing based localization in wireless sensor network. In: Proc. IEEE 30th Annual Conference on Local Computer Networks, pp. 513–514.
74. Cheung KW, So HC, Ma WK & Chan YT (2004) Least squares algorithms for time-of-arrival-based mobile location. IEEE Transactions on Signal Processing 52(4): 1121–1128.
75. Caffery JJ (2000) A new approach to the geometry of TOA location. In: Proc. IEEE Vehicular Technology Conference, Boston (MA), volume 4, pp. 1943–1949.
76. Venkatesh S & Buehrer RM (2006) A linear programming approach to NLOS error mitigation in sensor networks. In: Proc. IEEE 5th International Conference on Information Processing in Sensor Networks, pp. 301–308.
77. Li Z, Trappe W, Zhang Y & Nath B (2005) Robust statistical methods for securing wireless localization in sensor networks. In: Proc. IEEE 4th International Symposium on Information Processing in Sensor Networks, pp. 91–98.
78. Alfakih AY, Wolkowicz H & Khandani A (1999) Solving Euclidean distance matrix completion problems via semi-definite programming. Journal Computational Optimization and Applications - Special issue on computational optimization—a tribute to Olvi Mangasarian, part I 12(1): 13 – 30.
79. Caffery JJ (1998) Overview of radiolocation in CDMA cellular systems. IEEE Communications Magazine 36(4): 38–45.
80. Gezici S & Sahinoglu Z (2204) UWB geolocation techniques for IEEE 802.15.4a personal area networks. Technical report, MERL, Cambridge, MA.
81. Guvenc I, Chia-Chin C & Watanabe F (2007) NLOS identification and mitigation for UWB localization systems. In: Proc. IEEE Wireless Communications and Networking Conference, pp. 1571 – 1576.
82. Costa JA, Patwari N & Hero AO (2006) Distributed multidimensional scaling with adaptive weighting for node localization in sensor networks. ACM Journal on Sensor Networks 2(1): 39–64.
83. Hero AOI & Blatt D (2005) Sensor network source localization via projection onto convex sets (POCS). In: Proc. IEEE International Conference on Acoustics, Speech, and Signal Processing, volume 3, pp. 689–692.
84. Gholami HSERM MR; Wymeersch (2011) Robust distributed positioning algorithms for cooperative networks. In: Proc. IEEE International Workshop on Signal Processing Advances in Wireless Communications, pp. 156–160.

85. Caffery J J & Stuber G (1998) Subscriber location in cdma cellular networks. IEEE Transactions on Vehicular Technology 47(2): 406–416.
86. Venkatesh S & Buehrer RM (2007) NLOS mitigation using linear programming in ultra-wide band location-aware networks. IEEE Transactions on Vehicular Technology 56(5, Part 2): 3182 – 3198.
87. Chen CL & Feng KT (2005) An efficient geometry-constrained location estimation algorithm for NLOS environments. In: Proc. IEEE International Conference Wireless Networks, Communications and Mobile Computing, Hawaii, USA, pp. 244–249.
88. Wuk K, Lee J & Jee GI (2006) The interior-point method for an optimal treatment of bias in tri-lateration location. IEEE Transactions on Vehicular Technology 55(4): 1291–1301.
89. Biggs N (1994) Algebraic Graph Theory. Cambridge University Press, second edition.
90. Macagnano D, Destino G & Abreu: G (2011) Hybrid initialization for non-convex network localization problems. In: Proc. IEEE International Conference on Ultra-Wideband, pp. 145 – 149.
91. Golub GH & van Loan CF (1996) Matrix Computations. Johns Hopkins Univ. Press, New York, NY, 3 edition.
92. Jourdan D, Dardari D & Win M (2006) Position error bound for UWB localization in dense cluttered environments. In: Proc. IEEE International Conference on Communications, volume 8, pp. 3705–3710.
93. Alsindi N, Alavi B & Pahlavan K (2009) Measurement and modeling of ultra-wide band TOA-based ranging in indoor multipath environments. IEEE Transactions on Vehicular Technology 58(3): 1046 –1058.
94. Dardari D, Conti A, Ferner U, Giorgetti A & Win M (2009) Ranging with ultra-wide bandwidth signals in multipath environments. Proceedings of the IEEE 97(2): 404–426.
95. Chen PC (1999) A non-line-of-sight error mitigation algorithm in location estimation. In: Proc. IEEE Wireless Communications and Networking Conference, volume 1, pp. 316–320.
96. Denis B, Pierrot JB & Abou Rjeily C (2006) Joint distributed synchronization and positioning in UWB ad hoc networks using TOA. IEEE Transactions on Microwave Theory and Techniques 54(2): 1896–1911.
97. Denis B, He L & Ouvry L (2007) A flexible distributed maximum log-likelihood scheme for UWB indoor positioning. In: Proc. IEEE 4th Workshop on Positioning, Navigation and Communication, pp. 77–86.

98. Feingold DG & Varga RS (1962) Block diagonally dominant matrices and generalizations of the gerschgorin circle theorem. Pacific Journal of Mathematics 12: 1241–1250.
99. Graepel T (2002) Kernel matrix completion by semi-definite programming. In: Dorronsoro JR (ed.) ENNS 12th International Conference on Artificial Neural Networks, volume Vol. 2415, pp. 694 – 699. Springer-Verlag.
100. Lui K, Chan F & So H (2009) Semi-definite programming approach for range-difference based source localization. IEEE Transactions on Signal Processing 57(4): 1630–1633.
101. Cheng M, Zhi D & Dasgupta S (2008) A semi-definite programming approach to source localization in wireless sensor networks. IEEE Signal Processing Letters 15: 253–256.
102. Boyd S, Ghaoui LE, Feron E & Balakrishnan V (1994.) Linear Matrix Inequalities in System and Control Theory. SIAM.
103. Macagnano D & de Abreu GTF (2011) Gershgorin analysis of random Gramian matrices with application to MDS tracking. IEEE Transactions on Signal Processing 59(4): 1785 – 1800.
104. Platt JC (2004) Fastmap, metricmap, and landmark mds are all Nyström algorithms. Technical Report MSR-TR-2004-26, Microsoft Research Technical Report.
105. Guvenc I, Chong CC & Watanabe F (2007) Analysis of a linear least-squares localization technique in LOS and NLOS environments. In: Proc. IEEE 65th Vehicular Technology Conference (Spring), pp. 1886–1890.
106. Shen Y & Win MZ (2010) Fundamental limits of wideband localization— part I: A general framework. IEEE Transactions on Information Theory, 56(10): 4956 – 4980.
107. Shen Y, Wymeersch H & Win MZ (2010) Fundamental limits of wideband localization— part II: Cooperative networks. IEEE Transactions on Information Theory, 56(10): 4981–5000.
108. Mazuelas A, Shen Y & Win MZ (2011) information coupling in cooperative localization. IEEE Communications Letters 15(7): 737–739.
109. Wang H, Yip L, Yao K & Estrin D (2004) Lower bounds of localization uncertainty in sensor networks. In: Proc. IEEE International Conference on Acoustics, Speech, and Signal Processing, volume 3, pp. 917–20.
110. Alfakih AY (2007) On dimensional rigidity of joint-and-bar frameworks. ACM Discrete Applied Mathematics 155: 1244–1253.
111. Alfakih A (2001) On rigidity and realisability of weighted graphs. Elsevier Linear Algebra and its Applications 325: 57–70.

112. Alfakih A (2006) On the nullspace, the rangespace and the characteristic polynomial of the euclidean distance matrices. Elsevier Linear Algebra and Its Applications 416(2-3): 348–354.
113. Alfakih A (2008) On the eigenvalues of euclidean distance matrices. Elsevier Computational&Applied Mathematics 27(3): 237–250.
114. Alfakih AY & Wolkowicz H (1998) On the embeddability of weighted graphs in euclidean spaces. Technical report, University of Waterloo, Dept. of Combinatorics and Optimization.
115. Goldenberg A, Krishnamurthy D, Maness A, Yang W, Young Y, Morse A & Savvides A (2005) Network localization in partially localisable networks. In: Proc. IEEE 24th International Conference on Computer Communications, volume 1, pp. 313–326.
116. Connely R (2005) Generic global rigidity. Discrete & Computational Geometry 33: 549–563.
117. PN Eren TG, Whiteley O, Yang W, Morse Y, Anderson A & Belhumeur B (2004) Rigidity, computation, and randomization in network localization. In: Proc. IEEE 23rd International Conference on Computer Communications, 4, pp. 2673–2684.
118. Laman G (2002) On graphs and rigidity of plane skeletal structures. Springer Journal of Engineering Mathematics 4: 331–340.
119. Lovász L & Yemini Y (1982) On generic rigidity in the plane. SIAM Journal on Algebraic and Discrete Methods 3(1): 91–98.
120. Servatius B & Servatius H (2002) Rigidity Theory and Applications, chapter Generic and Abstract Rigidity, pp. 1–19. Fundamental Materials Research. Springer US.
121. Jackson B & Jackson B (2003) Connected rigidity matroids and unique realization of graphs. Technical report, Egerváry Research Group on Combinatorial Optimization.
122. Aspnes J, Eren T, Goldenberg DK, Morse AS, Whiteley W, Yang YR, Anderson BDO & Belhumeur PN (2006) A theory of network localization. IEEE Transactions on Mobile Computing 5(12): 1663–1678.
123. Saxe J (1979) Embeddability of weighted graphs in k-space in strongly NP-hard. In: Proc. Allerton Conference in Communications, Control and Computing, pp. 480–489.
124. Engle RI & McFadden D (eds.) (2003) Handbook of Econometrics, volume 4, chapter 36, pp. 2120–2241. Elsevier Science.

125. Wylie-Green M (2005) Comparison of the bhattacharyya and cramer-rao lower bounds for the position estimation of an OFDM transmitter. In: Proc. IEEE International Conference on Acoustics Speech and Signal Processing, volume 4, pp. 729–732.
126. Tabrinkian J & Krolik J (1999) Barankin bounds for source localization in an uncertain ocean environment. IEEE Transactions on Signal Processing 47(11): 2917–2927.
127. Lehmann EL (1983) Theory of Point Estimation. New York: Jhon Wiley.
128. Rendas M & Moura J (1998) Ambiguity in radar and sonar. IEEE Transactions on Signal Processing 46(2): 294–305.
129. Renaux A, Najjar-Atallah L, Forster P & Larzabal P (2007) A useful form of the Abel bound and its application to estimator threshold prediction. IEEE Transactions on Signal Processing, 55(5): 2365–2369.
130. Gentile C & Kik A (2006) An evaluation of ultra wideband technology for indoor ranging. In: Proc. IEEE 49th Global Telecommunications Conference, pp. 1–6.
131. Conti A, Guerra M, Dardari D, Decarli N & Win M (2012) Network experimentation for cooperative localization. IEEE Journal on Selected Areas in Communications 30(2): 467–475.
132. Wang X, Wang Z & Dea BO (2003) A TOA based location algorithm reducing the errors due to NLOS propagation. IEEE Transactions on Vehicular Technology 52(1): 112–116.
133. Kannan A, Fidan B & Guoqiang M (2010) Analysis of flip ambiguities for robust sensor network localization. IEEE Transactions on Vehicular Technology 59(4): 2057 –2070.
134. Gill PE & Murray W (1978) Algorithms for the solution of the non-linear least-squares problem. SIAM Journal on Numerical Analysis 15(5): 977–992.
135. Shang Y & Ruml W (2004) Improved MDS-based localization. In: Proc. IEEE 23rd International Conference on Computer Communications, volume 4, pp. 2640 – 2651. Hong-Kong, China.
136. de Leeuw J (1988) Convergence of the majorization method for multi-dimensional scaling. Journal of Classification 5: 163–180.
137. Allgower EL & Georg K (2003) Introduction to Numerical Continuation Methods, volume 45. SIAM Classics in Applied Mathematics.
138. Abramowitz M & Stegun IA (1965) Handbook of Mathematical Functions with Formulas, Graphs, and Mathematical Tables. Dover Publications, 10 edition.
139. Gradshteyn IS & Ryzhik IM (2000) Table of Integrals, Series, and Products. Academic Press, 6 edition.

140. Proakis JG (2000) Digital Communications, Fourth Edition. Mc-Graw-Hill, New York, NY.
141. Moon P & Spencer DE (1988) Field Theory Handbook, Including Coordinate Systems, Differential Equations, and Their Solutions. Springer-Verlag, New York.
142. Ipsen ICF & Nadler B (2009) Refined perturbation bounds for eigenvalues of Hermitian and non-Hermitian matrices. SIAM Journal on Matrix Analysis and Applications 31(1): 40 – 53.
143. Moré JJ & Wu Z (1994) ϵ-optimal solutions to distance geometry problems via global continuation. Preprint MCS–P520–0595, Mathematics and Computer Science Division, Argonne National Laboratory, Argonne, Ill.
144. Gibbons J (1992) Non-parametric Statistical Inference. Marcel Dekker.
145. Agresti A (1990) Categorical Data Analysis. Wiley Series in Probability and Mathematical Statistics. Applied Probability and Statistics. John Wiley & Sons.
146. Patton MQ (1987) How to Use Qualitative Methods in Evaluation. Sage Publications, Newbury Park, CA.
147. Shannon CA (1948) A mathematical theory of communications. Bell System Technical Journal 27: 379 – 423.
148. Bertoluzza C & Poggi C (1990) Non-probabilistic uncertainty measures. In: Proc. IEEE 1st International Symposyum on Uncertainty Modelling and Analysis, pp. 647–651.
149. Girod L & Estrin D (2000) Robust range estimation for localization in ad-hoc sensor networks. Technical report, UCLA.
150. Borras J, Hatrack P & Mandayam N (1998) Decision theoretic framework for NLOS identification. In: Proc. IEEE 48th Vehicular Technology Conference, volume 2, pp. 1583–1587.
151. Macagnano D & Abreu G (2011) Gershgorin analysis of random gramian matrices with application to MDS tracking. IEEE Transactions on Signal Processing 59(4): 1785 – 1800.
152. Khan UA, Kar S & Moura JMF (2010) DILAND: an algorithm for distributed sensor localization with noisy distance measurements. IEEE Transactions on Signal Processing 58(3): 1940–1947.
153. Khan UA, Kar S & Moura JMF (2009) Distributed sensor localization in random environments using minimal number of anchor nodes. IEEE Transactions on Signal Processing 57(5): 2000–2016.
154. Kannan AA, Mao G & Vucetic B (2006) Simulated annealing based wireless sensor network localization with flip ambiguity mitigation. In: Proc. IEEE 63rd Vehicular Technology Conference, volume 2, pp. 1022–1026.

155. Domain T PulseON 210 Reference Design Technical Brochure.
URI: http://www.timedomain.com/products/P2101RD.pdf.
156. Joon-Yong L & Scholtz R (2002) Ranging in a dense multipath environment using an UWB radio link. IEEE Journal on Selected Areas in Communications 20: 1667–1683.
157. Bhagwat N, Kunpeng L & Jabbari B (2010) Robust bias mitigation algorithm for localization in wireless networks. In: Proc. IEEE International Conference on Communications, pp. 1–5.
158. Gholami MR, Ström EG, Wymeersch H & Rydström M (2012) On geometric upper bounds for positioning algorithms in wireless sensor networks. Http://arxiv.org/abs/1201.2513.

Appendix 1 Algorithm Pseudo-Codes

DC-WC Pseudo-code

Algorithm 1 WC-DC localization

1: Get the matrix $\tilde{\mathbf{D}} \in \mathbb{R}^{N \times N}$;
2: **if** $B_D \neq \emptyset$ **then**
3: $\quad \vec{\hat{\mathbf{z}}}_0 \leftarrow \frac{1}{N_v} \sum_{i=1}^{N_v} \mathbf{p}_i^{B_D}$;
4: **else**
5: $\quad$ Solve $\vec{\hat{\mathbf{z}}}_0 \leftarrow \arg \min_{\hat{\mathbf{z}} \in \mathbb{R}^{\eta}} \sum_{i=1}^{N_{\mathrm{A}}} (\tilde{d}_i^2 - \hat{d}_i^2)^2$;
$\qquad\qquad\qquad\quad$ s.t. $\hat{\mathbf{z}} \in \mathcal{C}(\mathbf{P}_A)$
6: **end if**
7: $\hat{\boldsymbol{\Omega}} \leftarrow O([\mathbf{P}_A; \vec{\hat{\mathbf{z}}}_0])$;
8: Solve $\hat{\boldsymbol{\rho}} \leftarrow \arg \min_{\hat{\boldsymbol{\rho}} \in \mathbb{R}^{N_{\mathrm{A}}}} \hat{\boldsymbol{\rho}} \hat{\boldsymbol{\Omega}} \hat{\boldsymbol{\rho}}^{\mathrm{T}}$;
$\qquad\qquad$ s.t. $\tilde{d}_i + \rho_i \leq 0 \, \forall i$,
9: $[\boldsymbol{\omega}^{\boldsymbol{dc}}]_i \leftarrow \hat{\rho}_i / \tilde{d}_i$;
10: $\hat{z} \leftarrow \boldsymbol{\omega}^{dc} \mathbf{P}_A$.

To evaluate the computational complexity of the WC-DC algorithm we consider the most relevant operations: *a*) the calculation of the initial point (line 2-line 6) and *b*) the estimation of the contraction vector $\hat{\boldsymbol{\rho}}$ objective function (line 8). If the feasibility region B_D is not empty, then the cost of line 3 can be neglected since the intersection points $\mathbf{p}_i^{B_D}$ can be computed in closed-form. On the other hand, if B_D is empty the optimization problem can be solved as in equation (194), which implies a complexity of the order $\mathcal{O}(N_{\mathrm{A}}^3)$ (size of the linear system corresponding to the interior point method). The estimation of the contraction vector also involves a quadratic programming, with a computational complexity of the order $\mathcal{O}(N_{\mathrm{A}}^3)$.

NLS-DC Pseudo-code

Algorithm 2 NLS-DC localization

1: Get the matrix $\tilde{\mathbf{D}} \in \mathbb{R}^{N \times N}$;
2: **if** $B_D \neq \emptyset$ **then**
3: $\quad \vec{\hat{\mathbf{z}}}_0 \leftarrow \frac{1}{N_v} \sum_{i=1}^{N_v} \mathbf{p}_i^{B_D}$;
4: **else**
5: $\quad$ Solve $\vec{\hat{\mathbf{z}}}_0 \leftarrow \arg \min_{\hat{\mathbf{z}} \in \mathbb{R}^\eta} \sum_{i=1}^{N_\mathrm{A}} (\tilde{d}_i^2 - \hat{d}_i^2)^2$; s.t. $\hat{\mathbf{z}} \in \mathcal{C}(\mathbf{P}_A)$
6: **end if**
7: $\hat{\mathbf{\Omega}} \leftarrow O([\mathbf{P}_A; \vec{\hat{\mathbf{z}}}_0])$;
8: Solve $\hat{\boldsymbol{\rho}} \leftarrow \arg \min_{\hat{\boldsymbol{\rho}} \in \mathbb{R}^{N_\mathrm{A}}} \hat{\boldsymbol{\rho}} \hat{\mathbf{\Omega}} \hat{\boldsymbol{\rho}}^\mathrm{T}$; s.t. $\tilde{d}_i + \rho_i \leq 0 \, \forall i$,
9: $\hat{z} \leftarrow \arg \min_{\hat{\mathbf{z}} \in \mathbb{R}^\eta} \sum_{i=1}^{N_\mathrm{A}} (\tilde{d}_i - \hat{\rho}_i - \hat{d}_i)^2$.

Similar to the WC-DC algorithm, the computational complexity of the NLS-DC technique can be computed from the relevant operations: *a*) the calculation of the initial point (line 2-line 6), *b*) the estimation of the contraction vector $\hat{\boldsymbol{\rho}}$ objective function (line 8) and *c*) the minimization of the modified WLS objective function (line 9). Thus, the overall cost can be estimated in the order $\mathcal{O}(N_\mathrm{A}^3)$.

R-GDC Pseudo-code

Algorithm 3 R-GDC localization

1: Get the matrices $\tilde{\mathbf{D}} \in \mathbb{R}^{N\times N}$, $\mathbf{W} \in \mathbb{R}^{N\times N}$;
2: Set the Stop-Criteria $\chi_Z = 10^{-8}$, $\chi_F = 10^{-8}$ and $T_{\mathrm{MAX}} = 51$;
3: $\lambda^{(1)} \leftarrow \frac{\sqrt{\pi}}{2} \max_{ij\in E} \tilde{d}_{ij}$;
4: $K \leftarrow 5$;
5: $\vec{\tilde{\mathbf{z}}} \leftarrow \mathrm{rand}(N_{\mathrm{T}}\eta, 1)$;
6: $T_{\mathrm{s}} \leftarrow \lceil T_{\mathrm{MAX}}/K \rceil$;
7: **for** $k = 0$ to K **do**
8: $\quad\lambda \leftarrow \lambda^{(1)} \frac{(K-k)}{K}$;
9: $\quad t \leftarrow 0$;
10: $\quad\tilde{\boldsymbol{H}}_{\lambda}^{-1} \leftarrow \mathbf{I}$; (approximation of the Hessian inverse)
11: $\quad$**repeat**
12: $\quad\quad t \leftarrow t + 1$;
13: $\quad\quad$Evaluate $\nabla_{\vec{\tilde{\mathbf{z}}}} \langle f_{\mathrm{R}} \rangle_{\lambda}(\vec{\tilde{\mathbf{z}}})$;
14: $\quad\quad\boldsymbol{\delta}_z^{(t)} \leftarrow -\tilde{\boldsymbol{H}}_{\lambda}^{-1} \cdot \nabla_{\vec{\tilde{\mathbf{z}}}} \langle f_{\mathrm{R}} \rangle_{\lambda}(\vec{\tilde{\mathbf{z}}}^{(t-1)})$; (search direction)
15: $\quad\quad r \leftarrow 0$;
16: $\quad\quad\vec{\tilde{\mathbf{z}}}_{old} \leftarrow \vec{\tilde{\mathbf{z}}}$;
17: $\quad\quad$**repeat**
18: $\quad\quad\quad r \leftarrow r + 1$;
19: $\quad\quad\quad$Select the step-length α_z; (backtracking method)
20: $\quad\quad\quad\vec{\tilde{\mathbf{z}}} \leftarrow \vec{\tilde{\mathbf{z}}}_{old} + \alpha_z \boldsymbol{\delta}_z$;
21: $\quad\quad\quad\Delta_{\mathbf{f}} \leftarrow \langle f_{\mathrm{R}} \rangle_{\lambda}(\vec{\tilde{\mathbf{z}}}) - \langle f_{\mathrm{R}} \rangle_{\lambda}(\vec{\tilde{\mathbf{z}}}_{old})$;
22: $\quad\quad$**until** $\Delta_{\mathbf{f}} < 0$;
23: $\quad\quad$Update $\tilde{\boldsymbol{H}}_{\lambda}^{-1}$; (Shermam-Morrison-Woodbury formula)
24: $\quad\quad\Delta_{\mathbf{z}} \leftarrow \|\vec{\tilde{\mathbf{z}}} - \vec{\tilde{\mathbf{z}}}_{old}\|_{\mathrm{F}}$;
25: $\quad$**until** $(\boldsymbol{\Delta}_{\mathbf{z}} \leq \chi_Z)$ && $(t \geq T_{\mathrm{s}})$ && $(\mathrm{abs}(\Delta_{\mathbf{f}}) \leq \chi_F)$
26: **end for**

To evaluate the computational complexity of the R-GDC algorithm we consider the most relevant operations: *a*) the calculation of the search direction (line 14), *b*) the evaluation of the gradient and the objective function (line 13 and line 21) and *c*) the update of the inverse Hessian approximation $\tilde{\boldsymbol{H}}_{\lambda} \in \mathbb{R}^{N_V \times N_V}$ (line 23). Thus, the cost of the R-GDC method can be estimated as

$$\mathcal{C}_{\text{R-GDC}}(N_V;t) \approx \sum_{k=1}^{K} t_k \Big(\underbrace{\tfrac{N}{2}(N-1)C_2}_{\text{line 13}} + \underbrace{2N_V^2 - N_V}_{\text{line 14}} + \underbrace{6N_V^2}_{\text{line 23}}\Big) + r(t_k)\,\underbrace{\tfrac{N}{2}(N-1)C_1}_{\text{line 21}},$$

$$= \frac{1}{2}\sum_{k=1}^{K} t_k\big((N^2-N)C_2 + 16N_V^2 - 2N_V\big) + r(t_k)(N^2-N)C_1, \qquad (283)$$

where $r(t_k)$ is the number of iterations in the inner loop obtained with $\lambda^{(k)}$, C_1 and C_2 are the costs for the calculation of the Hypergeometric functions of equations (207) and (222), respectively.

LM-WLS Pseudo-code

Algorithm 4 LM-WLS localisation

1: Get the matrices $\tilde{\mathbf{D}} \in \mathbb{R}^{N\times N}$, $\mathbf{W} \in \mathbb{R}^{N\times N}$
2: Set the Stop-Criteria $\chi_Z = 10^{-8}$, $\chi_F = 10^{-8}$, $\chi_g = 10^{-8}$ and $T_{\text{MAX}} = 51$;
3: Set the initial estimate $\hat{\mathbf{Z}} \leftarrow \hat{\mathbf{Z}}_0 \in \mathbb{R}^{N_{\text{T}}\times\eta}$
4: **repeat**
5: Evaluate the vector function $\vec{\hat{\boldsymbol{\mathcal{F}}}}$
6: Evaluate the Jacobian $\boldsymbol{J}_{\vec{\mathbf{p}}}(\hat{\boldsymbol{\mathcal{F}}})$
7: Evaluate the magnitude of the gradient $\boldsymbol{\epsilon}_g \leftarrow \boldsymbol{J}^{\text{T}}_{\vec{\mathbf{p}}}(\hat{\boldsymbol{\mathcal{F}}})\vec{\hat{\boldsymbol{\mathcal{F}}}}$
8: **repeat**
9: $r \leftarrow r + 1$;
10: Estimate the descending step $\boldsymbol{\Delta}_{\mathbf{z}}$
11: $\Delta_{\mathbf{f}} \leftarrow f_{\text{R}}(\hat{\mathbf{Z}} + \boldsymbol{\Delta}_{\mathbf{z}}) - f_{\text{R}}(\hat{\mathbf{Z}})$;
12: **until** $\Delta_{\mathbf{f}} < 0$
13: $\hat{\mathbf{Z}} \leftarrow \hat{\mathbf{Z}} + \boldsymbol{\Delta}_{\mathbf{z}}$;
14: **until** $(\boldsymbol{\Delta}_{\mathbf{z}} \leq \chi_Z)$ && $(t \geq T_{\text{MAX}})$ && $(|\Delta_{\mathbf{f}}| \leq \chi_F)$&& $(\boldsymbol{\epsilon}_g < \chi_g)$

The computational complexity of the LM-WLS method is determined by: *a*) the total number of flops for the evaluations of the objective function, the Jacobian and the gradient magnitude and *b*) the number of elementary operations required by the estimation of the descending step. In modern LM algorithm the latter is given by a constrained optimization problem known as the trust-region sub-problem, which can be solved with the aid of a pre-conditioned conjugate gradient.

Finally, the computational complexity of the algorithm can be computed as

$$\begin{aligned}\mathcal{C}_{\text{LM-WLS}}(N_V;t) &\approx t(\underbrace{\tfrac{N_V^2}{\eta^2}+\tfrac{N_V}{\eta}(2N_{\text{A}}-1)}_{\text{line5+line6}}+\underbrace{\tfrac{N_V^3}{\eta^2}+\tfrac{2N_V^2}{\eta}(N_{\text{A}}-1)+N_V)}_{\text{line7}}+ \\ &\quad r(t)(\underbrace{N_V^3}_{\text{line10}}+\underbrace{\tfrac{N}{2}(N-1)}_{\text{line11}}) \qquad (284)\\ &= t(\tfrac{N_V^3}{\eta^2}+(\tfrac{N_V^2}{\eta^2}+\tfrac{N_V}{\eta})(2N_{\text{A}}-1)+N_V)+ \\ &\quad r(t)(N_V^3+\tfrac{N}{2}(N-1)).\end{aligned}$$

SMACOF Pseudo-code

Algorithm 5 SMACOF localization

1: Get the matrices $\tilde{\mathbf{D}} \in \mathbb{R}^{N\times N}$, $\mathbf{W} \in \mathbb{R}^{N\times N}$
2: Set the Stop-Criteria $\chi_Z = 10^{-8}$, $\chi_F = 10^{-8}$ and $T_{\mathrm{MAX}} = 51$;
3: Compute $\mathbf{H}_S \in \mathbb{R}^{N\times N}$ as

$$[\mathbf{H}_S]_{ij} \triangleq \begin{cases} \sum_{q=1}^{N} w_{iq}^2 - w_{ii}^2, & \text{if } i = j, \\ -w_{ij}^2, & i \neq j; \end{cases}$$

4: Compute $\mathbf{H}_S^{\dagger}$;
5: $\hat{\mathbf{P}} \leftarrow [\mathbf{a}_1; \cdots; \mathbf{a}_{N_{\mathrm{A}}}; \hat{\mathbf{Z}}_0] \in \mathbb{R}^{N\times\eta}$;
6: $t \leftarrow 0$;
7: **repeat**
8: $\quad t \leftarrow t + 1$;
9: $\quad \hat{\mathbf{P}}_{old} \leftarrow \hat{\mathbf{P}}$
10: $\quad$ Compute $\mathbf{A}_S \in \mathbb{R}^{N\times N}$ as

$$[\mathbf{A}_S]_{ij} = \begin{cases} \sum_{\substack{i=1 \\ i\neq j}}^{N} [\mathbf{A}_S]_{ij}\ , & i = j, \\ w_{ij}^2 \cdot \dfrac{\tilde{d}_{ij}}{\|\hat{\mathbf{p}}_i - \hat{\mathbf{p}}_j\|_{\mathrm{F}}}\ , & i \neq j; \end{cases}$$

11: $\quad \hat{\mathbf{P}} \leftarrow \mathbf{H}_S^{\dagger} \cdot \mathbf{A}_S \cdot \hat{\mathbf{P}}_{old}$;
12: $\quad \Delta_{\mathbf{P}} \leftarrow \|\hat{\mathbf{P}} - \hat{\mathbf{P}}_{old}\|_{\mathrm{F}}$;
13: $\quad \Delta_{\mathbf{f}} \leftarrow f_{\mathrm{R}}(\hat{\mathbf{P}}) - f_{\mathrm{R}}(\hat{\mathbf{P}}_{old})$;
14: **until** $(\Delta_{\mathbf{P}} \leq \chi_Z)$ && $(t \geq T_{\mathrm{MAX}})$ && $(\mathrm{abs}(\Delta_{\mathbf{f}}) \leq \chi_F)$

The complexity of the SMACOF algorithm is determined by: *a*) the calculation of the pseudo-inverse $\mathbf{H}^{\dagger}$, the update $\hat{\mathbf{P}}$ and *c*) the evaluation of the objective function. Specifically,

$$\begin{aligned} \mathcal{C}_{\mathrm{SMACOF}}(M;t) \;&\approx \underbrace{N^3}_{\text{line4}} + t\left(\underbrace{\eta N(2N-1)}_{\text{line10}} + \underbrace{\tfrac{N}{2}(N-1)}_{\text{line11}}\right) \\ &= \; N^3 + t\big(N^2(2\eta+\tfrac{1}{2}) - N(\eta+\tfrac{1}{2})\big)\,. \end{aligned} \tag{285}$$

419. Hietakangas, Simo (2012) Design methods and considerations of supply modulated switched RF power amplifiers

420. Davidyuk, Oleg (2012) Automated and interactive composition of ubiquitous applications

421. Suutala, Jaakko (2012) Learning discriminative models from structured multi-sensor data for human context recognition

422. Lorenzo Veiga, Beatriz (2012) New network paradigms for future multihop cellular systems

423. Ketonen, Johanna (2012) Equalization and channel estimation algorithms and implementations for cellular MIMO-OFDM downlink

424. Macagnano, Davide (2012) Multitarget localization and tracking : Active and passive solutions

425. Körkkö, Mika (2012) On the analysis of ink content in recycled pulps

426. Kukka, Hannu (2012) Case studies in human information behaviour in smart urban spaces

427. Koivukangas, Tapani (2012) Methods for determination of the accuracy of surgical guidance devices : A study in the region of neurosurgical interest

428. Landaburu-Aguirre, Junkal (2012) Micellar-enhanced ultrafiltration for the removal of heavy metals from phosphorous-rich wastewaters : From end-of-pipe to clean technology

429. Myllymäki, Sami (2012) Capacitive antenna sensor for user proximity recognition

430. Jansson, Jussi-Pekka (2012) A stabilized multi-channel CMOS time-to-digital converter based on a low frequency reference

431. Soini, Jaakko (2012) Effects of environmental variations in *Escherichia coli* fermentations

432. Wang, Meng (2012) Polymer integrated Young interferometers for label-free biosensing applications

433. Halunen, Kimmo (2012) Hash function security : Cryptanalysis of the Very Smooth Hash and multicollisions in generalised iterated hash functions

Book orders:
Granum: Virtual book store
http://granum.uta.fi/granum/

UNIVERSITY OF OULU P.O.B. 7500 FI-90014 UNIVERSITY OF OULU FINLAND

ACTA UNIVERSITATIS OULUENSIS

ISBN 978-951-42-9973-5 (Paperback)
ISBN 978-951-42-9974-2 (PDF)
ISSN 0355-3213 (Print)
ISSN 1796-2226 (Online)

UNIVERSITY of OULU
OULUN YLIOPISTO